Formation and evolution of early-type galaxies

van Dokkum, Pieter Gerhardus

RIJKSUNIVERSITEIT GRONINGEN

Formation and Evolution of Early-Type Galaxies

Proefschrift
ter verkrijging van het doctoraat in de
Wiskunde en Natuurwetenschappen
aan de Rijksuniversiteit Groningen
op gezag van de
Rector Magnificus, dr. D. F. J. Bosscher,
in het openbaar te verdedigen op
maandag 21 juni 1999
om 14.15 uur

door

Pieter Gerhardus van Dokkum
geboren op 29 juni 1972
te Zwolle

Promotores: Prof. dr. M. Franx
Prof. dr. G. D. Illingworth

Cover:

Part of a mosaic of Hubble Space Telescope images of galaxy cluster MS 1054–03 at $z = 0.83$. This is one of the most distant clusters known; its redshift corresponds to the time when the Universe was only 45 % of its present age.

Dimensions of the image are $3.3' \times 3.0'$, corresponding to $1.9 \times 1.7\, h_{50}^{-1}$ Mpc at the distance of MS 1054–03. In this thesis, morphologies, colors, masses and luminosities of galaxies in distant clusters are measured and compared to those of galaxies in nearby clusters.

A large fraction of galaxies in MS 1054–03 is colliding and merging. Images of some of these colliding galaxies are displayed on the back cover. Each image spans $6\farcs0 \times 5\farcs0$, or $56 \times 47\, h_{50}^{-1}$ kpc.

Contents

1 Introduction and Summary

ABSTRACT

Early-type galaxies are the dominant population in nearby rich clusters. In this thesis early-type galaxies in four clusters at $0.33 < z < 0.83$ are studied, to determine their star formation history and time of assembly. The evolution of the mean M/L ratio of early-type galaxies is measured from the Fundamental Plane. The M/L ratio evolves as $\Delta \log M/L_B \propto -0.40z$, for $\Omega_m = 0.3$ and $\Omega_\Lambda = 0$. From the slow luminosity evolution of massive early-types it is inferred that most of their stars were formed before $z \approx 2$. Early-type galaxies appear to have formed more recently than the stars within them. From a study of the cluster CL 1358+62 at $z = 0.33$ it is inferred that many low luminosity S0s in nearby clusters are probably dead remnants of star forming field galaxies, that suffered truncation of their star formation after entering the cluster environment. Furthermore, a population of luminous merging galaxies is discovered in the most distant cluster in the sample, MS 1054–03 at $z = 0.83$. It is estimated that more than half of present-day luminous ($\sim 2L_*$) cluster ellipticals experienced a major merger at $z < 1$. The mergers already have evolved stellar populations, consistent with the homogeneity and old stars of low redshift ellipticals. The discovery of a high merger fraction in this young cluster is direct evidence against formation of massive galaxies in a "monolithic collapse" at high redshift, and in qualitative agreement with hierarchical models for structure formation.

1.1 Introduction

1.1.1 Galaxy Formation

One of the major questions in astronomy is how galaxies were formed and how they subsequently evolved. As far as we know, virtually all stars and metals in the Universe were formed inside galaxies; the subject of galaxy formation therefore has close ties with the star formation history of the Universe, and the evolution of its metal content. Furthermore, galaxy formation is a probe of structure formation. In the past ~ 15 Gyr the Universe evolved from the smooth Cosmic Microwave Background with variations $\sim 10^{-5}$ on $\sim 10^{\circ}$ scales (Banday et al. 1998) to the rich structure of stars, galaxies, clusters and superclusters seen today. Currently popular models assume this structuring process is driven by the evolution of dark matter halos (e.g., White & Rees 1978), but because dark matter is very difficult to observe, galaxies can serve as luminous probes of the evolution of these halos.

In recent years there has been tremendous progress in the fields of galaxy formation and evolution, largely because of advances in telescope design and instrumentation. Telescopes such as the Hubble Space Telescope (HST), the 10 m W. M. Keck telescope on Hawaii, and the Very Large Telescope in Chile provide the means to study galaxies at cosmological distances, enabling us to observe the young progenitors of today's galaxies directly (e.g., Steidel et al. 1996). The study of galaxy formation has moved from extrapolating properties of nearby galaxies back in time to interpolating properties of galaxy populations at different epochs.

1.1.2 Properties of Early-Type Galaxies

This thesis deals with the formation and evolution of early-type galaxies, i.e., ellipticals and S0 galaxies. These galaxies form the dominant population in rich clusters such as the nearby Coma cluster (Dressler 1980). Early-type galaxies can be very luminous; the luminosities of giant ellipticals extend to $M_B^{\mathrm{T}} \sim -23$. These properties make early-type galaxies very suitable for studies of galaxy evolution; they can be observed to large distances due to their high luminosities, and it is relatively easy to obtain a large sample at the same distance by observing high redshift rich clusters.

Early-type galaxies are very homogeneous in their properties. They obey tight relations between their luminosities, velocity dispersions, colors, and structural parameters (e.g., Bower, Lucey, & Ellis 1992, Djorgovski & Davis 1987, Dressler et al. 1987). The usual interpretation of this homogeneity is that the stellar populations of early-type galaxies formed in a short timespan at very high redshift. Age differences between galaxies lead to a spread in colors and M/L ratios, and the small scatter in these properties at a given mass implies a small scatter in luminosity weighted ages. As an example, the upper limit of $\sigma_{U-V} < 0.035$ on the scatter in the $U-V$ color-magnitude relation of Coma ellipticals (Bower et al. 1992) implies an upper limit on the spread in luminosity weighted ages of $\delta\tau/\langle\tau\rangle \lesssim 0.12$. This upper limit indicates that most of the stars were formed at early times, and/or star formation in different galaxies was somehow synchronized.

Early-type galaxies can thus be considered relics of processes that took place in the early Universe, and studies of the evolution of early-type galaxies have been motivated by the desire to identify and quantify these processes.

1.1.3 Formation Theories

The homogeneity of early-type galaxies is consistent with the idea of galaxy formation in a "monolithic" collapse at high redshift. In these models, galaxies were formed in a single event

at very high redshift, from the collapse of proto-galactic gas clouds (Eggen, Lynden-Bell, & Sandage 1962; Searle, Sargent, & Bagnuolo 1973; Larson 1975; Rees & Ostriker 1977). Star formation in early-type galaxies ceased shortly after the collapse, followed by a smooth and regular dimming of the stellar light. These models naturally explain the homogeneity of early-type galaxies at $z = 0$, and predict little evolution in their properties or number density from the time of collapse to the present (see Jimenez et al. 1998).

A prediction of monolithic collapse models is the presence of massive star forming young galaxies at high redshift, with star formation rates of order $10^{2-3} M_\odot$ yr^{-1} (Jimenez et al. 1998). Star formation rates of galaxies at $z > 3$ selected by their continuum break at 912 Å are typically much lower ($\sim 10 M_\odot$ yr^{-1}; Steidel et al. 1996). However, massive star bursting systems at high redshift may have escaped detection in optical surveys if they are enshrouded in dust (e.g., Thompson et al. 1995). Dusty star bursting high redshift galaxies have been detected in the sub-mm (Blain et al. 1999), but it is difficult to determine their masses.

Massive star bursting young galaxies may be extremely rare. In semi-analytical models for galaxy formation in Cold Dark Matter (CDM) cosmologies (White & Frenk 1991; Cole 1991) the only objects that can form at $z \gtrsim 3$ are of low mass. These low mass galaxies can merge as their dark halos merge, and high mass galaxies such as ellipticals and S0s are slowly built up in many generations of mergers. Mergers form bulges and ellipticals; spirals are formed by accretion of gas after a merger, which then settles into a disk (e.g., Kauffmann, White, & Guiderdoni 1993). In the hierarchical models explored until now early-type galaxies are relatively newcomers to the galaxy population (Kauffmann 1996; Baugh, Cole, & Frenk 1996); Baugh et al. (1996) predict 50 % of present-day massive ellipticals experienced a major merger at $z < 0.5$.

These semi-analytical CDM models are currently unable to reproduce simultaneously the present-day luminosity function and the Tully-Fisher relation (Kauffmann et al. 1993; Cole et al. 1994; Heyl et al. 1995; Kauffmann et al. 1999). They also have difficulty explaining the homogeneity of early-type galaxies at $z = 0$; as an example, Baugh et al. (1996) predict a scatter in the $U-V$ color-magnitude relation of $\sigma_{U-V} = 0.074$, a factor 2 larger than the observed upper limit $\sigma_{U-V} < 0.035$ (Bower et al. 1992).

On the other hand, observations and simulations of mergers and merger remnants in the field demonstrate that at least some ellipticals were formed in mergers (e.g., Schweizer & Seitzer 1992, Barnes 1999). Furthermore, the number fraction of galaxies in close pairs increases with redshift (Patton et al. 1997), indicating that mergers were more prevalent at earlier times. Similarly, many galaxies in the Hubble Deep Field are irregular and may be mergers in progress (Mobasher et al. 1996). Note that mergers are rare in present-day rich clusters, because the probability of a low velocity encounter is small. Therefore, if cluster ellipticals formed in mergers they must have occurred at early times, before or during the collapse of the cluster (Roos & Aarseth 1982; Merritt 1984).

1.1.4 Testing Hierarchical Formation

Although the predictions of the monolithic collapse model are very different from those of hierarchical models it is at present unclear which provides a better description of galaxy formation. The fundamental difference between these models is the evolution of the mass function $\phi(M)$ with time, but the mass function is very difficult to measure. It is relatively straightforward to measure the redshift evolution of the *luminosity* function (Lilly et al. 1995; Ellis et al. 1996). Although the evolution of the luminosity function depends on the evolution of the underlying mass function, it also depends on luminosity evolution of the galaxies. Even in the absence of star formation the luminosities of stellar populations are expected to evolve, because stars turn off the main sequence. Additional measurements are necessary to

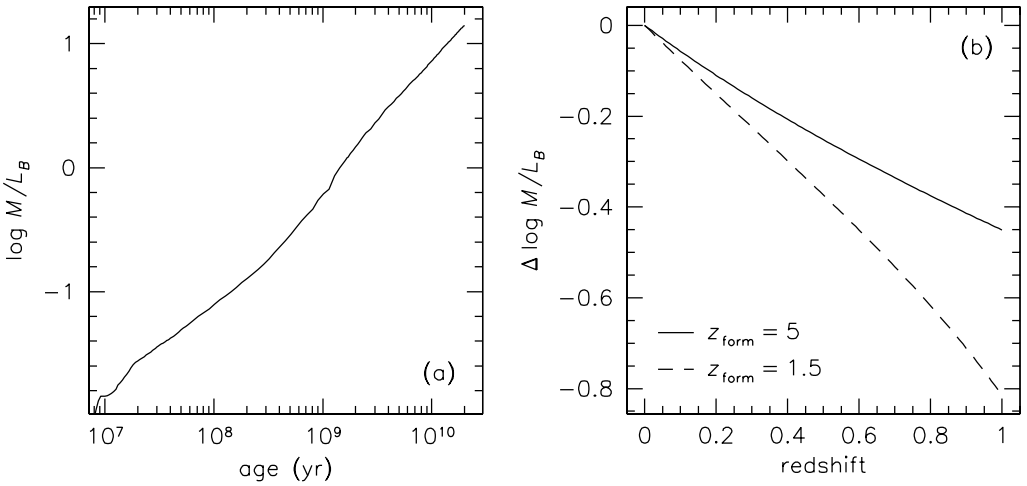

Figure 1.1: (a) Evolution of the M/L_B ratio of a single age stellar population (Bruzual & Charlot 1999). (b) Predicted redshift evolution of the M/L_B ratio for two stellar populations, formed at $z = 5$ and $z = 1.5$. The formation redshift of stellar populations can be determined from the observed evolution of their M/L ratios.

disentangle the effects of mass evolution and luminosity evolution on the evolution of the luminosity function.

By measuring mass-to-light ratios of galaxies the evolution of the luminosity function can be corrected for the luminosity evolution of stellar populations. If it is established that mass-to-light ratios evolve as $M/L(z)$ luminosities of high redshift galaxies can be transformed to masses, and through the transformation

$$\phi(M, z) = M/L(z)\phi(L, z) \tag{1.1}$$

the evolution of the mass function can be obtained.

Furthermore, the measured evolution of M/L ratios of galaxies provides important constraints on the properties of their stars, because it depends on the Initial Mass Function (IMF), and the formation redshift. The light of a young stellar population is dominated by massive stars which have a short lifetime on the main sequence. Therefore, the M/L ratio of a young population evolves faster than the M/L ratio of an old population. As illustrated in Fig. 1.1 the formation redshift of a stellar population can be determined from the measured evolution of its M/L ratio (see Franx 1995).

1.2 Outline and Summary

In this thesis, two approaches are followed to constrain theories for the formation and evolution of early-type galaxies. Constraints on the ages of their stars are obtained from the observed evolution of their M/L ratios (Chapter 2 – 4), and constraints on the time and process of their formation are obtained from morphological and spectral studies of large samples of galaxies in distant clusters (Chapter 5 – 7).

1.2.1 Ages of Stars in Early-Type Galaxies

In Chapters 2 – 4 the evolution of the M/L ratio of early-type galaxies is determined from the evolution of the Fundamental Plane (FP) in clusters to $z = 0.83$ (corresponding to a time when the Universe was $\approx 45\,\%$ of its present age). The FP is a tight relation between the effective radii r_e of galaxies, their surface brightness at the effective radii I_e, and their velocity dispersions σ, of the form

$$r_e \propto I_e^{-0.83} \sigma^{1.20} \tag{1.2}$$

in the B band (Djorgovski & Davis 1987; Dressler et al. 1987; Jørgensen, Franx, & Kjærgaard 1996). The implication of the existence of the FP is that M/L ratios of early-type galaxies are well behaved, and scale with the mass raised to a low power. Using $M \propto \sigma^2 r_e$ and $L \propto I_e r_e^2$ Eq. 1.2 can be rewritten as

$$M/L \propto M^{0.25} \tag{1.3}$$

(Faber et al. 1987). Therefore, the evolution of the FP traces the evolution of the M/L ratios of early-type galaxies, and the evolution of the offset of the FP is proportional to the evolution of the mean M/L ratio.

Determination of the high z FP requires measurements of r_e, I_e, and σ for samples of high redshift early-type galaxies. Because effective radii are typically $\sim 10\,\mathrm{kpc}$ (or $\sim 1''$ for galaxies at high redshift) high resolution imaging with HST is required to determine r_e and I_e. Velocity dispersions can be measured from the broadening of absorption lines in moderate resolution ($\sigma \lesssim 100\,\mathrm{km\,s^{-1}}$) spectra of early-type galaxies, obtained with high throughput spectrographs on large ground based telescopes.

These measurements were obtained for galaxies in four high redshift clusters. In Chapter 2 the methods for measuring r_e, I_e and σ of high redshift galaxies are described. Furthermore, these parameters are measured of galaxies in the cluster CL 0024+16 at $z = 0.39$. The Fundamental Plane is derived, and the evolution of the M/L ratio is established to $z = 0.39$. In Chapter 3 M/L ratios are measured of galaxies in CL 1358+62 at $z = 0.33$ and MS 2053+04 at $z = 0.58$. In Chapter 4, the analysis is extended to the cluster MS 1054–03 at $z = 0.83$ and these measurements are combined with those presented in Chapters 2 and 3. In this Chapter the implications for the formation redshift of the stars in early-type galaxies, the slope of the IMF, and Ω are discussed.

The M/L ratio evolves as $\Delta \log M/L_B \propto -0.40z$, for $\Omega_m = 0.3$ and $\Omega_\Lambda = 0$. The observed evolution provides a combined constraint on the formation redshift of the stars, the IMF, and cosmological parameters. The evolution is slow when compared to predictions from population synthesis models (e.g., Bruzual & Charlot 1999), indicating that the stars in early-type galaxies are very old. Furthermore, the data are inconsistent with $\Omega_m = 1$, unless the IMF is steeper than the standard Salpeter (1955) IMF. For a Salpeter IMF it is found that $z_{\mathrm{form}} > 2.8$ and $\Omega_m < 0.86$ with 95 % confidence. If the cosmological constant is non-zero lower formation redshifts are consistent with the data: $z_{\mathrm{form}} > 1.7$ if $\Omega_m = 0.3$ and $\Omega_\Lambda = 0.7$.

The luminosity evolution of massive early-type galaxies has now been determined with sufficient accuracy to place strong constraints on their epoch of star formation, and on cosmological models. The main uncertainty in the interpretation is the poor understanding of the IMF in the mass range around $1 M_\odot$. Nevertheless, the current measurement can be used directly to correct the evolution of the luminosity function for the brightening of stellar populations with redshift. This can provide an important constraint on the mass evolution of galaxies.

1.2.2 Ages of Early-Type Galaxies

In chapters 5 – 7 morphologies and colors are studied of large samples of galaxies in two clusters, CL 1358+62 at $z = 0.33$ and MS 1054–03 at $z = 0.83$. Although the stars in massive early-types formed at high redshift, the formation of the early-type galaxies *themselves* did not necessarily coincide with the formation of their stars. If all early-type galaxies were formed at very high redshift, their number density and properties are expected to show little evolution at $z < 1$. However, if early-type galaxies were formed in mergers, or by stripping of spiral galaxies, their number density is expected to evolve. Furthermore, if early-types formed in mergers these mergers should be seen, even though the timescales are short (typically $\lesssim$ 1 Gyr; e.g., Barnes 1998). The approach in this thesis is to perform large field surveys of a few clusters at different redshifts using a combination of large HST mosaics in two passbands and extensive spectroscopy from the ground, with the aim to constrain the relevance of processes such as stripping and merging for the formation of early-type galaxies.

In Chapter 5 the color-magnitude relation in CL 1358+62 at $z = 0.33$ is presented and discussed, using a sample of 194 spectroscopically confirmed cluster members observed with HST. It is found that S0s in the outer parts of the cluster are bluer on average and have a larger scatter in their colors than S0s in the inner parts of the cluster, implying they have younger stellar populations. This result is consistent with the idea that clusters at $z = 0.33$ continue to accrete galaxies and groups from the field and that infall extinguishes star formation. It is inferred that the population of S0s in clusters probably evolves as star forming galaxies are converted into passively evolving galaxies, fully consistent with morphological studies of galaxies in clusters at slightly higher redshift (Dressler et al. 1998). The young S0s are of low luminosity; the most luminous galaxies in clusters are already in place at $z = 0.33$, and must have formed at higher redshift.

Chapter 6 and 7 discuss the morphological mix and color-magnitude relation in MS 1054–03 at $z = 0.83$. A spectroscopic and photometric survey of this cluster yielded a sample of 81 spectroscopically confirmed cluster galaxies observed with HST. The most striking result of this survey is the large fraction of luminous ongoing mergers in MS 1054–03. Properties of these mergers and implications of their existence are discussed in Chapter 6. Most of the mergers will likely evolve into luminous ($\sim 2L_*$) elliptical galaxies. From the number fractions of mergers and ellipticals in MS 1054–03 it is estimated that $\gtrsim 50\,\%$ of present-day cluster ellipticals experienced a major merger at $z < 1$. Morphologies, spectra and colors of the mergers show that the merging galaxies are E/S0s or early-type spirals, with stellar formation redshifts $z \gtrsim 1.7$. The high merger fraction in this young cluster is direct evidence against formation of massive ellipticals in a "monolithic" collapse at high redshift, and in qualitative agreement with hierarchical formation scenarios.

In Chapter 7 the color-magnitude relation of MS 1054–03 is presented. The scatter and slope of the color-magnitude relation of early-type galaxies are very similar to those of the nearby Coma cluster. No trend with radius in the cluster is seen, but the data are consistent with the weak trend observed for S0s in the cluster CL 1358+62 at $z = 0.33$. A model is described which explains both the rapid evolution of the early-type fraction in clusters and the roughly constant scatter in the color-magnitude relation. The model assumes that star forming galaxies are continuously transformed to passively evolving galaxies, with the transformation rate determined by the observed evolution of the early-type fraction. Furthermore, it is assumed early-type galaxies are not immediately recognized as such after star formation ceases. The model reproduces the observed evolution of the scatter in the color-magnitude relation and the zeropoint of the Fundamental Plane, provided that early-type galaxies are recognized as such ~ 1 Gyr after star formation ceases.

1.3 Conclusions and Prospects

In conclusion, evidence is presented that the stars of early-type galaxies in clusters are old, whereas the early-types themselves have been assembled relatively recently. Specifically, we have shown that most stars in massive early-types were formed before $z \approx 2$, whereas it is inferred that more than half of present-day massive ellipticals were assembled in mergers at $z < 1$. The discovery of a large population of luminous mergers with evolved stellar populations in the outskirts of the cluster MS 1054–03 at $z = 0.83$ has far reaching implications; their presence is direct evidence against galaxy formation in a "monolithic" collapse at high redshift, and in qualitative agreement with hierarchical theories for structure formation. More wide field studies of high redshift clusters are necessary to establish whether MS 1054–03 is typical for its redshift, and to determine whether the merger fraction in distant clusters correlates with the dynamical state of the cluster itself.

It is difficult, but not impossible, to extend the studies presented in this thesis to higher redshifts. Several clusters have been discovered at $z \gtrsim 1$ (e.g., Deltorn et al. 1997, Stanford et al. 1997, Rosati et al. 1999). Because the 4000Å-break is redshifted to > 8000 Å the part of the spectrum of these galaxies that is usually observed is redshifted to the IR; IR imaging and spectroscopy will therefore be important aspects of studies of $z > 1$ early-types.

Furthermore, it is important to extend these studies to groups and the field at intermediate and high redshift. Currently popular hierarchical galaxy formation models predict that massive field ellipticals are several Gyr younger than cluster ellipticals, because galaxy formation is accelerated in dense environments (e.g., Kauffmann 1996). Therefore, comparison of the luminosity weighted ages and assembly time of field ellipticals and cluster ellipticals is an important test of these models.

References

Banday, A. J., Gorski, K. M., Bennett, C. L., Hinshaw, G., Kogut, A., Lineweaver, C., Smoot, G. F., & Tenorio, L. 1997, ApJ, 475, 393
Barnes, J. E. 1999, in After the Dark Ages: When Galaxies Were Young, 9th October Astrophysics Conference, University of Maryland, in press (astro-ph/9811242)
Baugh, C. M., Cole, S., & Frenk, C. S. 1996, MNRAS, 283, 1361
Blain, A. W., Smail, I., Ivison, R. J., & Kneib, J.-P. 1999, MNRAS, 302, 632
Bower, R. G., Lucey, J. R., & Ellis, R. S. 1992, MNRAS, 254, 601
Bruzual, G., & Charlot, S. 1999, in preparation
Cole, S. 1991, ApJ, 367, 45
Cole, S., Aragon-Salamanca, A., Frenk, C. S., Navarro, J. F., & Zepf, S. E. 1994, MNRAS, 271, 781
Deltorn, J.-M., Le Fevre, O., Crampton, D., & Dickinson, M. 1997, ApJ, 483, L21
Djorgovski, S., Davis, M. 1987, ApJ, 313, 59
Dressler, A. 1980, ApJ, 236, 351
Dressler, A., Lynden-Bell, D., Burstein, D., Davies, R. L., Faber, S. M., Terlevich, R. J., & Wegner, G. 1987, ApJ, 313, 42
Eggen, O. J., Lynden-Bell, D., & Sandage, A. R. 1962, ApJ, 136, 748
Ellis, R. S., Colless, M., Broadhurst, T., Heyl, J., Glazebrook, K. 1996, MNRAS, 280, 235
Faber, S. M., Dressler, A., Davies, R. L., Burstein, D., Lynden-Bell, D., Terlevich, R., Wegner, G. 1987, Faber, S. M., ed., Nearly Normal Galaxies. Springer, New York, p. 175
Franx, M. 1995, P. C. van der Kruit, & G. Gilmore, eds., Stellar Populations, IAU 164. Kluwer, Dordrecht, p. 269
Heyl, J. S., Cole, S., Frenk, C. S., & Navarro, J. F. 1995, MNRAS, 274, 755
Jimenez, R., Friaça, C. S., Dunlop, J. S., Terlevich, R. J., Peacock, J. A., & Nolan, L. A. 1998, preprint (astro-ph/9812222)
Jørgensen, I., Franx, M., & Kjærgaard, P. 1996, MNRAS, 280, 167
Kauffmann, G. 1996, MNRAS, 281, 487
Kauffmann, G., White, S. D. M., & Guiderdoni, B. 1993, MNRAS, 264, 201

Kauffmann, G., Colberg, J. M., Diaferio, A., & White, S. D. M. 1999, MNRAS, 303, 188
Larson, R. B. 1975, MNRAS, 173, 671
Lilly, S. J., Tresse, L., Hammer, F., Crampton, D., & Le Fevre, O. 1995, ApJ, 455, 108
Merritt, D. 1984, ApJ, 276, 26
Mobasher, B., Rowan-Robinson, M., Georgakakis, A., & Eaton, N. 1996, MNRAS, 282, L7
Patton, D. R., Pritchet, C. J., Yee, H. K. C., Ellingson, E., & Carlberg, R. G. 1997, ApJ, 475, 29
Rees, M. J., & Ostriker, J. P. 1977, MNRAS, 179, 541
Roos, N., & Aarseth, S. J. 1982, A&A, 114, 41
Rosati, P., Stanford, S. A., Eisenhardt, P. R., Elston, R., Spinrad, H., Stern, D., & Dey, A. 1999, AJ, in press (astro-ph/9903381)
Salpeter, E. 1955, ApJ, 121, 161
Schweizer, F., & Seitzer, P. 1992, AJ, 104, 1039
Searle L., Sargent W. L. W., & Bagnuolo W. G. 1973, ApJ, 179, 427
Stanford, S. A., Elston, R., Eisenhardt, P. R., Spinrad, H., Stern, D., & Dey, A. 1997, AJ, 114, 2232
Steidel, C. C., Giavalisco, M., Dickinson, M., & Adelberger, K. L. 1996, AJ, 112, 352
Thompson, D., Djorgovski, S., & Trauger, J. 1995, AJ, 110, 963
White, S. D. M., & Rees, M. J. 1978, MNRAS, 183, 341
White, S. D. M., & Frenk, C. S. 1991, ApJ, 379, 52

2 The Fundamental Plane at $z = 0.39$: Implications for the Evolution of M/L Ratios[†]

ABSTRACT

We present results on the Fundamental Plane of early-type galaxies in the rich cluster CL 0024 + 16 at z=0.391. The internal velocity dispersions of the galaxies have been measured from a 19 hour integration at the MMT. The photometric parameters of the galaxies have been measured from deep HST images. The galaxies satisfy a tight Fundamental Plane relation which is similar to that at low redshift. The scatter is 15 % in $\log r_e$, also very similar to that at low redshift. The data show that massive early-type galaxies existed at z=0.4, and extends earlier studies of the luminosities and colors of early-types in rich clusters.

The evolution of the M/L ratio is derived from the Fundamental Plane, by a comparison with Coma. The M/L ratio increases by 31 ± 12 % between $z = 0.391$, and $z = 0.023$. The evolution is low when compared to models for stellar populations. The expected evolution depends on the IMF, q_0, and the formation redshift of the galaxies. The data are in agreement with high formation redshifts. The modeling is still uncertain, however, because of various possible biases. The most serious bias may be the progenitor bias: if the progenitors of some current day early-types are spirals at $z = 0.4$, they would not be included in the sample, and the sample would be biased towards the oldest galaxies.

More data are needed to measure the evolution of the Fundamental Plane more precisely, and its scatter. There is a hint that the form of the Fundamental Plane changes with redshift, and this needs to be determined better. Deeper samples on more clusters would be valuable. Studies of the richest nearby clusters may help to test the underlying hypothesis that the Fundamental Plane is identical in all clusters.

[†]Pieter G. van Dokkum and Marijn Franx, *Mon. Not. R. Astron. Soc.*, **281**, 985 (1996)

2.1 Introduction

There is substantial evidence that galaxy evolution is a complex process. In contrast to the earliest ideas, involving an early formation and subsequently a smooth and regular dimming of the stellar light (e.g., Searle, Sargent, & Bagnuolo 1973), it is now believed that galaxies may evolve in an irregular way. Interactions, star bursts, and infall of material may drive the evolution of a typical galaxy. Observational evidence comes from the evolution of cluster galaxies (e.g., Butcher & Oemler 1978, 1984, Dressler & Gunn 1983, Couch & Sharples 1987), and studies of field galaxies (e.g., Broadhurst, Ellis, & Shanks 1988, Lilly et al. 1995). Similarly, hierarchical formation scenarios predict that galaxy evolution may be an irregular process (e.g., White & Frenk 1991).

Such complex evolution makes the interpretation of the observations more ambiguous, as the luminosities of galaxies can vary rapidly due to star bursts, and the morphologies of galaxies can change with time. As a result, the progenitors of current galaxies may have had different morphologies and masses. Detailed studies of the evolution of galaxy morphology, luminosity, and mass are necessary to determine the relevance of these processes. Such work has now become possible with the high resolution imaging capability of the Hubble Space Telescope (e.g., Dressler et al. 1994), and deep spectroscopy from the ground. An essential aspect of such studies is the measurement of the evolution of the masses and mass-to-light ratios (M/L) of galaxies. These measurements constrain the mass evolution of galaxies, and thereby infall and merging. They are necessary for a correct interpretation of the evolution of the luminosity function.

As the total masses of galaxies are very difficult to measure, relations such as the Tully-Fisher relation (Tully & Fisher 1977), the Faber-Jackson relation (Faber & Jackson 1976), or the Fundamental Plane (Dressler et al. 1987; Djorgovski & Davis 1987) can be used to constrain the mass evolution of galaxies. The small intrinsic scatter of these relations makes them very useful for studies of evolutionary effects.

Here we present results on the Fundamental Plane relation at high redshift. The Fundamental Plane is a relation between effective radius r_e, effective surface brightness I_e, and central velocity dispersion σ of the form $r_e \propto \sigma^{1.24} I_e^{-0.82}$ (Bender, Burstein, & Faber 1992, Jørgensen, Franx & Kjærgaard 1995c [JFK95c]). As shown originally by Faber et al. (1987), the implication of the relation is that the M/L ratio of galaxies is well-behaved, and of the form $M/L \propto r_e^{0.22}\sigma^{0.49} \propto M^{0.24}$. Recent studies indicate that the scatter in the M/L for cluster galaxies is small (23%, e.g., Lucey et al. 1991, JFK95c). The small scatter makes the Fundamental Plane especially useful to measure the evolution of galaxies with redshift, as small samples can provide useful answers. Furthermore, biases due to sample selection effects are small, if the scatter is small. The study of the Fundamental Plane at higher redshift has recently become possible with high throughput, high spectral resolution spectrographs (e.g., Franx 1993a,b).

In this paper, we report on measurements of velocity dispersions and structural parameters of galaxies in the rich and concentrated cluster CL 0024 + 1654 at $z = 0.39$. The Fundamental Plane is derived, and the implications for the evolution of the mass-to-light ratio are discussed. Sections 2 and 3 present the spectroscopy and the photometry. Those readers who are not interested in the details of the data analysis can proceed directly to sections 4 and 5, where the Fundamental Plane is presented and discussed.

Table 2.1: Spectroscopic Parameters

DGS[a]	BO[b]	PK[c]	Spectral Description[d]	σ	$\delta\sigma$	Remarks
84	15	122	Weak H,K,G,Bal abs	–	–	Insufficient S/N
111	26	105	E-type	156	28	
130		68		243	22	
137	42	80		–	–	Insufficient S/N
158	62	87	E-type	317	23	
161	65	86	E-type	275	20	
162	72	108	E-type	167	19	
169	71	88	E-type	342	25	
186	87	61	E-type:	382	34	
194	96	85	O II, Bal abs	–	–	Insufficient S/N
202	100	70	Weak E-type	248	20	
218				145	33	
229	125	64		–	–	Insufficient S/N

Notes:
[a] Dressler, Gunn & Schneider (1985) [DGS] number.
[b] Butcher & Oemler (1978) number.
[c] Pickles & van der Kruit (1991) number.
[d] Description of low resolution spectra from DGS.

2.2 Spectroscopy

Objects in the CL 0024 + 1654 field were observed with the Multiple Mirror Telescope (MMT) in September 1992. A mask with 14 slitlets was used. Each slitlet had a width of 1.6 arcsec, and variable length. Objects were selected on the basis of their *R* band flux (restframe $\sim B$). The slit positions were optimized to include as many of the brightest 20 galaxies as possible, and fainter galaxies were used to fill in remaining positions. The total integration time was 70 200 s, consisting of thirteen 5 400 s exposures in three nights. One object turned out to be a star, the thirteen galaxies are listed in Table 1, along with descriptions of low resolution spectra taken by Dressler, Gunn, & Schneider (1985) [DGS]. In this paper, we will use the numbering system of DGS throughout.

2.2.1 Reduction

Each slitlet was treated as a separate, long slit spectrum. For the reduction, we primarily used the standard IRAF tasks. Some tasks were written for the removal of the cosmic ray hits. After bias subtraction a smooth gradient was present in the residual bias frames. The peak-to-peak variation in this gradient proved to be small (0.4 %), and stable in time. We measured the gradient by fitting a low-order function to the residual of an average bias frame of each night, and we subtracted this fit from the data. The remaining variations in the individual bias frames are due to noise. Internal flatfields were used to correct for the pixel-to-pixel variations in the CCD response. The position of the slits on the chip was relatively stable during the observations: total shifts were of order ~ 2 pixels during each night. Several

averaged internal flatfields were created for each night to minimize the effects of these shifts. Since internal flatfields were taken before and after each 5 400 s exposure, small changes in the flatfields over time (e.g., the accumulation of dust grains) could be monitored well.

Cosmic ray hits were removed in several steps. First, exposures in each night were median filtered. The median frames were subtracted from the exposures, and the residual galaxy light and the residuals of skylines were modeled with appropriate functions. Cosmic ray hits were identified automatically as significant deviations from the function fits. The results from the program were inspected by eye, and corrected if necessary. Left over cosmic rays (~ 10 per exposure) and bad pixels were removed interactively. Finally, the separate exposures of each night were aligned and combined, with optimal weighting.

For each night, a wavelength solution was obtained from exposures of He-Ne-Ar lamps. The frames were transformed to a common $\log \lambda$ scale. The He-Ne-Ar exposures were reduced and combined in the same way as the galaxy exposures. The response function along each slitlet was determined from twilight sky exposures. After removal of the response function systematic variations in the spatial direction were $< 1\,\%$. The sky spectrum was derived from the spectra at the edges of each slitlet. After sky-subtraction, the average frames of the three nights were combined to form averaged, wavelength calibrated spectra of the 14 objects.

2.2.2 Instrumental Resolution

The usual procedure to determine velocity dispersions is to compare a galaxy spectrum with a star spectrum taken through the same spectrograph with the same setup. This ensures that the instrumental resolution of the star spectrum is the same as the instrumental resolution of the galaxy spectrum. Spectroscopy of high redshift galaxies does not allow this method, as the star and galaxy spectra cannot be obtained with the same setup. For the observation of stellar spectra, the grating angle needs to be changed to cover the same rest wavelengths as the spectra of the high redshift galaxies. Since the resolution is roughly constant in Å, it will change significantly in $\mathrm{km\,s^{-1}}$ (Franx 1993a,b). Furthermore, the resolution is usually dependent on the position on the CCD. Hence an absolute determination of the resolution, over the whole CCD, is necessary.

We determined the instrumental resolution from the He-Ne-Ar exposures, by fitting Gaussians to the emission lines. The fits were made for each slitlet, and for each observing night separately. Then, smooth functions were fit to the measured dispersions. The procedure is illustrated in Fig. 2.1. The instrumental resolution proved to be approximately constant at $\sigma_{\mathrm{instr}} = 1.4$ Å ($70\,\mathrm{km\,s^{-1}}$ at 6000 Å) for $\lambda \gtrsim 6100$ Å. At shorter wavelengths, the instrumental resolution is larger: it rises to $\sim 150\,\mathrm{km\,s^{-1}}$ at 5500 Å. The resolution also depends on the spatial coordinate: for the top and bottom slitlets σ_{instr} is $\sim 10\,\%$ larger than for the middle slitlet. The resolution was stable from night to night. Since each cluster exposure was bracketed by He-Ne-Ar exposures, the resolution could be determined through the nights. The resolution proved to be stable during each night, and consistent with the results derived from the mean He-Ne-Ar exposure.

The profile of a single line is determined by the instrumental characteristics, and can deviate from a Gaussian. This is especially likely to occur when the camera is out of focus on parts of the CCD. We verified the camera focus, and the shapes of the He-Ne-Ar lines by means of two exposures taken through two Hartman masks. These masks mask out either half of the parallel beam in the spectrograph. If the camera is out of focus, then there will be an offset between the two exposures in the wavelength direction. The offsets were small (~ 0.6 Å) in the spectral region that we used. Furthermore, we modeled the total instrumental

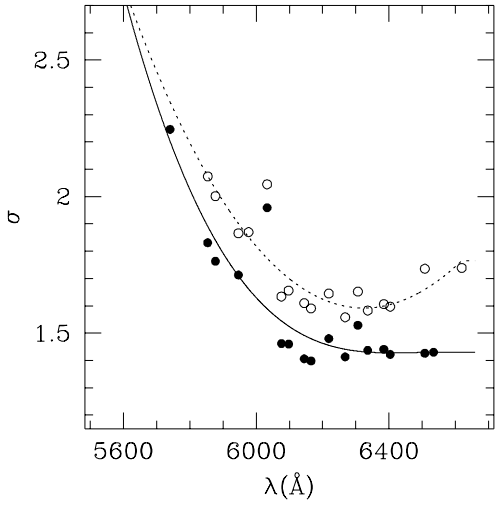

Figure 2.1: The instrumental resolution as a function of wavelength and position on the CCD. The instrumental resolution has been measured from He-Ne-Ar exposures. Solid symbols indicate the resolution for the central slitlet, open symbols the resolution for the slitlet closest to the edge of the chip. The deviant point at 6050 Å is a doublet. The resolution is highest in the center of the chip. The lines show the smooth functions that were fit to the measurements. We used the wavelength interval from 5895 to 6400 Å to measure the velocity dispersions.

resolution by taking the sum of the two separate Hartman exposures. The He-Ne-Ar lines on each Hartman exposure were fitted separately, and the instrumental resolution was now defined as the sum of two Gaussians, with different widths, and an offset. The resulting line profiles were very similar to those derived from a single Gauss fit, and the profiles did not affect the final velocity dispersions of the galaxies. This gives us confidence that the modeling is adequate.

The instrumental resolution can also be determined from sky emission lines, present in the galaxy spectra. This method has the advantage that the actual galaxy exposures are used, but suffers from the fact that many sky lines are blends. Gaussians were fit to bright lines which appeared to be no blends, using the final, summed spectra. No systematic differences between the thus determined resolution and the results from the He-Ne-Ar exposures were found. Since all determinations of the instrumental resolution give consistent values, we are confident the instrumental resolution is correctly modeled.

High spectral resolution template stars were kindly made available by R. van der Marel. The observations were done May 22, 1992, with the William Herschell Telescope (WHT) on La Palma, with the blue arm of ISIS (van der Marel et al. 1994). The spectral types of the 16 stars range from G0 to M0. The spectral resolution was measured again from comparison lamp spectra, similar to our measurements of the resolution of the MMT data. The spectral resolution is constant as a function of wavelength, but depends on the width of the slit used in the observations: $\sigma_* = 0.35$ Å (1″ slit) and $\sigma_* = 0.62$ Å (1.″8 slit). The spectra cover the spectral range 4215 – 4615 Å. The spectra were smoothed, rebinned, and smoothed again to have identical resolution as the galaxy exposures. Since the resolution of the galaxy spectra depends on the position on the chip, a separate template star was produced for each galaxy spectrum. We checked our method for consistency by comparing velocity dispersions obtained from template star spectra observed through the wide and the narrow slit. The differences in the output dispersion are of order 1%, and are not systematic. Hence our procedure correctly compensates for the differences in spectral resolution.

Eight additional template stars were made available by D. Fisher. They were observed May 16, 1993, with the Kast Spectrograph on the Lick Observatory 3 m telescope. The Lick spectra have a lower spectral resolution ($\sigma_* = 1.36$ Å), but cover a larger spectral range (4215 – 5617 Å) than the WHT stellar spectra. The stars were redshifted and rebinned to mimic

the MMT galaxy data. Since the instrumental resolution is comparable to the instrumental resolution of our data, no further transformations were performed.

2.2.3 Fourier Fitting

Velocities and velocity dispersions were determined with the Fourier Fitting method (Franx, Illingworth, & Heckman 1989 [FIH]). This method minimizes the residuals of the fitted stellar spectrum to the galaxy spectrum

$$\chi^2 = \sum_{i=1}^{N} (G_i - [B \circ S]_i)^2 / s^2 \tag{2.1}$$

where G is the galaxy spectrum, B is the broadening function, S is the stellar spectrum, $\circ$ denotes a convolution, and s is the noise in the galaxy spectrum. The fit is done in Fourier space, which speeds up the computation. The technique is described in detail in FIH. Several other methods exist for the determination of velocities and velocity dispersions from galaxy spectra (see, e.g., Rix & White 1992). One of our objectives is to compare our results with a low redshift comparison sample. Jørgensen, Franx, & Kjærgaard (1995b) [JFK95b] have used the Fourier Fitting method for the determination of velocity dispersions of a large sample of galaxies, and they found results consistent with earlier literature data. We use the same program in a very similar setup, to limit any systematic errors.

The spectra were summed in the spatial direction to increase the S/N ratio. The three central spectra were added to give an effective aperture size of $1\farcs8 \times 1\farcs6$. The S/N decreases very rapidly at larger distances from the galaxy centers, and the effective S/N ratio cannot be improved by adding more spectra. No weighting was applied in the summation. The Fourier program subtracted the continuum of the spectra, tapered them at the ends, and calculated the Fourier transform. The spectra were filtered with a low bandpass filter, and the fit was performed. The filter was set to give zero power at Fourier wavenumbers zero to l_o, and to rise slowly to unity at $2l_o$. We chose l_o equivalent to 110 Å^{-1}. This is identical to the value used by JFK95b when expressed in units of inverse km s^{-1}.

Since the spectra are not flux calibrated, the shape of the continuum is partly determined by the response function of the detector. The continuum shapes of the galaxy spectra and the star spectra are somewhat different, because they were taken with different instruments. The error introduced by this difference was estimated by dividing out the slope of the stellar spectrum, and comparing the results from the fitting program. The resulting rms differences in σ are ~ 1 %. Hence the fitting technique is insensitive to the shape of the continuum.

Various wavelength intervals for the fits were tried. The blue limit of the (redshifted) WHT and Lick star spectra is 5863 Å. Inclusion of the interval 5863 – 5895 Å resulted in a large increase in χ^2 for several spectra, due to the presence of a strong sky emission line at 5890 Å. Therefore, only the part of the spectrum redward of 5895 Å (rest wavelength 4238 Å) was used in the fits. For the fits with the WHT template stars, the upper limit of the wavelength interval was determined by the red limit of the redshifted star spectrum at 6420 Å. When fitting the WHT stars, we thus used the interval 5895 – 6400 Å. The Lick stellar spectra cover a larger wavelength range. The red limit is not determined by the stellar spectrum, but by the galaxy spectrum. This limit is different for each galaxy; it is determined by the layout of the multi-aperture mask. Typically it is $\sim$ 6530 Å. The results of the Fourier Fitting did not change when a red limit of 6400 Å was used.

The match between the template star spectrum and the galaxy spectrum will never be perfect, since the galaxy spectrum consists of a mix of stellar populations. In practice, template

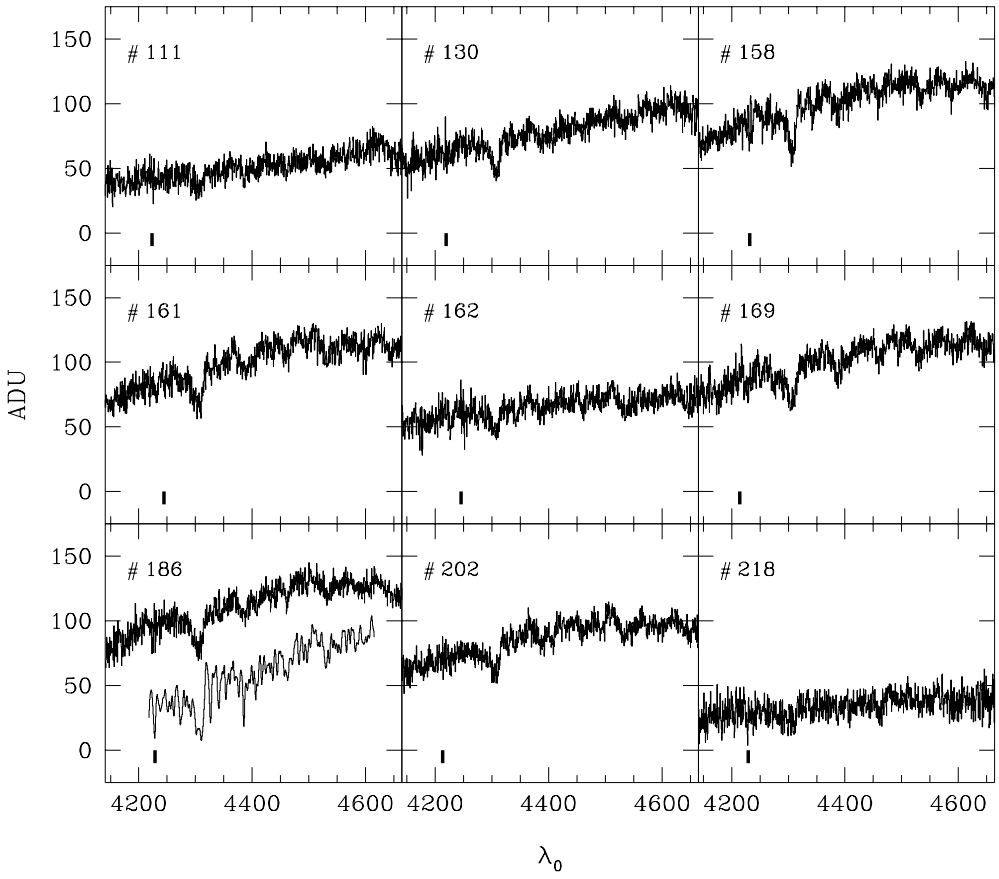

Figure 2.2: Spectra of galaxies with sufficient signal to determine internal velocity dispersions. The numbering system is from Dressler, Gunn & Schneider (1985) [DGS]. The lower left panel shows the template spectrum which was used to determine velocity dispersions. The units on the vertical axes are instrumental counts. Redshifts and velocity dispersions are listed in Table 1. Prominent spectral features are, e.g., the G-band at 4300 Å and the lines at Fe 4383, 4531, and Ca 4455 Å.

mismatch can be minimized by fitting template stars of various spectral types and using a star of the spectral type that gives the lowest χ^2 residual. Since the total number of template stars is 24, and the number of galaxies is 13, the best fitting templates could be determined reliably. The χ^2 residual has a minimum at spectral types G9 – K1, and it rises gradually for cooler or hotter stars. The dependence of χ^2 on spectral type is strongest for the galaxies with the highest S/N. Three of the WHT stars and five of the Lick stars have spectral types in the range G9 – K1. The consistency of the results of the fitting program was estimated by comparing σ and $\delta\sigma$ obtained with these template stars. The agreement between the Lick stars and the WHT stars is good. For the highest S/N spectra the distributions of the individual measurements of σ and $\delta\sigma$ are indistinguishable; for a few galaxies the differences are up to 10 %. There is no systematic effect, i.e., the differences average out for the galaxies. The agreement gives confidence in the stability of the results. Given the fact that the instrumental

resolution of the Lick stars is not precisely that of the galaxy spectra (especially blueward of 6100 Å, where the resolution of the galaxy spectra is no longer constant), the good agreement was not expected *a priori*.

Since the spectral resolution of the WHT templates is the same as the instrumental resolution of the galaxy spectra over the whole wavelength region used in the fits, we chose a good fitting WHT template (the K0 III giant HD 132737) for the final determinations of the velocities and velocity dispersions. Several galaxy spectra did not have sufficient S/N to derive a proper velocity dispersion. These galaxies were omitted from the list, as low S/N spectra produce biased estimates of the velocity dispersion (see, e.g., FIH). Fig. 2.2 shows the spectra of the galaxies for which reliable velocity dispersions could be determined. The position of the brightest sky emission line is indicated by bars.

Early-type galaxies have radial gradients in the velocity dispersion (e.g., Illingworth 1981, Davies et al. 1983, FIH, Jedrzejewski & Schechter 1989, van der Marel, Binney, & Davies 1990, Fisher, Illingworth, & Franx 1995). Therefore, the measured velocity dispersion through an aperture depends on the distance of the object and the aperture size. For a meaningful comparison between galaxies, the measured velocity dispersions must be corrected to a common physical aperture size. JFK95b have established aperture corrections from empirical models, based on published photometry and spectroscopy of 51 galaxies. They found that the correction to a physical aperture size of $d_{\rm corr}$ kpc can be approximated well by a power law:

$$\log \sigma_{\rm corr} = \log \sigma_{\rm obs} + 0.04 (\log d_{\rm obs} - \log d_{\rm corr}), \qquad (2.2)$$

where $d_{\rm obs}$ is the physical size in kpc of the aperture used in the observations. The correction is a simple power-law, and therefore the effective radius does not enter the expression if the aperture is corrected to a fixed physical size in kpc. We use the same normalization as JFK95b: a $3\farcs4$ diameter circular aperture projected on a galaxy in Coma. In our observations, the effective aperture was $1\farcs6 \times 1\farcs8$. This is equivalent to a circular aperture of $1\farcs96$ diameter (JFK95b). Using Eq. 2.2, we find that the correction to the distance of Coma and an aperture size of $3\farcs4$ is $\sigma_{\rm corr} = 1.072\,\sigma_{\rm obs}$, where we used a value of $q_0 = 0.5$.

Corrected velocity dispersions are listed in Table 1. The errors are the formal errors from the Fourier fitting program. Systematic errors in the velocity dispersion may be produced by two effects: spectral type mismatch, and incorrect filtering. We estimated these from the results obtained with template stars with different spectral type, and by changing the filter l_o by a factor of 1.5. Each effect is on the order of 3%, and we estimated the combined systematic error at 5%.

2.3 Photometry

Hubble Space Telescope (HST) Wide Field Camera (WFC) images of CL 0024 + 1654 were obtained from the Space Telescope Science Institute (STScI) archive. The cluster was observed through the *F*702*W* filter on two occasions: October 6, 1991 and October 1, 1992. The pointings were offset by $62''$. Therefore, approximately one half of the objects were imaged in both observations. Each observation consists of six separate exposures. The images of the 1992 observation are not aligned: between the third and fourth exposure the telescope moved $3\farcs7$. Total exposure times are 11 200 seconds (1991 observation) and 13 100 seconds (1992 observation).

2.3.1 Reduction

The pipeline processing was performed at STScI. For each observation we checked whether the recommended calibration files were used. The pipeline bias frames were different from the recommended frames. We retrieved the used and recommended bias frames from the archive and subtracted them; no differences were found. Bad columns were interpolated. Cosmic rays were removed in three steps. In the first step, individual exposures of the same field were compared, and pixel values which were significantly different from the mean were rejected. Then, the exposures were averaged, and left-over hits were removed using the COSMICRAYS task in IRAF. Finally, the images were carefully checked by eye for both left over cosmic rays and pixels which were wrongly recognized as cosmic ray hits (e.g., the central pixels of stars are sometimes marked as cosmic rays by the software).

The resulting images show a large ($\sim 20\,\%$) gradient in the background across the four chips. This is probably caused by non-uniformity in the throughput of the $F122M$ filter, which was used as a neutral density filter when Earth flatfields were taken (Faber 1992). Furthermore, "doughnut" like features are present ($\sim 5\,\%$ variations), probably images of the secondary mirror assembly (see, e.g., Ratnatunga et al. 1994). First, we tried to remove the gradient by applying a correction flatfield, constructed from the "superskyflats" in the $F555W$ and $F785LP$ filters created by the Medium Deep Survey (MDS) team (Phillips et al. 1994; Ratnatunga et al. 1994): the MDS flatfields were divided by the stacked earth flatfield in the same filter, yielding a $F122M$ filter flatfield. These flatfields removed the "doughnuts", but did not remove the gradient satisfactorily. Therefore, we created correction flats from the exposures themself, by fitting a low order function to the background, carefully avoiding all objects. The correction frames were normalized to the center of WF2. These flats do not remove the "doughnuts", but do reduce the large scale fluctuations to $\sim 1.5\,\%$. The doughnuts were modeled and divided out separately, using the constructed $F122M$ flats. As an independent test, we obtained images of the cluster Abell 370 from the STScI archive, taken November 11, 1992, also through the $F702W$ filter. In these observations, the same background structures are present, confirming that the source of the gradient is a flatfielding problem. After division of the Abell 370 images by our correction flats, the background was flat within $2\,\%$.

Finally, we combined the two averaged images from the 1992 observations, which were offset by $3\farcs7$. Since the shape of the HST PSF is dependent on the position on the chip, this step requires justification. We have tested the effect on galaxy parameters by refitting all (43) objects on chip 1 of the 1991 observation with PSFs offset by 18 pixels, and comparing the resulting parameters with the original ones (cf. Sect. 2.3.3). The average difference in r_e is $0.2 \pm 0.9\,\%$ and in I_e $0.3 \pm 1.7\,\%$. The difference in the product $r_e I_e^{0.8}$ is $< 0.1\,\%$. The differences in galaxy parameters do not correlate with distance from the center of the chip. Since the differences are small and are not systematic, no significant error was introduced by combining the six exposures of the 1992 observation.

2.3.2 Zeropoints

A meaningful comparison between magnitudes of galaxies at large z and magnitudes of nearby galaxies requires a transformation to a common photometric band in the restframe of the galaxies. For this purpose, the filterband needs to be shifted with the redshift of the galaxies. The $F702W$ band for the HST observations is fairly close to the redshifted V band, which we denote by "V_z". We use a small color correction to bring the HST observations on the V_z system. The steps are outlined in detail in Appendix A.

In summary, we have used groundbased data to determine a proper zeropoint for the HST

instrumental magnitudes, and to determine the color correction. We find

$$V_z = m_{F702W} - (0.47 \pm 0.05)(R-I-0.82) - (2.04 \pm 0.01), \tag{2.3}$$

The uncertainties in the steps are small. The systematic zeropoint uncertainty in the V_z magnitude is 0.03. The noise added by the color term is small, on the order of 0.02 mag. As a result, the method produces the true V_z magnitudes for galaxies. It is very different from applying a K-correction to magnitudes taken in a fixed filter in the observers frame. As noted by many authors, such K-corrections produce errors due to color variations between ellipticals, and because of color evolution of galaxies with redshift. As an example, the scatter in $V-R$ for Coma ellipticals is ~ 0.06 magnitudes. Furthermore, the models of Worthey (1994) predict an evolution in $V-R$ of ~ 0.10 magnitudes between $z = 0.4$ and the present. Therefore, the various K-corrections in the literature can easily produce errors of order 0.1 mag. Our resulting magnitudes behave like the standard K-corrected magnitudes, i.e., as fluxes, and not as flux densities. This is relevant for the surface brightness dimming correction. We determined the galactic extinction in the R and I band from Burstein & Heiles (1984), and Seaton (1979). We obtain an extinction of 0.09 in R, and 0.07 in I. All photometry is corrected for this extinction.

2.3.3 Analysis

Fitting Program

For an accurate measurement of length scales and central surface brightnesses it is necessary to account for the Point Spread Function (PSF). Especially for the HST, with its extended and asymmetrical PSF, an understanding of the effects of the PSF is crucial for a reliable determination of galaxy parameters. We fitted galaxies with a code which uses the full 2D information, taking the PSF into account. The program convolves a 2D model of a galaxy with the image of the PSF, and iteratively minimizes the residual

$$\chi^2 = \sum_{i=1}^{N} w_i (I_i - [M \circ P]_i)^2, \tag{2.4}$$

where I is the observed intensity, M is the model, P is the PSF, and $\circ$ denotes convolution. The summation is over all pixels within some fixed radius. A weighting function w is applied:

$$w_i = \frac{I_i + \langle I_e \rangle}{\langle I_e \rangle}. \tag{2.5}$$

This weighting ensures that the weight of pixels at the effective radius is roughly half of that of the central pixels. As a stability check, we also fitted objects with a uniform weighting (i.e., $w_i = 1$) and investigated the change in derived parameters. The effect of the applied weighting function on r_e and I_e is $< 2\%$, and the effect on the FP parameter $r_e I_e^{0.8} < 0.5\%$. This shows that the derived parameters do not depend critically on the applied weighting function.

The models are parameterized by 7 parameters: x and y center position, effective radius r_e, surface brightness at an effective radius I_e, ellipticity ϵ, position angle, and sky value. An additional parameter is object type: exponential, de Vaucouleurs $r^{1/4}$, exponential + $r^{1/4}$, or a δ-function, for the modeling of stars. All objects are fit simultaneously. For each object, a different PSF can be used. The advantage of fitting to the original data rather than to restored data (e.g., CLEANed data) is that the method requires a convolution instead of a

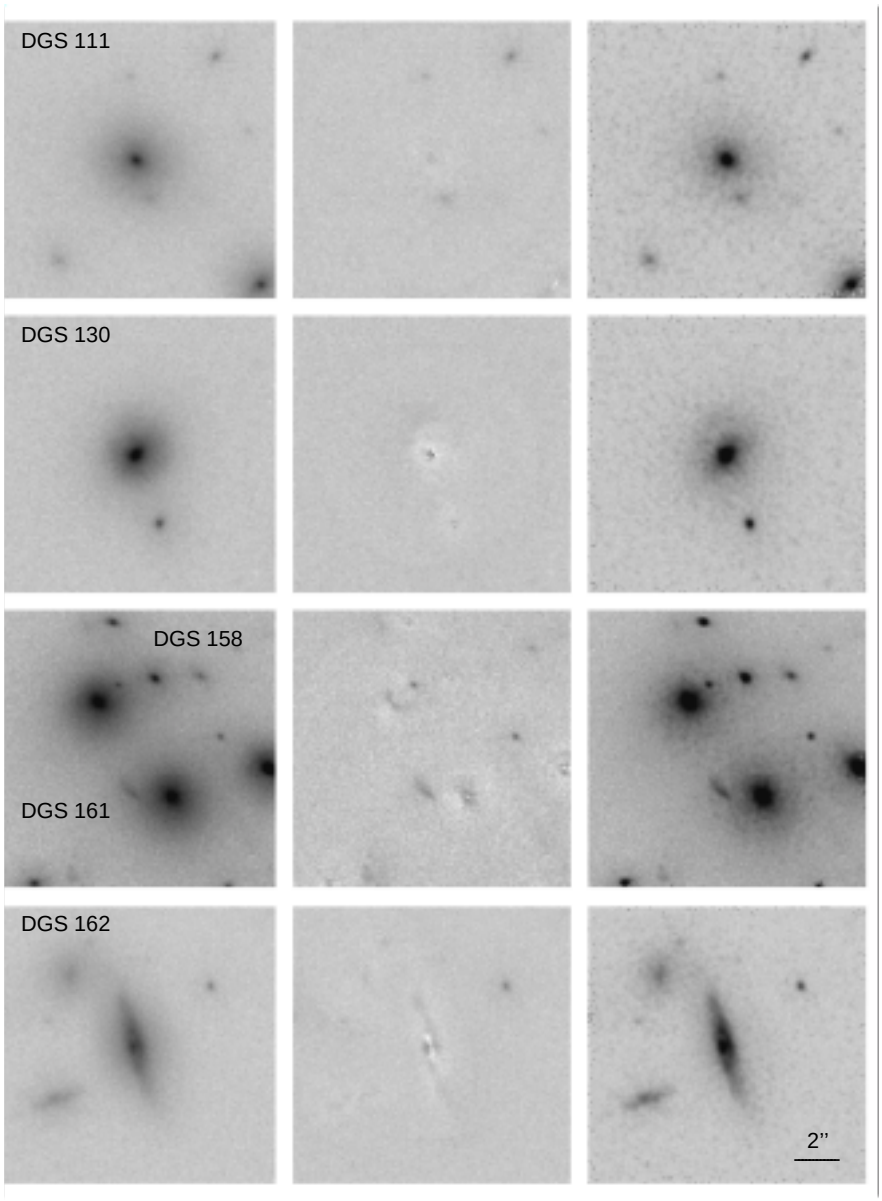

Figure 2.3: Hubble Space Telescope Wide Field Camera images of galaxies with measured velocity dispersions. Each panel is $13'' \times 13''$. North is up, East is to the left. For each galaxy, the original data, the residual of the model fits to the data, and a CLEAN restoration is shown. Apart from DGS 186, which has a triple nucleus, the galaxies are fit well. The CLEANing tends to sharpen and emphasize features already marginally visible in the original data.

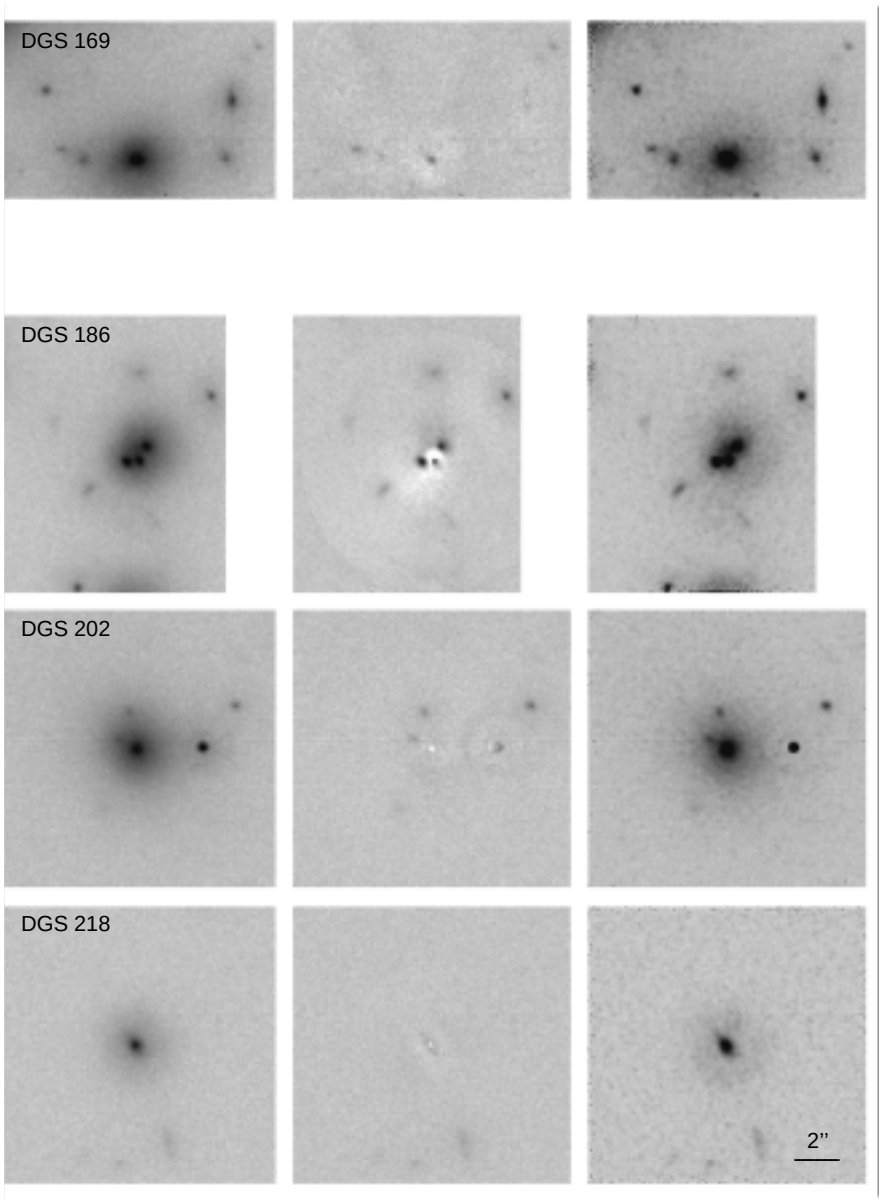

Figure 2.3: (continued)

Table 2.2: Photometric Parameters

Iden	[a]m_r	Type	χ^2	$\log r_e$ ″	μ_e^I	μ_e^V	$R_c - I_c$
111	19.51	S0	4.1	0.295	23.28	24.11	0.62
130	19.47	Interact	44	–0.048	21.49	22.37	0.84
158	18.48	E	12	0.773	23.81	24.69	0.83
161	18.37	E	13	0.535	23.21	24.11	0.85
162	19.48	S0/S	12	0.594	23.94	24.81	0.78
169	18.57	E	15	0.348	22.56	23.45	0.86
186	19.20	Triple	205	0.601	23.52	24.40	0.81
202	19.08	E/S0	14	0.759	24.08	24.96	0.82
218	20.55	SB0	5.6	–0.089	22.06	22.95	0.91

Notes:
[a] Gunn r magnitude from Schneider, Dressler & Gunn (1986).

deconvolution. This ensures that our method is repeatable and stable, and gives direct error estimates. Furthermore, the correlations between the parameters follow directly from the least squares fit. This is relevant here, because r_e and I_e are generally strongly coupled in these determinations. Fortunately, the correlation is usually parallel to the line of constant $r_e I_e^{0.8}$, and produces very little scatter in the Fundamental Plane (e.g., Jørgensen, Franx, & Kjærgaard 1993). The other advantage of this procedure is that overlapping galaxies are treated properly.

Results from the Fits

All objects in the observed CL 0024 + 1654 field with instrumental magnitudes $m_{F702W} < 24.6$ were fit. We used Tiny Tim 4.0 (Krist 1994) to calculate PSFs with a total size of $6'' \times 6''$. These were calculated for all object positions, to account for the dependence of the shape of the PSF on the position on the chip. Each galaxy was fit three times: in the first two fits, an exponential profile and an $r^{1/4}$ profile were fit respectively, to determine which profile type has the lowest χ^2 residual. Then, a third fit was performed with the best profile type for each galaxy.

For eight galaxies in our sample an $r^{1/4}$ profile gives the lowest χ^2 residual. Galaxy DGS 162 is best fit by an exponential profile. We tested how well we can discriminate between disk-dominated and bulge-dominated galaxies by simulations. We constructed model galaxies, with S/N and structural parameters typical for the observations. The models cover a range in inclination and bulge-to-disk ratio. We found that galaxies with bulge to disk ratios higher than 2/3 are best fit by $r^{1/4}$ law profiles. Hence, galaxies that are best fit by an $r^{1/4}$ profile may have significant disks, contributing up to $\sim 60\,\%$ of the light. The S/N is very high for the observations, and does not influence this result.

Fig. 2.3 shows the images of the galaxies with measured velocity dispersions (cf. Sect. 2.2.3). For each galaxy, the panels show the original image, the residual from the fits to the data, and a CLEAN restoration (Högbom 1974) of the image respectively. The CLEANing was performed with a 1.5σ stopping criterion and a loop gain of 0.02. The results are stable with respect to changes in these parameters. Table 2 lists the values of χ^2, and the effective

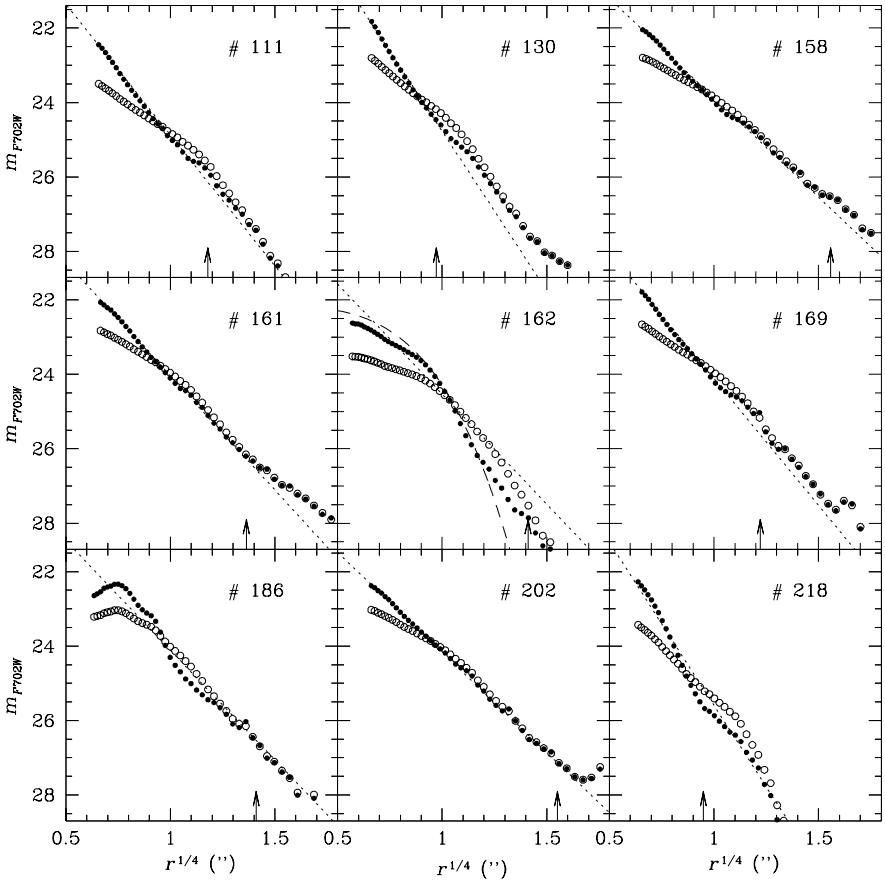

Figure 2.4: Surface brightness profiles of galaxies with measured velocity dispersions. Open circles represent the original data, filled circles a CLEAN restoration. Dotted lines indicate $r^{1/4}$ profiles as found by our fit to the original data. Some galaxies exhibit deviations from an $r^{1/4}$ profile, due to the presence of disks, or other galaxies. Galaxy DGS 162 is best fit by an exponential profile, indicated with the dashed line. Galaxy DGS 186 has a triple nucleus.

parameters r_e and μ_e for the galaxies. The value of χ^2 is significantly higher than 1 for all galaxies. This is no surprise, as ellipticals are well known to have radial variations in ellipticity and position angle, and intensity profiles which deviate from an $r^{1/4}$ law. The galaxies with the largest χ^2 are interacting galaxies (see 3.3.3).

As an independent check on our procedure, surface brightness (SB) profiles were extracted from the original and CLEANed images by integrating along ellipses with ellipticities and position angles as found by our fitting program. The profiles are shown in Fig. 2.4. The dotted lines indicate the result from the fit to an $r^{1/4}$ model; for DGS 162 the dashed line indicates the result from the fit to an exponential model. We also verified that the direct fitting method did not miss flux within an r_e. To that end, we derived the fluxes of the convolved model and that of the data within an effective radius of each galaxy. The differences were small, smaller than 0.03 magnitudes.

Morphologies of Galaxies with Measured Velocity Dispersions

Interestingly, several of the SB profiles depicted in Fig. 2.4 show significant deviations from a perfect $r^{1/4}$ law. The profiles are measured along ellipses with constant ellipticity, position angle and center position. The profiles do not change when the shapes and the centers of the ellipses are allowed to vary. We briefly discuss the morphological characteristics of the individual galaxies, on the basis of the ellipse fits, the CLEAN restorations of the images, and the residuals from the fits to the original images. We note that the distinction between ellipticals and S0's is difficult to make for lower luminosity galaxies, as face-on disks can be difficult to detect (e.g., Rix & White 1990, Jørgensen & Franx 1994).

DGS 111 – This galaxy has the appearance of an S0 close to face-on. The inner part of the galaxy is well fit by an $r^{1/4}$ profile. At $r = 1\farcs8$ a small companion galaxy causes a bump in the profile. The profile in the outer parts ($r > 2''$) is best fit by an exponential profile, indicating this galaxy probably has a disk.

DGS 130 – The CLEANed image, and the residual map shows a tidal tail to the North. The profile changes abruptly at $r \approx 1\farcs5$; the fit represents the inner part well. The outer part, containing most of the light, is fit badly. This is where the galaxy has an asymmetric extension to the North. We conclude that this galaxy is most likely interacting.

DGS 158 – Elliptical. This is one of the four bright galaxies in the center of the cluster. The light profile is consistent with an $r^{1/4}$ law.

DGS 161 – Elliptical. This is the central galaxy of the central group in the cluster. This group consists of four galaxies, including DGS 169 and DGS 158. The profile outside of $5''$ is affected by other galaxies. The inner $5''$ are well fit by an $r^{1/4}$ law.

DGS 162 – This is an edge-on disk galaxy. The residual image and the CLEAN image indicate dust absorption near the center and in the disk. The morphological type is S0/S. The profile is best fit by an exponential light distribution. The galaxy is red ($R-I = 0.78$); it resembles the bright, red spirals observed in nearby rich clusters. Since we intend to limit the biases as much as possible, this galaxy was treated as an elliptical (i.e., an $r^{1/4}$ law was fit to the profile). In Fig. 2.4, this fit is indicated with the dotted line.

DGS 169 – Elliptical. The galaxy image is close to the edge of the chip, therefore, points at $r > 2''$ have large uncertainties. The inner part of the profile is well fit with an $r^{1/4}$ profile.

DGS 186 – The CLEAN image of DGS 186 clearly shows the presence of three nuclei (cf. Fig 3), separated $\sim 0\farcs5$ (3 kpc), a characteristic of nearby Brightest Cluster Galaxies (e.g., Hoessel 1980). The galaxy is not located at the center of the cluster, but at a projected distance of $35''$ (0.22 Mpc). The bright nuclei severely affect the fit to the galaxy light profile. Therefore, we do not include this galaxy in our analysis.

DGS 202 – This galaxy appears to be an elliptical, or a close to face-on S0. It is difficult to distinguish faint ellipticals from face-on S0 galaxies. The light profile is consistent with an $r^{1/4}$ law.

DGS 218 – Probably a barred S0 galaxy. The galaxy has a high ellipticity at $r \approx 0\farcs7$. There is a break in the light profile at $r = 0\farcs7$, and a position angle twist. The profile is exponential in the outer parts, consistent with the presence of a disk.

From the analysis of the HST images, it is clear that various types of galaxies are represented in our sample, ranging from a disk dominated spiral galaxy (DGS 162) to apparently 'bona fide' giant ellipticals like DGS 158. Three galaxies show evidence for disks, one galaxy is probably interacting. DGS 186 has three nuclei, and is not considered in the analysis of the Fundamental Plane.

Internal Accuracy of the Fit Results

The fact that no systematic signal is present in the residual maps (see Fig. 2.3) is reassuring. Also, from Fig. 2.4 it is clear that the fit results generally are consistent with a CLEAN restoration. Differences between fits and data can be attributed to characteristics of the galaxies (e.g., disks or tidal features), and do not stem from systematic errors in the fitting procedure. Although the formal error in the derived parameters is small (typically $\sim 1-2\,\%$), we suspect the true uncertainty is larger, and primarily due to lack of knowledge of the HST PSF.

The shape of the HST PSF is position dependent due to camera vignetting, and changes over time (Faber 1992; Baggett & MacKenty 1994). Therefore, galaxies observed at different times on different chips and chip positions are ideally suited to estimate the uncertainties caused by lack of knowledge of the Point Spread Function. Approximately 40 % of the total number of objects in the cluster have been observed two times, 12 months apart, on different chips and/or at different chip positions. Therefore, we are able to derive reliable error estimates from a comparison of galaxy parameters derived from the two observations. A total of 75 objects were observed twice. Fig. 2.5 shows the differences in galaxy parameters derived from the two independent sets of observations. Galaxies situated close to the edge of a WFC chip are not considered in this comparison.

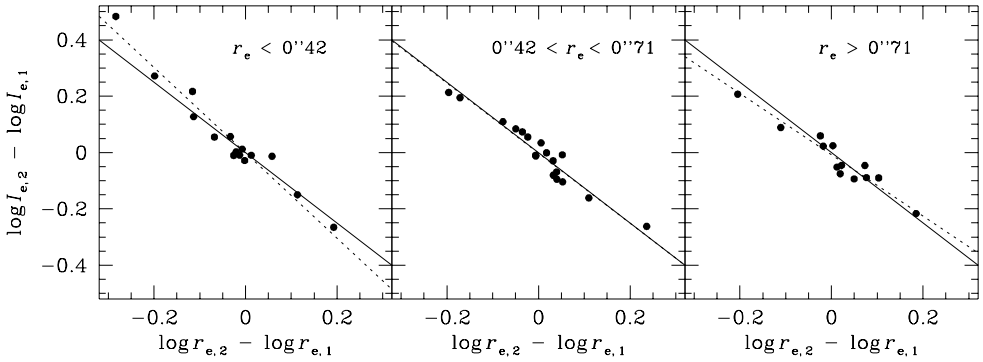

Figure 2.5: Comparison of galaxy parameters derived from the 1991 observations (labeled 1) and the 1992 observations (labeled 2). As expected, the differences in r_e and I_e are strongly correlated. The dotted lines are fits to the data. The uncertainty in r_e and I_e is lower for larger (i.e., larger r_e) galaxies. The observed correlations are almost parallel to the lines of constant $r_e I_e^{0.8}$ (solid lines), i.e., the Fundamental Plane parameter $r_e I_e^{0.8}$ can be determined to high accuracy. The error is estimated at 0.022 per single observation.

As expected, the differences in r_e and μ_e are strongly correlated. The slope of the correlation and the spread in r_e and μ_e is somewhat dependent on r_e; the data are grouped in three bins of r_e to show this behavior. The slope of the correlation is parallel to the line of constant $r_e I_e^{0.8}$, which enters the Fundamental Plane. There is no systematic offset between the two exposures. With these results, we can establish the errors in the determinations of r_e and I_e. For galaxies with $r_e > 0''.71$ the rms errors in $\log r_e$ and $\log I_e$ are 0.04 and 0.05, respectively. The rms error for $\log r_e I_e^{0.8}$, which enters the Fundamental Plane, is 0.022.

Comparison with Growth Curve Analysis

The structural parameters of nearby early-type galaxies are usually determined through curve-of-growth fitting. We verified that our technique gives similar results. To that end, we applied

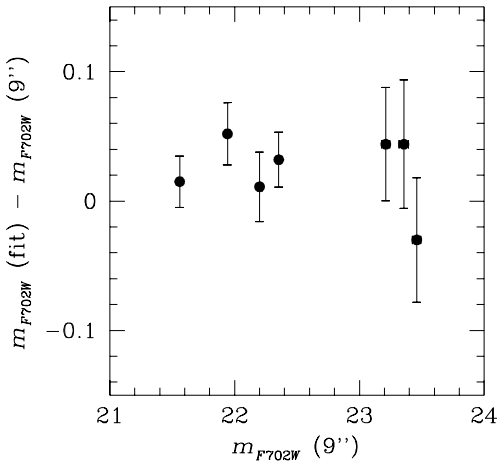

Figure 2.6: Comparison of magnitudes derived with our fitting program and magnitudes derived from aperture photometry. The fitting program used PSFs with Tiny Tim 4.0 with a size of $9'' \times 9''$. The aperture magnitudes were derived within $9''$. The mean difference is 0.02 ± 0.03 magnitudes. We infer that the Tiny Tim PSFs are a reasonable approximation of the true PSF.

a curve-of-growth analysis to the CLEANed data. Except for the interacting galaxies, the resulting combination of $r_e I_e^{0.8}$ was very similar to that derived from the direct fit. The difference was generally below 5 %, except for the SB0 galaxy in the sample. The median difference in $r_e I_e^{0.8}$ was 2 %. Hence, the direct fitting method does not introduce large systematic effects.

Recovery of Flux

We also tested whether the fitting program recovered all flux, for stars and galaxies. For stars, we tested this by fitting $9''$ x $9''$ PSFs, generated with Tiny Tim 4.0, to the stars used in the calibration of the HST data (cf. Sect. 2.5). The aperture magnitudes were measured through an aperture with a diameter of $9''$. Figure 6 shows the differences between the aperture magnitudes and magnitudes from the fits. The mean difference is $\langle F702W_{\rm fit} - F702W_{9''} \rangle = 0.02 \pm 0.03$ magnitudes. From this, we infer that the results of the fitting program and the results from the stellar photometry are consistent, and the Tiny Tim construction of the PSF is a good approximation of the true PSF.

Since the wings of the HST PSF extend beyond $3''$, it may be that there are systematic errors in the derived parameters I_e and/or r_e. We tested this by constructing model galaxies and fitting the models using PSFs with different sizes, $6''$x$6''$ and $12''$x$12''$ respectively. The differences in r_e and I_e were smaller than 3 %, whereas the combination of $r_e I_e^{0.8}$ was stable to 1 %. In conclusion, we are confident that the parameters listed in Table 2 are not systematically different from the true galaxy parameters. The typical errors are 0.04 in $\log r_e$, 0.05 in $\log I_e$, and 0.022 in $\log r_e I_e^{0.8}$.

2.4 The Fundamental Plane

In the late 1980s, it was found that early-type galaxies occupy a surface in (r_e, I_e, σ)-space, now known as the Fundamental Plane (Dressler et al. 1987; Djorgovski & Davis 1987). The scatter in the edge-on projection of the FP is small (< 17 % in $\log r_e$), but not entirely explained by measurement uncertainties (Lucey et al. 1991, JFK95c). The source of the intrinsic scatter in the FP is not understood at present; the residuals do not correlate with other structural parameters like ellipticity or isophotal shape (e.g., JFK95c).

The form of the Fundamental Plane is given by

$$\log r_e = \alpha \log \sigma + \beta \log I_e + \gamma. \quad (2.6)$$

The precise values of α and β are not well known; different authors find different values, due to differences in sample selection and fitting methods. The coefficients depend on passband. However, since most data sets are not complete in more than one passband, it is often very hard to disentangle the effects of differences in passbands and sample selection. We therefore use the coefficients measured by JFK95c, who studied 225 early-type galaxies in nearby clusters. They found $\alpha_{\mathrm{Gunn}\ r} = 1.24 \pm 0.07$ and $\beta_{\mathrm{Gunn}\ r} = 0.82 \pm 0.02$. We use these values throughout the analysis, and we test how the conclusions change if we use their coefficients for a bluer passband (e.g., $\alpha_{\mathrm{Gunn}\ g} = 1.16 \pm 0.10$ and $\beta_{\mathrm{Gunn}\ g} = 0.76 \pm 0.04$).

The Fundamental Plane implies that the M/L ratio of galaxies is well-behaved. Under the assumption that galaxies are a homologous family, the M/L ratio scales like

$$M/L \propto \sigma^{0.49} r_e^{0.22} \propto M^{0.24} r_e^{-0.02} \quad (2.7)$$

with a scatter of 23 % (Faber et al. 1987, JFK95c). The Fundamental Plane is a good tool to study galaxy evolution, because the internal scatter is so low. It is therefore sensitive to relatively small changes. In general, evolution of the Fundamental Plane is expected, because the M/L ratios of galaxies are expected to evolve with time. This is due to the evolution of the stellar population. Stellar populations with a fixed mass are expected to evolve like

$$L \propto 1/(t - t_{\mathrm{form}})^{\kappa} \quad (2.8)$$

To first order, $\kappa = 1.3 - 0.3x$, where x is the slope of the IMF (Tinsley 1980). However, κ depends also on passband and metallicity. As an example, the models of Buzzoni (1989) and Worthey (1994) produce values of κ between 0.6 and 0.95 in the V band, for various IMFs and metallicities.

The evolution of the M/L ratio implies that the zeropoint of the Fundamental Plane is expected to change. Furthermore, if the luminosity evolution depends on the mass of the galaxy, the coefficients of the Fundamental Plane can change (e.g., Renzini & Ciotti 1993). The evolution of the M/L ratio is generally measured as a function of redshift. Equation (9) implies that the M/L evolves in the following way

$$\ln M/L(z) = \ln M/L(0) - \kappa \left(1 + q_0 + z_{\mathrm{form}}^{-1}\right) z, \quad (2.9)$$

where z_{form} is the formation redshift z_{form} of the population (Franx 1995, Franx & van Dokkum 1996). This equation is valid to first order in z, for $q_0 \approx 0$ and high values of z_{form}. The logarithm of the M/L ratio is therefore expected to evolve in a linear way with redshift, and the slope depends on a combination of κ(IMF), q_0, and the formation redshift z_{form}. In general, the M/L ratio decreases with redshift, because the luminosity increases.

2.4.1 The Fundamental Plane of CL 0024

We show the Fundamental Plane for our sample of galaxies in CL 0024 in Fig. 2.7. The galaxies follow a tight relation, similar to nearby cluster galaxies. The scatter is 0.06 in $\log r_e$, or 15 % in r_e. Is is comparable to the observational scatter, and similar to the scatter for Coma. Fig. 2.7a shows the Fundamental Plane along one of its longest axes, whereas Fig. 2.7b shows it along a short axis. Similar to nearby clusters, it appears tighter in one projection than in the other, but the implied scatter is the same for both projections. The

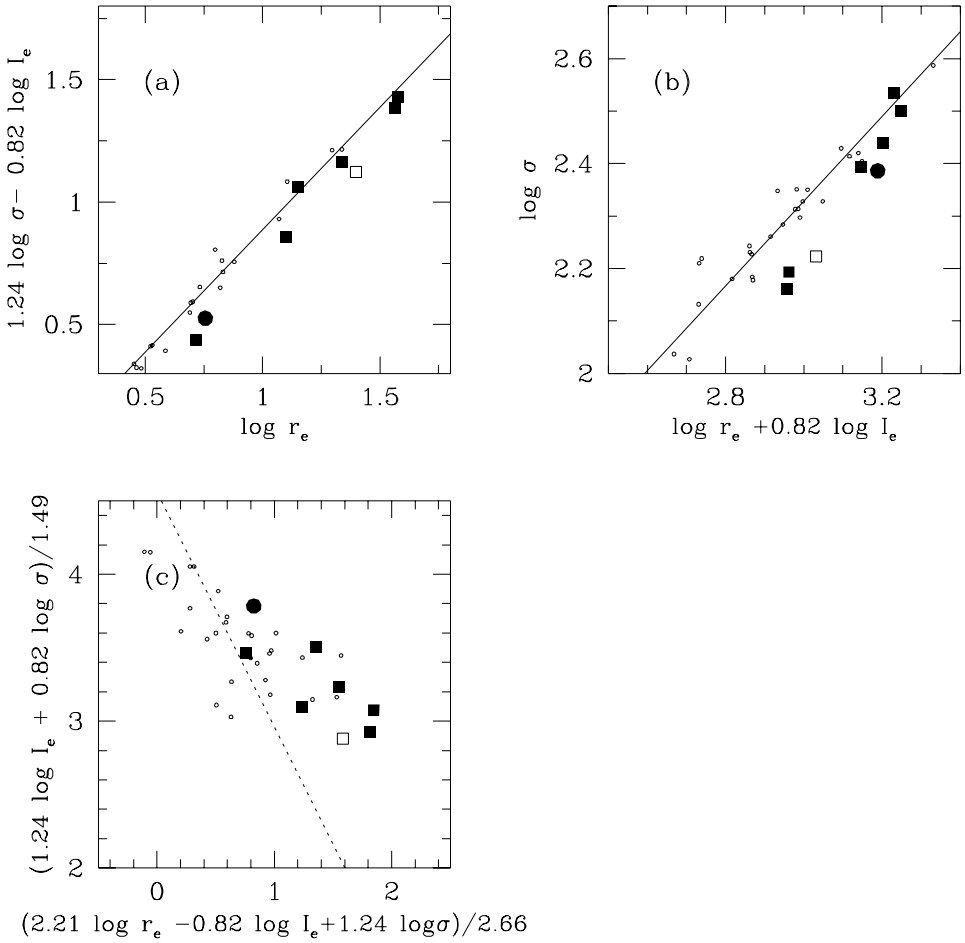

Figure 2.7: The Fundamental Plane of CL 0054 + 1654 in the *V* band. a) An edge-on view of the Fundamental Plane. The two axes are two long axes of the Fundamental Plane. The large symbols are the galaxies in CL 0024, the small circles are galaxies in Coma. The open square indicates galaxy DGS 162, which is treated in the same way as the other galaxies, but probably is a spiral galaxy. The filled circle is the interacting galaxy. The solid line is the fit to the galaxies in Coma by JFK95c. The Fundamental Plane is very similar at $z = 0.4$. b) A similar edge-on Fundamental Plane. The two axes are two of the shortest axes. The Fundamental Plane appears compressed. The scatter is more prominent. c) The face-on view of the Fundamental Plane. The galaxies in CL 0024 occupy a smaller region in the Plane, which is due to the bias in favor of luminous galaxies. The dashed line is a line of constant luminosity.

small scatter in Fundamental Plane implies a scatter in age of 20-30 %, depending on the value of κ (Renzini & Ciotti, 1993).

It is hazardous to determine the coefficients of the Fundamental Plane from the small sample presented here, because of systematic errors. Nevertheless, if we use the same algorithm

as JFK95c, we find coefficients of

$$\alpha = 0.97 \pm 0.09, \beta = 0.77 \pm 0.06 \tag{2.10}$$

which are not significantly different from the coefficients for Gunn *g* derived by JFK95c. The difference in α is the largest, $\Delta\alpha = 0.19 \pm 0.14$. More, and deeper data are needed to measure these coefficients to higher accuracy. If future observations confirm that α declines with redshift, then the implication is that the *M/L* ratio of low mass galaxies evolves faster than that of high mass galaxies. This could be due to low mass galaxies being younger (as advocated by Trager et al. 1993), to differences in the IMF (e.g., Renzini and Ciotti 1993), or unknown effects of stellar evolution.

2.4.2 The Surface Brightness Test with the Fundamental Plane

We can compare the zeropoints of the Fundamental Plane at high redshift and low redshift directly. For the low redshift sample, we use the data of Jørgensen, Franx, & Kjaergaard (1995a,b) for Coma. Their photometric parameters are based on CCD photometry, whereas the velocity dispersions come from a variety of sources. The details can be found in the Appendix. The Coma Fundamental Plane has a scatter of 16% in the *V* band.

Fig. 2.8 shows the evolution of the zeropoint of the Fundamental Plane expressed in surface brightness. The zeropoint surface brightness is the surface brightness of a galaxy on the Fundamental Plane with an effective radius of 3 h_{50}^{-1} kpc, and a velocity dispersion of 200 km s^{-1}. The decrease in surface brightness is due to the cosmological surface brightness dimming. Kjærgaard, Jørgensen, & Moles (1993) have proposed the Fundamental Plane as a method to verify the cosmological surface brightness dimming, but we note that the Cosmic Background Radiation provides a much better test. If the surface brightness would not evolve like $(1+z)^{-4}$, then the CBR would have satisfied a Planck curve for only a very short time after the photons were generated. Since it satisfies a Planck curve to 0.03 % (Mather et al. 1994), the cosmological surface brightness dimming must hold to very high accuracy.

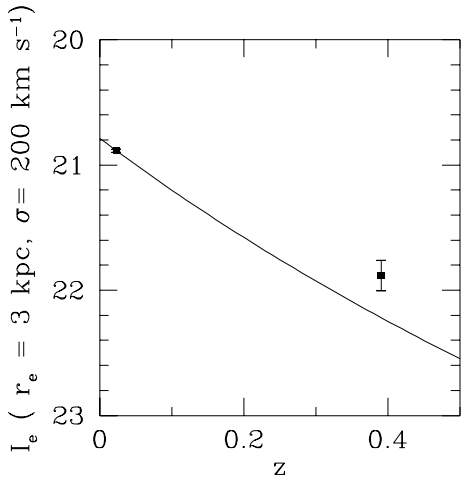

Figure 2.8: The evolution of the zeropoint of the Fundamental Plane as a function of redshift. The zeropoint is expressed as the observed *V* surface brightness for a galaxy on the Fundamental Plane with r_e = 3 kpc and σ = 200 km s^{-1}, in units of mag arcsec^{-2}. The surface brightness decreases rapidly with redshift, which is due to surface brightness dimming. The drawn line is the predicted cosmological effect $I_e \propto (1+z)^{-4}$. The zeropoint for CL 0024 lies above this line, which is due to evolutionary brightening of the stellar population.

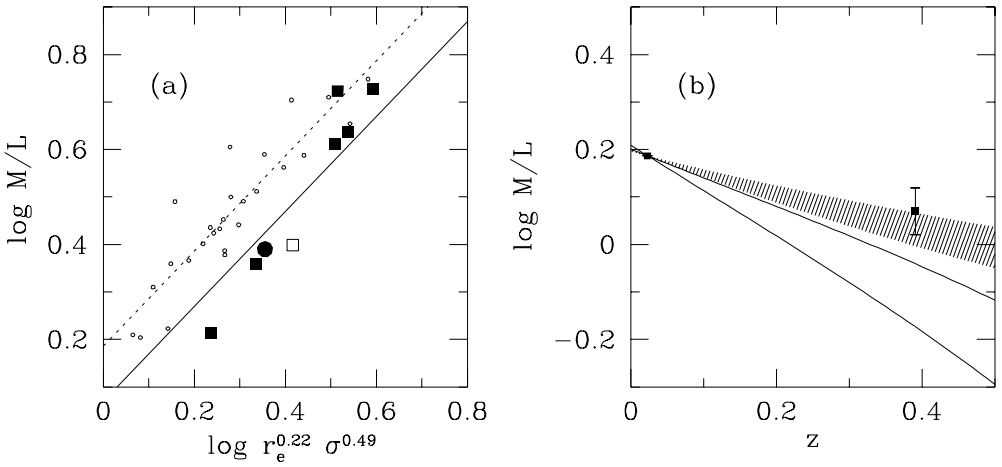

Figure 2.9: The evolution of the *M/L* ratio of early-type galaxies in CL 0024. a) The individual measurements of the *M/L* ratio for galaxies in CL 0024 (large symbols), and Coma (small circles). The Fundamental Plane implies that the *M/L* ratio is proportional to the parameter plotted along the horizontal axis. The drawn line is the relation for the CL 0024 sample, the dashed line is the relation for the Coma sample. The offset between the Coma sample and the CL 0024 is due to the evolution of the *M/L* ratio. The *M/L* ratio for CL 0024 is 31 % $\pm$ 12% lower than that for Coma. The filled circle is the interacting galaxy in CL 0024, the open square is the spiral galaxy in CL 0024. There is a suggestion that the *M/L* ratios of the low luminosity galaxies in Cl0024 are lower than expected from the Fundamental Plane. b) The evolution of the *M/L* ratio against redshift. The *M/L* ratio for a galaxy on the Fundamental Plane with r_e = 3 kpc and σ = 200 km s^{-1}, in arbitrary units. The hatched area indicates the values allowed by stellar population models with $z_{form} = \infty$ and $q_0 = 0$. The thick lines delineate the area allowed by models with $z_{form} = 1$. The data are marginally consistent with such models.

2.4.3 Evolution of the *M/L* Ratio Indicated by the Fundamental Plane

Fig. 2.9 shows the *M/L* ratios for galaxies in Coma and CL 0024 as a function of $\sigma^{0.49} r_e^{0.22}$ ($\propto M^{0.24} r_e^{-0.02}$). If galaxies evolve in a simple way, without merging or accretion, then the parameter $\sigma^{0.49} r_e^{0.22}$ remains constant, and only the *M/L* ratio will evolve with time. The figure suggests that the tilt of the Fundamental Plane may be slightly different for CL 0024, as found earlier. The reality of the effect remains uncertain.

We can derive the mean evolution in the *M/L* ratio by determining the offsets between both data sets. It turns out, however, that a straight fit to the data points produces an evolutionary effect which depends strongly on the coefficients of the Fundamental Plane. This is caused by the different selection of galaxies. The Coma data are dominated by much lower mass galaxies than the CL 0024 data. If the coefficients of the Fundamental Plane change, then the Coma zeropoint will be determined mostly by these low mass galaxies, whereas the CL 0024 zeropoint will be determined by the high mass galaxies. This difference in the mean mass of the galaxies results in a strong correlation between the zeropoint difference and the tilt of the lines. The difference in $\langle \log M \rangle$ for the two dataset is 0.7, equivalent to a factor of 5. The problem can be avoided by giving the low-mass galaxies in Coma low weight. All galaxies with masses lower than the lowest mass galaxy in CL 0024 were given weight 0, whereas the other galaxies were given a weight inversely proportional to the number of galaxies per mass bin. As a result, each mass bin has equal weight, both for the Coma sam-

ple, and the CL 0024 sample (which was treated in the same way). The range in masses is now very similar, and the weighted mean masses are the same.

The fits are shown as lines in Fig. 2.9(a). The mean offset between the two datasets is 31% in the M/L ratio. The offset changes very little when different coefficients are used. The coefficients for Gunn g give an almost identical offset of 33%. This can be contrasted to the results when no weighting is applied: the offsets are 26% and 41% for the two sets of coefficients. The uncertainty in the offset due to random errors is very small, and it is dominated by systematic effects. The systematic effects in the structural parameters produce an uncertainty of 9 %, whereas the uncertainty due to the sample selection is estimated at 7%. The total uncertainty is therefore on the order of 12 %. Here we assumed that the systematic uncertainties can be added quadratically.

Figure 2.9(a) suggests that the slope for the galaxies in CL0024 might be somewhat different from that for Coma. This is equivalent to saying that the lower luminosity galaxies have evolved faster in their M/L, which is consistent with a change in the coefficient α in the Fundamental Plane. However, as we noted earlier, the reality of this effect is not clear, and many more data points are needed for verification.

2.4.4 Modeling the Evolution of the M/L Ratio

When we apply the simple formula for a single, co-eval population to our result, we obtain a constraint of the form

$$\kappa(1+q_0+1/z_{\rm form})0.37 = 0.31 \pm 0.12 \tag{2.11}$$

As the models for stellar populations imply $0.6 < \kappa < 0.95$, the constraint is satisfied for a model with $z_{\rm form} = \infty$ and $q_0 = 1/2$. A model with values of $z_{\rm form} = 2$ and $q_0 = 1/2$ lies 1 σ away, for $\kappa = 0.6$. For high values of κ, such models predict an evolution of 70%, and that is ruled out firmly.

These results, however, should be treated with caution. As pointed out by Franx (1995) and Franx and van Dokkum (1996) the results from the Fundamental Plane may be biased if the fraction of early-type galaxies in clusters evolves with redshift. In such a case, the set of early-type galaxies at low redshift is not the same as the set of early-type galaxies at high redshift. Specifically, some of the early-type galaxies at $z = 0$ may be spirals at $z = 0.39$, and they should be included to derive the proper constraints on the mean formation redshift of all early-type galaxies in nearby clusters. Alternatively, we can try to measure the morphological evolution, and correct for it.

Another uncertain parameter in the equation is κ, the luminosity evolution. It depends directly on the IMF, and the IMF has not been well determined for early-type galaxies. Hence it could be that the model values of κ are incorrect. The measurement of good optical and IR colors may help towards a resolution of this issue. The color evolution of the galaxies is also linked to the IMF, and the value of κ. For steep IMF's, κ is small, but the color evolution will be rapid (e.g., Tinsley 1980). We notice that Stanford, Eisenhard, & Dickinson (1995) found an inconsistency between the color evolution of galaxies and the population models. The modeling of these observations needs further study.

Finally, but maybe most fundamentally, we have made the assumption that the Fundamental Plane evolves in an identical way in Coma and CL 0024. Although there is good evidence that the Fundamental Plane is very similar in Coma, and other rich nearby clusters (e.g., JFK95c), the cluster CL 0024 may not be typical of the progenitors of clusters like Coma at $z = 0.39$. Its high richness at $z = 0.39$ might imply that it will evolve into a cluster of much higher richness at $z = 0$. It is therefore valuable to probe the richest clusters at $z = 0$, to test whether the zeropoint of the Fundamental Plane is the same.

2.5 Discussion and Conclusions

We have measured photometric parameters and velocity dispersions of galaxies in the cluster CL 0024 + 1654 at z=0.39. The Fundamental Plane at this redshift is similar to the Fundamental Plane for nearby galaxies. The scatter is small, and dominated by measurement errors. Since the scatter is expected to increase with redshift, due to the fact that fractional age differences between galaxies become larger, this is rather surprising. More data are needed to measure the shape and scatter of the Fundamental Plane in greater detail. The low number of galaxies in our sample makes a good determination of these parameters difficult. Furthermore, the current sample is biased towards the most massive galaxies.

The data demonstrate that massive ellipticals existed at z=0.39 which are very similar to those in nearby clusters. The formation of these galaxies must have occurred at significantly higher redshift. This conclusion is in agreement with earlier studies on the colors and color magnitude relation (e.g., Bower, Lucey, & Ellis 1992). The analysis shows a weak evolution of the M/L ratio of the galaxies, on the order of 31% $\pm$ 12%. Such evolution is expected from the evolution of stellar populations in general. The speed of the evolution depends on the IMF, the formation redshift of the galaxy, and q_0. Our low evolution of the M/L ratio is difficult to reconcile with a low formation redshift. However, large uncertainties in the interpretation remain, relating to the IMF, and the progenitor problem: since it is not known what the progenitors of present-day ellipticals look like at z=0.39, it may be that we are selecting preferentially old progenitor galaxies at z=0.39 and then conclude that they are old. Detailed studies of the morphological evolution of cluster galaxies is needed to address that issue.

Our results can be compared to other measurements of the luminosity evolution in rich clusters. Aragon-Salamanca et al. (1993) derived the evolution of the K band luminosity function of rich clusters. They found no significant evolution. Their errors are large enough, however, to be consistent with the current observations. More such data would be valuable. The luminosity function does not necessarily evolve in the same fashion as the M/L ratio. If dissipationless merging occurs frequently, then its effect on the luminosities is much larger than on the M/L ratio. The combined measurement of the evolution of the luminosity function, and the M/L ratio can constrain such merging.

We can also compare our results to the evolution of the luminosity function of field galaxies. Lilly et al. (1995) and Ellis et al. (1996) find little evolution of the luminosity function at high luminosities for z=0.5. This is consistent with our results. Furthermore, Lilly et al. analyzed their red galaxies separately, and found small evolution for the red sample as a whole. These results are in qualitative agreement with the current result. A passive evolution of 1 magnitude, or higher, at z=0.5 appears to be inconsistent with all results.

It may be more difficult to reconcile the low luminosity evolution with the low, or absent color evolution of early-type galaxies at z=0.4 (e.g., Aragon-Salamanca et al. 1993, Rakos & Schombert 1995). Stellar population models predict rapid color evolution when the luminosity evolution is low, and vice versa (Tinsley 1980). The datasets therefore agree on a qualitative level, in the sense that evolution is small, but more data are needed to quantify all evolutionary effects more accurately. Data are needed on more galaxies in similar clusters to determine the scatter and form of the Fundamental Plane in greater detail. Such data can be used to confirm the hint that the low mass galaxies have evolved faster than high mass galaxies. Furthermore, it will be of interest to study poorer clusters at higher redshifts, to test for a dependence of the evolution on cluster properties. Finally, the comparison sample at low redshift needs to be extended towards the richest clusters.

Acknowledgements

The staff of KPNO and MMT are thanked for their assistance with the observations. Dan Fabricant helped with the fabrication of the aperture masks. Roeland van der Marel and David Fisher are thanked for making their data available in digital form. This research was partly funded by Hubble Fellowship grant HF-1016.01.91A and a grant from the University of Groningen. The comments of the referee, Roger Davies, helped to improve the text.

References

Aragon-Salamanca A., Ellis R. S., Couch W. J., Carter D., 1993, MNRAS, 262, 764
Baggett S., MacKenty J., 1994, J. C. Blades, S. J. Osmer, eds., Calibrating Hubble Space Telescope. STScI, Baltimore, p. 20
Bender R., Burstein D., Faber S. M., 1992, ApJ, 399, 462
Bower R., Lucey J. R., Ellis R. S. 1992, MNRAS, 254, 589
Broadhurst T. J., Ellis R. S., Shanks T., 1988, MNRAS, 235, 827
Burstein D., Heiles C., 1984, APJS, 54, 33
Butcher H., Oemler A., 1978, ApJ, 219, 18 [BO]
Butcher H., Oemler A., 1984, ApJ, 285, 426
Buzzoni A., 1989, APJS, 71, 817
Coleman G. D., Wu C.-C., Weedman D. W., 1980, APJS, 43, 393
Couch W. J., Sharples R. M., 1987, MNRAS, 229, 423
Davies R. L., Efstathiou G., Fall S. M., Illingworth G., Schechter P. L., 1983, ApJ, 266, 41
Davies R. L., Burstein D., Dressler A., Faber S. M., Lynden-Bell D., Terlevich R. J., Wegner G., 1987, ApJS, 64, 581
Djorgovski S., Davis M., 1987, ApJ, 313, 59
Dressler A., Gunn J. E., 1983, ApJ, 270, 7
Dressler A., Gunn J. E., Schneider D. P., 1985, ApJ, 294, 70 [DGS]
Dressler A., 1987, ApJ, 317, 1
Dressler A., Lynden-Bell D., Burstein D., Davies R. L., Faber S. M., Terlevich R. J., Wegner G., 1987, ApJ, 313, 42
Dressler A., Oemler A. J., Butcher H. R., Gunn J.E., 1994, ApJ, 424, 79
Ellis R. S., Colless M., Broadhurst T., Heyl J, Glazebrook K., 1996, MNRAS, 280, 235
Faber S. M., 1992, (Ed.), WFPC Final Orbital/Science Verification Report. STScI, Baltimore
Faber S. M., Dressler A., Davies R. L., Burstein D., Lynden-Bell D., Terlevich R., Wegner G., 1987, Faber S. M., ed., Nearly Normal Galaxies. Springer, New York, p. 175
Faber S. M., Jackson R. E., 1976, ApJ, 204, 668
Fisher D., Illingworth G., Franx M., 1995, ApJ, 438, 539
Franx M., 1993a, ApJ, 407, L5
Franx M., 1993b, PASP, 105, 1058
Franx M., 1995, van der Kruit P. C., Gilmore G., eds, Proc. IAU Symp. 164, Stellar Populations. Kluwer, Dordrecht, p. 269
Franx M., Illingworth G., Heckman T., 1989, ApJ, 344, 613 [FIH]
Franx M., van Dokkum P. G., 1996, Davies R., Bender R., eds., Proc. IAU Symp. 171, New Light on Galaxy Evolution. Kluwer, Dordrecht, p. 233
Frei Z., Gunn J. E., 1994, AJ, 108, 1476
Guzmán R., Lucey J. R., Carter D., Terlevich R. J., 1992, MNRAS, 257, 187
Harris H. C., Baum W. A., Hunter D. A., Kreidl T. J., 1991, AJ, 101, 677
Hamuy M., Suntzeff N. B., Heathcote S. R., Walker A. R., Gigoux P., Phillips M. M., 1994, PASP, 106, 566
Hoessel J. G., 1980, ApJ, 241, 493
Högbom J. A., 1974, A&AS, 15,417
Illingworth G., 1981, Fall S. M., Lynden-Bell D., eds., The Structure and Evolution of Normal Galaxies. Cambridge University Press, Cambridge, p. 27
Jedrzejewski R., Schechter P. L., 1989, AJ, 98, 147
Jørgensen I., 1994, PASP, 106, 967
Jørgensen I., Franx M., 1994, ApJ, 433, 553
Jørgensen I., Franx M., Kjærgaard P., 1992, A&AS, 95, 489

Jørgensen I., Franx M., Kjærgaard P., 1993, ApJ, 411, 34
Jørgensen I., Franx M., Kjærgaard P., 1995, MNRAS, 273, 1097 [JFK95a]
Jørgensen I., Franx M., Kjærgaard P., 1995, MNRAS, 276, 1341 [JFK95b]
Jørgensen I., Franx M., Kjærgaard P., 1995, MNRAS, 280, 167 [JFK95c]
Kjærgaard P., Jørgensen I., Moles M., 1993, ApJ, 418, 617
Krist J. 1994, The Tiny Tim User's Manual, version 4.0. STScI, Baltimore
Landolt A. U., 1992, AJ, 104, 340
Lilly S. J., Tresse L., Hammer F., Crampton D., Le Fèvre O., 1995, ApJ, in press.
Lucey J. R., Guzmán R., Carter D., Terlevich R. J., 1991, MNRAS, 253, 584
Mather J. C., et al., 1994, ApJ, 420, 439
Oke J. B., 1990, AJ, 99, 1621
Oke J. B., Gunn J. E., 1983, ApJ, 266, 713
Pence W., 1976, ApJ, 203, 39
Phillips A. C., Forbes D. A., Bershady M. A., Illingworth, G. D., Koo D. C., 1994, AJ, 107, 1904
Pickles A. J., van der Kruit P. C., 1991, A&AS, 91, 1 [PK]
Renzini A., Ciotti L., 1993, ApJ, 416, L49
Rakos K., Schombert J., 1995, ApJ, 439, 47
Ratnatunga K. U., Griffiths R. E., Casertano S., Neuschaefer L. W., Wyckoff E. W., 1994, Blades J. C., Osmer S. J., eds., Calibrating Hubble Space Telescope. STScI, Baltimore, p. 59
Rix H.-W., White S. D. M., 1990, ApJ, 362, 52
Rix H.-W., White S. D. M., 1992, MNRAS, 254, 389
Searle L., Sargent W. L. W., Bagnuolo W. G., 1973, ApJ, 179, 427
Seaton M. J., 1979, MNRAS, 187, 73
Schneider D. P., Dressler A., Gunn J. E., 1986, AJ, 92, 523
Stanford S. A., Eisenhardt P. R. M., Dickinson M., 1995, ApJ, 450, 512
Trager, S. C., Faber, S. M., Gonzalez, J. J., Worthey, G., 1993, BAAS, 183, 4205.
Tinsley B. M., 1980, Fundamentals of Cosmic Physics, 5, 287
Tully R. B., Fisher J. R., 1977, AA, 54, 661
van der Marel R. P., Binney J. J., Davies R. L., 1990, MNRAS, 245, 582
van der Marel R. P., Rix H., Carter D., Franx M., White S. D. M., de Zeeuw T., 1994, MNRAS, 268, 521
White S. D. M., Frenk C. S., 1991, ApJ, 379, 52
Worthey G., 1994, APJS, 95, 107

2.A Transformation from m_{F702W} Magnitudes to Redshifted V Magnitudes

2.A.1 Zeropoints

The HST $F702W$ zeropoint has an uncertainty of order 0.1 magnitudes (Faber 1992), primarily due to the flatfielding problems (cf. Sect. 2.3.1) and the uncertainty in the contamination correction. Accurate zeropoints (derived by the Medium Deep Survey team; Phillips et al. 1994) exist only for the $F555W$ and $F785LP$ filters. Hence, we used ground based observations of CL 0024 + 1654 to derive the $F702W$ zeropoint and the transformation to Cousins R and I magnitudes.

The observations were done on December 12, 1991, on the Kitt Peak National Observatory 2.1 m telescope, in the Cousins R and I bands. The integration times were 1800 s in I and 300 s in R. The standard photometric reduction was applied, using the IRAF package. The photometric zeropoints and color terms were calculated with the PHOTCAL package. Fluxes of 19 standard stars (Landolt 1992) were measured through a $9''$ diameter aperture. The color terms were small, and the published magnitudes could be reproduced to an rms accuracy of 0.02 magnitude.

The HST data of CL 0024 + 1654 were smoothed to the same resolution as the ground based data. The magnitudes of the stars and galaxies were measured through a $9''$ aperture.

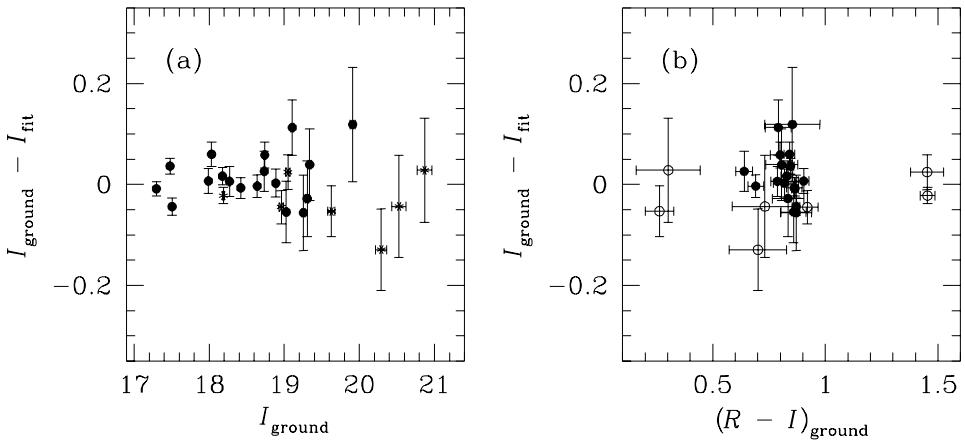

Figure 2.10: Comparison of ground based I magnitudes with I band magnitudes calculated from HST data using $I_{\rm fit} = F702W - 0.70(R-I-0.82) - 2.92$. Filled circles indicate galaxies, open circles indicate stars. In (a), the difference $I_{\rm ground} - I_{\rm fit}$ is plotted against ground based I. In (b), $I_{\rm ground} - I_{\rm fit}$ is plotted against $R-I$ color. No systematic trends are apparent. The scatter is consistent with the measurement errors.

We define $F702W$ instrumental magnitudes:

$$m_{F702W} = 25 - 2.5 \log \left(\frac{\rm ADU}{\rm exptime} \right). \tag{2.12}$$

A transformation of the form

$$I = m_{F702W} - \alpha(R-I-\langle R-I \rangle_{\rm gal}) + \beta \tag{2.13}$$

was derived, where $\langle R-I \rangle_{\rm gal} = 0.82$. A least squares fit to the data gave the following transformation:

$$I = m_{F702W} - (0.70 \pm 0.05)(R-I-0.82) - (2.92 \pm 0.01). \tag{2.14}$$

The residuals from the fit are shown in Fig. 2.10. The scatter is consistent with the measurement errors. This transformation can be compared to the transformations of Harris et al. (1991) between the HST filter system and the Kron-Cousins filter system, and to the in-flight $F702W$ zeropoint derived in Faber (1992) from observations of ω Cen. We derived $V-I = 2.13(R-I)$ from the observed standard stars. Hence the equivalent expression to Eq. 2.14 is given by

$$I = F702W - 0.72(R-I-0.82) - 2.95. \tag{2.15}$$

The $R-I$ colors of the galaxies fall into a narrow range: $\langle R-I \rangle = 0.82 \pm 0.06$. Therefore, our transformation (Eq. 2.14) is consistent with the transformation from Harris et al. (1991) and the zeropoint from Faber (1992) to ~ 0.03 magnitudes. This difference is well within the uncertainty of ~ 0.1 magnitudes for the $F702W$ zeropoint (Faber 1992). The $9''$ diameter aperture magnitudes have the advantage that no aperture correction is needed to compare them to the standard star measurements, making them suitable for the derivation of Eq. 2.14. However, they have large errorbars. In the application of eq. A2 to our galaxy photometry, we used $R-I$ colors measured through $5''$ apertures. These colors have much smaller errors. The measured values, corrected for galactic extinction, are listed in Table 2.

2.A.2 Correction to Redshifted V Magnitude

The resulting R and I magnitudes can be related to the magnitude through a redshifted V filter in the following way. Each magnitude is interpreted as a fluxdensity at the central frequency ν_i : $m_i = c_i - 2.5 \log F(\nu_i)$ The conversion constants are taken from Frei & Gunn (1994). Their constants are based on broad band observations of the spectrophotometric standards of Oke & Gunn (1983). The uncertainty in the constants is determined by the uncertainty in the spectrophotometry.

Next we assume that the flux density at the redshifted V band is related to the flux densities in the R and I band by $F(\nu_V(z)) = F(\nu_R)^{\alpha} F(\nu_I)^{1-\alpha}$. It is straightforward to derive the magnitude in the redshifted V band system

$$V_z = I + \alpha(R-I) + c_R + \alpha(c_R - c_I) - c_V + 2.5 \log(1+z) \tag{2.16}$$

The last term $2.5 \log(1+z)$ makes the magnitude behave as if it is a flux, and not a fluxdensity. This implies that the surface brightness decreases as $(1+z)^{-4}$, and not as $(1+z)^{-3}$ as for surface brightness flux densities. The corrected magnitude V_z behaves therefore as K-corrected magnitude.

We calculated α for galaxy spectral energy distributions from Coleman et al. (1980) and Pence (1976), for $z = 0.39$. The value of α is 0.23 ± 0.01 for early-type galaxies and early-type spirals. The resulting transformation

$$V_z = I + 0.23(R-I) + 0.69 \tag{2.17}$$

if correct for all galaxy types to 0.01 magnitude. The most significant error in the transformation comes from the uncertainty in the spectrophotometry. We estimate this uncertainty at 0.03 from a comparison of synthetic $V-I$ colors of stars observed by both Oke (1990) and Hamuy et al. (1994).

2.B The Coma Data

The low redshift comparison sample consists of E and S0 galaxies in the Coma cluster at $z = 0.023$. The surface photometry is from Jørgensen, Franx & Kjærgaard (1995a) [JFK95a]. The data were taken in the Johnson B and the Gunn r photometric filters. The effective radii and surface brightnesses in V were calculated from the B band photometry, and $B-V$ colors. The B band is the best band to use for this purpose, as the V band is closer to the B band than the Gunn r band. Color gradients in $B-V$ are very small, and can be ignored.

The $B-V$ color was calculated from the $B-r$ color. The transformation is given by Jørgensen (1994):

$$B-V = 0.673(B-r) + 0.184 \qquad (\sigma_{\rm fit} = 0.021). \tag{2.18}$$

The $B-r$ colors were taken from Jørgensen et al. (1992), and seeing corrected as described in JFK95a. JFK95a listed the mean surface brightness within an effective radius. These are K-corrected, and corrected for cosmological surface brightness dimming. We removed the correction for surface brightness dimming, and converted the surface brightnesses to the surface brightnesses at an r_e. The typical error in the V surface brightness is 0.03 mag.

The velocity dispersions listed by JFK95b were used. These are based on velocity dispersions published by Davies et al. (1987), Dressler (1987), Lucey et al. (1991), and Guzmán et al. (1992). JFK95b corrected these dispersions to an aperture size of $3\farcs4$.

3 The Fundamental Plane to $z = 0.58$ using Keck Spectroscopy and HST Imaging[†]

ABSTRACT

We present new results on the Fundamental Plane of galaxies in two rich clusters, Cl1358+62 at $z = 0.33$ and MS2053–04 at $z = 0.58$, based on Keck and HST observations. Our new data triple the sample of galaxies with measured Fundamental Plane parameters at intermediate redshift. The early-type galaxies in these clusters define very clear Fundamental Plane relations, confirming an earlier result for Cl0024+16 at $z = 0.39$. This large sample allows us to estimate the scatter reliably. We find it to be low, at 0.067 dex in $\log r_e$, or 17% in re, similar to that observed in comparable low redshift clusters. This suggests that the structure of the older galaxies has changed little since $z = 0.58$.

The M/L_V ratios of early-type galaxies clearly evolve with redshift; the evolution is consistent with $\Delta \log M/L_V \sim -0.3z$. The M/L_V ratios of two E+A galaxies in Cl1358+62 are also lower by a factor of ~ 3, consistent with the hypothesis that they underwent a star burst 1 Gyr previously. We conclude that the Fundamental Plane can therefore be used as a sensitive diagnostic of the evolutionary history of galaxies. Our data, when compared to the predictions of simple stellar population models, imply that the oldest cluster galaxies formed at high redshift ($z > 2$). We infer a different evolutionary history for the E+A galaxies, in which a large fraction of stars formed at $z < 1$. Larger samples spanning a larger redshift range are needed to determine the influence of star bursts on the general cluster population.

[†]Daniel D. Kelson, Pieter G. van Dokkum, Marijn Franx, Garth D. Illingworth, and Daniel Fabricant, *Astrophysical Journal Letters*, **478**, L13 (1997)

3.1 Introduction

Evidence for evolution in galaxies at intermediate redshifts has been found in a number of pioneering studies, both in clusters (e.g., Butcher & Oemler 1978, 1984; Dressler & Gunn 1983, Couch & Sharples 1987) and in the field (e.g., Kron 1980, Broadhurst, Ellis & Shanks 1988). Large spectroscopic surveys with 4 m class telescopes, coupled with HST images, have begun to clarify the nature of this evolution. The CFRS redshift survey of $\sim 10^3$ field galaxies (Le Févre *et al.* 1995; Lilly *et al.* 1995) is one such example. Here we pursue a complementary approach involving the detailed structural and kinematic study of smaller samples of individual galaxies using HST images and higher resolution spectroscopy with the Keck telescope. With these data, we can exploit the power of the Tully-Fisher relation for spirals (*e.g.*, Vogt *et al.* 1996) and the Fundamental Plane relation for early-type (E/S0) galaxies (see Franx 1993).

The Fundamental Plane (Djorgovski & Davis 1987; Dressler *et al.* 1987) is particularly valuable due to its low intrinsic scatter (Jørgensen, Franx and Kjærgaard 1993). For the Coma cluster, the Fundamental Plane relation,

$$r_e \propto \sigma^{1.24} I_e^{-0.82}, \tag{3.1}$$

where r_e is the effective radius, I_e is the surface brightness at that effective radius in the visible, and σ is the central velocity dispersion, has a scatter of only 17% *rms* (Jørgensen, Franx and Kjærgaard 1996 [JFK96]). This low scatter implies that the following well-defined relation exists for early-type galaxies (Faber *et al.* 1987):

$$M/L_V \propto r_e^{0.22} \sigma^{0.49} \propto M^{0.24} r_e^{-0.02}. \tag{3.2}$$

Thus, the Fundamental Plane is valuable because it explicitly incorporates galaxy masses. Franx (1995) and van Dokkum and Franx (1996 [vDF]) have demonstrated the value of this relation for studying evolution in early-type galaxies at intermediate redshift. The latter authors showed that the Fundamental Plane in the rich cluster Cl0024+16 is well defined, and consistent with simple evolutionary models, but the observed sample was very small.

Here we present new results for two additional clusters at intermediate redshifts. These new data triple the galaxy sample, and extend the observed redshift range to $z = 0.58$.

3.2 Observations and Data Reduction

The spectroscopic sample was selected on the basis of *R*-band magnitude. Blue galaxies were rejected to avoid field contamination, though the color restriction was chosen such that star-forming and post-starburst cluster members were not excluded.

Slit masks were designed to include as many bright galaxies as possible, though we only present data here for galaxies with HST imaging (see Figure 3.1). In addition, two known "E+A" (Dressler & Gunn 1983) galaxies were added to the Cl1358 mask. These galaxies are not included in the general sample, but are discussed separately. Thus, ten galaxies in Cl1358, and five in MS2053, are analyzed in this paper.

3.2.1 Spectroscopy

The spectroscopic observations were made using multi-slit masks with the Low Resolution Imaging Spectrograph (LRIS) at the Keck telescope. We observed at a typical resolution of σ_{instr} = 60-85 km s^{-1}. The data reduction was very similar to the data reduction of vDF for

Cl0024. The resulting spectra were very high S/N (typically 20-60 per resolution element). We show spectra of two galaxies in Figure 3.1(c,d).

We modeled the spectral resolution of the spectrograph in great detail, for the template stars as well as the galaxies. This is necessary to ensure that the template stars used for the determination of the velocity dispersions have the correct spectral resolution. This procedure is the most essential technical aspect of measuring velocity dispersions of galaxies at intermediate redshift.

Some galaxies showed peculiar features in their spectra. These features, either strong Balmer absorption lines, emission lines, residual sky lines, or atmospheric absorption bands, were given zero weight in the template fitting. We corrected the central velocity dispersions to an aperture of $3\farcs4$ at the distance of Coma, using the procedure of Jørgensen, Franx, & Kjærgaard (1995b). The corrections are small, 1.065 for Cl1358+62 and 1.066 for MS2053–04 ($q_0 = 0.05$). The resulting velocity dispersions and random errors are listed in Table 1.

3.2.2 Imaging

We used WFPC2 HST images to measure the structural parameters. Observations were taken in the filters F606W and F814W for Cl1358+62, and in F702W and F814W for MS2053–04. These data were processed in the usual way for cosmic rays and removal of the sky background. The field for Cl1358+62 was very large, $\sim 8' \times 8'$. For MS2053-04, only 1 central pointing was available. As a result we have more Fundamental Plane measurements for Cl1358+62.

We determined the photometric parameters in two different ways, following the procedures used by vDF. We first used Point-Spread Function images to fit convolved $r^{1/4}$-law profiles to the galaxy images. In addition, we deconvolved the images with the CLEAN procedure (Högbom 1974), and derived growth curves for the galaxies. The results from both methods were compared to estimate the errors. It is worth noting that the median differences in r_e and μ_e were +7.4% and –9.7%, but the combined parameter $r_e I_e^{0.82}$ only differed by –1.2% for Cl1358+62 and –1.4% for MS2053–04. This is the combination of parameters that enters the Fundamental Plane, and as a result, our subsequent analysis is insensitive to the individual errors in r_e and I_e.[1] Because the Coma data were derived from growth curves, we proceeded to use the growth curve results in the following analysis. After calibration using Holtzman *et al.* (1995), the photometry was transformed to the redshifted V-band, for direct comparison to the Coma photometry. This is possible, because we have observations in multiple passbands close to the redshifted V-band. Colors were measured within an aperture of $r < 3r_e$, and Galactic extinctions were derived from Burstein and Heiles (1982) and Cardelli, Clayton & Mathis (1989).

3.2.3 Errors

Errors have been determined directly from the spectroscopic, structural and photometric fits, as well as the photometric transformations. The random errors are listed in Table 1, and the typical random error bars are shown in Figure 3.2 (as thin error bars). We have considered possible sources of systematic errors and we have estimated their contribution (shown as thick error bars in Figure 3.2). We have several sources of systematic errors: (i) photometric transformations at ± 0.05 mag, which is dominated by the uncertainties in the absolute zeropoint of the F814W passband; (ii) velocity dispersions, where our procedures may have relative

[1] The same applies for previous measurements at intermediate and low redshift (Jørgensen, Franx & Kjærgaard 1995a).

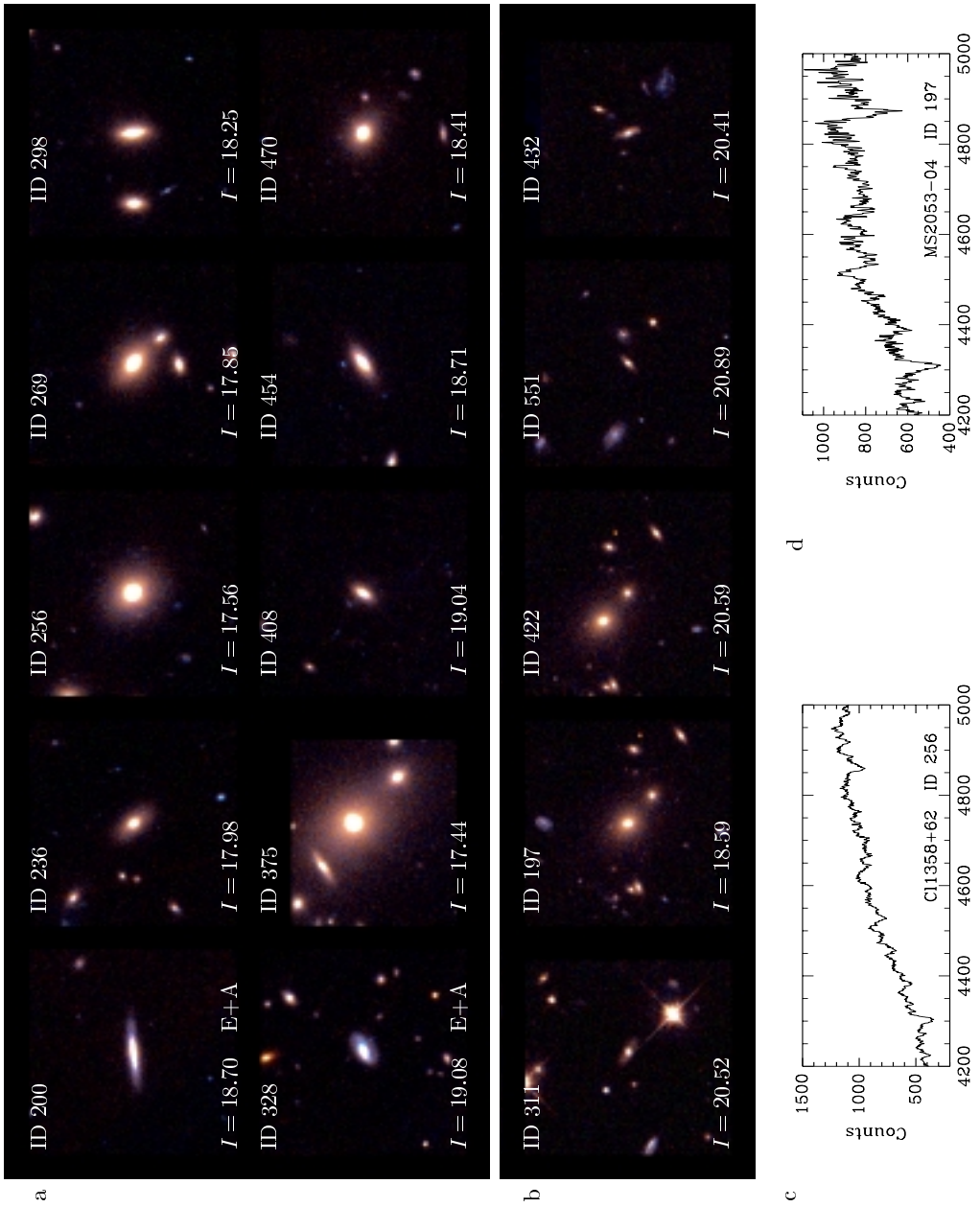

Figure 3.1: (a) Montage of color images for the sample galaxies in Cl1358+62, using F606W and F814W; and in (b) MS2053–04 using F702W and F814W; (c) Spectrum of galaxy #256 in Cl1358+62; and (d) #197 in MS2053–04.

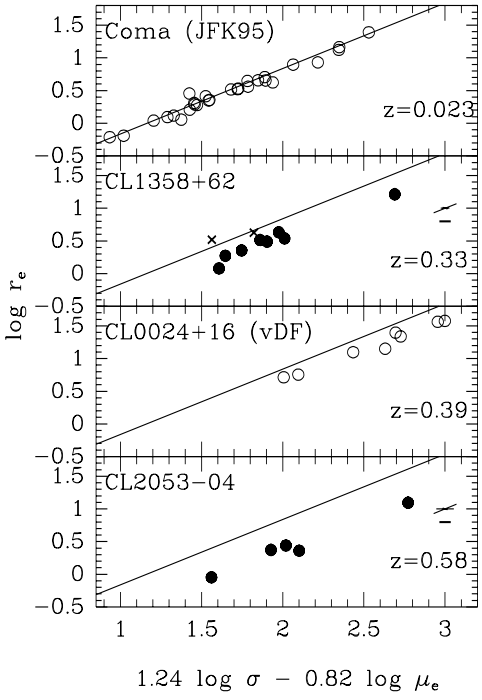

Figure 3.2: The FP for the four clusters with the mean FP for Coma (JFK96) plotted on each panel. Note that the two E+As in Cl1358+62, shown as "x"s, lie to the left of the mean relation of the "old" Cl1358+62 early-type galaxies. The previous results of JFK96 and vDF are shown as open circles. The new data are shown as filled circles. Typical random (thin) and systematic (thick) errors are shown.

errors of $\pm$3% with respect to similar measurements at low redshift (the absolute velocity dispersions may be in error systematically by up to $\pm$5-7%); (iii) structural parameters (r_e and μ_e), where deviations from an $r^{1/4}$-law model could cause systematic errors on the level of $\pm$1% in the combined parameter $r_e {\mu_e}^{0.82}$.

Another source of uncertainty is due to departures from homology (see, *e.g.*, Capelato *et al.* 1995, Ciotti *et al.* 1996). Non-homology can affect our measurement of evolution through the aperture correction for the velocity dispersions. Jørgensen *et al.* (1995b) determined the aperture corrections empirically, by using long slit data on nearby galaxies. They found no strong effect out to an effective radius. Therefore, these aperture corrections are likely to be appropriate for most of our galaxies. However, for the smallest galaxies, this correction is more uncertain and may require future observations of velocity dispersion profiles to large radii in a broad sample of nearby galaxies (*e.g.*, Corollo *et al.* 1995).

3.3 The Fundamental Plane in Cl1358+62 and MS2053–04

The Fundamental Plane for the clusters are shown in Figure 3.2 along with the FPs for Cl0024+16 (vDF) and Coma (JFK96). We use the coefficients for the FP determined by JFK96 from a large sample of 225 early-type galaxies in ten nearby clusters. The figure shows clearly that a well defined Fundamental Plane exists, *despite the fact that the galaxies in the intermediate redshift clusters were chosen without morphological information*. Furthermore, the sample is large enough to derive the scatter about the Coma Fundamental Plane. We find surprisingly low *rms* scatters in $\log r_e$ of $\pm$0.064, $\pm$0.065, $\pm$0.060, and $\pm$0.072 for Coma, Cl1358+62, Cl0024+16, and MS2053–04, respectively. The galaxies also show a large offset from the Coma relation, due mainly to cosmological surface brightness dimming.

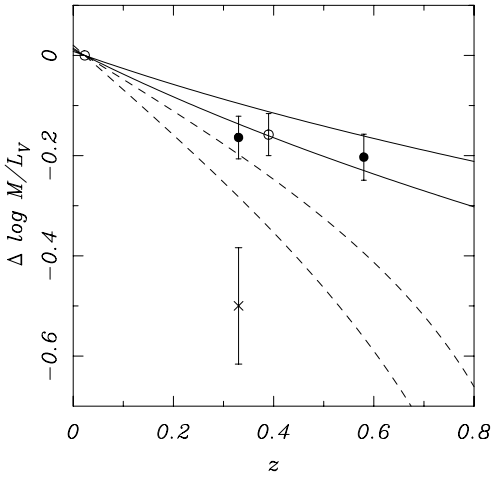

Figure 3.3: The mean M/L_V offsets with redshift, for $q_0 = 0.05$. The area enclosed by solid lines corresponds to single burst models with $z_f = \infty$ and a range of IMFs. The region marked by dash lines corresponds to the equivalent $z_f = 1$ models. The previous results of JFK96 and vDF are shown as open circles. The new data are shown as filled circles. The "x" marks the M/L_V offset derived from the two E+A galaxies in Cl1358+62. The errors were estimated by adding the random and systematic errors in quadrature.

One interesting question is whether the coefficients of the FP are the same in higher redshift clusters, *i.e.*, are the luminous and less luminous galaxies evolving at the same rate? However, the current sample is too small to provide a definitive answer. The weak indication that the slope is flatter when the distant galaxies are taken together needs to be verified with larger samples before any conclusions should be made (see also vDF).

We determined the mean M/L_V ratio for each cluster directly from the Fundamental Plane zeropoint, adopting the slopes of the Fundamental Plane of JFK96 and $q_0 = 0.05$. The resulting evolution of M/L_V ratio is shown in Figure 3.3. The errors are taken from §2.3 and have been added in quadrature. Weighting the individual galaxies by their random errors does not change the results significantly.

Clearly, the M/L_V ratio is lower at higher redshift, consistent with evolution of the stellar populations. We have drawn simple, single-burst model predictions in the same plot, adopting formation redshifts z_{form} of infinity, and $z_{form} = 1$. The current data are not consistent with the predictions for co-eval populations which have formed recently. More data are needed to test whether more complex models with recent star formation can be accommodated (see, e.g., Franx and van Dokkum 1996 and Poggianti & Barbaro 1996).

3.4 Discussion

We have measured structural parameters and central velocity dispersions for galaxies in two clusters at intermediate redshift, Cl1358+62 at $z = 0.33$ and MS2053–04 at $z = 0.58$. The Fundamental Plane relations in the intermediate redshift clusters are very similar to that found in Coma. This observation demonstrates that mature early-type galaxies existed in these clusters at $z \approx 0.6$; their primary epochs of star formation must have occurred at much higher redshifts.

The sample is also large enough to measure the scatter in the Fundamental Plane relation reliably. We find it to be low: ± 0.067 in $\log r_e$, or $\pm 17\%$ in M/L_V. This suggests that the populations are very homogeneous, and that the age differences between the galaxies are not very large (Ciotti, Lanzoni, & Renzini 1996).

The mean M/L_V ratio of the galaxies was clearly lower several Gyr ago, consistent with passively evolving stellar populations. This evolution depends on the formation redshift(s)

of the population, the IMF(s), and cosmological model (*e.g.*, Franx 1995). We show model predictions for formation redshifts of $z = 1$ and $z = \infty$ in Figure 3.3 (Tinsley & Gunn 1976) using $q_0 = 0.05$. The new data are fully consistent with a high formation redshift, $z_{form} > 2$, strengthening the conclusion of vDF. This result is a lower limit; the constraints are even stronger if $q_0 = 0.5$.

This interpretation, however, is complicated by the fact that mergers, interactions, star bursts, and other processes may continue to transform late-type galaxies into early-type galaxies: the early-type galaxies we observe at high redshift may only be a subset of the early-type galaxies we observe at low redshift. In this case, the early-type galaxies observed at high redshift (if they remained undisturbed until the present) should be compared to the oldest early-type galaxies locally. In some sense, these high redshift early-type galaxies have been compared to a *mean* low redshift counterpart, probably not as old as the comparison requires. Thus, the formation redshift estimated from the M/L evolution can be biased upwards (see, *e.g.*, Franx and van Dokkum 1996).

We included two Cl1358+62 "E+A" galaxies in our sample to test whether these galaxies are progenitors of early-type galaxies in low redshift clusters.[2] They are shown in Figure 3.2 by the "x" symbols. We can use the Coma Fundamental Plane to measure the M/L_V ratios of these "E+A" galaxies, assuming that their structural properties are similar to nearby early-type systems. This assumption may not necessarily be correct, as the Franx (1993) analysis of an E+A in Abell 665 ($z = 0.18$) shows that it is essentially bulgeless; it is not clear whether it will become an S0 or remain a spiral system.

With this caveat in mind, we show the mean M/L_V offset for the two E+A galaxies in Figure 3.3 as an "x." This M/L_V is consistent with a "formation" redshift of $z_f \approx 0.5$, a V-band luminosity weighted mean of the formation redshifts of the subcomponents. This is consistent with the hypothesis that the E+As have undergone a burst of star formation 1-2 Gyr before they have been observed (Dressler and Gunn 1983). We conclude that a fraction of nearby cluster early-type galaxies has undergone secondary bursts of star formation at $z < 1$.

At this point, more work is needed to assess the relevance of the E+A galaxies to the evolution of early-type galaxies and we will study the E+As in these clusters in greater detail elsewhere. Observations of higher redshift clusters will be needed to test whether star formation and star bursts were even more prevalent at earlier times, as suggested by Lubin (1996) and Rakos & Schombert (1995). Our sample can also be compared to surveys of nearby field galaxies, in which the data of González (1993) and Faber *et al.* (1995) suggest that a large age spread ($\sim$ 2-18 Gyr) exists. Thus, a large fraction of these experienced bursts of star formation at $z < 1$. Our data suggest that it might be hard, but not impossible, to model the evolutionary history of the cluster galaxies in the same way as the field galaxies.

Acknowledgements

We appreciate the effort of all those in the HST program that made this unique Observatory work as well as it does. The assistance of those at STScI who helped with the acquisition of the HST data is gratefully acknowledged. We also appreciate the effort of those at the Keck, MMT and KPNO telescopes who developed and supported the facility and the instruments that made this program possible. Support from STScI grants GO05989.01-94A, GO05991.01-94A, and AR05798.01-94A is gratefully acknowledged.

[2]These galaxies have spectra which can be interpreted as a superposition of an old population (the "E" for early type), and a young population with the spectrum of an A star (Dressler and Gunn 1983).

TABLE 1
FUNDAMENTAL PLANE PARAMETERS

ID	I	$R-I$	σ	r_e	$\mu_{e,V}$
	(mag)	(mag)	km s^{-1}	(arcsec)	mag arcsec^{-2}
(1)	(2)	(3)	(4)	(5)	(6)
200	18.70	0.68	135 ± 11	0.913	22.50
236	17.98	0.80	166 ± 11	0.541	21.93
256	17.56	0.78	273 ± 7	1.024	21.81
269	17.85	0.82	342 ± 10	0.826	21.55
298	18.25	0.82	280 ± 8	0.448	20.77
328	19.08	0.60	98 ± 7	0.712	22.24
375	17.44	0.81	301 ± 11	3.910	23.83
408	19.04	0.77	265 ± 17	0.287	20.74
454	18.71	0.73	171 ± 6	0.780	22.23
470	18.41	0.79	185 ± 6	0.738	22.23
311	20.52	1.12	223 ± 25	0.402	22.53
197	18.59	1.20	319 ± 18	2.182	23.99
422	20.59	1.20	158 ± 22	0.413	22.57
551	20.89	1.14	217 ± 19	0.157	20.93
432	20.41	1.08	161 ± 20	0.483	22.82

Notes:
(1) Galaxy identification;
(2) Integrated I magnitude (± 0.1 mag);
(3) $R-I$ color within a $3r_e$ aperture (± 0.05 mag);
(4) Velocity dispersion with formal (random) errors;
(5) Effective radius r_e from CLEAN/growth curve fit of $r^{1/4}$-law to HST images;
(6) Surface brightness in rest frame V-band from that fit at r_e

References

Broadhurst T. J., Ellis R. S., & Shanks T. 1988, MNRAS, 235, 827
Burstein D., & Heiles C. 1982, AJ, 87, 1165
Butcher H., & Oemler A. 1978, ApJ, 219, 18
Butcher H., & Oemler A. 1984, ApJ, 285, 426
Capelato, H. V., de Carvalho, R. R., & Carlberg, R. G. 1995, ApJ, 451, 525
Cardelli, J. A., Clayton, G. C., & Mathis, J. S. 1989, ApJ, 345, 245
Ciotti, L., Lanzoni, B., & Renzini, A. 1996, MNRAS, 282, 1
Corollo, C. M., de Zeeuw, P. T., van der Marel, R. P., Danziger, I. J., & Qian, E. E. 1995, ApJ, 441, L25
Couch W. J., & Sharples R. M. 1987, MNRAS, 229, 423
Djorgovski S., & Davis M. 1987, ApJ, 313, 59
Dressler A., & Gunn J. E. 1983, ApJ, 270, 7
Dressler A., Lynden-Bell D., Burstein D., Davies R. L., Faber S. M., Terlevich R. J., & Wegner G. 1987, ApJ, 313, 42
Faber S. M., Dressler A., Davies R. L., Burstein D., Lynden-Bell D., Terlevich R., & Wegner G. 1987, Faber S. M., ed., Nearly Normal Galaxies. Springer, New York, p. 175
Faber, S. M., Trager, S. C., González J. J., & Worthey, G. 1995, IAU Symp. 164, Stellar Populations (Dordrecht: Kluwer), 255
Franx M. 1993, PASP, 105, 1058
Franx M. 1995 IAU Symp. 164, Stellar Populations (Dordrecht: Kluwer), 269
Franx M., & van Dokkum, P. G. 1996, *New Light on Galaxy Evolution*, eds. Bender, R., & Davies, R. L., p. 233
González, J. J. 1993, Ph.D. Thesis, Univ. California, Santa Cruz
Högbom J. A. 1974, A&AS, 15,417

Holtzman, J. A., Burrows, C. J., Casertano, S., Hester, J. J., Trauger, J. T., Watson, A. M., & Worthey, G. 1995, PASP, 107, 1065
Jørgensen I., Franx M., & Kjærgaard P. 1993, ApJ, 411, 34
Jørgensen I., Franx M., & Kjærgaard P. 1995a, MNRAS, 273, 1097
Jørgensen I., Franx M., & Kjærgaard P. 1995b, MNRAS, 276, 1341
Jørgensen I., Franx M., & Kjærgaard P. 1996, MNRAS, 280, 167 [JFK96]
Kron, R. 1980, APJS, 43, 305
Le Févre, O., *et al.* 1995, ApJ, 461, 534
Lilly S. J., Tresse L., Hammer F., Crampton D., & Le Fèvre O. 1995, ApJ, 455, 50
Lubin, L. 1996, AJ, 112, 23
Poggianti, B. M., & Barbaro, G. 1996, AA, 314, 379
Rakos, K. D., & Schombert, J. M. 1995, ApJ, 439, 47
Tinsley, B. M., & Gunn, J. E. 1976, ApJ, 203, 52
van Dokkum, P. G., & Franx M. 1996, MNRAS, 281, 985 [vDF] **[Chapter 2]**
Vogt, N. P., Forbes, D. A., Phillips, A. C., Gronwall, C., Faber, S. M., Illingworth, G. D., & Koo, D. C. 1996, ApJ, 465, L15

4 Luminosity Evolution of Early-Type Galaxies to $z = 0.83$: Constraints on Formation Epoch and Ω[†]

ABSTRACT

We present deep spectroscopy with the Keck telescope of eight galaxies in the luminous X-ray cluster MS 1054–03 at $z = 0.83$. The data are combined with imaging observations from the *Hubble Space Telescope* (HST). The spectroscopic data are used to measure the internal kinematics of the galaxies, and the HST data to measure their structural parameters. Six galaxies have early-type spectra, and two have "E+A" spectra. The galaxies with early-type spectra define a tight Fundamental Plane (FP) relation. The evolution of the mass-to-light ratio is derived from the FP. The M/L ratio evolves as $\Delta \log M/L_B \propto -0.40z$ ($\Omega_m = 0.3$, $\Omega_\Lambda = 0$). The observed evolution of the M/L ratio provides a combined constraint on the formation redshift of the stars, the IMF, and cosmological parameters. For a Salpeter IMF ($x = 2.35$) we find that $z_{form} > 2.8$ and $\Omega_m < 0.86$ with 95 % confidence. The constraint on the formation redshift is weaker if $\Omega_\Lambda > 0$: $z_{form} > 1.7$ if $\Omega_m = 0.3$ and $\Omega_\Lambda = 0.7$. At present the limiting factor in constraining z_{form} and Ω from the observed luminosity evolution of early-type galaxies is the poor understanding of the IMF. We find that if $\Omega_m = 1$ the IMF must be significantly steeper than the Salpeter IMF ($x > 2.6$).

[†]Pieter G. van Dokkum, Marijn Franx, Daniel D. Kelson, and Garth D. Illingworth, *Astrophysical Journal Letters*, **504**, L17 (1998)

4.1 Introduction

Measurements of the masses and mass-to-light (M/L) ratios of early-type galaxies in distant clusters provide important constraints on galaxy evolution. The luminosity evolution of early-type galaxies can be determined by comparing the luminosities of galaxies of similar masses at different redshifts. Also, mass measurements can be used to constrain the merger rate.

The evolution of the M/L ratio can be measured from the evolution of the fundamental plane of early-type galaxies. The fundamental plane (FP) is a tight correlation between the structural parameters and the velocity dispersion of the form $r_e \propto I_e^{-0.83}\sigma^{1.20}$ in the B band (Djorgovski & Davis 1987; Dressler et al. 1987; Jørgensen, Franx & Kjærgaard 1996 [JFK]). Assuming homology, the existence of the FP implies that $M/L \propto M^{0.25}r_e^{-0.04}$, with low scatter (Faber et al. 1987). Therefore, the evolution of the intercept of the FP is proportional to the evolution of the mean M/L ratio (see Franx 1993a).

Studies of the FP out to $z \approx 0.6$ have shown that the M/L ratio of massive cluster galaxies evolves slowly (van Dokkum & Franx 1996 [vDF]; Kelson et al. 1997 [KvDFIF]; Bender et al. 1998; Pahre 1998). The implication is that the stars in massive cluster galaxies were probably formed at much higher redshifts. These results are consistent with other studies of the evolution of the luminosities, colors, and absorption line strengths of bright cluster galaxies (e.g., Aragon-Salamanca et al. 1993, Bender, Ziegler, & Bruzual 1996, Schade, Barrientos, & Lopez-Cruz 1997, Ellis et al. 1997, Stanford, Eisenhardt, & Dickinson 1998).

The constraints on the formation epoch of massive galaxies can be made stronger by extending the studies of the evolution of the M/L ratio to higher redshifts. In this *Letter*, we report on spectroscopic and photometric observations of eight bright galaxies in the luminous X-ray cluster MS 1054–03 at $z = 0.83$. The fundamental plane is derived, and the evolution of the M/L ratio is established out to $z = 0.83$, when the universe was 50 % of its present age ($q_0 = 0.15$).

4.2 Spectroscopy

Galaxies in MS 1054–03 were selected on the basis of their I band flux ($I < 22.1$), and their location in the $B-R$ versus $R-I$ plane. The allowed range in color was broad, thus minimizing any bias against passively-evolving blue cluster galaxies. There was no selection on morphology. The ground based imaging data used for the selection were kindly provided by G. Luppino, and are described in Luppino & Kaiser (1997).

The cluster was observed on February 11, 1997 with LRIS (Oke et al. 1995) on the 10 m W. M. Keck telescope. The multi-aperture slitlets were 1.″0 wide, and the seeing was 0.″9 – 1.″0. The instrumental resolution $\sigma_{\rm instr} \approx 50$ km s^{-1}. The total exposure time was 14 400 s. A bright blue star was included in the masks for the purpose of correcting for the H_2O absorption at 7600 Å from our atmosphere. The reduction procedures were very similar to those described by vDF and KvDFIF. Eight of the observed galaxies are covered by a deep HST image of the cluster core. In this *Letter*, we will limit the discussion to these galaxies.

The spectra of the galaxies are shown in Fig. 4.1. Two of the eight galaxies (1430 and 1583) have strong Balmer absorption lines (EW$>$ 4 Å in the rest frame), indicating the presence of a young stellar component. Subsequent low resolution spectroscopy covering a larger wavelength range showed that both galaxies have O II 3727 EW$<$ 5 Å, and hence are classified "E+A" galaxies (Dressler & Gunn 1983).

We determined the central velocity dispersions of the galaxies from a fit to a convolved template star in real space, following the procedures outlined in vDF and KvDFIF. The spectral regions that are dominated by bright sky lines were given low weight in the fit. The

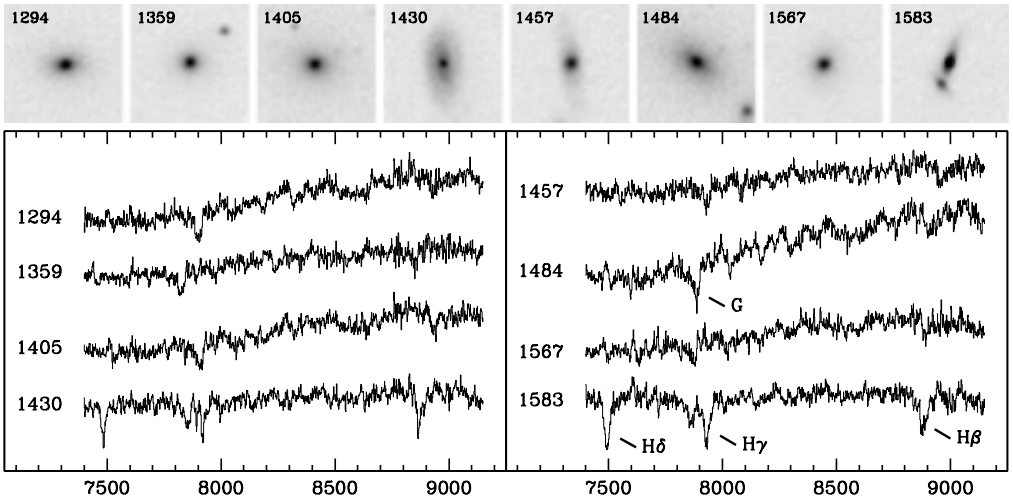

Figure 4.1: HST images and Keck spectra of the galaxies in MS 1054–03 with measured dispersions. The most prominent spectral feature in most galaxies is the 4300 Å G band observed at $\approx$ 7870 Å. Galaxies 1430 and 1583 have strong Balmer absorption lines, and are "E+A" galaxies. Galaxy 1484 is the brightest cluster galaxy.

Balmer lines in the E+A galaxies were masked. The resulting dispersions, corrected to an aperture of 3.″4 at the distance of Coma (cf. vDF), are listed in Table 1. We experimented with the choice of template star, the continuum filtering, and the fitting method (e.g., fitting in Fourier space rather than real space) to assess the systematic uncertainties, and estimate them to be $\sim 5\,\%$.

There are several galaxies with dispersions in the range 250 – 300 km s^{-1}, showing that massive galaxies exist at $z = 0.83$. The dispersions of the two E+A galaxies are 153 ± 12 km s^{-1} and 212 ± 25 km s^{-1}. These values are significantly higher than the typical dispersions of E+A galaxies at lower redshift (~ 100 km s^{-1}; Franx 1993b, KvDFIF).

4.3 Photometry

Hubble Space Telescope (HST) WFPC2 imaging data of the central parts of MS 1054–03 were taken by Donahue et al. (1998) on March 13, 1996 through the *F*814*W* filter. The total exposure time was 15 600 s. Following the usual reduction process the images were deconvolved with the CLEAN algorithm (Høgbom 1974), using Tiny Tim (Krist 1995) PSFs appropriate for the positions of the galaxies on the WFPC2 chips. The six galaxies with early-type spectra appear to be unperturbed E and S0 galaxies (Fig. 4.1). The two E+A galaxies have more peculiar morphologies. Galaxy 1430 has a disk with faint spiral structure, and is lopsided. Galaxy 1583 also has a disk, and a very luminous, compact bulge. It may be interacting with the small companion galaxy to the South.

We determined effective radii and effective surface brightnesses of the galaxies using the 2D fitting method outlined in vDF. The values of r_e (in arcseconds) and $\mu_{e,F814W}$ are listed in Table 1. As noted by many authors (e.g., JFK), the errors in r_e and I_e are correlated, and the correlation is almost parallel to the Fundamental Plane. Therefore, the product $r_e I_e^{0.83}$, which enters the FP, can be determined to high accuracy.

4.4 The Fundamental Plane and Evolution of the M/L Ratio

The edge-on projection of the fundamental plane in MS 1054–03 is shown in Fig. 4.2. The surface brightnesses ($I_e \equiv 10^{-0.4\,\mu_e}$) have been corrected for the $(1+z)^4$ cosmological dimming. The effective radii were converted using $q_0 = 0.15$ and $H_0 = 50\,\mathrm{km\ s^{-1}\,Mpc^{-1}}$. The open symbols are the two E+A galaxies. The small dots are galaxies in Coma at $z = 0.023$, taken from JFK. The line is the fit from JFK. The six galaxies with early-type spectra define a clear FP, with low scatter (~ 0.045 in $\log r_e$). The slope is similar to that of the Coma cluster. A larger sample is needed to determine the scatter and the slope reliably. The offset of the FP of MS 1054–03 with respect to the FP of Coma is due to the evolution of the M/L ratio between $z = 0.83$ and the present.

The E+A galaxies are over-luminous with respect to the prediction from the FP defined by the other galaxies in MS 1054–03, consistent with the presence of a young population. The E+As have lower masses than the other galaxies in the sample. In the following analysis, we will only consider the galaxies with early-type spectra. Therefore, our conclusions may only apply to a subset of the galaxy population. We will return to this point in Sect. 4.5.

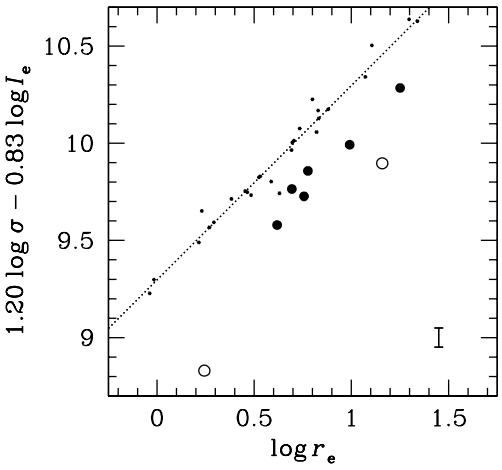

Figure 4.2: Edge-on projection of the fundamental plane in MS 1054–03 at $z = 0.83$. The open symbols are two E+A galaxies. The errorbar indicates the typical uncertainty. The small dots are galaxies in Coma at $z = 0.023$, from JFK. The line shows the fit from JFK. The fundamental plane for the six galaxies with early-type spectra is very similar to the FP of Coma. The offset with respect to the FP of Coma is due to luminosity evolution of the galaxies.

We determined the evolution of the M/L ratio from the FP. In Fig. 4.3, the evolution of the M/L ratio from $z = 0.02$ to $z = 0.83$ is plotted. Included in the Figure are data for Coma at $z = 0.02$ from JFK, for CL 0024+16 at $z = 0.39$ from vDF, and for CL 1358+62 at $z = 0.33$ and MS 2053+03 at $z = 0.58$ from KvDFIF. All data were transformed to a common rest frame band, equivalent to the $F814W$ band in the observed frame at $z = 0.83$. This band is very close to the B band redshifted to $z = 0.83$, and is denoted B'_z. For MS 1054–03 at $z = 0.83$, $B'_z \equiv F814W + 2.5\log(1+z)$. The transformations for the other clusters were derived in a similar way as is described in vDF. For all clusters, the observed bands are close to the redshifted B band, and the color terms in the transformations are small. Since the observed colors of the galaxies are used in the transformations, the procedure is very different from a K-correction, and is independent of the spectral types of the galaxies. Using spectral energy distributions from Pence (1976), we estimate the error induced by the transformations is $\lesssim 0.03$ magnitudes for all spectral types. Because the scatter in the FP is very small, the errorbars in Fig. 4.3 are mainly due to systematic errors. We have assumed that the systematic errors in the dispersions, in the photometric zeropoints, and the errors caused by the sample selection (see vDF) can be added in quadrature. The M/L ratio evolves as

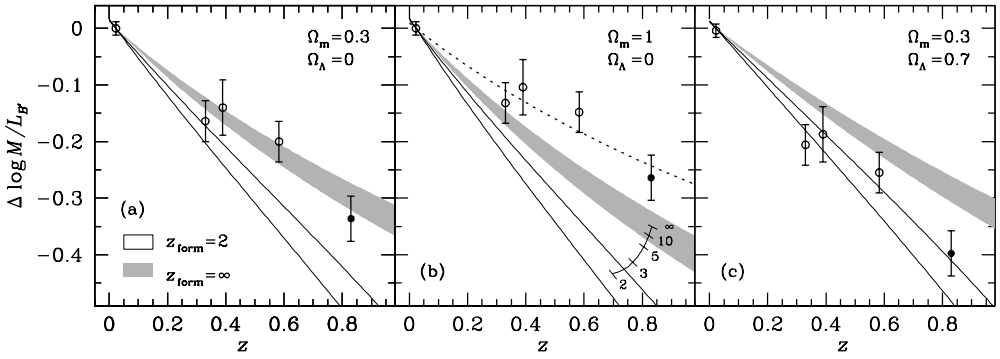

Figure 4.3: Evolution of the M/L ratio with redshift, for $q_0 = 0.15$ (a), $q_0 = 0.5$ (b), and for a non-zero cosmological constant (c). The open symbols are Coma at $z = 0.02$ (JFK), CL 1358+62 at $z = 0.33$ (KvDFIF), CL 0024+16 at $z = 0.39$ (vDF), and MS 2053+03 at $z = 0.58$ (KvDFIF). The solid symbol is MS 1054–03 at $z = 0.83$ (this paper). Model predictions for different formation redshifts of the stars are shown, assuming a Salpeter IMF ($x = 2.35$) and a range of metallicities. The data favor high formation redshifts and a low value of q_0. The broken line in (b) indicates a model with $z_{\rm form} = \infty$ and a steep IMF ($x = 3.35$). The conclusions are very sensitive to the IMF.

$\Delta \log M/L_B \propto (-0.40 \pm 0.04)z$ if $\Omega_{\rm m} = 0.3$, or $\Delta \log M/L_B \propto (-0.31 \pm 0.04)z$ if $\Omega_{\rm m} = 1$. This is consistent with other measurements of the luminosity evolution of early-type galaxies to $z \approx 0.8$ (e.g., Schade et al. 1997). However, our measurement has a much smaller uncertainty, due to the low scatter in the FP.

4.5 Discussion

The observed evolution of the M/L ratio with redshift can be compared to predictions for the evolution of single age stellar populations formed at redshift $z_{\rm form}$. The luminosity evolution of a single age stellar population behaves as a power law: $L \propto (t - t_{\rm form})^{\kappa}$. The evolution depends on κ, the cosmology, and $z_{\rm form}$ (vDF). The value of κ depends on the passband, the IMF, and the metallicity. The models of Bruzual & Charlot (1999), Vazdekis et al. (1996) and Worthey (1999) give $0.86 < \kappa_B < 1.00$ for a Salpeter (1955) IMF ($x = 2.35$) and $-0.5 <$ [Fe/H] < 0.5. Model predictions are shown in Fig. 4.3(a) for $z_{\rm form} = 2$ (open area) and $z_{\rm form} = \infty$ (shaded area), for a universe with $\Omega_{\rm m} = 0.3$ and no cosmological constant ($q_0 = 0.15$). Note that the models as well as the data points in Fig. 4.3 are independent of the value of H_0. The formal 95 % confidence lower limit on the formation redshift is $z_{\rm form} > 2.8$, for solar metallicity, a Salpeter IMF and $q_0 = 0.15$.

The slow evolution of massive galaxies in clusters not only provides a constraint on their formation redshift, but also on cosmological models (e.g., Bender et al. 1998). This is illustrated in Fig. 4.3(b), which shows the same models as in Fig. 4.3(a) for $\Omega_{\rm m} = 1$ ($q_0 = 0.5$) rather than $\Omega_{\rm m} = 0.3$. The models fail to fit the data in this cosmology, and we find $\Omega_{\rm m} < 0.86$ (95 % confidence). The constraint on $\Omega_{\rm m}$ is considerably stronger than the constraint derived by Bender et al. (1998) from the combination of the $\mathrm{Mg}_b - \sigma$ relation and the fundamental plane at $z = 0.375$, due to the higher redshift of MS 1054–03.

These results are based on the assumption that massive early-type galaxies in clusters have a Salpeter IMF. There is considerable uncertainty in the slope and form of the IMF in the mass range around $\sim 1 M_\odot$ (Scalo 1997), and there are only indirect constraints on the

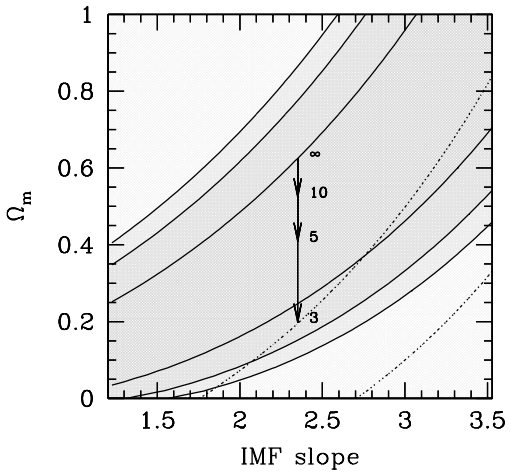

Figure 4.4: Combined constraint on the slope of the IMF of massive early-type galaxies and Ω_m, for $\Omega_\Lambda = 0$, solar metallicity and $z_{form} = \infty$. The solid contours represent confidence limits of 66 %, 90 % and 95 %. The arrow shows the effect of changing z_{form} to lower values. The 66 % confidence limits for $z_{form} = 3$ are indicated with broken lines.

IMF of massive ellipticals in clusters (e.g., Gibson & Matteucci 1997). The value of κ, and hence the rate of evolution, is quite sensitive to the logarithmic slope of the IMF: the Worthey (1999) models give $\Delta\kappa_B = -0.22\Delta x$.

Since the IMF is very uncertain, we express our results as a combined constraint on Ω_m and the slope of the IMF in Fig. 4.4. The IMF is steep if $\Omega_m = 1$. The 95 % confidence lower limit on the slope is $x > 2.6$ for $\Omega_m = 1$. As an illustration, the broken line in Fig. 4.3(b) indicates a model with $\Omega_m = 1$, $z_{form} = \infty$ and $x = 3.35$. This model fits the data very well. The case $z_{form} = \infty$ is extreme; the dependence on the formation redshift of the constraints on Ω_m and x is indicated with an arrow in Fig. 4.4. For lower formation redshifts (or higher metallicities) the constraints are stronger. As an example, for $z_{form} = 5$ rather than ∞ we find that $\Omega_m < 0.60$ for $x = 2.35$, and $x > 3.0$ for $\Omega_m = 1$.

We note that if $\Omega_\Lambda > 0$, as is indicated by distant supernovae (Riess et al. 1998), the constraints on z_{form} and the slope of the IMF are much weaker. Figure 4.3(c) shows the evolution of the M/L ratio if $\Omega_m = 0.3$ and $\Omega_\Lambda = 0.7$. The lower limit on the formation redshift is $z_{form} > 1.7$. In this cosmology, the data provide no meaningful constraint on the slope of the IMF.

The implicit assumption in this type of study that the set of high redshift early-types is similar to the set of low redshift early-types (e.g., Kauffmann 1995, van Dokkum & Franx 1996) is probably justified for the high mass galaxies considered here. It seems unlikely that a significant fraction of the high mass galaxies in clusters at $z = 0$ was added to the sample between $z = 0.83$ and $z = 0$, given the tightness of the color-magnitude relation of luminous galaxies in intermediate z clusters (e.g., Ellis et al. 1997, van Dokkum et al. 1998), and the low masses of the E+A galaxies (Franx 1993b, KvDFIF). However, our conclusions may not hold for low mass galaxies: there is good evidence that a significant fraction of the low luminosity early-type galaxies at $z = 0$ was accreted from the field at $z < 1$ (e.g., Abraham et al. 1996, van Dokkum et al. 1998). The two E+A galaxies in our sample may be galaxies that were recently accreted. Larger samples to fainter magnitudes are needed to assess the fraction of galaxies with young populations in $z \approx 0.8$ clusters, and their masses.

In conclusion, the luminosity evolution of massive early-type galaxies to $z \approx 0.8$ has now been determined to sufficient accuracy to place strong constraints on the epoch of formation of the galaxies, and on cosmological models. The main uncertainty in the interpretation is the poor understanding of the IMF in the mass range around one solar mass. Other applications of the FP suffer from the same uncertainty (e.g., Bender et al. 1998). Nevertheless, our current

measurement can be used directly to correct the evolution of the luminosity function for the brightening of the stellar populations with redshift. This can provide direct constraints on the mass evolution of galaxies.

Acknowledgements

We thank M. Donahue for providing us with the HST image of MS 1054–03, and G. Luppino for the ground based images. The University of Groningen and the Leids Kerkhoven-Bosscha Fonds are thanked for support. Support from STScI grants GO07372.01-96A, GO05991.01-94A, and AR05798.01-94A is gratefully acknowledged.

TABLE 1
GALAXY PARAMETERS

ID	σ	$\log r_e$	μ_e	spectral type
1294	316 ± 21	–0.200	22.62	early-type
1359	225 ± 19	–0.359	22.33	early-type
1405	259 ± 21	0.015	23.34	early-type
1430	153 ± 12	0.183	23.88	E+A
1457	210 ± 24	–0.220	22.88	early-type
1484	330 ± 20	0.274	23.84	early-type
1567	261 ± 27	–0.283	22.65	early-type
1583	212 ± 25	–0.733	20.16	E+A

References

Abraham, R. G., Smecker-Hane, T. A., Hutchings, J. B., Carlberg, R. G., Yee, H. K. C., Ellingson, E., Morris, S., Oke, J. B., & Rigler, M. 1996, ApJ, 471, 694
Aragon-Salamanca, A., Ellis, R. S., Couch, W. J., & Carter, D. 1993, MNRAS, 262, 764
Bender, R., Saglia, R. P., Ziegler, B., Belloni, P., Greggio, L., Hopp, U., & Bruzual, G. 1998, ApJ, 493, 529
Bender, R., Ziegler, B., & Bruzual, G. 1996, ApJ, 463, L51
Bruzual, G., & Charlot, S. 1999, in preparation
Djorgovski, S., & Davis, M. 1987, ApJ, 313, 59
Donahue, M., Voit, G. M., Gioia, I. M., Luppino, G., Hughes, J. P., & Stocke, J. T. 1998, ApJ, 502, 550
Dressler, A., & Gunn, J. E. 1983, ApJ, 270, 7
Dressler, A., Lynden-Bell, D., Burstein, D., Davies, R. L., Faber, S. M., Terlevich, R. J., & Wegner, G. 1987, ApJ, 313, 42
Ellis, R. S., Smail, I., Dressler, A., Couch, W. J., Oemler, A., Jr., Butcher, H., & Sharples, R. M. 1997, ApJ, 483, 582
Faber, S. M., Dressler, A., Davies, R. L., Burstein, D., Lynden-Bell, D., Terlevich, R., Wegner, G. 1987, Faber, S. M., ed., Nearly Normal Galaxies. Springer, New York, p. 175
Franx, M. 1993a, PASP, 105, 1058
Franx, M., 1993b, ApJ, 407, L5
Gibson, B. K., & Matteucci, F. 1997, MNRAS, 291, L8
Jørgensen, I., Franx, M., & Kjærgaard, P. 1996, MNRAS, 280, 167
Kauffmann, G. 1995, MNRAS, 274, 153
Kelson, D. D., van Dokkum, P. G., Franx, M., Illingworth, G. D., & Fabricant, D. 1997, ApJ, 478, L13 **[Chapter 3]**
Krist, J. 1995, in Astronomical Data Analysis Software and Systems IV, ASP Conference Series, 77, R. A. Shaw, H. E. Payne, and J. J. E. Hayes, eds., p. 349
Luppino, G. A., & Kaiser, N. 1997, ApJ, 475, 20
Oke, J. B., et al. 1995, PASP, 107, 375
Pahre, M. 1998, Phd thesis, California Institute of Technology
Pence, W. 1976, ApJ, 203, 39
Riess, A. G., et al. 1998, AJ, 116, 1009

Salpeter, E. 1955, ApJ, 121, 161
Scalo, J. 1997, in The Stellar Initial Mass Function Proceedings of the 38th Herstmonceux Conference, G. Gilmore, I. Parry, & S. Ryan, eds., in press (astro-ph/9712317)
Schade, D., Barrientos, L. F., & Lopez-Cruz, O. 1997, ApJ, 477, L17
Stanford, S. A., Eisenhardt, P. R., & Dickinson, M. 1998, ApJ, 492, 461
van Dokkum, P. G., & Franx, M. 1996, MNRAS, 281, 985 **[Chapter 2]**
van Dokkum, P. G., Franx, M., Kelson, D. D., Illingworth, G. D. I., Fisher, D., & Fabricant, D. 1998, ApJ, 500, 714 **[Chapter 5]**
Vazdekis, A., Casuso, E., Peletier, R. F., & Beckman, J. E., 1996, APJS, 106, 307
Worthey, G. 1999, in preparation

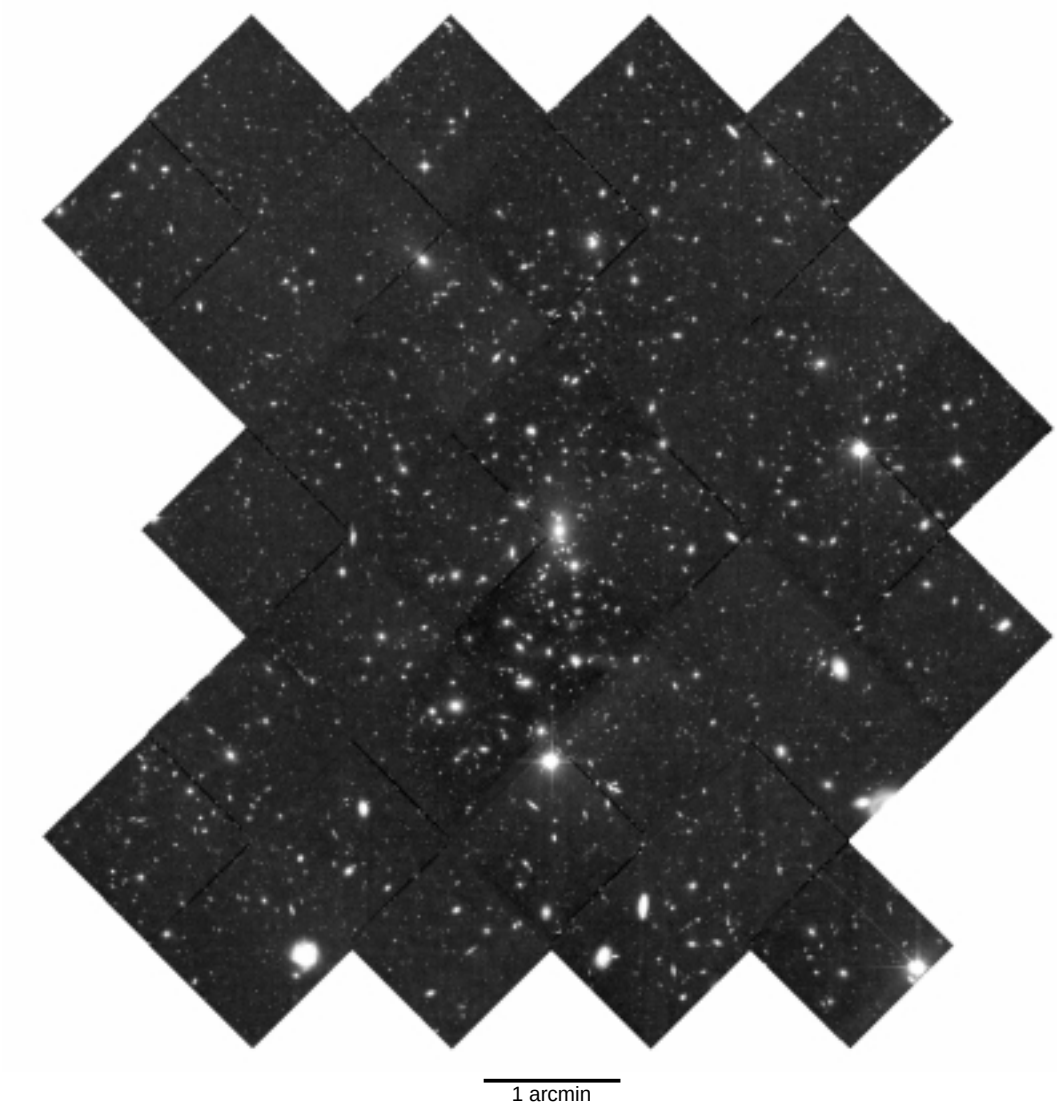

Figure 5.1: [Plate 1] *Hubble Space Telescope* WFPC2 mosaic of the cluster CL 1358+62 at $z = 0.33$. The image is a mosaic of twelve adjacent HST pointings, in two filters ($F606W$ and $F814W$). The $F606W$ and $F814W$ images were added to increase the S/N, giving a total exposure time of 7200 s per pointing (3600 s in each filter). North is up and East is to the left. The length of the scalebar is 1 arcmin, or $350\,h_{50}^{-1}$ kpc at the distance of CL 1358+62 ($q_0 = 0.5$). The total area of the image is 49 arcmin^2. The galaxy density decreases with distance from the cluster center and BCG. The galaxy population in this intermediate z cluster can be studied in lower density regions than in previous studies with HST, which focussed on the cluster cores.

Figure 5.2: [Plate 2] Color representation of the central part of Fig. 5.1 [Plate 1, page 55], created from the $F606W$ and $F814W$ exposures. The cluster members are easily recognized by their yellow colors. However, many of the bluer galaxies are also cluster members.

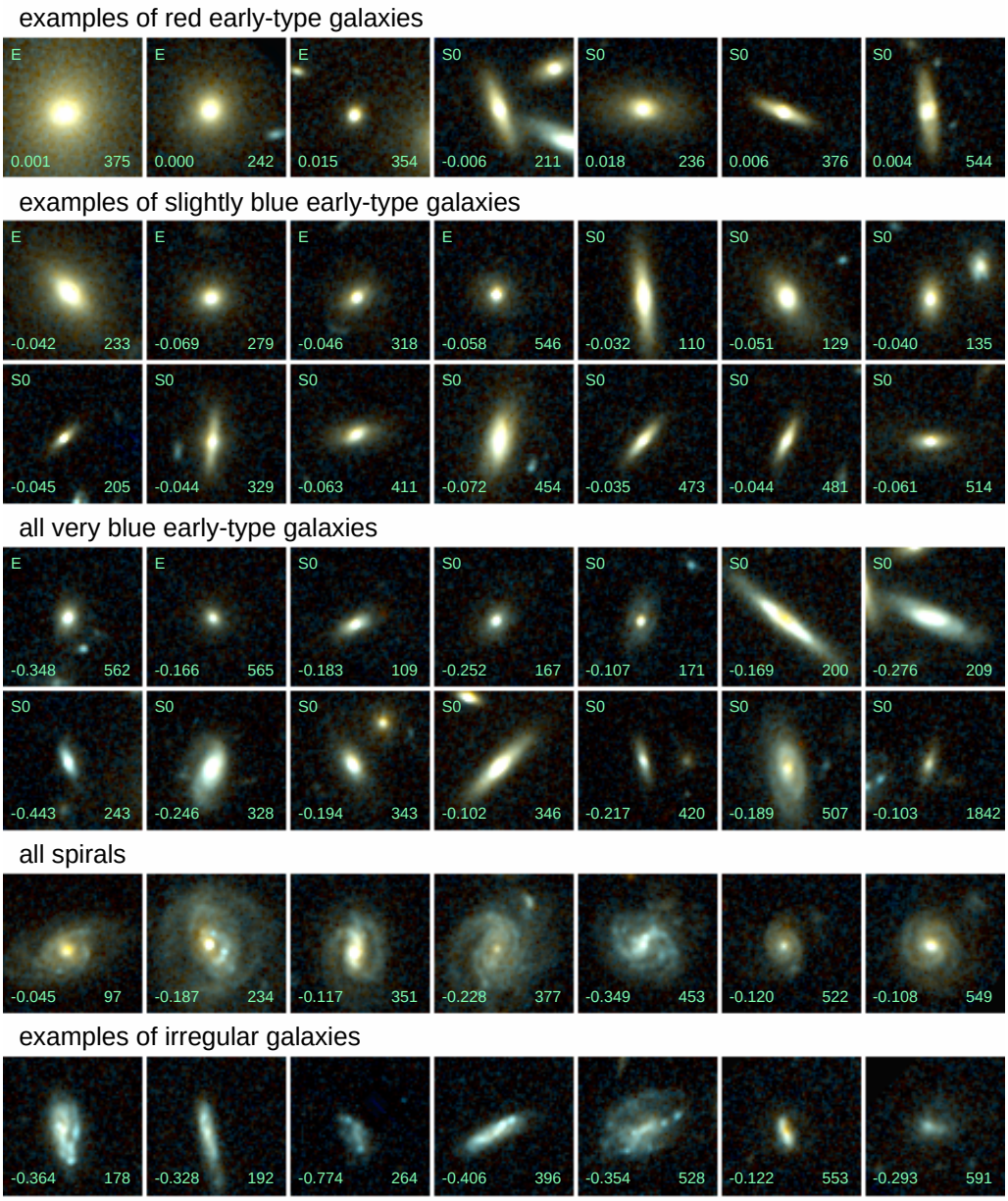

Figure 5.4: [Plate 3] Examples of early-type galaxies on the CM relation, examples of slightly blue early-types, all very blue early-types, all spirals, and examples of irregular galaxies. Each box is $6\farcs4 \times 6\farcs4$ ($37 \times 37\,h_{50}^{-1}$ kpc). The number in the lower right of each box is the galaxy identification, the number in the lower left is the restframe $B-V$ color with respect to the CM relation. The slightly blue early-type galaxies have very similar morphologies to the early-types on the CM relation. The very blue early-types have low luminosities and generally have significant disks.

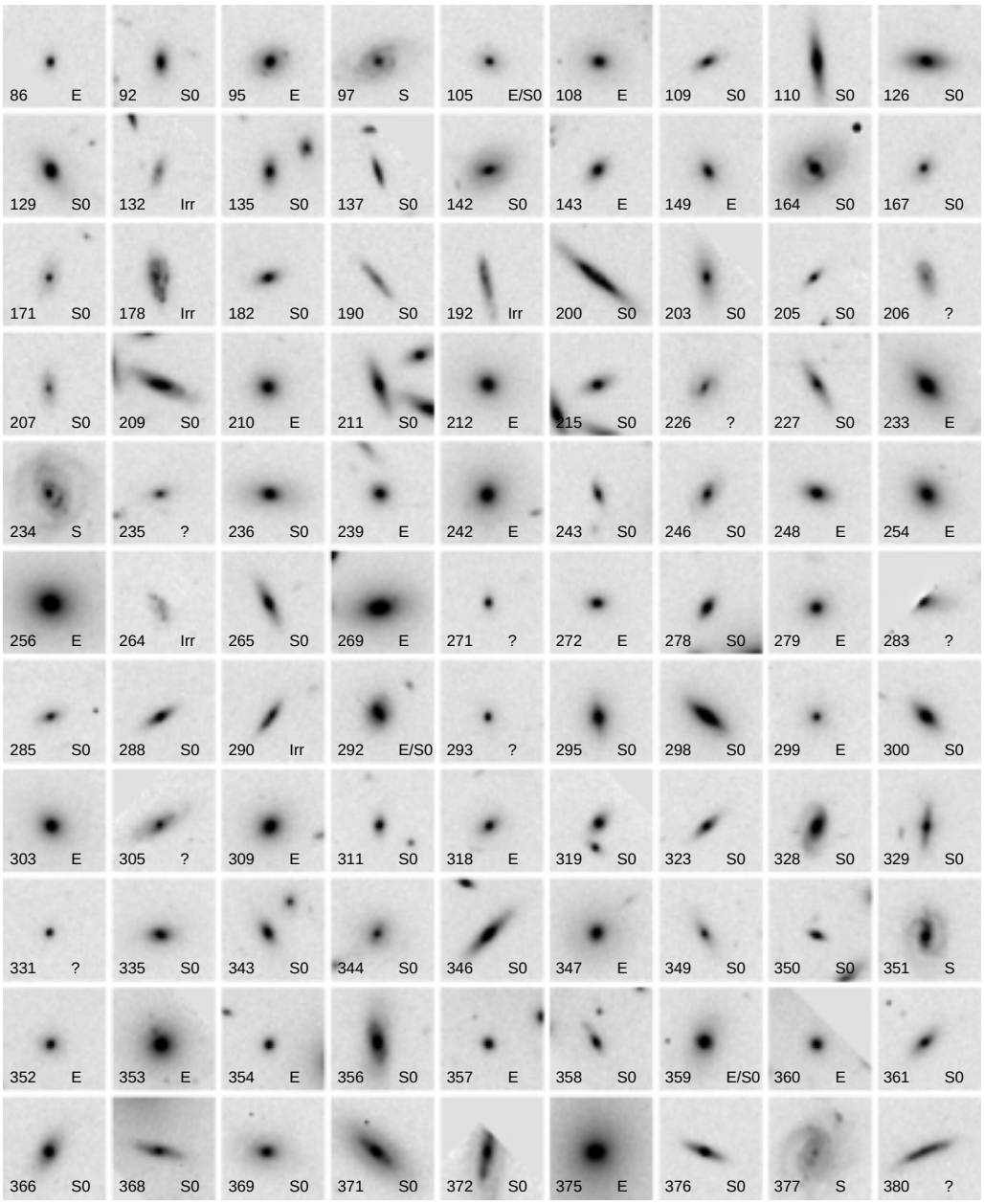

Figure 5.3: [Plate 4] Greyscale representations of all spectroscopically confirmed cluster members in the CL 1358+62 HST mosaic. The boxes are $6\farcs4$, or 37 h_{50}^{-1} kpc ($q_0 = 0.5$), on a side.

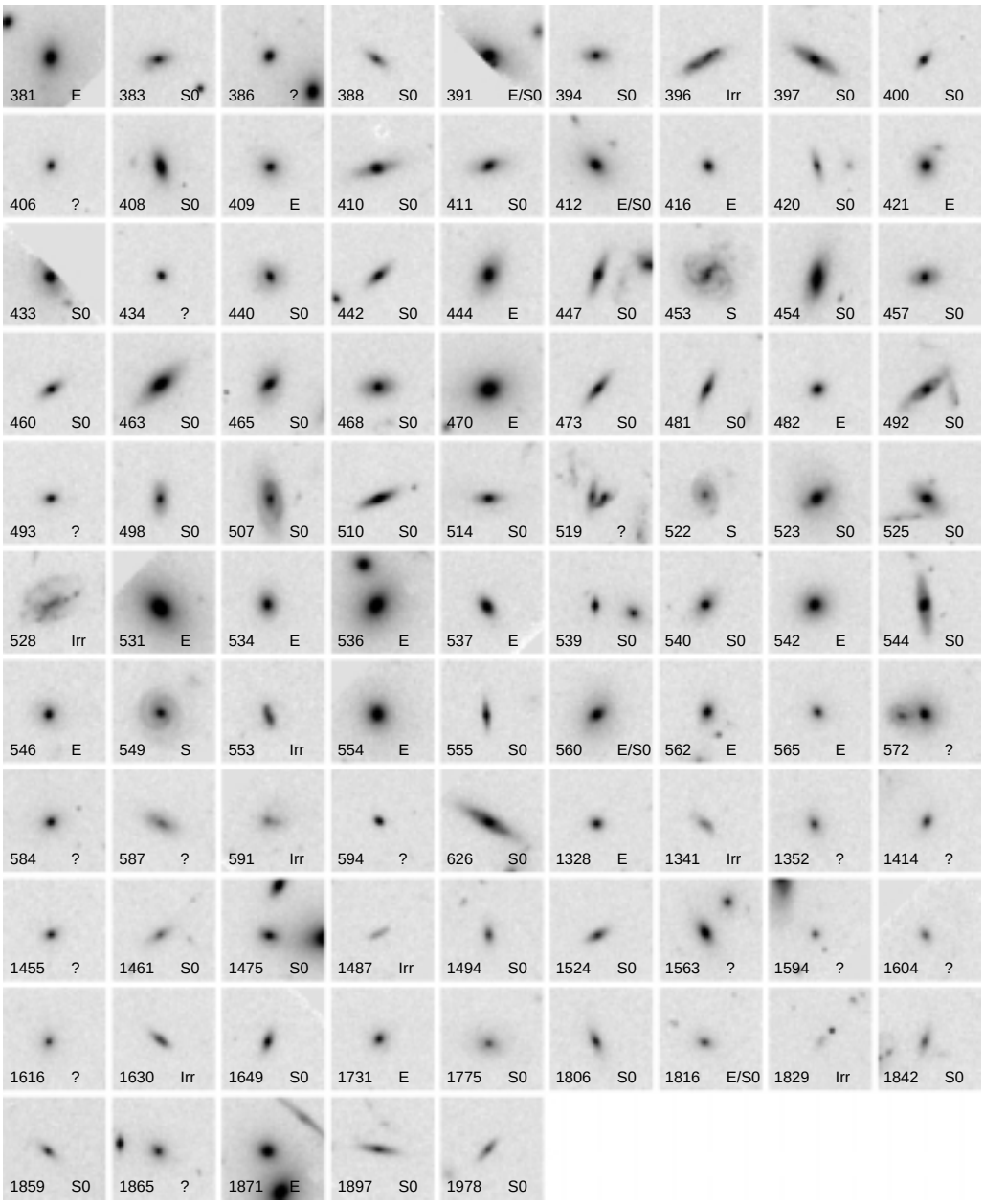

Figure 5.3: [Plate 4] (continued)

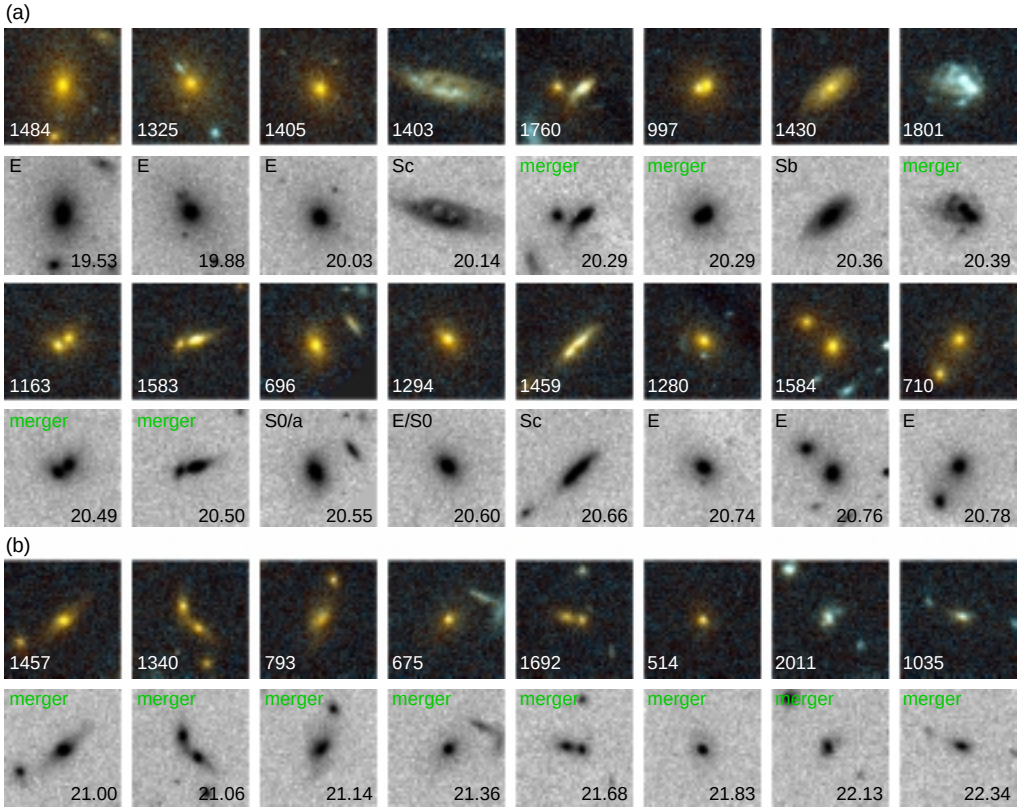

Figure 6.1: [Plate 5] (a) The sixteen most luminous galaxies in the cluster, ordered by total F814W magnitude. Of each galaxy a color image and the F814W image are shown. The size of each image is $5\farcs9 \times 5\farcs9$ ($56 \times 56\,h_{50}^{-1}$ kpc); the pixel size is $0\farcs07$. At low redshift the bright end of the luminosity function in clusters is dominated by ellipticals and S0 galaxies. In MS 1054–03 at $z = 0.83$ we find five mergers among the most luminous sixteen galaxies. (b) The eight fainter galaxies classified as "merger/peculiar".

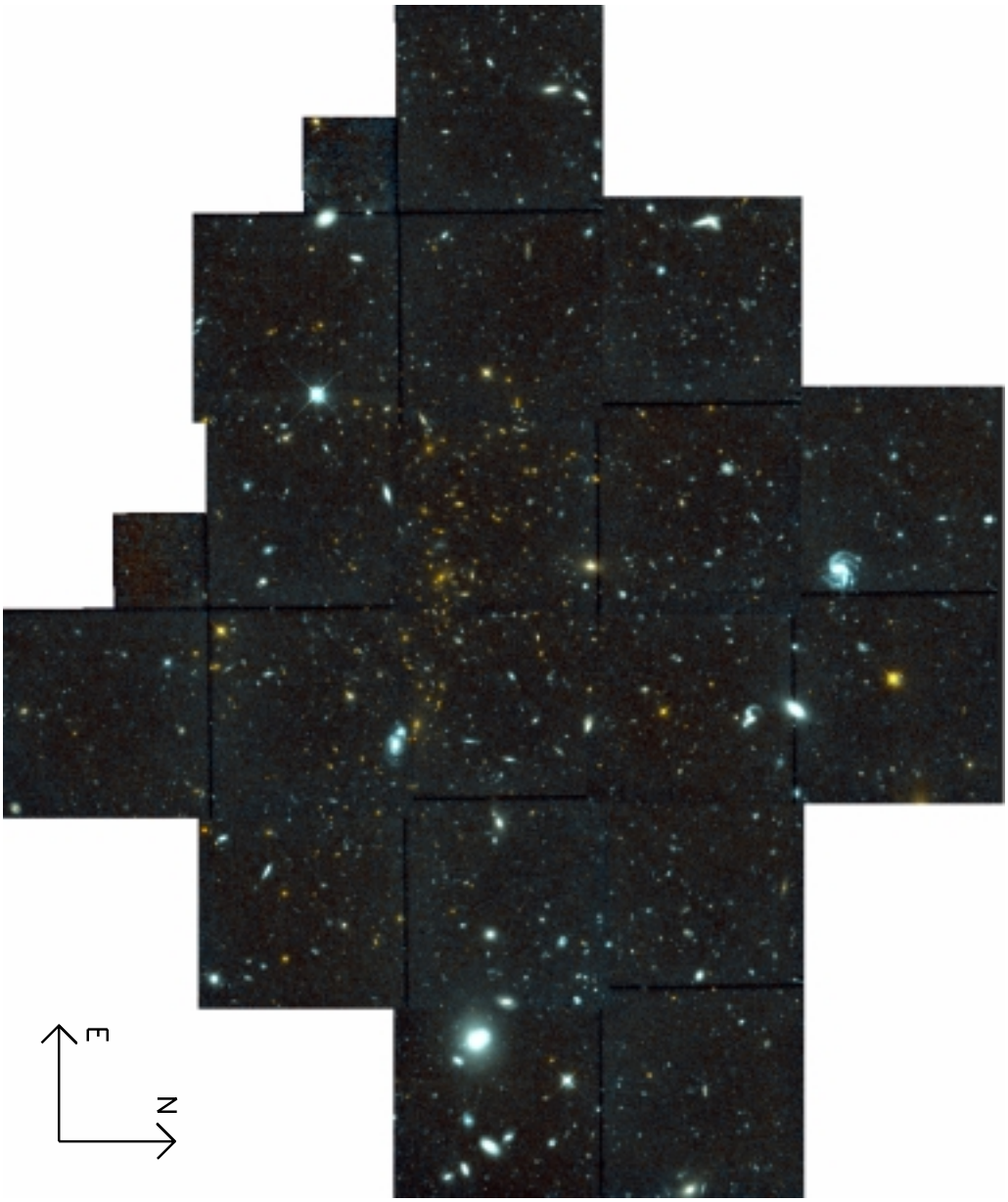

Figure 7.5: [Plate 6] Hubble Space Telescope WFPC2 mosaic of the cluster MS 1054–03 at $z = 0.83$. This color image was created from the F606W and F814W exposures, and spans roughly $4 \times 6'$ ($2 \times 3\,h_{50}^{-1}$ Mpc). The red cluster galaxies are conspicuous. Note their irregular and elongated distribution.

5 The Color-Magnitude Relation at $z = 0.33$: Evidence for Significant Evolution in the S0 Population[†]

ABSTRACT

We use a large, multi-color mosaic of HST WFPC2 images to measure the colors and morphologies of 194 spectroscopically confirmed members of the rich galaxy cluster CL 1358+62 at $z = 0.33$. We study the color-magnitude (CM) relation as a function of radius in the cluster, to a limit of 4.6 arcmin from the center, equivalent to 1.6 h_{50}^{-1} Mpc. The intrinsic scatter in the restframe $B-V$ CM relation of the elliptical galaxies is very small: $\sim$0.022 magnitudes. The CM relation of the ellipticals does not depend significantly on the distance from the cluster center. In contrast, the CM relation for the S0 galaxies does depend on radius: the S0s in the core follow a CM relation similar to the ellipticals, but at large radii ($R > 0.7\,h_{50}^{-1}$ Mpc) the S0s are systematically bluer and the scatter in the CM relation approximately doubles to $\sim$0.043 magnitudes. The blueing of the S0s at large radii is significant at the 95 % confidence level. These results imply that the S0 galaxies in the outer parts of the cluster have formed stars more recently than the S0s in the inner parts. A likely explanation is that clusters at $z = 0.33$ continue to accrete galaxies and groups from the field and that infall extinguishes star formation. The apparent homogeneity of the elliptical galaxy population implies that star formation in recently accreted ellipticals was terminated well before accretion occurred. We have constructed models to explore the constraints that these observations place on the star formation history of cluster galaxies. The best constrained parameter is the scatter in the luminosity-weighted age $\Delta\tau_L/\langle\tau_L\rangle$, which is less than 18 % for the ellipticals and the S0s in the cluster core, and less than 35 % for the S0s in the outer parts of the cluster. The constraints on the most recent period of star formation are model dependent, but we show that star formation in ellipticals likely ceased at $z = 0.6$ or higher. If we assume that the galaxies have a constant star formation rate up to a randomly distributed truncation time, we find that the S0s in the outer parts of the cluster have experienced star formation until the epoch of observation at $z = 0.33$. We conclude that the population of S0s in clusters is likely to evolve as star forming galaxies are converted into passively evolving galaxies. Assuming a constant accretion rate after $z = 0.33$, we estimate $\sim$15% of the present day early-type galaxy population in rich clusters was accreted between $z = 0.33$ and $z = 0$. The ellipticals (and the brightest S0s) are probably a more stable population, at least since $z = 0.6$.

[†]Pieter G. van Dokkum, Marijn Franx, Daniel D. Kelson, Garth D. Illingworth, David Fisher, and Daniel Fabricant, *Astrophysical Journal*, **500**, 714 (1998)

5.1 Introduction

Early-type galaxies in nearby rich clusters form a homogeneous population. The elliptical and S0 galaxies in clusters such as Coma follow a tight color-magnitude (CM) relation (Bower, Lucey, & Ellis 1992b), Mg_2–σ relation (Guzman et al. 1992), and Fundamental Plane (e.g., Jørgensen, Franx, & Kjærgaard 1993). The low scatter in these relations implies that the spread in the metallicities and ages of the galaxies is small at a given mass or luminosity.

The homogeneity of the early-type galaxies constrains models for the formation and evolution of these galaxies (e.g., Sandage & Visvanathan 1978, Faber et al. 1987, Bower et al. 1992b). In particular, the small intrinsic scatter in the CM relations of Coma and Virgo implies that the early-type galaxies in these clusters either formed at high redshift, or that their formation was synchronized (Bower et al. 1992b).

If the intrinsic scatter is due to age differences between the galaxies, one expects the scatter to be higher at larger lookback times. Hence, the scatter in the CM relation is expected to increase with redshift. Ellis et al. (1997) studied the CM relation in three clusters at $z \sim 0.55$ using Hubble Space Telescope (HST) data. Surprisingly, Ellis et al. (1997) found that the CM relation of the ellipticals and S0s is still very tight at $z = 0.55$. This led these authors to conclude that the star formation in early-type galaxies likely ceased at much higher redshifts. A similar conclusion was reached by Andreon, Davoust, & Heim (1997), who found a tight CM relation of the early-type galaxies in Abell 851 at $z = 0.4$. These results were further strengthened by Stanford, Eisenhardt, & Dickinson (1998), who found that the scatter in the CM relation of early-type galaxies in rich clusters is nearly constant with redshift to $z \sim 0.9$. Similarly, studies of the Fundamental Plane relation in clusters to $z \sim 0.6$ show that the scatter in the relation is not very different from that in local clusters (van Dokkum & Franx 1996; Kelson et al. 1997; Bender et al. 1997), indicating that the population of early-type galaxies has been stable and homogeneous over a significant fraction of the age of the universe.

The result of Ellis et al. (1997) is surprising, because it seems difficult to reconcile with the strong evolution of the cluster population implied by the Butcher-Oemler effect. The enhanced fraction of blue galaxies in intermediate redshift clusters as observed by Butcher & Oemler (1978, 1984) is often interpreted as the result of the transformation of blue field galaxies to red cluster galaxies (e.g., Butcher & Oemler 1984, Abraham et al. 1996b). A key question is whether the end products of this transformation are early-types (e.g., Dressler et al. 1997), or whether the Butcher-Oemler effect can be largely explained by blue spirals turning red (Butcher & Oemler 1984). Many blue galaxies in intermediate redshift clusters have the characteristics of normal (field) spirals (e.g., Couch & Sharples 1987, Andreon et al. 1997). However, some have a star burst or a post starburst spectrum (Dressler & Gunn 1983; Couch & Sharples 1987), and it seems natural to link these post starburst galaxies to today's early-type galaxies. If a population of recently transformed early-types exists, they are expected to be bluer than the pre-existing early-types, and to increase the scatter in the CM relation. Apparently, such galaxies are not in the samples studied by Ellis et al. (1997) and Stanford et al. (1998). On the other hand, the strong evolution with redshift of the morphology-density relation claimed by Dressler et al. (1997) is in qualitative agreement with the continuous transformation of spirals to S0s.

The studies of Ellis et al. (1997) and Stanford et al. (1998) suffer from two limitations: membership information is sparse, and the field sizes are small. The membership information is important because it is crucial to measure the full distribution of galaxies in the color-magnitude plane, and the blue side of the CM relation is heavily contaminated by field galaxies. Usually, a correction is applied by subtracting the expected number of field galaxies based on number counts. Since the number counts can vary in a small field, it is obviously preferable to have direct spectroscopic membership information.

A large angular coverage is of particular importance, since there is good evidence that the blue galaxies are more abundant at larger distances from the cluster center (e.g., Butcher & Oemler 1984, Pickles & van der Kruit 1991, Abraham et al. 1996b). An environmental dependence is also indicated by the evidence for young populations in early-type galaxies in the field (e.g., Larson, Tinsley, & Caldwell 1980, Bothun & Gregg 1990). If there are (mildly) blue early-type galaxies in intermediate redshift clusters, it seems likely that they reside in the transition region between the cluster and the field.

In the present study, we extend the study of the CM relation to larger radii, using a large $8' \times 8'$ HST mosaic of the cluster CL 1358+62 at $z = 0.33$. We determine morphologies, colors, and magnitudes for 194 spectroscopically confirmed cluster members within the HST mosaic. The color-magnitude relation in intermediate redshift clusters has been studied extensively (e.g., Aragon-Salamanca et al. 1993, Rakos & Schombert 1995, Abraham et al. 1996b, Ellis et al. 1997, Stanford et al. 1998), but never before with high resolution, large format images. The aims of this study are to constrain the star formation histories of the galaxies, and to establish whether the histories depend on morphology or environment. In particular, we test whether star formation in the ellipticals and S0 galaxies in the outer parts of the cluster has persisted to more recent epochs than star formation in early-type galaxies in the cluster core.

5.2 Data

5.2.1 Sample Selection

The present sample is based on a large spectroscopic survey of the cluster. The spectra were obtained with multislit masks at the Multiple Mirror Telescope and the William Herschel Telescope. The sample selection and the reduction and analysis of the spectroscopic data are described in detail in Fabricant, McClintock, & Bautz (1991), and Fisher et al. (1998). Here, we briefly summarize the sample selection.

The spectroscopic sample was selected on the basis of R magnitude. Twenty multislit aperture masks were exposed within a $\sim 10' \times 11'$ field centered on the brightest cluster galaxy in CL 1358+62, and redshifts for 387 galaxies were determined. The sample of galaxies with redshifts is $> 80\,\%$ complete to $R = 21$, or $F814W \sim 20.2$, dropping steeply to $\sim 20\,\%$ at $R = 22$ ($F814W \sim 21.2$). The completeness within the $8' \times 8'$ HST WFPC2 field (see below) is somewhat higher: $> 90\,\%$ to $R = 21$, and $\sim 30\,\%$ at $R = 22$. This incompleteness is caused by the limited number of galaxies that was observed, and not by the inability to measure the redshifts of observed galaxies. The "success rate" of measuring the redshift is 100 % to $R = 21.1$. The success rate drops to 70 % at $R = 22.3$ ($F814W \sim 21.5$), and 50 % at $R = 23$. The success rate does not depend strongly on color, for $R < 23.5$ (Fisher et al. 1998).

We refer the reader to Fisher et al. (1998) for a discussion of cluster membership and substructure in the cluster. Following Fisher et al., we include as cluster members all galaxies in the interval $0.31461 < z < 0.34201$. The subsample used for this paper consists of all 194 confirmed cluster members in the $8' \times 8'$ HST WFPC2 field (see below). For the analysis in Sect. 5.3, we furthermore impose a magnitude limit of $F814W = 21.5$, reducing the sample to 188 galaxies.

5.2.2 Imaging

WFPC2 images from twelve HST pointings were combined to give an $\sim 8' \times 8'$ field centered on the brightest cluster galaxy (BCG) in CL 1358+62. The cluster was observed with the

*F*606*W* and *F*814*W* filters (close to rest frame *B* and *V*), on February 15, 1996. Exposure times were 3600 s in each filter, for each pointing. Figure 5.1 [Plate 1, page 55] shows the field layout.

Reduction

The pipeline reduction was performed at the Space Telescope Science Institute (STScI). No recalibration was done, and we verified that the most recent calibration files had been used in the pipeline processing. The crucial step in the data reduction was the sky subtraction. The cluster was observed in the Continuous Viewing Zone (CVZ) of HST. The sky background is fairly high in most exposures, due to reflected Earth light. The Earth light reflects off the Optical Telescope Assembly (OTA) and scatters throughout the WFPC2 field. In most exposures, dark diagonal bands are present; these appear when the OTA vanes pass into the shadow of the WFPC2 camera relay spiders (see Biretta, Ritchie, & Rudloff 1995).

Three identical 1200 s exposures were obtained in each filter. The exposures were timed to minimize the scattered light in one of the three exposures. For the majority of exposures, we modeled the background in two steps. First, the image with the lowest background was subtracted from the two other images. Second, the residual images (containing the background structure + noise) were fitted with high order 2D polynomials. These fits were then subtracted from the high background images. Finally, we checked the results by eye and iterated to minimize the residuals of the cross patterns. In all *F*606*W* exposures this method worked well. However, in four of the twelve *F*814*W* pointings the background structure was present in all three exposures. For these pointings, the cross pattern in the lowest background image was carefully fitted and subtracted before subtracting this image from the higher background images.

In 10 of the 72 exposures bright linear features are present, due to the passage of bright objects through the field of view during the exposures (Biretta et al. 1995). The areas affected by these features were masked before the three exposures of each field were combined. When both a high background and a bright streak are present, the bright streak was masked before modeling the background.

The individual exposures were combined with the CRREJECT task, incorporated in the IRAF STSDAS reduction package. The output cosmic ray mask files were visually checked to verify that only cosmic rays were removed. Hot pixels were corrected by creating a "dark" frame from the exposures themselves; the twelve pointings were median filtered to identify the locations of hot pixels. Bad pixels and bad columns were removed by interpolation.

The full field is shown in Fig. 5.1 [Plate 1, page 55]. The total area of the image is 49 arcmin^2. The galaxy density decreases with distance from the BCG, allowing us to study the dependence of the properties of the cluster galaxies on local galaxy density. Fig. 5.2 [Plate 2, page 56] is a color image of the central part of the cluster. Clearly, most of the cluster galaxies have very similar colors, but our spectroscopy shows that many of the blue galaxies are also cluster members (Fisher et al. 1998).

Zeropoints

The *F*606*W* and *F*814*W* HST WFPC2 filters are close to the rest frame *B* and *V* bands for an object with $z = 0.33$. As noted by many authors, standard *K*-corrections may introduce large errors, due to the effects of spectral evolution and intrinsic scatter in galaxy colors. Therefore, we followed the procedure described in van Dokkum & Franx (1996), and derived direct transformations from the HST filters to the redshifted *V* band, denoted with V_z, and

$(B-V)_z$ colors:

$$V_z = F814W + 0.20(F606W - F814W) + 0.65 \tag{5.1}$$

$$(B-V)_z = 0.82(F606W - F814W) - 0.13 \tag{5.2}$$

For the early-type galaxies in CL 1358+62, $V_z \sim F814W + 0.9$. The zero points of the $F814W$ and $F606W$ filters are based on the Vega spectrum, and taken from Table 41.1 in the HST Data Handbook (Leitherer 1995). Using spectral energy distributions from Pence (1976), we find the transformations are independent of galaxy type to ~ 0.01 magnitudes, for early-types and early-type spirals.

5.2.3 Morphologies and Photometry

Visual Classification

We have extracted $6\farcs4 \times 6\farcs4$ images of all 194 galaxies from the WFPC2 frames. Greyscale representations of these images are presented in Fig. 5.3 [Plate 4, page 58]. Four of us (PvD, MF, DK, and GDI) morphologically classified the galaxies. Our classification scheme is identical to that used by Dressler (1980) for galaxies in nearby clusters. Five morphological types are distinguished: E, S0, S, Irregular, and unclassified. These morphological types were assigned on the basis of two qualifiers: early-type / late-type / irregular, and disk / no disk / irregular. The division between late-type and early-type is determined by the presence of spiral arms and the smoothness of the image. The disk qualifier is based on the presence of a disk. Because faint, face-on disks in S0 galaxies are very difficult to detect, early-type galaxies that were classified as diskless may contain disks at low inclinations (see, e.g., Rix & White 1990, Jørgensen & Franx 1994).

If at least three out of four authors agreed on the value of the qualifier the value was set to the median of the values of the four authors. If there was no such agreement, the type qualifier and / or disk qualifier were set to "uncertain". Our classifications fit directly into Dressler's (1980) scheme. Ellipticals are early-type galaxies without a disk, S0s are early-type galaxies with a disk, and spirals are late-type galaxies with a disk. Galaxies with type and / or disk qualifier "irregular" are classified as irregulars. The classifications are listed in Table 1, and labeled in Fig. 5.3 [Plate 4, page 58]. Color representations of several examples of galaxies of different morphologies are shown in Fig. 5.4 [Plate 3, page 57].

The reliability of visual classifications has been discussed extensively (e.g., Abraham et al. 1996a, Smail et al. 1997). It appears that the robustness of the classification of HST images of galaxies at $z \lesssim 0.5$ is not very different from that of the classification of galaxies in nearby clusters observed from the ground; even at $z = 0$ it is difficult to distinguish between adjacent Hubble types. The robustness of the classification can be assessed by comparing the classifications of different authors. Figure 5.5 illustrates the consistency of the classifications. Three of the four authors agree on $> 85\,\%$ of the galaxies to $V_z = 21$. The improvement in the consistency of the classifications at magnitudes fainter than $V_z = 22$ is probably real. The galaxy sample is dominated by irregular galaxies below this magnitude, and these galaxies are more easily distinguished from the other types than, e.g., ellipticals from S0s.

Some of the galaxies in the sample have faint, smooth spiral structure (e.g., galaxy 328). In the adopted classification scheme, these galaxies could either be classified as spirals (on the basis of the spiral features), or S0s (on the basis of the absence of star formation regions and dust). It is not clear how these galaxies fit into the Hubble sequence. We will discuss the properties of these galaxies in more detail in future papers on the morphology-density

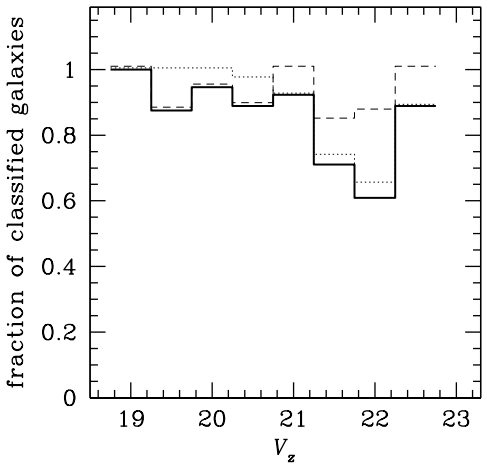

Figure 5.5: The agreement between visual classifications of different authors. The histograms show the fraction of galaxies within a magnitude bin that were given identical classifications by at least three out of four authors. The agreement on the type qualifier is indicated by the dashed line, and the agreement on the disk qualifier by the dotted line. The drawn line indicates the agreement on the type qualifier and the disk qualifier simultaneously. The magnitude bins are 0.5 magnitudes wide. Adjacent points are independent.

relation, and the "E+A" galaxies in CL 1358+62. We note here that four of these ambiguous galaxies were classified as S0s, the remainder as spirals.

We compared the limiting magnitude of our classifications to the limits adopted by Smail et al. (1997) and Ellis et al. (1997). Smail et al. classify galaxies to a limit (in signal-to-noise) ~ 1 magnitudes fainter than in our study, and Ellis et al. to a limit ~ 0.5 magnitudes fainter.

Quantitative Classification from Structural Parameters

The visual classifications are by their nature not very quantitative, nor can we assess systematic errors. Because the vast majority of cluster galaxies in the present sample are early-type galaxies, it is desirable to have a quantitative indicator of the bulge-to-disk ratios of these galaxies, to have an alternative way to discriminate between bulge dominated and disk dominated galaxies. As noted by Saglia et al. (1997), the Sérsic (1968) n parameter provides a rough measure of the bulge-to-disk ratio. The value of n that gives the lowest χ^2 in a fit of the galaxy profile to an $r^{1/n}$ law depends on the relative contributions of the bulge and the disk. If the disk dominates, n will be close to 1 (i.e. an exponential profile), if the bulge dominates, n will be close to 4 (i.e. the de Vaucouleurs $r^{1/4}$ law).

All images of the cluster galaxies were fitted with two-dimensional $r^{1/n}$-law models (Sérsic 1968), with $1 \leq n \leq 4$, which were convolved with the HST Point Spread Function (PSF). The PSFs were generated with Tiny Tim 4.0b (Krist 1995). For each galaxy, a separate PSF was used, appropriate to the galaxy position on the WF chip. The fitting method uses the full 2D information rather than an azimuthally averaged light profile. The fitting program determines the position, ellipticity, position angle, effective radius r_e, and the surface brightness at the effective radius μ_e. The method is described for the $n = 4$ case (the de Vaucouleur $r^{1/4}$-law) in van Dokkum & Franx (1996). Models with $n = 1, 2, 3, 4$ were fitted to the galaxy images. The χ^2 values of the four fits were compared to choose the 'best fitting profile type' for each galaxy.

We have performed simulations to test how well the n parameter correlates with bulge-to-disk ratio. Artifical galaxies were created with varying bulge-to-disk ratios, inclinations, and effective radii of the bulges and the disks. The effective radii of the disks span a range from half the effective radius of the bulge to twice the effective radius of the bulge. In the simulations, the surface brightness profiles of the bulges follow $r^{1/4}$ laws, and the surface brightness

profiles of the disks are exponential. The artificial galaxies were convolved with Tiny Tim PSFs, before determining the n parameter. We used the same procedure to determine the best fitting profile type n as for the cluster galaxies.

The simulations show that the n parameter does indeed correlate with bulge-to-disk ratio, but that it is also somewhat dependent on the effective radius of the disk relative to the bulge: large, faint disks relative to the bulge give rise to higher n values than small, bright disks. Bulge fractions $\leq 20\,\%$ give rise to $n \leq 2$ in 90 % of the cases, and bulge fractions $\geq 70\,\%$ always give rise to $n \geq 3$ in our simulations.

In reality, galaxy profiles cannot always be described by the combination of a de Vaucouleurs bulge and an exponential disk. As an example, galaxy 86 is one of 2 galaxies that are best fitted by an exponential profile ($n = 1$), but are visually classified as elliptical. A closer examination of its surface brightness profile reveals that it is best fitted by a combination of two exponentials. Also, bars and other non-axisymmetric features complicate the interpretation of the n parameter.

In summary, the n parameter is a rough measure of the bulge-to-disk ratio, but one should be cautious in drawing conclusions for individual galaxies on the basis of the n parameter. We stress that the n parameter is not intended as a refinement of the visual classifications, but as an independent and quantitative measure of the morphology. We will express our results in the context of both the visual classifications, and the best fitting profile type.

Colors and Magnitudes

The colors were measured from aperture photometry using the PHOT task in IRAF. For each galaxy, the radius of the aperture r_c was set equal to the effective radius, r_e, as determined from the fit to an $r^{1/4}$-law. The advantage of using the effective radius rather than a larger aperture is that sky subtraction errors are small. Furthermore, this procedure minimizes the effects of color gradients.

For many galaxies, the effective radii are $\lesssim 0\farcs5$. Within such small radii, the galaxy profiles are significantly affected by the Point Spread Function (PSF). The shape of the HST PSF depends on the passband, and the measured colors within an effective radius are affected by the differences between the $F606W$ and $F814W$ PSFs. We determined the importance of this effect by constructing a model galaxy with an effective radius of $0\farcs3$, and convolving it with $F606W$ and $F814W$ PSFs generated by Tiny Tim. The measured color within r_c turned out to be 0.016 magnitudes bluer than the true color. After deconvolution of the model galaxy, the true color could be obtained within 0.001 magnitudes. We tested whether the Tiny Tim PSF is a reasonable approximation of the true PSF by constructing a model galaxy using the $F606W$ and $F814W$ images of a star in the field, and deconvolving it using a Tiny Tim PSF. Again, the true color could be obtained within 0.001 magnitudes after deconvolution.

To correct for the effects of the PSF, we deconvolved all images before measuring the colors. For the deconvolutions the CLEAN algorithm (Högbom 1974) was used, which ensures flux conservation. For each galaxy a PSF was created with Tiny Tim, appropriate for the position of the galaxy on the chip. The deconvolution does not influence the scatter in the CM relation significantly. However, the deconvolution has a small, but systematic, effect on the slope of the CM relation.

We performed extensive tests to establish how our conclusions depend on the choice of aperture. We explored the effect of apertures with radii $r_e/2$, $2r_e$, and $3r_e$, as well as apertures with a fixed angular radius ($0\farcs2$, $0\farcs6$, $1\farcs0$, and $1\farcs5$). The systematic trends discussed in Sect. 5.3.2 also apply for all these apertures. However, the colors of individual galaxies may depend substantially on the aperture size because some galaxies have significant color gradients. We will return to this issue later.

"Total" magnitudes were measured through 1.″5 radius apertures. The error in the total magnitude contributes to the scatter in the CM relation. This can be estimated at $|\alpha|\delta V$, where α is the slope of the CM relation and δV is the error in the magnitude. Since $|\alpha| \sim 0.018$ (cf. Sect. 5.3.1) this contribution to the scatter in the CM relation is negligible, for $\delta V < 1$ magnitude. The colors and magnitudes of all 194 galaxies in the sample are listed in Table 1.

Photometric Accuracy

It is difficult to calibrate HST WFPC2 observations to higher absolute accuracy than 5 % (see, e.g., Holtzman et al. 1995, Whitmore 1997). One of the main uncertainties is the charge transfer efficiency (CTE) which leads to efficiency variations of a few percent over individual WFPC2 chips (Whitmore 1997). Fortunately, all uncertainties that are effectively efficiency variations over the WFPC2 field (such as the CTE problem) cancel out when determining colors, provided the effect is not very wavelength dependent. Therefore, in principle, color differences between galaxies can be measured to very high accuracy despite limitations in the absolute calibration.

The signal to noise (S/N) ratio in the HST observations of the spectroscopically confirmed cluster members is very high; the formal errors in the colors measured within r_c are $\lesssim 0.005$ magnitudes for all galaxies. However, other systematic sources of error remain, e.g., the flatfielding, the sky subtraction, and uncertainties in the PSF.

The HST pointings were chosen to allow an overlap of $\sim 5''$ between adjacent observations. Therefore, a number of objects in the CL 1358+62 field were observed twice. These repeated observations allow us to directly assess the errors in the photometry. We found 23 objects that were well exposed in two pointings; 15 of these are spectroscopically confirmed cluster members. The galaxy colors were measured within 0.″7 radius apertures, which is the median r_e of the 194 cluster members.

The $1\,\sigma$ spread in the differences between the two color measurements of the 23 objects is 0.015 magnitudes, implying an uncertainty for a single observation of $0.015/\sqrt{2} = 0.011$ magnitudes. The 23 objects span a similar range in magnitude as the sample of 194 cluster members, and have a median magnitude of $V_z = 21$. We divided the sample into two bins to determine whether the measurement uncertainty depends on the magnitude. For galaxies with $V_z < 21$ the uncertainty is 0.009. For galaxies with $V_z \geq 21$ the uncertainty rises to 0.017 magnitude.

We noticed that the differences between the two observations were often close to −0.010 or +0.010. This is almost certainly due to systematic differences between the WFPC2 chips: after adding 0.010 to the $F606W$ zeropoint of chip 3, the measurement uncertainty for galaxies in the bright half of the sample was reduced to 0.002 magnitudes.

The errors in the sky subtraction and the flat fielding are probably largest near the edges of the chips. In addition, the shape of the PSF has a strong positional dependence near the chip edges. Therefore, the color measurement errors for galaxies near the centers of the chips are likely to be smaller than the preceding estimates. The measured scatter in the CM relation of the ellipticals and S0s ranges from 0.021 to 0.043 (cf. Sect. 5.3), which is significantly larger than the measurement error (0.011). Therefore, the contribution of measurement errors to the measured scatter in the CM relation is generally negligible. However, for consistency, we computed the intrinsic scatter in the CM relation by removing an uncertainty of 0.011 magnitudes in quadrature from the measured scatter.

TABLE 1
GALAXY CATALOG

Id	$x(''$)	$y(''$)	type	n	$F814W$	V_z	$F606W-F814W$	$(B-V)_z$	$r_c(''$)
86	−60.9	−252.6	E	1	20.78	21.68	1.179	0.837	0.32
92	137.2	−237.1	S0	2	19.84	20.75	1.201	0.855	0.60
95	63.5	−235.4	E	3	19.32	20.25	1.249	0.894	0.52
97	−64.2	−233.8	S	2	19.67	20.57	1.162	0.823	2.95
105	130.4	−222.1	E/S0	4	20.52	21.42	1.214	0.866	0.32
108	−131.1	−225.0	E	4	19.67	20.58	1.219	0.870	0.75
109	73.7	−222.1	S0	3	20.46	21.32	0.978	0.672	0.44
110	58.6	−221.7	S0	3	18.98	19.89	1.194	0.849	0.71
126	67.9	−208.2	S0	4	19.10	20.01	1.201	0.855	0.60
129	127.7	−201.7	S0	3	19.06	19.96	1.169	0.829	0.42
132	87.4	−200.9	Irr	1	21.12	21.97	0.940	0.641	2.04
135	−21.1	−199.5	S0	4	19.78	20.68	1.166	0.826	0.36
137	86.0	−196.9	S0	1	20.44	21.33	1.130	0.797	2.17
142	−50.9	−191.3	S0	4	19.34	20.26	1.202	0.856	1.25
143	58.0	−189.6	E	2	19.94	20.85	1.214	0.866	0.54
149	−147.6	−187.0	E	3	19.95	20.85	1.188	0.844	0.57
164	−105.1	−172.2	S0	4	18.98	19.88	1.219	0.870	1.15
167	89.3	−168.2	S0	3	20.71	21.55	0.889	0.599	0.54
171	93.7	−164.3	S0	4	20.90	21.77	1.061	0.740	0.59
178	−1.6	−155.1	Irr	1	19.86	20.67	0.771	0.502	3.04
182	−177.6	−152.3	S0	3	20.07	20.97	1.182	0.839	0.50
190	61.3	−142.7	S0	1	20.80	21.69	1.158	0.820	1.85
192	13.8	−142.9	Irr	1	20.48	21.30	0.801	0.527	2.09
200	−12.6	−138.4	S0	1	19.16	20.02	1.023	0.709	3.09
203	25.2	−137.4	S0	3	19.87	20.76	1.183	0.840	1.03
205	−106.8	−135.9	S0	3	20.96	21.84	1.135	0.801	0.23
206	−165.3	−135.6	?	1	20.58	21.43	1.095	0.768	2.23
207	73.4	−130.8	S0	2	20.87	21.75	1.136	0.802	1.25
209	29.2	−130.8	S0	2	19.28	20.09	0.891	0.601	1.52
210	−185.0	−132.1	E	3	19.37	20.28	1.249	0.894	0.83
211	26.1	−129.4	S0	4	19.24	20.12	1.220	0.870	0.77
212	135.6	−127.7	E	4	19.16	20.04	1.217	0.868	0.64
215	28.5	−127.4	S0	4	19.90	20.78	1.187	0.843	0.38
226	−208.3	−120.3	?	2	20.46	21.31	0.989	0.681	1.77
227	15.9	−117.1	S0	2	20.02	20.91	1.272	0.913	1.00
233	−164.9	−114.3	E	4	18.60	19.47	1.191	0.847	0.61
234	111.8	−110.8	S	4	19.30	20.14	0.999	0.689	2.17
235	−46.5	−111.3	?	4	20.74	21.60	1.141	0.806	0.71
236	−37.2	−110.4	S0	4	19.27	20.16	1.249	0.894	0.61
239	−26.8	−103.9	E	3	19.78	20.67	1.255	0.899	0.42
242	−8.6	−101.2	E	2	18.92	19.81	1.234	0.882	2.34
243	−13.8	−99.7	S0	3	20.83	21.59	0.655	0.407	0.50
246	78.1	−96.1	S0	3	20.09	20.97	1.182	0.839	0.78
248	−59.8	−96.2	E	4	19.30	20.20	1.289	0.927	0.32
254	−63.5	−91.2	E	4	19.03	19.91	1.220	0.870	0.96
256	−51.6	−88.5	E	4	18.06	18.95	1.226	0.875	1.04
264	−3.1	−79.3	Irr	1	21.86	22.57	0.229	0.058	2.20

TABLE 1
(CONTINUED)

Id	$x('')$	$y('')$	type	n	$F814W$	V_z	$F606W-F814W$	$(B-V)_z$	$r_c('')$
265	59.0	–77.9	S0	3	19.59	20.47	1.229	0.878	0.59
269	–16.7	–76.9	E	4	18.19	19.12	1.272	0.913	0.93
271	–138.2	–78.1	?	1	21.16	21.93	0.649	0.402	0.25
272	–53.0	–76.5	E	3	20.02	20.90	1.238	0.885	0.31
278	–19.7	–73.6	S0	2	19.75	20.66	1.234	0.882	0.48
279	69.2	–72.4	E	3	19.71	20.60	1.133	0.799	0.58
283	–176.7	–72.4	?	3	20.40	21.29	1.266	0.908	0.49
285	1.9	–68.6	S0	3	20.76	21.67	1.215	0.866	0.51
288	–75.1	–68.2	S0	3	19.83	20.75	1.214	0.866	0.40
290	16.0	–65.5	Irr	1	20.32	21.16	0.907	0.614	1.14
292	38.9	–64.6	E/S0	2	19.14	20.00	1.105	0.776	1.16
293	27.1	–64.3	?	3	20.78	21.69	1.193	0.848	0.21
295	–5.0	–61.3	S0	3	19.29	20.19	1.205	0.858	0.82
298	–19.7	–58.8	S0	2	18.52	19.44	1.273	0.914	0.93
299	–45.1	–54.6	E	4	20.55	21.45	1.176	0.834	0.49
300	–15.0	–53.9	S0	2	19.10	20.01	1.230	0.879	0.48
303	–89.0	–53.8	E	3	19.12	20.03	1.206	0.859	0.60
305	150.7	–48.4	?	2	20.08	20.98	1.170	0.829	1.46
309	–26.3	–46.3	E	4	18.94	19.86	1.255	0.899	0.51
311	–2.5	–45.5	S0	3	20.42	21.32	1.185	0.842	0.28
318	212.5	–37.6	E	3	20.14	21.05	1.151	0.814	0.49
319	29.7	–39.7	S0	3	19.71	20.64	1.259	0.902	0.48
323	23.3	–38.1	S0	3	20.23	21.14	1.189	0.845	0.47
328	–4.0	–36.8	S0	3	19.26	20.11	0.927	0.630	1.15
329	199.2	–34.2	S0	3	19.88	20.77	1.160	0.821	0.79
331	–146.6	–36.9	?	1	20.96	21.86	1.213	0.865	0.19
335	9.2	–32.2	S0	4	19.67	20.58	1.207	0.860	0.59
343	–64.3	–25.3	S0	3	19.95	20.80	0.976	0.670	0.56
344	–38.2	–24.9	S0	3	19.98	20.87	1.169	0.829	1.70
346	–8.2	–23.1	S0	4	18.98	19.87	1.109	0.779	0.39
347	–51.9	–22.9	E	4	19.25	20.14	1.202	0.856	0.74
349	63.6	–19.7	S0	3	20.65	21.54	1.174	0.833	0.74
350	–9.5	–20.0	S0	1	20.34	21.26	1.240	0.887	0.25
351	–109.0	–21.2	S	4	19.26	20.15	1.084	0.759	0.90
352	–6.1	–17.7	E	3	20.08	20.99	1.225	0.875	0.39
353	7.8	–17.6	E	4	18.50	19.41	1.243	0.889	1.25
354	3.7	–16.3	E	3	20.20	21.11	1.224	0.874	0.31
356	–23.2	–11.2	S0	4	18.73	19.64	1.244	0.890	0.86
357	–1.6	–10.8	E	3	19.99	20.90	1.217	0.868	0.23
358	4.9	–10.2	S0	4	20.02	20.92	1.223	0.873	0.44
359	66.7	–9.0	E/S0	3	19.01	19.91	1.196	0.851	0.61
360	1.8	–9.2	E	1	19.78	20.69	1.208	0.861	0.93
361	56.9	–8.4	S0	3	20.12	21.01	1.197	0.852	0.64
366	137.9	–4.7	S0	3	19.32	20.22	1.211	0.863	0.75
368	0.8	–5.0	S0	4	19.53	20.43	1.208	0.861	3.55
369	122.5	–3.4	S0	4	19.53	20.43	1.230	0.879	1.04
371	87.2	–2.9	S0	3	18.77	19.67	1.221	0.871	2.07

TABLE 1
(CONTINUED)

Id	$x(''$)	$y(''$)	type	n	$F814W$	V_z	$F606W-F814W$	$(B-V)_z$	$r_c(''$)
372	−103.6	−3.8	S0	2	19.16	20.07	1.216	0.867	2.77
375	0.0	0.0	E	4	18.14	19.05	1.249	0.894	2.86
376	54.1	1.5	S0	2	19.55	20.46	1.227	0.876	0.40
377	184.2	3.8	S	1	19.71	20.55	0.939	0.640	9.06
380	−27.8	5.0	?	1	20.13	20.95	0.805	0.530	1.99
381	−0.1	6.0	E	3	19.06	19.94	1.215	0.866	1.48
383	10.3	7.6	S0	3	20.38	21.28	1.182	0.839	0.98
386	−2.7	8.3	?	4	19.81	20.69	1.220	0.870	0.53
388	−63.6	12.0	S0	1	21.03	21.93	1.204	0.857	0.76
391	−18.8	13.2	E/S0	3	18.67	19.55	1.255	0.899	1.68
394	110.5	20.2	S0	1	20.46	21.33	1.182	0.839	1.38
396	−66.4	18.8	Irr	1	20.33	21.13	0.710	0.452	1.98
397	−82.6	19.3	S0	4	19.63	20.52	1.197	0.852	0.78
400	53.2	22.9	S0	3	20.61	21.51	1.191	0.847	0.22
406	−121.2	24.1	?	3	21.04	21.90	1.081	0.756	0.37
408	−5.3	25.9	S0	3	19.33	20.21	1.207	0.860	0.46
409	−90.6	25.5	E	3	20.19	21.07	1.250	0.895	0.55
410	49.3	30.7	S0	3	19.75	20.65	1.220	0.870	0.59
411	115.1	31.7	S0	3	20.16	21.03	1.131	0.797	0.72
412	−78.3	30.4	E/S0	1	19.55	20.42	1.186	0.843	1.31
416	2.9	33.7	E	3	20.57	21.44	1.183	0.840	0.27
420	−18.9	36.7	S0	3	21.32	22.14	0.919	0.624	0.41
421	−32.3	37.3	E	4	19.87	20.75	1.251	0.896	0.37
433	52.3	43.8	S0	4	19.24	20.13	1.195	0.850	0.69
434	1.3	45.5	?	1	20.71	21.59	1.232	0.880	0.20
440	−120.6	49.8	S0	4	20.09	20.97	1.187	0.843	0.59
442	14.9	52.3	S0	3	20.28	21.16	1.196	0.851	0.36
444	154.2	56.4	E	3	19.35	20.23	1.250	0.895	1.14
447	165.0	57.9	S0	2	19.88	20.77	1.255	0.899	0.68
453	194.7	63.3	S	2	19.81	20.60	0.792	0.519	3.50
454	46.6	62.0	S0	2	19.04	19.94	1.143	0.807	1.50
457	−143.9	63.3	S0	1	20.04	20.94	1.191	0.847	1.44
460	51.5	70.7	S0	3	20.54	21.44	1.187	0.843	0.44
463	8.0	75.9	S0	3	18.97	19.86	1.236	0.884	0.75
465	3.4	76.8	S0	3	19.61	20.49	1.224	0.874	0.65
468	171.8	83.2	S0	4	19.45	20.36	1.214	0.866	0.68
470	131.2	84.6	E	3	18.65	19.57	1.222	0.872	1.06
473	47.4	87.3	S0	3	20.19	21.09	1.163	0.824	0.55
481	−44.2	91.1	S0	2	20.38	21.27	1.148	0.811	0.56
482	40.8	94.8	E	3	20.41	21.32	1.208	0.861	0.34
492	110.3	100.0	S0	3	19.70	20.64	1.304	0.939	1.26
493	11.7	98.9	?	3	20.80	21.70	1.144	0.808	0.27
498	67.8	106.8	S0	3	20.41	21.31	1.163	0.824	0.76
507	−181.3	112.4	S0	2	19.66	20.52	0.987	0.679	3.07
510	55.5	117.3	S0	2	19.63	20.55	1.211	0.863	0.46
514	−58.3	119.2	S0	3	20.28	21.17	1.130	0.797	0.39
519	−32.4	124.4	?	2	20.23	21.06	0.788	0.516	1.38

TABLE 1
(CONTINUED)

Id	$x(''$)	$y(''$)	type	n	$F814W$	V_z	$F606W-F814W$	$(B-V)_z$	$r_c(''$)
522	−125.4	124.3	S	1	20.39	21.26	1.056	0.736	2.56
523	37.5	126.6	S0	3	19.30	20.23	1.262	0.905	1.16
525	−137.7	125.5	S0	3	19.57	20.47	1.199	0.853	0.63
528	−17.8	132.9	Irr	1	20.23	21.04	0.776	0.506	4.41
531	−68.8	136.3	E	3	18.28	19.19	1.240	0.887	1.34
534	−124.7	140.4	E	4	19.83	20.74	1.242	0.888	0.50
536	17.0	144.9	E	4	18.48	19.39	1.224	0.874	1.20
537	31.7	145.2	E	3	19.73	20.63	1.239	0.886	0.41
539	108.7	146.8	S0	3	20.53	21.42	1.163	0.824	0.22
540	68.3	147.1	S0	3	19.95	20.86	1.241	0.888	0.39
542	−4.3	150.0	E	4	19.27	20.18	1.234	0.882	0.53
544	−195.7	151.4	S0	2	19.52	20.42	1.226	0.875	0.79
546	100.4	157.4	E	3	20.16	21.04	1.136	0.802	0.31
549	47.6	161.1	S	3	19.75	20.61	1.085	0.760	2.05
553	−150.3	160.5	Irr	1	20.74	21.60	1.045	0.727	1.22
554	−252.3	160.3	E	4	19.04	19.94	1.253	0.897	0.59
555	82.8	164.6	S0	3	20.57	21.47	1.218	0.869	0.41
560	21.7	170.5	E/S0	4	19.51	20.41	1.192	0.847	0.73
562	57.0	175.1	E	3	20.32	21.11	0.781	0.510	0.25
565	140.2	177.7	E	3	21.03	21.86	0.987	0.679	0.55
572	−198.7	181.7	?	4	19.39	20.29	1.229	0.878	0.97
584	−54.2	201.3	?	4	20.54	21.41	1.182	0.839	0.36
587	43.7	206.8	?	1	20.86	21.72	1.119	0.788	1.89
591	−204.2	209.1	Irr	2	21.25	22.05	0.828	0.549	2.08
594	−169.5	213.7	?	1	21.05	21.90	1.031	0.715	0.16
626	−56.5	255.2	S0	2	19.43	20.32	1.232	0.880	1.48
1328	−192.3	−159.6	E	3	20.87	21.77	1.191	0.847	0.41
1341	−242.3	−150.0	Irr	1	21.94	22.74	0.734	0.472	1.15
1352	−139.8	−144.5	?	2	20.97	21.85	1.110	0.780	0.90
1414	116.3	−115.1	?	2	21.23	22.08	1.104	0.775	0.64
1455	−3.5	−89.4	?	3	21.13	22.03	1.156	0.818	0.44
1461	97.0	−83.4	S0	3	21.41	22.31	1.096	0.769	1.24
1475	−19.9	−76.9	S0	4	19.99	20.89	1.188	0.844	1.82
1487	139.1	−58.6	Irr	1	22.75	23.56	0.717	0.458	1.27
1494	−77.5	−58.5	S0	1	21.34	22.25	1.194	0.849	0.64
1524	82.2	−39.6	S0	1	21.01	21.91	1.181	0.838	0.66
1563	−63.0	−23.7	?	3	19.95	20.80	0.976	0.670	0.56
1594	−21.4	−14.7	?	4	21.72	22.60	1.138	0.803	0.60
1604	95.4	−5.1	?	1	21.81	22.70	1.160	0.821	0.66
1616	30.7	−1.9	?	4	21.15	22.04	1.145	0.809	0.56
1630	92.4	12.8	Irr	1	21.37	22.18	0.857	0.573	0.79
1649	71.6	20.5	S0	3	20.72	21.60	1.153	0.816	0.41
1731	−75.9	67.6	E	2	20.87	21.74	1.165	0.825	0.58
1775	116.9	97.8	S0	3	20.84	21.74	1.130	0.797	1.42
1806	93.6	118.9	S0	2	20.99	21.88	1.168	0.828	0.58
1816	77.8	123.9	E/S0	2	21.33	22.22	1.137	0.802	0.78
1829	136.7	131.1	Irr	3	21.82	22.62	0.689	0.435	0.42

TABLE 1
(CONTINUED)

Id	$x(''$)	$y(''$)	type	n	$F814W$	V_z	$F606W-F814W$	$(B-V)_z$	$r_c(''$)
1842	−14.4	133.8	S0	2	21.40	22.27	1.055	0.735	1.06
1859	−76.8	142.1	S0	3	21.12	22.01	1.163	0.824	0.51
1865	111.1	146.4	?	4	20.69	21.58	1.129	0.796	1.33
1871	16.3	147.2	E	3	19.31	20.21	1.240	0.887	4.29
1897	139.0	166.8	S0	2	20.73	21.61	1.216	0.867	0.80
1978	140.5	229.0	S0	1	21.38	22.27	1.252	0.897	0.74

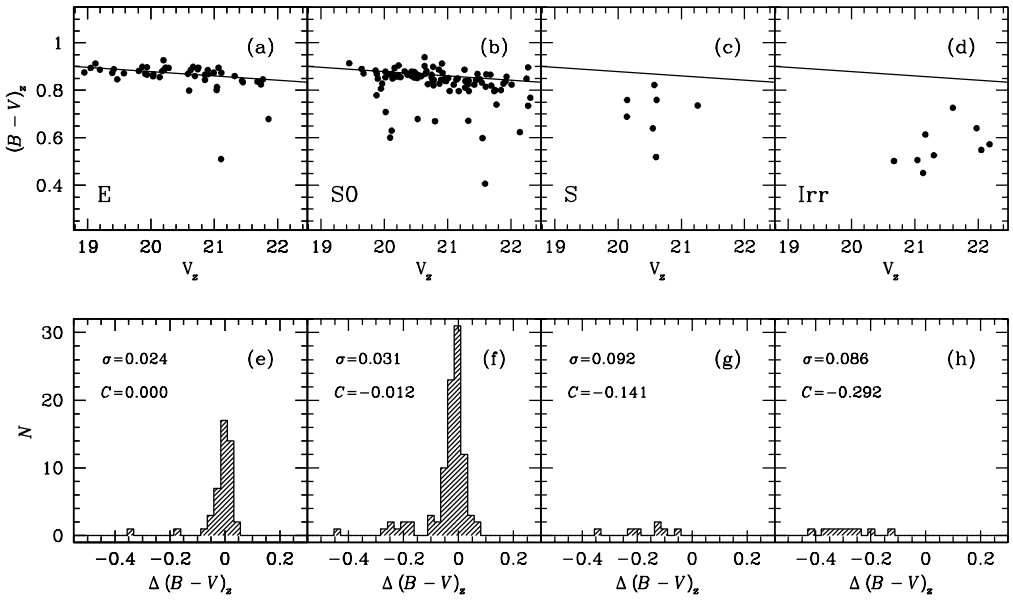

Figure 5.6: The restframe $B-V$ color-magnitude relation for galaxies of different morphological types (a-d). The line is a least squares fit to the CM relation of the ellipticals, and is repeated in each plot. Panels e-h show the distributions of the colors after subtracting the CM relation of the ellipticals. (see text).

5.3 The Color-Magnitude Relation

5.3.1 The Color-Magnitude Relation for Different Morphological Types

The CM relations of cluster members of different morphological types are presented in Figure 5.6(a-d). The figure shows that the CM relation depends strongly on morphological type. Only the ellipticals and S0s show a well defined relation, whereas the spirals and the irregulars show a large scatter in the color. Few ellipticals are significant outliers from the "ridge line" of this relation, but the fraction of outliers is higher for the S0s. The distribution about the ridge line appears to be tighter for the ellipticals than for the S0s.

We quantified these effects as follows. First, we determined the CM relation for the

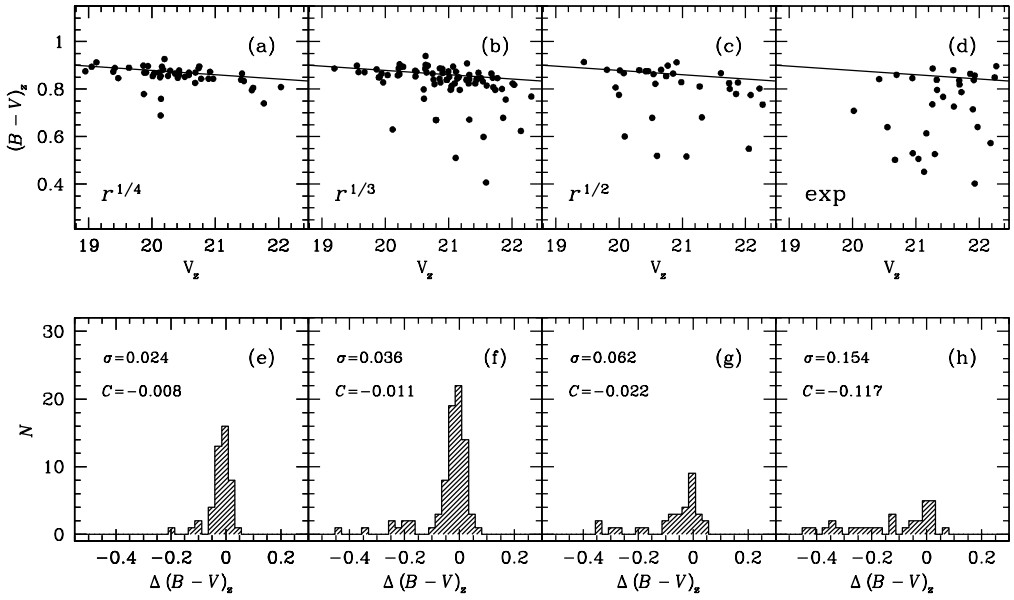

Figure 5.7: The color-magnitude relation for galaxies with different best fitting profile types. Galaxies are systematically bluer and the scatter in the CM relation increases with decreasing n.

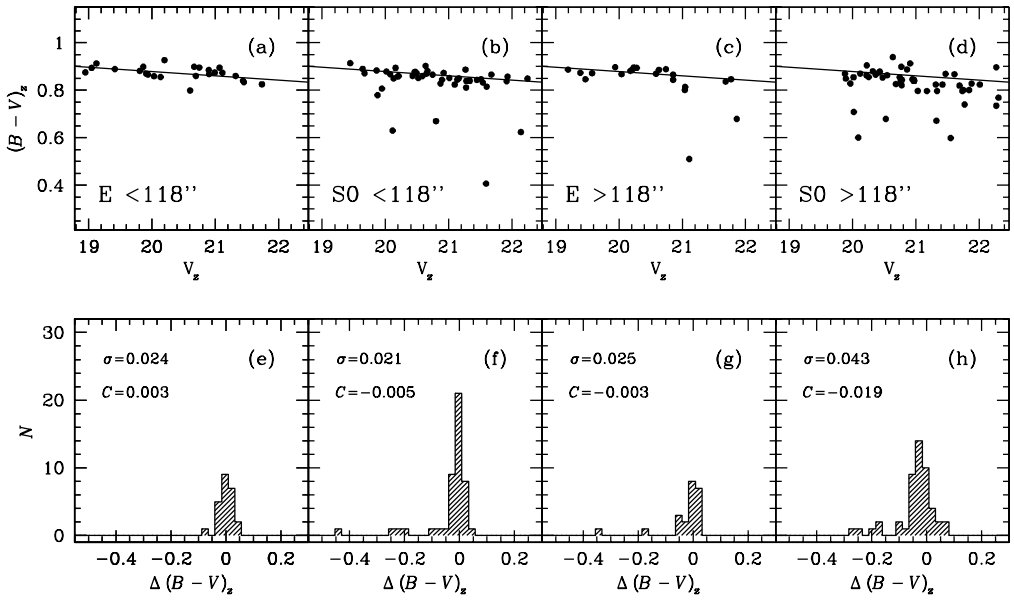

Figure 5.8: Comparison of the color-magnitude relations for ellipticals and S0s in the inner parts and in the outer parts of the cluster. The scatter in the CM relation of the S0s and the Es is very similar inside $R = 118''$. Outside $R = 118''$, the scatter in the S0 colors is larger than that of the ellipticals by a factor 2.

ellipticals with a least squares fit, excluding the two bluest galaxies. The form of this fit is

$$(B-V)_z = (0.866 \pm 0.004) - (0.018 \pm 0.005)(V_z - 20.7). \quad (5.3)$$

and it is shown in all upper panels of Fig. 5.6. For each galaxy we determined the residual color relative to the fiducial CM relation of the ellipticals: $\Delta(B-V)_z \equiv (B-V)_z + 0.018V_z - 1.240$. From the distributions of $\Delta(B-V)_z$ for the different morphological types we determined the offset C relative to the CM relation of the ellipticals, and the scatter σ. Histograms of the distributions of $\Delta(B-V)_z$ are shown in Fig. 5.6(e-h).

The offset and the scatter were calculated using the biweight estimators for the location and the scale of a distribution. This estimator was also used by Stanford et al. (1998). The biweight estimator gives higher weight to points that are closer to the center of the distribution (see Beers, Flynn, & Gebhardt 1990). Therefore, the biweight estimator is insensitive to outliers. For a Gaussian distribution the biweight scale estimator reduces to the conventional rms. The values that we obtain are characteristic of the scatter of the points close to the ridge line, and are insensitive to the blue outliers.

Bower et al. (1992b) and Ellis et al. (1997) use the normalized median absolute deviation (MAD) as a scatter estimator. The biweight estimator is more robust than the MAD estimator (Beers et al. 1990). We checked if our results are sensitive to the choice of estimator by computing the median and the normalized MAD for the distributions, and comparing the results to the biweight estimators. In the present study, the median and the normalized MAD give values very similar to those obtained with the biweight estimators.

Table 2 and Fig. 5.6 show the offset and the scatter of the CM relation. The error in the scatter was determined from bootstrap resampling. The blue outliers were not excluded from the analysis, although the biweight estimator gives them lower weight. The visual impression of an increased scatter for the S0 galaxies when compared to ellipticals is confirmed (0.031 ± 0.004 compared to 0.024 ± 0.003). Furthermore, we find that the CM relation of the S0 galaxies is offset to the blue with respect to that of the ellipticals by 0.012 ± 0.003 magnitudes. The significance of the difference in the offsets of the ellipticals and the S0s can be evaluated with the (non-parametric) Mann-Whitney test. The probability that the ellipticals and the S0s are drawn from the same sample is $< 1\,\%$. The difference in the scatter for the ellipticals and S0s is also significant, given the formal errors. We directly determined the significance of the difference between the distributions of the residuals of the CM relations of the ellipticals and the S0s with the Kolgomorov-Smirnov (KS) test. The probability that the distributions were drawn from the same parent sample is $3\,\%$.

We tested whether the scatter and offset of the CM relation are functions of the n value derived from the surface brightness profile fits. In Fig. 5.7(a-d) the CM relation is shown for different best fitting profile types, ranging from $r^{1/4}$ ($n = 4$) to exponential ($n = 1$). The distributions of the residuals from the CM relation are shown in Fig. 5.7(e-h). The offset and the scatter of the CM relation vary systematically with n, towards a bluer offset and a larger scatter for more disk dominated systems. This trend is exactly the same as the trend with morphology, confirming the distinction between S0s and ellipticals.

This difference in properties between ellipticals and S0s in intermediate redshift clusters has not been seen before. Similar studies of the CM relation with HST have found very low scatter for both ellipticals and S0s (e.g., Ellis et al. 1997). The main difference with this study is that our large-area imaging extends beyond the cluster core regions covered by previous studies with HST of intermediate redshift clusters. This raises the question whether this effect is related to distance from the cluster center.

5.3.2 Radial Dependence of the Color-Magnitude Relation

We investigated whether the scatter in the CM relation of the ellipticals and S0s depends on R, the distance from the BCG. As a first test, the galaxy sample was divided into two radial bins. The bin size, 118 arcsec ($\sim 0.7\,h_{50}^{-1}$ Mpc), was chosen such that half of the galaxies classified as early-type are contained in each bin.

Figure 5.8 shows the CM relation of the ellipticals and S0s inside and outside $R = 118''$. The scatter in the CM relation of the ellipticals and the S0s in the inner regions of the cluster is very similar: the observed scatter is 0.024 ± 0.004 for the ellipticals, compared to 0.021 ± 0.004 for the S0s, and the difference in mean color between the ellipticals and the S0s within $R = 118''$ is not significant.

Although the CM relations of the ellipticals and the S0s appear to be similar in the core of the cluster, they are very different in the outer parts of the cluster. The CM relation of the elliptical galaxies remains essentially unchanged, but the scatter for the S0s increases substantially in the outer parts. The CM relation of the S0s in the outer parts is offset to the blue by 0.019 magnitudes, and the scatter is 0.043 ± 0.009, almost a factor 2 higher than for the ellipticals in the outer parts, and the ellipticals and S0s in the core. The difference in the mean color between the S0s in the inner parts and the S0s in the outer parts is significant at the 95 % confidence level.

The dependence of the CM relation on the distance to the cluster center can be studied in more detail. In Fig. 5.9 the residuals of the CM relation are plotted against R, for visually classified ellipticals and S0s, and for early-type galaxies separated by best fitting profile type. We experimented with the size of the radial bins, and found that the results are robust when there are at least ~ 20 galaxies in each radial bin.

There is a very clear trend of the scatter and mean color for the S0 galaxies, and for the early-type galaxies with $n \leq 3$. The trend is much weaker, or absent, for the ellipticals and the early-type galaxies best fitted by a de Vaucouleur $r^{1/4}$-law. The scatter in the S0 colors increases from 0.017 at $R = 40''$ to 0.043 at $R = 200''$. The intrinsic scatter increases from 0.013 to 0.042. The S0s in the outer parts of the cluster are 0.015 magnitudes bluer than the S0s in the inner parts of the cluster. The scatter in the colors of the ellipticals is nearly constant with radius, at 0.024. The ellipticals in the outer parts of the cluster do not appear to be much bluer than the ellipticals in the inner parts. However, the number of elliptical

TABLE 2
OFFSET AND SCATTER OF THE CM RELATION

Sample	N	Offset	Error	Obs. Scatter	Intr. Scatter	Error
All	188	–0.012	0.003	0.041	0.040	0.006
E	46	0.000	0.003	0.024	0.022	0.003
S0	95	–0.012	0.003	0.031	0.029	0.004
S	7	–0.141	0.032	0.092	0.091	0.051
Irr	9	–0.292	0.027	0.086	0.085	0.023
$n = 4$	46	–0.008	0.003	0.024	0.022	0.005
$n = 3$	80	–0.011	0.004	0.036	0.034	0.006
$n = 2$	32	–0.022	0.010	0.061	0.060	0.026
$n = 1$	30	–0.117	0.026	0.154	0.154	0.021
E $< 118''$	24	0.003	0.005	0.024	0.021	0.004
E $\geq 118''$	22	–0.003	0.005	0.025	0.023	0.006
S0 $< 118''$	46	–0.005	0.003	0.021	0.018	0.004
S0 $\geq 118''$	49	–0.019	0.006	0.043	0.041	0.009

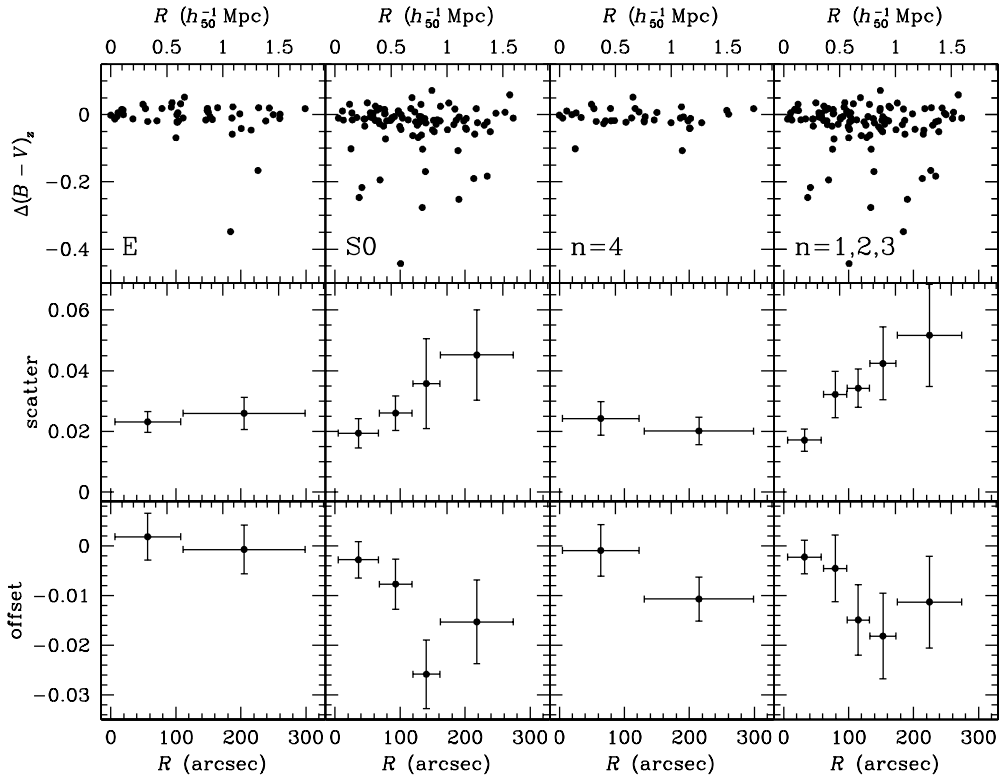

Figure 5.9: The dependence of the residuals from the CM relation on the distance from the BCG, for visually classified ellipticals and S0s, and for early-type galaxies with $n = 4$ and $n \leq 3$, where n is the value that gives the lowest χ^2 in a fit to an $r^{1/n}$ profile. The scatter and offset determined with the biweight estimators are calculated in radial bins, each containing at least 20 galaxies. Adjacent data points are independent. The biweight statistics give low weight to outliers so the scatter is not a direct function of the number of outliers. The scatter in the $(B-V)_z$ colors of the S0s and the early-types with $n \leq 3$ increases with R. These galaxies are also bluer at larger distance from the cluster center. In contrast, the ellipticals and the galaxies best fitted by an $r^{1/4}$-law do not show a significant trend with radius, but the number of galaxies is too small to rule out a change with radius in the scatter or mean color of $\lesssim 0.01$ magnitudes.

galaxies in the sample is small. We cannot rule out a change in color of ~ 0.01 magnitudes.

These results are confirmed with the objective classification provided by the best fitting profile types; the radial trend for the early-types with $n \leq 3$ is very similar to the trend for the visually classified S0s. In contrast, there is no evidence for a radial trend in the scatter for the galaxies best fitted by an $r^{1/4}$-law, confirming the result for the visually classified ellipticals. The early-types with $n = 4$ in the outer parts are bluer than those in the inner parts by 0.01 magnitudes, but a Mann-Whitney test shows that this difference is not statistically significant.

One might be concerned that the gradient in the S0 population is driven by the radially increasing fraction of blue outliers. We tested the effect of outliers by excluding from the analysis the S0 galaxies that are more than 0.1 magnitudes bluer than the CM relation. We

stress that since we have full membership information there is no justification for removing the blue outliers from the sample, other than to test whether these galaxies drive the trends with radius. The trend in the S0 colors proved to be very similar for $R < 150''$. The scatter in the outermost bin goes down from 0.046 to 0.031 when the four blue outliers in this bin are removed, indicating that the scatter in individual radial bins has considerable uncertainty. The robustness of the trends in the scatter and the mean color demonstrate that the scatter and mean color are a good approximation to the width and location of the CM ridge line. Our results therefore describe the bulk of the population, and are not unduly influenced by a small interfering population.

We tested whether the trends with radius of the S0 galaxies could be caused by the misclassification of a few early-type spirals as S0s in the outer part of the cluster. Assuming a scatter of 0.021 for the S0 population, and a three times larger scatter for Sa galaxies, we find that $\sim 55\,\%$ of the S0 galaxies in the outer parts of the cluster must be misclassified spirals to explain the observed scatter of 0.043 magnitudes. We conclude that our conclusions are robust against the misclassification of a few spirals as S0s.

We also tested whether the gradient in color and scatter in the CM relation is caused by a gradient in bulge-to-disk ratio: it may be that there are more disk dominated galaxies in the outer parts of the cluster, and that the disks are bluer than the bulges. When we subdivide our sample by best fitting profile parameter n, we find that the gradients are independent of n, for $n \leq 4$. In particular, the trends with R are very clear in the $n = 3$ galaxies, which have significant bulges. In Fig. 5.10, the radial trend of the scatter in the CM relation is plotted for galaxies classified as early-type with $n = 3$ (solid circles), and $n \leq 2$ (open circles). The colors of the S0 galaxies with strong bulges ($n = 3$) depend similarly on R as the colors of S0s with weak bulges ($n \leq 2$). This result strongly suggests that both bulges and disks are responsible for the color differences. We return to this issue in Sect. 5.4.

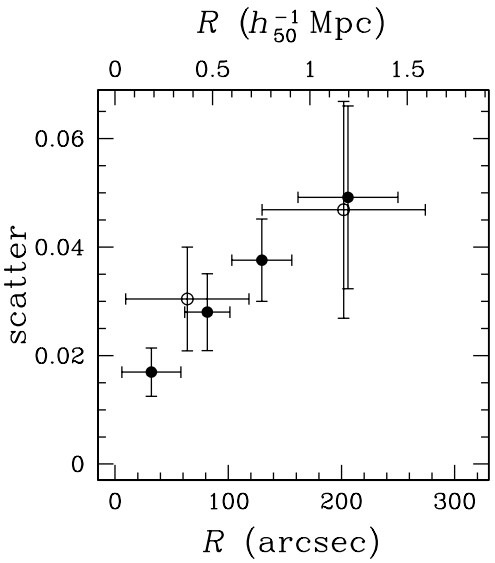

Figure 5.10: The dependence of the scatter in the CM relation on R, the distance from the BCG, for early-type galaxies with $n = 3$ (solid circles), and $n = 1,2$ (open circles), with n the value that gives the lowest χ^2 in profile fits of the form $r^{1/n}$. The $n = 3$ galaxies often have strong bulges. The trend with R of the $n = 3$ galaxies is very similar to the trend of the $n \leq 2$ galaxies. This shows that the trend of the colors of the S0 galaxies with R is not driven by bulge-to-disk ratio.

We investigated whether either the red or blue galaxies are located in subclumps. Figure 5.11 shows the spatial distributions of the S0s in various color bins. For comparison, the spatial distribution of the ellipticals is also shown. The differences between the spatial distributions of the various subsamples are striking. The blue S0s avoid the cluster core, and their

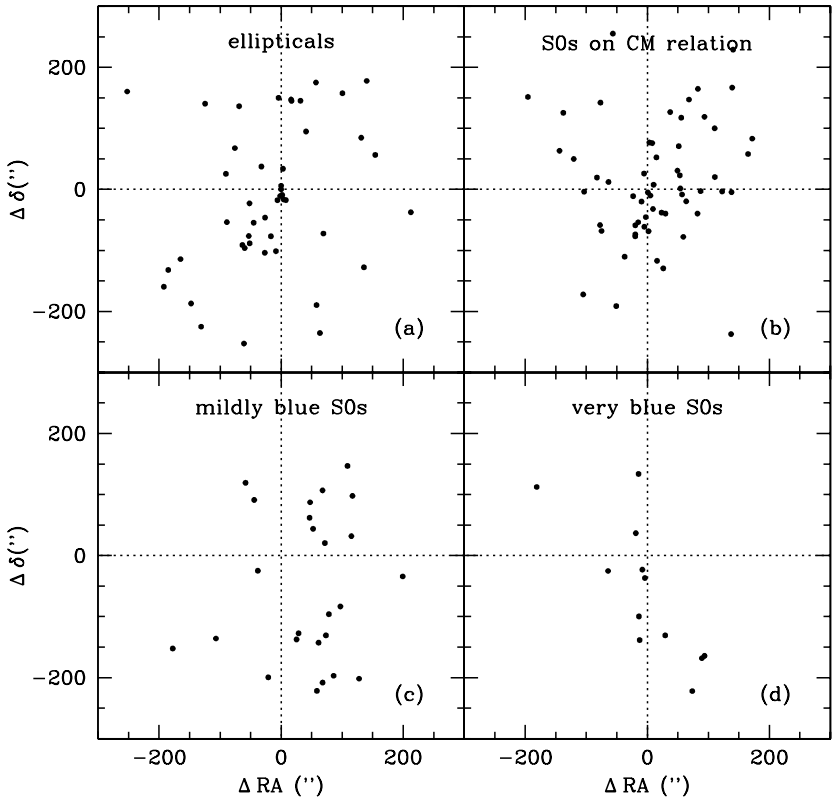

Figure 5.11: The spatial distributions of the ellipticals (a), and the S0s in various color bins (b-d). In (b), the distribution of S0s within 0.021 magnitudes (the 1σ scatter in the CM relation of the S0s in the inner parts of the cluster) of the CM relation is shown. In (c), mildly blue ($-0.10 < \Delta(B-V)_z < -0.021$ are shown, where $\Delta(B-V)_z$ is the distance to the CM relation) S0s are shown, and (d) shows the distribution of very blue S0s ($\Delta(B-V)_z \leq -0.10$). The distributions of the various subsamples are very different. In contrast to the S0s on the CM relation, the mildly blue S0s avoid the cluster core.

spatial distribution does not appear relaxed. There seem to be more mildly blue S0s to the West of the cluster center than to the East. These results confirm that the S0 galaxies in the core are redder than the S0 galaxies in the outskirts of the cluster.

We conclude that the differences between the CM relations of the ellipticals and the S0 galaxies discussed in the previous Section are caused by the increased scatter and bluer colors of the S0s in the outer part of the cluster. The S0s in the inner parts follow a similar CM relation as the ellipticals, whereas those in the outer parts have characteristics indicative of more recent, or more intense, star formation. We cannot exclude a small (≤ 0.01) trend of the elliptical colors with radius, but the trend of the S0 colors is much more significant. These are the key observational results of the paper; they are discussed more extensively below.

5.4 Blue Bulges and Disks

It is natural to expect that the color differences between S0 galaxies are caused in a large part by blue disks, as it is usually assumed that star formation in disks lasts much longer than star formation in bulges. Some bulge dominated galaxies also show blue colors, hence the process must be more complex. The high resolution of our HST data allows us to study the radial color gradients in the S0 galaxies, and to directly test if the central parts behave differently than the outer parts.

As a first test, we determined the colors within 0.5 r_e, instead of the 1 r_e used above. The color changes going to a smaller aperture do not appear correlated with radius in the cluster. We then examined the full color profiles of our sample galaxies. In general, the color gradients within the galaxies are small, but we find some galaxies with disks that are considerably bluer than their bulges or the reverse.

We show three typical color profiles in Fig. 5.12 (c). Color images of these galaxies are shown in Fig. 5.4 [Plate 3, page 57]. The radial surface brightness profiles of the galaxies are shown in Fig. 5.12 (a). These profiles were determined from the deconvolved images with the GALPHOT package (Franx, Illingworth, & Heckman 1989). The top profile in Fig. 5.12 (c) is a normal S0 on the CM relation, the middle profile is an S0 which is slightly blue, and the bottom profile is a very blue S0. Clearly, these color profiles do not show large radial changes.

Although the color differences between the bulges and the disks are small for most galaxies, some galaxies do have large color gradients. In particular, some of the bluest early-type galaxies have very blue bulges. In Fig. 5.12 (d) three examples of galaxies with extreme color gradients are shown. One has a blue disk, two have blue bulges. Images of the galaxies are shown in Fig. 5.4 [Plate 3, page 57]. At all radii these galaxies are bluer than galaxy 211, which falls on the CM relation.

We conclude that the trends in the S0 colors with distance from the BCG cannot solely be attributed to prolonged star formation in the disks of the S0s in the outer part of the cluster. Although there are a few galaxies with blue disks and red bulges, most S0 galaxies have small color gradients, implying that the bulges were affected as much as the disks, or that the star formation was stronger in the centers of the disks. Interestingly, we find that some of the bluest galaxies have very blue bulges compared to their disks.

5.5 Are There Luminous Blue Galaxies ?

Fig. 5.6 demonstrates that the brightest galaxies in CL 1358+62 are all red. There are no galaxies that are more than 0.1 magnitudes bluer than the CM relation among the brightest 29 galaxies in the sample. Their low scatter in color suggests that the population of bright galaxies is very stable between $z = 0.33$ and $z = 0$. The relatively low luminosity of the bluest galaxies has been noticed before in other clusters (e.g., Butcher & Oemler 1984, Thompson 1986).

Interestingly, the distribution along the ridge line of the CM relation of the bright S0 galaxies also seems tighter than that of the less luminous S0s. Also, judging from Fig. 5.7 it appears that the radial behavior of the colors of the brightest S0s is more similar to that of the ellipticals than to that of the fainter S0s, although the numbers are small.

We measured the scatter and offset of the CM relation of the brightest one third of the S0 galaxies ($V_z < 20.52$). The scatter in this sample is 0.019 ± 0.003, and the offset -0.003 ± 0.004. These values are similar to the scatter and offsets of the ellipticals (cf. Table 2) and of the S0s in the inner part of the cluster. The scatter for the bright S0s is significantly different

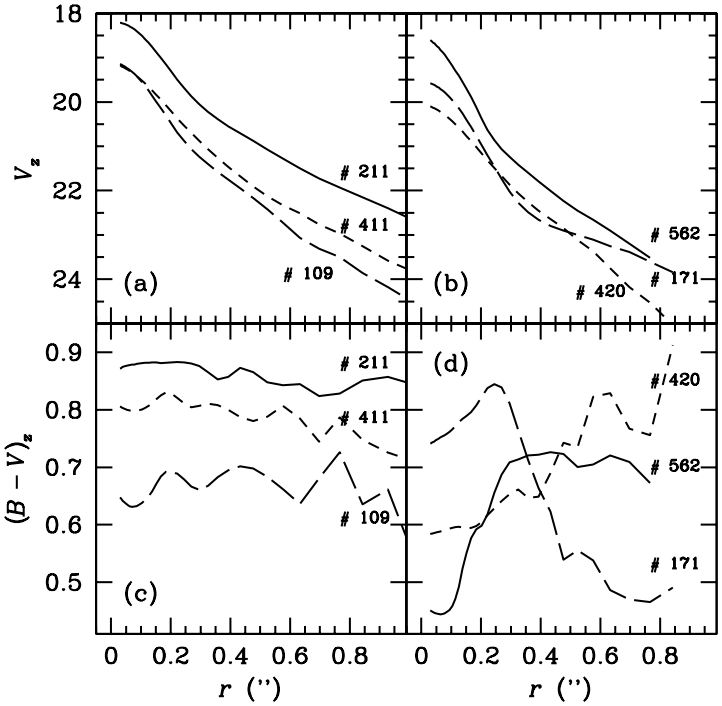

Figure 5.12: Radial surface brightness profiles (a,b) and color profiles (c,d) of early-type galaxies in CL 1358+62. In (a) and (c), surface brightness profiles and typical color profiles of an S0 galaxy on the CM relation (211), a mildly blue S0 (411), and a very blue S0 (109) are shown. The color gradients of these S0 galaxies are very similar, indicating that both the bulges and the disks of the blue S0s contain young populations. The majority of the blue S0s have shallow color gradients. In (b) and (d), examples of galaxies with extreme color gradients are shown: two galaxies with blue bulges compared to their disks (420 and 562), and a galaxy with a blue disk compared to its bulge (171). Images of the galaxies in this Figure are shown in Fig. 5.4 [Plate 3, page 57].

from that of the whole S0 sample. Furthermore, the S0s with $V_z < 20.52$ do not show the strong trend with radius that is evident for the whole S0 sample. The scatter for the bright S0s at $R > 118''$ is 0.021 ± 0.004, and the offset -0.010 ± 0.005. The scatter for the complete S0 sample in the outer parts is much higher, at 0.043 ± 0.009.

Although the brightest galaxies are generally very red, there are a few luminous early-types that are slightly bluer than the average CM relation. As an example, galaxy 233 is the 8th brightest galaxy in the sample, and is 0.04 magnitudes bluer than the CM relation. It is classified as an elliptical, and it is best fitted by a de Vaucouleur $r^{1/4}$-law. (see Fig. 5.4 [Plate 3, page 57]). It may be that the brightest galaxies in the cluster have had a different star formation history than the bulk of the cluster population, e.g., they may have had their star formation turned off at earlier times. The presence of a few bright galaxies with slightly bluer colors suggests that we may find luminous blue early-types in clusters at higher redshifts.

5.6 Implications for the Star Formation Histories

In this Section, we construct a range of models for the star formation histories of the ellipticals and the S0s. The aim is to constrain the most recent period of star formation in the ellipticals and the S0s from the observed scatter in the CM relation. We assume that the scatter in the CM relation arises from age differences among the galaxies. The fact that essentially all early-type galaxies that are more than 0.1 magnitudes bluer than the CM relation have strong Balmer absorption lines (Fisher et al. 1998) supports this interpretation.

5.6.1 Models

While the usual assumption is that most of the star formation in early-type galaxies occurred in single bursts, there is good evidence that many galaxies in clusters have more complicated star formation histories. The spectra of blue galaxies in intermediate z clusters can be fit by models that incorporate truncated star formation in disks, or secondary bursts of star formation in spirals or ellipticals (e.g., Couch & Sharples 1987, Poggianti & Barbaro 1996, Barger et al. 1996).

Motivated by these studies, we consider three scenarios: 1) formation of all the stars in a galaxy in a single burst of star formation, 2) formation of the bulk of the stars in a first burst, followed by a second burst of star formation involving a small fraction of the mass of the galaxy, and 3) a truncated uniform star formation rate. We use simple semi-analytical descriptions of the color evolution to predict the scatter in the CM relation. The derivation of the color evolution is given in Appendix A for each of the models.

The purpose of the modeling is to compare the model predictions to the observed scatter in the CM relation, under various assumptions. We focus on the scatter in the CM relation of the ellipticals and of the S0s in the outer parts of the cluster, since the scatter in the CM relation of the S0s in the inner parts is very similar to that of the ellipticals. The intrinsic scatter for the ellipticals is 0.022 magnitudes, and for the S0s in the outer parts of the cluster 0.042 magnitudes (cf. Table 2). A small (10 %) correction must be made to the intrinsic scatter because the increased luminosity of young galaxies artificially increases the scatter in the CM relation (cf. Appendix B). The corrected intrinsic scatter is 0.020 magnitudes for the ellipticals, and 0.038 for the S0s in the outer parts of the cluster.

5.6.2 Application of the Models to the Data

Constraints on the Most Recent Period of Star Formation

The scatter in the CM relation only constrains the scatter in the relative ages of the galaxies, and not the absolute ages (see Bower et al. 1992b, Appendix A). The galaxies could have an arbitrarily low mean age, provided that their formation was sufficiently synchronized. It is not possible to determine the most recent period of star formation from the models without making further assumptions.

To break this degeneracy, we assume simple top hat probability distributions in time for the star formation events that characterize the models (single bursts, secondary bursts, truncation of uniform star formation). In Sect. 5.6.2 we will investigate the effects of relaxing this assumption. In the single burst model, galaxies form in a δ-peak at a random time. In the secondary burst model, 80 % of the mass of the galaxies forms in a burst at $t = 0$, and 20 % in a second burst at a random time. In the truncated star formation model, the star formations starts at $t = 0$ for all galaxies, continues at a constant rate, and terminates at a random time.

The models are schematically represented in Fig. 5.13 and Fig. 5.14. The scatter in the CM relation of the ellipticals is reproduced in Fig. 5.13, and that of the S0s in the outer part of the cluster in Fig. 5.14. The bottom panels in Fig. 5.13 and Fig. 5.14 show the histograms of the residuals from the CM relation, derived from Monte-Carlo simulations with 5000 galaxies. The scatter and offset of these simulated distributions are measured in the same way as the observed parameters.

The scatter of 0.020 in the colors of the ellipticals can be reproduced by the three models (Fig. 5.13). In the single burst model, the youngest ellipticals formed at $z = 1.2$. In the secondary burst model, the most recent bursts occurred at $z = 0.5$. In the truncated star formation model, the youngest ellipticals were forming stars up to $z = 0.6$. The constraints on the most recent period of star formation thus depend on the assumed model for the star formation history. In particular, in the truncated star formation model the ages of the most recently formed galaxies are a factor of 2 lower than in the single burst model. This generic feature of the models can be derived analytically (cf. Appendix A).

The scatter in the colors of the S0s can be reproduced by the single burst model and the truncated star formation model (Fig. 5.14). In the single burst model, the youngest S0s formed at $z = 0.7$. The secondary burst model predicts a scatter of 0.035, if the mass fraction involved in the burst is 20 % and the bursts occur continuously up to $z = 0.33$. This is slightly lower than the observed scatter. Stronger bursts (involving mass fractions of ~ 25 %) are required to explain the observed scatter with this model. The truncated star formation model can reproduce the observed scatter if the youngest S0s were forming stars up to $z = 0.33$, the redshift of the cluster.

An important result is that all three models allow for quite recent star formation in the S0s in the outer part of the cluster. The formation time of the galaxies is pushed back furthest in the single burst model, but even in this model the youngest S0s formed as recently as $z \sim 0.7$.

Other Probability Distributions

The assumption in the preceding Section is that the probability distributions for the star formation events that characterize the models are simple top hats. Here, we investigate how stable our conclusions are when this assumption is relaxed. We consider two other probability distributions: an exponentially decreasing probability distribution, and a Gaussian. For simplicity, only single burst models are considered, and only the scatter in the ellipticals and the S0s in the core of the cluster is reproduced.

In Fig. 5.15 three probability distributions are shown that reproduce the scatter in the ellipticals and S0s in the core of CL 1358+62. The exponential distribution has the form $P = e^{-5t/t_{0.33}}$, where $t_{0.33}$ is the age of the universe at $z = 0.33$. The mean of the Gaussian is at $z = 2$, and the width is $0.13t_{0.33}$.

The formation time of the youngest galaxies is more difficult to define for other distributions than the top hat, since the Gaussian and exponential distribution have a tail extending to infinity. We calculated when 50 % and 75 % of the galaxies have formed assuming the three distributions (top hat, exponential, and an example of a Gaussian). The open dots indicate the time when 50 % of the galaxies have been formed, and the solid dots indicate the time when 75 % of the galaxies have been formed. In all the models ~ 25 % of the ellipticals and the S0 galaxies in the core of the cluster formed after $z = 2$. This is a generalization of the result that the youngest ellipticals and S0 galaxies in the core of the cluster formed at $z \sim 1.2$, which was derived for the top hat model in the previous Section.

Similar to the top hat distribution, the exponentially decreasing probability distribution has one free parameter, and is therefore fully determined by the observed scatter at $z = 0.33$. The Gaussian distribution has two free parameters: any Gaussian distribution that satisfies

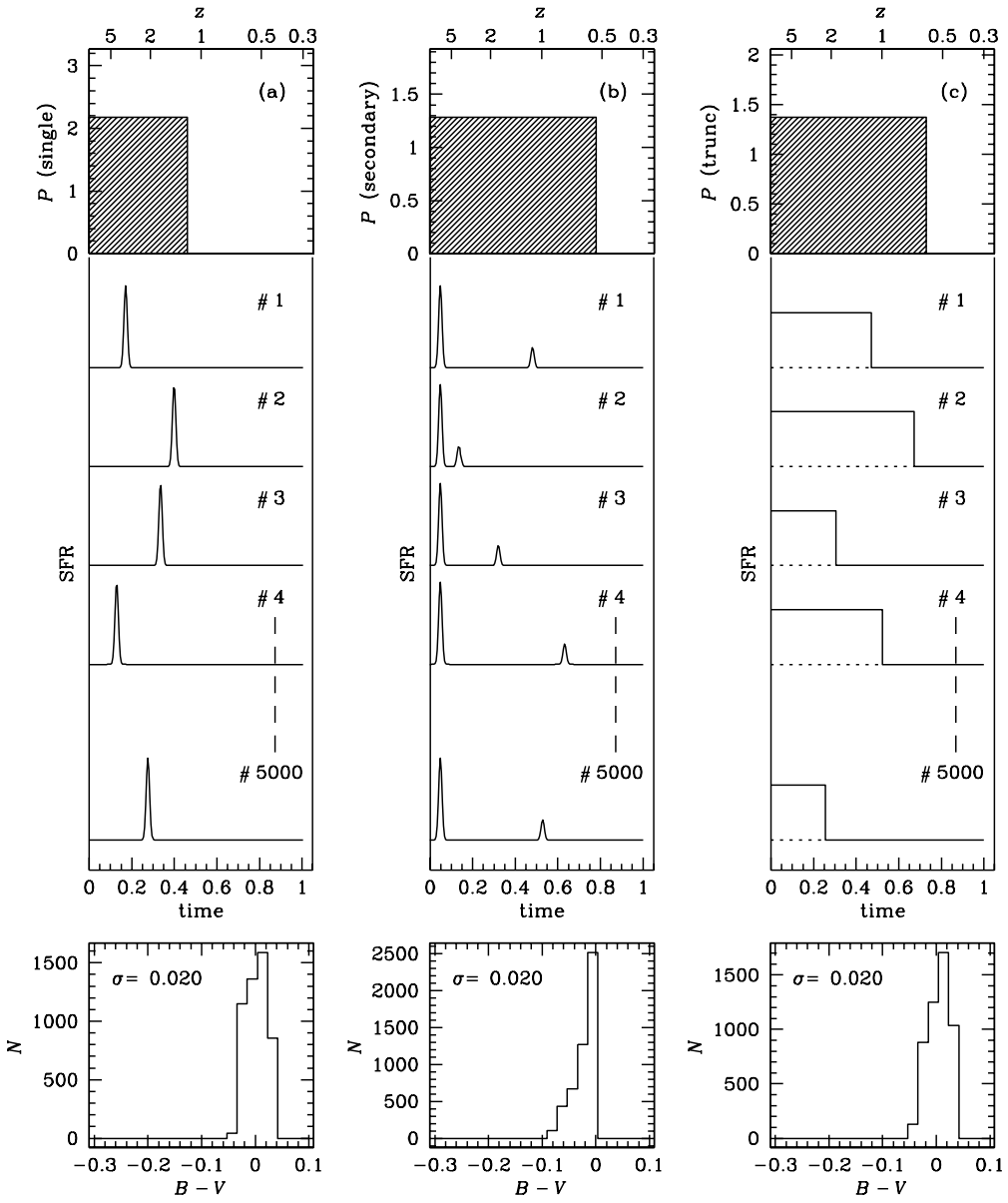

Figure 5.13: Reproduction of the scatter in the CM relation of the ellipticals (0.020) in three different models. In (a), galaxies form in a δ-peak at a random time between $t = 0$ and $t = 0.46$ ($z = 1.2$; $q = 0.5$). In (b), 80 % of the mass of the galaxies forms in a single burst at $t = 0$, and 20 % of the mass in a second burst at a random time between $t = 0$ and $t = 0.78$ ($z = 0.5$). In (c), the galaxies start forming stars at $t = 0$ and stop forming stars at a random time between $t = 0$ and $t = 0.73$ ($z = 0.6$). Note that t is scaled such that $t = 1$ corresponds to $z = 0.33$. The top panels show the probability distributions P for the events that characterize the models (single bursts, secondary bursts, truncation of star formation). The model color distributions at $z = 0.33$ are shown in the bottom panels, derived from Monte Carlo simulations with 5000 model galaxies. The constraints on the last period of star formation are very dependent on the model for the star formation history.

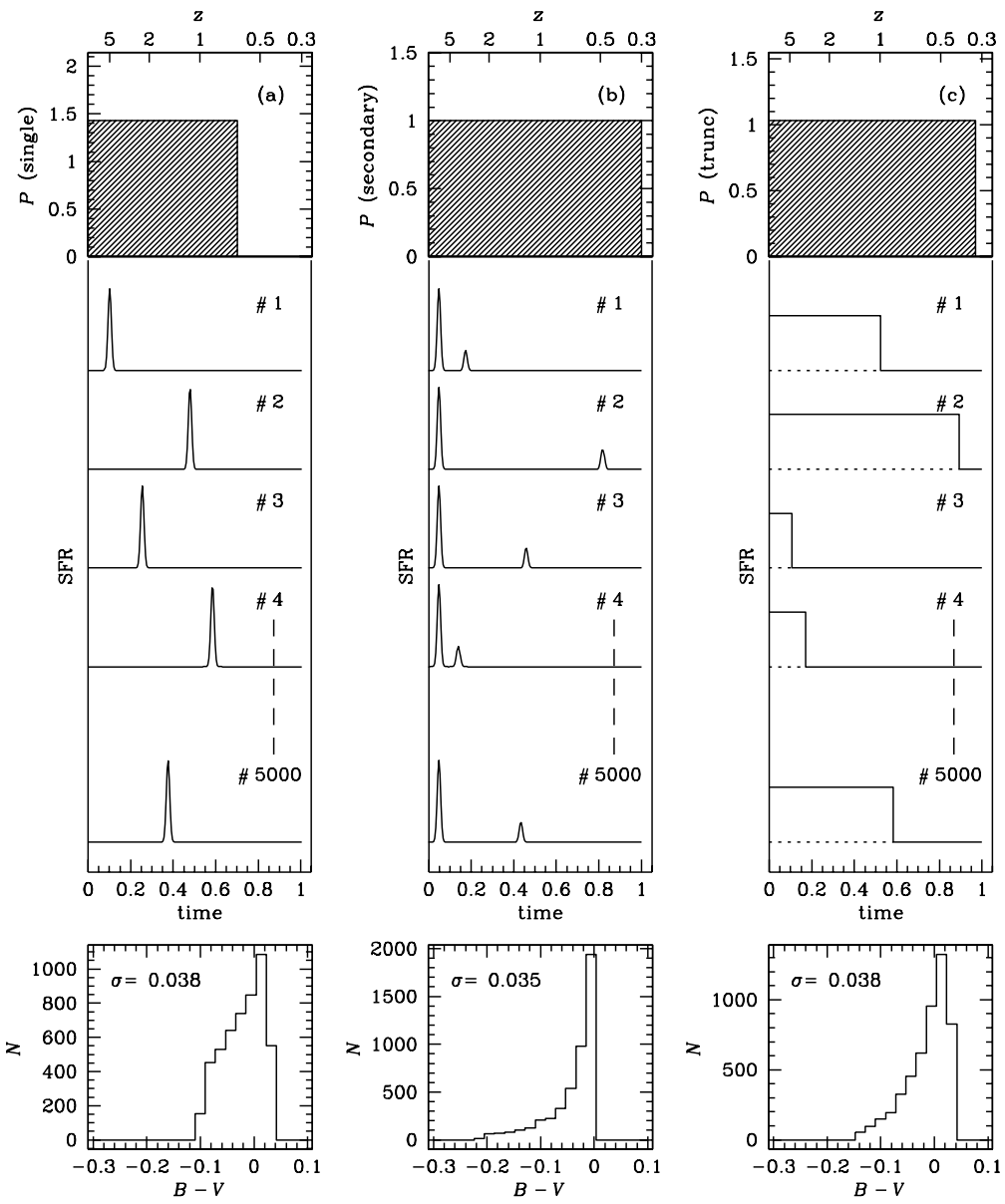

Figure 5.14: Reproduction of the scatter in the CM relation of the S0 galaxies in the outer parts (0.038) in three different models. In the single burst model, the youngest S0s formed at $z \approx 0.7$ (a). Secondary bursts involving 20 % of the mass that occur from $t = 0$ to the epoch of observation (b) predict a scatter that is somewhat lower than what is observed. The truncated star formation model (c) can reproduce the observed scatter if the youngest S0s were forming stars up to $z = 0.33$, the redshift of the cluster.

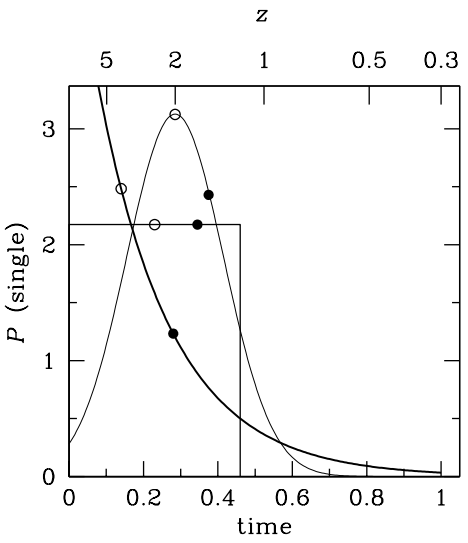

Figure 5.15: Three probability distributions for galaxy formation in single bursts of star formation that reproduce the observed scatter in the CM relation of the S0 galaxies in the core and the elliptical galaxies in CL 1358+62. Open dots indicate the times when 50 % of the galaxies have been formed, in each of the models. Solid dots indicate the times when 75 % of the galaxies have been formed.

the constraint $\sigma_t/(t_{0.33} - t') = 0.18$, where σ_t is the width of the Gaussian and t' is the mean, reproduces the observed scatter in the CM relation for the ellipticals and the S0s in the core of the cluster. We note that the Gaussian distribution has the general property that it allows for more recent star formation than the top hat or the exponential. In particular, the time when 75 % of the galaxies have been formed is always after $z = 2$, for any combination of σ_t and t'.

Constraints on the Scatter in the Luminosity Weighted Age

The constraint on the most recent period of star formation is very dependent on the model that is assumed for the star formation history (cf. Sect. 5.6.2). In particular, models with truncated continuous star formation allow for much later star formation than single burst models. Here, we investigate how well we can constrain the scatter in the mean ages and the mean luminosity weighted ages of the galaxies.

The scatter in the mean ages of the galaxies is also rather model dependent. In the models described in Sect. 5.6.2, $0.05 < \Delta\tau/\langle\tau\rangle < 0.20$ for the ellipticals, and $0.07 < \Delta\tau/\langle\tau\rangle < 0.35$ for the S0s in the outer parts of the cluster. This large range results from the fact that the color of a galaxy is mostly determined by the youngest stars that contribute most of the light.

The scatter in the *V* band luminosity weighted ages is better constrained. The expressions for the luminosity weighted ages τ_L for each of the models are given in the Appendix. For the ellipticals, the single burst model gives $\Delta \ln \tau_L = 0.18$, the truncated star formation model $\Delta \ln \tau_L = 0.16$, and the secondary burst model $\Delta \ln \tau_L = 0.13$. For the S0s in the outer parts, we find $\Delta \ln \tau_L = 0.35$ in the single burst model, and $\Delta \ln \tau_L = 0.30$ in the truncated star formation model.

Secondary burst models provide the strongest constraints on the scatter in the luminosity weighted ages; weaker but similar constraints are provided by the single burst model and in the truncated star formation models. The constraints on $\Delta \ln \tau_L$ are not very dependent on the distributions of the formation times and truncation times. The various probability distributions discussed in Sect. 5.6.2 give very similar results as the top hat distributions of Sect. 5.6.2. We consistently find $\Delta \ln \tau_L < 0.18$ for the ellipticals, and $\Delta \ln \tau_L < 0.35$ for the S0s in the outer part of the cluster. Since $\Delta \ln \tau_L = \Delta\tau_L/\langle\tau_L\rangle$, these numbers are a combined

constraint on the spread in ages of the galaxies, and the mean age of the galaxy population.

5.7 Evolution of the Scatter in the CM Relation

All of the models discussed in the previous Section reproduce the observed scatter in the CM relation of the ellipticals and S0s at $z = 0.33$. These models make very different predictions for the scatter in the CM relation at other redshifts. Therefore, in principle, the models can be constrained by observations of the scatter in the CM relation at different redshifts. In this Section, the predictions from the models discussed in Sect. 5.6.2 are compared to data from the literature on the central regions of the Coma cluster at $z = 0.02$, and the central regions of three clusters at $z \sim 0.55$. At present, there is no data available in the literature for the scatter in the CM relation of early-type galaxies in the outskirts of clusters, where we measure the high scatter for the S0 galaxies.

Figure 5.16(a,b) shows the predictions of the single burst and truncated star formation models in Sect. 5.6.2 for the evolution of the scatter in the CM relation with redshift. Predictions for the ellipticals and the S0s in the outer part of the cluster are shown. Note that the scatter is constant with time while the galaxies were being formed. For *any* continuous formation process the scatter is constant because it arises from $\Delta\tau/\langle\tau\rangle$, and the mean age of the galaxies increases at the same rate as the scatter in the ages. After the end of the formation phase of the galaxies, the scatter decreases monotonically, because the relative age differences between the galaxies become smaller. Therefore, a nearly constant scatter in the CM relation with redshift, such as observed by Stanford et al. (1998), implies that the galaxies either formed at very high redshift, or that galaxies are continuously formed and added to the sample.

For the ellipticals, it is not possible to distinguish between the truncated star formation model and the single burst model at $z \lesssim 0.8$. For the S0s in the outer parts, the predictions of the single burst model and the truncated star formation model discussed in Sect. 5.6.2 are already a factor two different at $z \geq 0.6$. Note that the scatter at $z = 0$ is not well constrained in the truncated star formation model (the broken line in Fig. 5.16b). The constraint is weak because the S0s are still forming at $z = 0.33$: the scatter may be as low as 0.015 at $z = 0$ if the production of S0s stops at $z = 0.33$, or remain constant at ~ 0.040 if the formation continues up to the present epoch.

The solid symbols indicate the observed scatter in the ellipticals (Fig. 5.16a) and the S0s in the outer parts of the cluster (Fig. 5.16b) at $z = 0.33$. The open symbols in Fig. 5.16(a) are derived from data for the central regions of the Coma cluster by Bower, Lucey, & Ellis (1992a,b), and from the Ellis et al. (1997) study of the CM relation in the cores of three clusters at $z \sim 0.55$. The Bower et al. (1992a) and Ellis et al. (1997) data are in restframe $U-V$. The color evolution in $U-V$ is a factor $1.5-2.5$ stronger than in $B-V$, depending on the metallicity (Worthey 1994). The $U-V$ data were transformed to $B-V$ through $\Delta U-V = 2\Delta B-V$.

As can be seen in Fig. 5.16(a), the measurements of the scatter at $z = 0.02$ and at $z = 0.55$ are consistent with the model predictions. The measurements we plot in Fig. 5.16(a) between $z = 0$ and $z = 0.55$ are in apparent conflict with Stanford et al. (1998), who found that the scatter in the "blue – red" (roughly $U-V$, cf. Stanford et al. 1998) CM relation in the cores of clusters out to $z \sim 0.9$ is approximately constant with redshift, at ~ 0.07, or equivalent to ~ 0.03 in $B-V$. The model predictions range from 0.02 at $z = 0.3$ to 0.045 at $z = 0.9$. However, judging from Fig. 6 in Stanford et al. (1998), their error bars are consistent with the modest increase in the scatter shown in Fig. 5.16(a).

We cannot compare our results for the scatter in the CM relation of the S0s in the outer

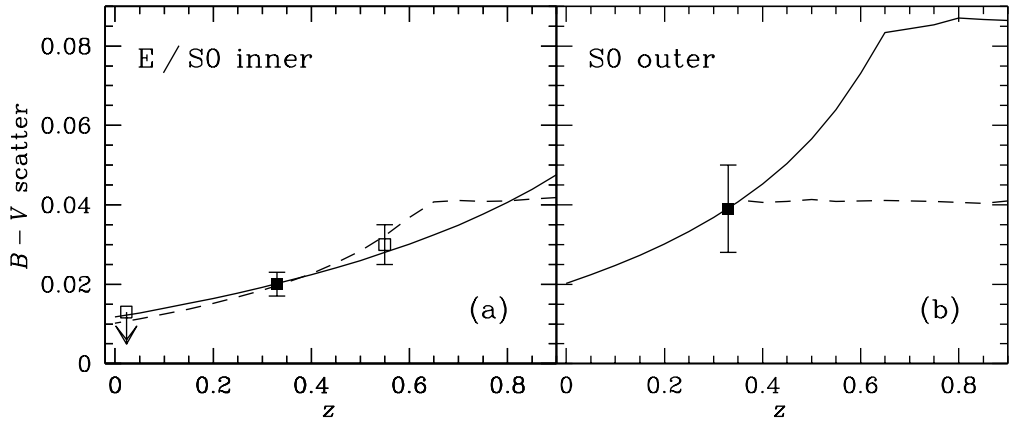

Figure 5.16: The evolution of the scatter in the CM relation. Solid symbols indicate the observed scatter of the ellipticals in CL 1358+62 (a), and of the S0s in the outer parts of CL 1358+62 (b). Open symbols in (a) represent the ellipticals in the core of the Coma cluster at $z = 0.02$ from Bower et al. (1992), and the ellipticals and S0s in the cores of three clusters at $z = 0.55$ from Ellis et al. (1997), transformed to restframe $B-V$. The lines are the predictions from the models discussed in Sect. 5.6.2. The models in (a) reproduce the scatter in the CM relation of the ellipticals in CL 1358+62, and of the S0s in the inner parts. The models in (b) reproduce the scatter of the S0s in the outer parts of CL 1358+62. Solid lines are single burst models, broken lines are truncated continuous star formation models (cf. Sect. 5.6.2). In the truncated star formation model of (b), the S0s are still forming at $z = 0.33$. Therefore, the scatter in the CM relation between $z = 0$ and $z = 0.33$ is not well constrained in this model.

part of the cluster to the above mentioned studies, since they do not extend far enough in radius ($R \sim 0.6 h_{50}^{-1}$ Mpc, compared to $R = 1.6 h_{50}^{-1}$ Mpc for our dataset). At present, large field photometric studies of the Coma cluster (e.g., Godwin et al. 1983, Mazure et al. 1988) are not sufficiently accurate to allow a meaningful comparison with the high z studies of the CM relation. Large field ground based studies of intermediate redshift clusters such as that of Abraham et al. (1996b) lack the resolution to determine galaxy morphologies, and sufficiently accurate colors. Our results, and those of Caldwell et al. (1993) for the Coma cluster, suggest that it may be of interest to extend accurate studies of the scatter in the CM relation of early-types to larger radii, at high and low redshift.

5.8 Infall and the Progenitors of Present-day Early-types

There is good evidence that many clusters of galaxies have significant substructure (e.g., Forman et al. 1981, Geller & Beers 1982, Dressler & Shectman 1988, White, Briel, & Henry 1993). This is consistent with theoretical predictions: it is expected that clusters accrete a significant amount of mass after their initial collapse (e.g., Gunn & Gott 1972, Evrard 1990, 1991, Frenk et al. 1996). During the accretion, it is likely that galaxies are transformed from star forming galaxies into non-star forming galaxies, to produce the passively evolving galaxies that are observed in rich clusters. The galaxies in which the star formation has been shut off will be observed as blue, non-star forming galaxies for a short period (~ 1 Gyr). These galaxies are expected to be more abundant in the outskirts of the cluster (Evrard 1991; Frenk et al. 1996). The blue early-type galaxies that we observe in CL 1358+62 may therefore

be recently accreted galaxies that have had their formation terminated upon entry.

The accretion process may be related to the Butcher-Oemler effect (e.g., Dressler & Gunn 1983, Butcher & Oemler 1984, Lavery & Henry 1994, Moore et al. 1996, Abraham et al. 1996b). It is often suggested that the Butcher-Oemler effect is caused by an enhanced accretion at higher redshifts (e.g., Kauffmann 1995). The cluster CL 1358+62 displays a mild Butcher-Oemler effect (Luppino et al. 1991; Fabricant et al. 1991), and it will be interesting to see whether the scatter of the early-type galaxies in the outer parts correlates with the Butcher-Oemler effect.

If galaxies are accreted from the field, with a subsequent cutoff in their star formation rate, then the set of non-star forming galaxies in clusters evolves with time. Hence the non-star forming galaxies at $z = 0.33$ are a subsample of the non-star forming galaxies at $z = 0$, for the same cluster. This evolution makes it harder to compare samples of early-type cluster galaxies at different redshifts: at high redshift there will be an observational bias towards the oldest progenitors of present day early type galaxies.

We calculate the importance of this effect by estimating the number of galaxies that will be added to the early-type galaxy population between $z = 0.33$ and $z = 0$. The subsample that is consistent with continuous accretion (the S0s in the outer parts of the cluster) comprises about $1/3$ of the early-type galaxy population of CL 1358+62. This implies that the accretion rate must have decreased considerably since the onset of the formation of the cluster, which is consistent with theoretical predictions (e.g., Lacey & Cole 1993, Kauffmann 1995). If we assume that the accretion rate remains constant after $z = 0.33$, we obtain an upper limit on the accreted and transformed fraction. For $q_0 = 0.5$ we derive that only $\sim 15\,\%$ of the early-type galaxy population at $z = 0$ has been added after $z = 0.33$. The main uncertainty is the limited field of view of our data.

The transformation rate is smaller when only bright galaxies are considered. As discussed in Sect. 5.5, the bluest galaxies have low luminosities. The most massive galaxies were therefore probably transformed into passively evolving systems at earlier times. It is difficult to add young bright galaxies to the cluster sample, even when we consider mergers. The merger of the two brightest galaxies that are more than 0.10 magnitudes bluer than the CM relation would produce a galaxy of $V_z \sim 19.3$. This galaxy would be placed among the brightest galaxies in CL 1358+62, but only for a short time. The luminosity of such a blue galaxy would be expected to fade by ~ 0.7 magnitudes, and the implication is that we have not (yet) observed the young progenitors of massive galaxies.

5.9 Summary and Conclusions

We have studied the color-magnitude relation in the rich cluster CL 1358+62 at $z = 0.33$. The elliptical galaxies in CL 1358+62 form a very homogeneous population: the observed scatter in the $B-V$ CM relation is only 0.024 magnitudes, and there is no evidence for an increase in the scatter with distance from the cluster center. We cannot presently exclude a small ($\lesssim 0.01$ magnitudes) trend in the mean color of the ellipticals.

The S0s are a more heterogeneous population. The scatter and the mean color of the CM relation are strong functions of galaxy distance from the cluster center. The CM relations of the ellipticals and the S0s in the inner parts of the cluster are very similar, as is the case for three clusters at $z \sim 0.55$ studied by Ellis et al. (1997). The S0s in the outer parts of CL 1358+62 are bluer by 0.02 magnitudes, and have a larger scatter than the S0s in the inner parts (0.043 vs. 0.021). Fig. 5.11 demonstrates that the mildly blue S0s avoid the cluster core. The morphologies of the mildly blue S0s are very similar to those of the red S0s (cf. Fig. 5.4 [Plate 3, page 57]). The very blue S0s generally have low luminosities.

The systematic blueing of the CM relation with radius has been observed before (in the cluster Abell 2390 at $z = 0.23$, by Abraham et al. 1996b), but this is the first time that the morphologies of the galaxies at large distances from the cluster center could be determined. Also, the colors in the study of Abraham et al. (1996b) are not accurate enough for the detection of the radial gradient in the scatter in the color-magnitude relation.

We have constructed a range of models to explain the scatter in the CM relation of the ellipticals and the S0s in the outer parts of the cluster. We find that truncated continuous star formation models allow for more recent star formation than single burst models. The youngest ellipticals formed before $z = 1.2$ if they formed in single bursts of star formation, and before $z = 0.6$ if they experienced a constant star formation rate until an abrupt truncation. In all models, the youngest S0s in the outer parts of the cluster formed stars until close to the epoch of observation. In the truncated star formation model, star formation in these galaxies continued until the epoch of observation.

The radial trend of the S0 colors is consistent with the hypothesis that galaxies and groups are continuously accreted from the field. In this picture, the blue S0s are the galaxies that have been accreted recently. The star formation in the infalling galaxies is turned off upon entering the cluster. The truncation of the star formation may be accompanied by a small star burst in the nucleus (e.g., Hernquist & Mihos 1995). This nuclear star burst would explain the blue bulges (and the small color gradients) that we see in many of the blue S0 galaxies (cf. Sect. 5.4). The accretion radius of the cluster is roughly $3\,h_{50}^{-1}$ Mpc (Carlberg, Yee & Ellingson 1997), which is just outside our HST mosaic. If the morphological transformation between spirals and S0s occurs before accretion into the denser regions of the cluster, while the galaxies are still in small groups, that process probably occurs at radii beyond the limit of our observations. This might explain the small fraction of spirals in this very rich cluster.

The continuous infall of field galaxies implies that the fraction of non-star forming galaxies in clusters evolves with time. This complicates the comparison between galaxy populations in high redshift clusters and local clusters. Assuming a constant accretion rate after $z = 0.33$, we estimate that $\sim 15\,\%$ of the present-day early-type galaxy population in clusters has been added between $z = 0.33$ and $z = 0$. We infer that the accretion rate was higher before $z = 0.33$, which is consistent with model predictions (e.g., Kauffmann 1995).

The infall and transformation process seems to affect mostly the faint end of the galaxy population: the bluest galaxies have low luminosities. There are a few bright early-types with slightly bluer colors than the CM relation. Their presence suggests that bright early-type galaxies with young populations may be found in clusters at higher redshifts.

The homogeneity of the ellipticals and luminous S0s suggests that their star formation had ceased before they were accreted onto the cluster. There are several possible mechanisms, e.g., the star formation may have ceased after the collapse of smaller subclumps (galaxy groups) in which the galaxies resided. Studies of early-type galaxies in the field will be valuable to determine the process that shuts off the star formation in bright early-types before they enter the cluster environment.

This study demonstrates the need for large field, high resolution observations of distant clusters. If only one HST WFPC2 pointing had been available, our conclusions would be quite different: inside $R = 80''$, there is no systematic difference in the scatter or offset of the CM relation for the ellipticals and the S0s. Additional wide field observations are needed to establish whether CL 1358+62 is typical of intermediate z clusters and to extend this study to higher redshifts. High quality data for nearby clusters extending over a wide field would also be valuable. It will be interesting to explore whether the differences between ellipticals and S0s, and the environmental dependence of the colors, are reflected in the Fundamental Plane of this cluster: the observed scatter of 0.043 in the S0 colors in the outer parts implies a scatter in the Fundamental Plane in the V band of $\sim 30\,\%$ in μ_e.

Acknowledgements

We thank the referee, Dr. Ian Smail, for his constructive comments, which improved the paper. Henk Hoekstra is thanked for a critical reading of the appendix. The University of Groningen and the Leids Kerkhoven-Bosscha Fonds are thanked for support. Support from STScI grants GO05989.01-94A, GO05991.01-94A, and AR05798.01-94A is gratefully acknowledged.

References

Abraham, R. G., van den Bergh, S., Glazebrook, K., Ellis, R. S., Santiago, B. X., Surma, P., & Griffiths, R. E. 1996a, APJS, 107, 1
Abraham, R. G., Smecker-Hane, T. A., Hutchings, J. B., Carlberg, R. G., Yee, H. K. C., Ellingson, E., Morris, S., Oke, J. B., & Rigler, M. 1996b, ApJ, 471, 694
Andreon, S., Davoust, E., & Heim, T. 1997, AA, 323, 337
Aragon-Salamanca, A., Ellis, R. S., Couch, W. J., & Carter, D. 1993, MNRAS, 262, 764
Barger, A. J., Aragon-Salamanca, A., Ellis, R. S., Couch, W. J., Smail, I., & Sharples, R. M. 1996, MNRAS, 279, 1
Beers, T. C., Flynn, K., & Gebhardt, K. 1990, AJ, 100, 32
Bender, R., Saglia, R. P., Ziegler, B., Belloni, P., Greggio, L., & Hopp, U. 1998, ApJ, 493, 529
Biretta, J., Ritchie, C., & Rudloff, K. 1995, STScI Science Report 95-06, A Field Guide to WFPC2 Image Anomalies
Bothun, G. D., & Gregg, M. D. 1990, ApJ, 350, 73
Bower, R. G., Lucey, J. R., & Ellis, R. S. 1992a, MNRAS, 254, 589
Bower, R. G., Lucey, J. R., & Ellis, R. S. 1992b, MNRAS, 254, 601
Butcher, H., & Oemler, A. 1978, ApJ, 219, 18
Butcher, H., & Oemler, A. 1984, ApJ, 285, 426
Caldwell, N., Rose, J. A., Sharples, R. M., Ellis, R. S., & Bower, R. G. 1993, AJ, 106, 473
Carlberg, R. G., Yee, H. K. C., & Ellingson, E. 1997, ApJ, 478, 462
Couch, W. J., & Sharples, R. M. 1987, MNRAS, 229, 423
Dressler, A. 1980, APJS, 42, 565
Dressler, A., & Gunn, J. E. 1983, ApJ, 270, 7
Dressler, A., & Shectman, S.A. 1988, AJ, 95, 985
Dressler, A., Oemler, A., Jr., Couch, W. J., Smail, I., Ellis, R. S., Barger, A., Butcher, H., Poggianti, B. M., & Sharples, R. M. 1997, ApJ, 490, 577
Ellis, R. S., Smail, I., Dressler, A., Couch, W. J., Oemler, A., Butcher, H., & Sharples, R. M. 1997, ApJ, 483, 582
Evrard, A. E. 1990, ApJ, 363,349
Evrard, A. E. 1991, MNRAS, 248, p8
Faber, S. M., Dressler, A., Davies, R. L., Burstein, D., Lynden-Bell, D., Terlevich, R., & Wegner, G. 1987, Faber S. M., ed., Nearly Normal Galaxies. Springer, New York, p. 175
Fabricant, D. G., McClintock, J. E., & Bautz, M. W. 1991, ApJ, 381, 33
Fisher, D., Fabricant, D., Franx, M., & van Dokkum, P. G. 1998, ApJ, 498, 195
Forman, W., Bechtold, J., Blair, W., Giacconi, R., Speybroeck, L., & Jones, C. 1981, ApJ, 243, L133
Franx, M., Illingworth, G., & Heckman, T. 1989, AJ, 98, 538
Frenk, C. S., Evrard, A. E., White, S. D. M., & Summers, F. J. 1996, ApJ, 472, 460
Geller, M. J., & Beers, T. C. 1982, PASP, 94, 421
Godwin, J. G., Metcalfe, N., & Peach, J.V. 1983, MNRAS, 202, 113
Gunn, J. E., & Gott, J. R. 1972, ApJ, 176, 1
Guzman, R., Lucey, J. R., Carter, D., & Terlevich, R. J. 1992, MNRAS, 257, 187
Hernquist, L., & Mihos, J. C. 1995, ApJ, 448, 41
Holtzman, J. A., Burrows, C. J., Casertano, S., Hester, J. J., Trauger, J. T., Watson, A. M., & Worthey, G. 1995, PASP, 107, 1065
Högbom, J. A. 1974, A&AS, 15, 417
Jørgensen, I., Franx, M., & Kjærgaard, P. 1993, ApJ, 411, 34
Jørgensen, I., & Franx, M. 1994, ApJ, 433, 553
Kauffmann, G. 1995, MNRAS, 274, 153

Kelson, D. D., van Dokkum, P. G., Franx, M., Illingworth, G. D., & Fabricant, D. 1997, ApJ, 478, L13 **[Chapter 3]**
Krist, J. 1995, in Astronomical Data Analysis Software and Systems IV, ASP Conference Series, 77, R. A. Shaw, H. E. Payne, and J. J. E. Hayes, eds., p. 349
Lacey, C., & Cole, S. 1993, MNRAS, 262, 627
Larson, R. B., Tinsley, B. M., & Caldwell, C. N. 1980, ApJ, 237, 692
Lavery, R. J., & Henry, J. P. 1994, ApJ, 426, 524
Leitherer 1995, ed., HST Data Handbook Version 2.0, STScI, Baltimore
Luppino, G. A., Cooke, B. A., McHardy, I. M., & Ricker, G. R. 1991, AJ, 102, 1
Mazure, A., Proust, D., Mathez, G., & Mellier, Y. 1988, A&AS, 76, 339
Moore, B., Katz, N., Lake, G., Dressler, A., & Oemler, A., Jr. 1996, Nature, 379, 613
Pence, W. 1976, ApJ, 203, 39
Pickles, A. J., & van der Kruit, P. C. 1991, A&AS, 91, 1
Poggianti, B. M., & Barbaro, G. 1996, A&A, 314, 379
Rakos, K. D., & Schombert, J. M. 1995, ApJ, 439, 47
Rix, H.-W., & White, S. D. M. 1990, ApJ, 362, 52
Saglia, R. P., Bertschinger, E., Baggley, G., Burstein, D., Colless, M., Davies, R. L., McMahan, R. K., Jr., & Wegner, G. 1997, APJS, 109, 79
Sandage, A., & Visvanathan, N. 1978, ApJ, 225, 742
Sérsic, J. L. 1968, Atlas de galaxias australes, Observatorio Astronómico de Córdoba, Argentina
Smail, I., Dressler, A., Couch, W. J., Ellis, R. S., Oemler, A., Jr., Butcher, H., & Sharples, R. M. 1997, APJS, 110, 213
Stanford, S. A., Eisenhardt, P. R., & Dickinson, M. 1998, ApJ, 492, 461
Thompson, L. A. 1986, ApJ, 306, 384
Tinsley, B. M. 1980, Fundam. Cosmic Phys., 5, 287
van Dokkum, P. G., & Franx, M. 1996, MNRAS, 281, 985 **[Chapter 2]**
White, S. D. M., Briel, U. G., & Henry, J. P. 1993, MNRAS, 261, L8
Whitmore, B. 1997, Photometry with the WFPC2, STScI, Baltimore
Worthey, G. 1994, APJS, 95, 107

5.A Models for the Color Evolution

5.A.1 Single Bursts

In this model the galaxies formed in single bursts of star formation at $t = t_0$. The luminosity evolution of a single age stellar population can be described by a power law:

$$L \propto \frac{1}{(t-t_0)^{\kappa}}, \tag{5.4}$$

with t the age of the universe at the epoch of observation, and t_0 the age of the universe at the time of formation of the population. The difference $t-t_0$ is the age of the population at the epoch of observation. The coefficient κ depends on the passband, but also on the metallicity Z and the IMF (Tinsley 1980; Worthey 1994).

The color evolution is

$$\frac{L_V}{L_B} \propto (t-t_0)^{\kappa_B-\kappa_V}, \tag{5.5}$$

or

$$B-V = 1.086(\kappa_B-\kappa_V)\ln(t-t_0)+C, \tag{5.6}$$

where we have set $B-V \equiv 2.5\log(L_V/L_B)$. The evolution of the color depends on the difference $\kappa_B-\kappa_V$, which is not very sensitive to differences in Z or the IMF. The Worthey (1994) models give $\kappa_B-\kappa_V \approx 0.10$ for $-2 < Z < 0.5$. In the single burst model, the scatter in the colors at time t is proportional to the scatter in $\ln(t-t_0)$.

5.A.2 Secondary Bursts

This model is an extension of the single burst model. A mass fraction $(1-f)$ forms in a burst at $t = t_0$, and a mass fraction f forms in a burst at $t = t_1$, with $t_1 > t_0$. The luminosity evolves as

$$L \propto \frac{1-f}{(t-t_0)^{\kappa}} + \frac{f}{(t-t_1)^{\kappa}}, \tag{5.7}$$

and the color as

$$\frac{L_V}{L_B} \propto \frac{(1-f)(t-t_0)^{-\kappa_V} + f(t-t_1)^{-\kappa_V}}{(1-f)(t-t_0)^{-\kappa_B} + f(t-t_1)^{-\kappa_B}}. \tag{5.8}$$

Expressed in magnitudes this is

$$B-V \approx 1.086(\kappa_B-\kappa_V)\ln(t-t_0) - 1.086\frac{f}{1-f}\left[\left(\frac{t-t_1}{t-t_0}\right)^{-\kappa_B} - \left(\frac{t-t_1}{t-t_0}\right)^{-\kappa_V}\right] + C, \tag{5.9}$$

where it is assumed that $f \ll \frac{t-t_1}{t-t_0}$, i.e., Eq. 5.9 is not valid shortly after a strong burst. In that case, the color evolution reduces to the single burst case (Eq. 5.6), with t_0 replaced by t_1.

The observed scatter in the colors can be expressed as a constraint on the relevance of star bursts. It is assumed the scatter in the colors is caused by a spread in ages of the bursts only (i.e., not by a spread in t_0 or f). Differentiating Eq. 5.9 with respect to $(t-t_1)$ gives an expression for the scatter in the colors as a function of the scatter in $(t-t_1)$:

$$\Delta(B-V) = 1.086\frac{f}{1-f}\left[\kappa_B\left(\frac{t-t_1}{t-t_0}\right)^{-\kappa_B-1} - \kappa_V\left(\frac{t-t_1}{t-t_0}\right)^{-\kappa_V-1}\right]\frac{\Delta(t-t_1)}{t-t_0}. \tag{5.10}$$

For $1.5 < (\kappa_B+\kappa_V) < 2$, a good approximation to Eq. 5.10 is

$$\Delta(B-V) \approx 1.086(\kappa_B-\kappa_V)\frac{f}{1-f}\left(\frac{t-t_0}{t-t_1}\right)^{1.5}\Delta\ln(t-t_1). \tag{5.11}$$

5.A.3 Truncated Star Formation

In this model the galaxies form stars at a constant rate from $t = t_0$ to $t = t_1$. The star formation is truncated at $t = t_1$. This model is appropriate for spiral galaxies in which the star formation suddenly terminates. The ages of the stellar populations in the galaxies range from $(t-t_0)$ to $(t-t_1)$. The contribution to the luminosity of each population is $dt_*(t-t_*)^{-\kappa}$. Therefore, the total luminosity after $t = t_1$ is

$$L \propto \frac{1}{t_1-t_0}\int_{t_0}^{t_1}\frac{dt_*}{(t-t_*)^{\kappa}}. \tag{5.12}$$

The factor $1/(t_1-t_0)$ normalizes the mass such that the mass of the galaxy after t_1 is independent of the length of the burst. For κ_B, $\kappa_V \neq 1$ the color evolution is

$$\begin{aligned}\frac{L_V}{L_B} &\propto \frac{1-\kappa_B}{1-\kappa_V}\left[(t-t_0)^{1-\kappa_V} - (t-t_1)^{1-\kappa_V}(t-t_0)^{1-\kappa_B} - (t-t_1)^{1-\kappa_B}\right] \qquad (5.13)\\ &= \frac{1-\kappa_B}{1-\kappa_V}(t-t_0)^{\kappa_B-\kappa_V}\left(\frac{t-t_1}{t-t_0}\right)^{\frac{1}{2}(\kappa_B-\kappa_V)}\frac{\left(\frac{t-t_1}{t-t_0}\right)^{-\frac{1}{2}(1-\kappa_V)} - \left(\frac{t-t_1}{t-t_0}\right)^{\frac{1}{2}(1-\kappa_V)}}{\left(\frac{t-t_1}{t-t_0}\right)^{-\frac{1}{2}(1-\kappa_B)} - \left(\frac{t-t_1}{t-t_0}\right)^{\frac{1}{2}(1-\kappa_B)}}.\end{aligned}$$

Since

$$\frac{x^{-\alpha}-x^{\alpha}}{x^{-\beta}-x^{\beta}} = \frac{\alpha\log x+\sum_{k=2}^{\infty}\frac{1}{(2k-1)!}(\alpha\log x)^{2k-1}}{\beta\log x+\sum_{k=2}^{\infty}\frac{1}{(2k-1)!}(\beta\log x)^{2k-1}} \approx \frac{\alpha}{\beta},$$

the color evolution reduces to

$$\frac{L_V}{L_B} \propto \left[\sqrt{(t-t_0)(t-t_1)}\right]^{\kappa_B-\kappa_V}. \tag{5.14}$$

In the truncated star formation model, galaxies are comprised of populations spanning a range of ages. The expression for the color evolution in this model is very similar to that for the color evolution in the single burst model (Eq. 5.5). However, the rate of evolution is determined by the geometric mean of the ages of the youngest stars and the oldest stars in the galaxy, rather than a single age.
Expressed in magnitudes, Eq. 5.14 reads

$$B-V = 0.543(\kappa_B-\kappa_V)\,[\ln(t-t_0)+\ln(t-t_1)]+C. \tag{5.15}$$

If it is assumed all galaxies have the same t_0, the scatter in the $B-V$ colors at time t only depends on the scatter in truncation times t_1.

5.A.4 Mean Ages

Here, we give expressions for the luminosity weighted mean ages τ_L in the three models. In the single burst model, all the stars have the same age, and therefore

$$\tau_L = t-t_0. \tag{5.16}$$

In the secondary burst model

$$\tau_L = \frac{(1-f)(t-t_0)^{1-\kappa}+f(t-t_1)^{1-\kappa}}{(1-f)(t-t_0)^{-\kappa}+f(t-t_1)^{-\kappa}}, \tag{5.17}$$

and in the truncated star formation model

$$\tau_L = \frac{1-\kappa}{2-\kappa}\left[\frac{(t-t_0)^{2-\kappa}-(t-t_1)^{2-\kappa}}{(t-t_0)^{1-\kappa}-(t-t_1)^{1-\kappa}}\right]. \tag{5.18}$$

5.B Correction for Luminosity Evolution

If the scatter in the CM relation is caused by age variations among the galaxies, the observed scatter in the CM relation is partly caused by the increased luminosity of young galaxies. The deviation for a given object in $B-V$ from the CM relation can be expressed as

$$\Delta(B-V)_{\rm obs} = \Delta(B-V)_{\rm evo}-\alpha\Delta V, \tag{5.19}$$

where α is the slope of the CM relation and ΔV is the amount of luminosity evolution for a color evolution of $\Delta(B-V)_{\rm evo}$. Since the relation between color evolution and luminosity evolution is

$$\Delta(B-V)_{\rm evo} = 1.086\left(\frac{\kappa_B}{\kappa_V}-1\right)\Delta V, \tag{5.20}$$

with κ_B, κ_V defined in Appendix A, it follows that

$$\Delta(B-V)_{\rm obs} = \left(1+\frac{\alpha}{1.086}\frac{\kappa_V}{\kappa_V-\kappa_B}\right)\Delta(B-V)_{\rm evo}. \tag{5.21}$$

The slope of the CM relation α = –0.018 (see Eq. 5.3). The Worthey (1994) models give $\kappa_B = 0.90$ and $\kappa_V = 0.80$ for solar metallicity. These values give a correction for the luminosity evolution of $\Delta(B-V)_{\rm evo} \approx 0.90\Delta(B-V)_{\rm obs}$.

6 A High Merger Fraction in the Rich Cluster MS 1054–03 at $z = 0.83$: Direct Evidence for Hierarchical Formation of Massive Galaxies[†]

ABSTRACT

We present a morphological study of the galaxy population of the luminous x-ray cluster MS 1054–03 at $z = 0.83$. The sample consists of 81 spectroscopically confirmed cluster members in a $3 \times 2\,h_{50}^{-1}$ Mpc area imaged in F606W and F814W with WFPC2. We find thirteen ongoing mergers in MS 1054–03, comprising 17 % of the $L \gtrsim L_*$ cluster population. Most of these mergers will likely evolve into luminous ($\sim 2L_*$) elliptical galaxies, and some may evolve into S0 galaxies. Assuming MS 1054–03 is typical for its redshift it is estimated that ~ 50 % of present-day cluster ellipticals experienced a major merger at $z < 1$. This implies that samples of ellipticals at $z \geq 1$ are special subsets of samples of low redshift ellipticals. The mergers are preferentially found in the outskirts of the cluster, and probably occur in small infalling clumps. Morphologies, spectra, and colors of the mergers show that their progenitors were typically E/S0s or early-type spirals with mean stellar formation redshifts $z_* \gtrsim 1.7$. The red colors of the merger remnants are consistent with the low scatter in the color-magnitude relation in rich clusters at lower redshift. The discovery of a high fraction of mergers in this young cluster is direct evidence against formation of ellipticals in a single "monolithic" collapse at high redshift, and in qualitative agreement with predictions of hierarchical models for structure formation.

[†]Pieter G. van Dokkum, Marijn Franx, Daniel Fabricant, Daniel D. Kelson, and Garth D. Illingworth, *Astrophysical Journal Letters*, submitted

6.1 Introduction

We do not know how and when luminous elliptical galaxies were assembled. Traditional models assume that all ellipticals are 10^{10} years old, and that they have experienced very little mass evolution after their initial collapse (e.g., Searle, Sargent, & Bagnuolo 1973). In contrast, galaxy formation models in cold dark matter (CDM) cosmologies predict that massive galaxies were assembled in many generations of mergers, and ellipticals experienced their last major mergers at $z < 1$ (Kauffmann 1996; Baugh, Cole, & Frenk 1996).

Ideally, the evolution of the mass function is determined directly from mass measurements of distant galaxies. An alternative approach is to determine the evolution of the merger fraction with redshift. Mergers in present-day rich clusters are rare because the probability of a low velocity encounter is small. Therefore, if cluster ellipticals formed in mergers, the mergers must have occurred before or during the initial collapse of the cluster (Roos & Aarseth 1982; Merritt 1984).

Morphological studies of intermediate redshift clusters have shown that mergers were indeed more common at earlier times (Lavery & Henry 1988 [LH88]; Lavery, Pierce, & McClure 1992 [LPM92]; Dressler et al. 1994 [D94]; Couch et al. 1998 [C98]). These studies indicate merger fractions of $\sim 5\,\%$ in clusters at $0.2 < z < 0.4$. However, since the mergers are generally blue and of low luminosity they are probably not very massive (e.g., C98). Furthermore, Dressler et al. (1997) suggest that disturbed galaxies in intermediate redshift clusters are generally disrupted disks rather than major mergers. These results indicate that massive cluster ellipticals were assembled at even higher redshift.

Recently it has become possible to extend morphological studies of rich clusters to $z \approx 1$ (e.g., Lubin et al. 1998). In this *Letter*, we present results from a large area survey of the x-ray selected cluster MS 1054–03 at $z = 0.83$. We determine the merger fraction using an I selected sample of 81 confirmed cluster members covered by a large HST WFPC2 mosaic. We assume $H_0 = 50\,\mathrm{km\ s^{-1}\ Mpc^{-1}}$ and $\Omega_0 = 0.3$.

6.2 Observations

The MS 1054–03 field was observed with LRIS (Oke et al. 1995) on the 10m Keck II telescope. Objects were selected on the basis of their I band flux ($20.0 < I < 22.7$). Spectra were taken through six multi-slit masks on 1998 February 28 and March 1. Exposure times were 2400 s for five of the masks and 1200 s for one mask. A cross-correlation program was used to determine redshifts for 186 galaxies in the MS 1054–03 field; 80 turned out to be cluster members. The redshifts were combined with the samples of Donahue et al. (1998) and Tran et al. (1999) giving a total of 89 confirmed cluster members.

We obtained a large HST WFPC2 mosaic of MS 1054–03, consisting of six independent pointings in two filters (F606W and F814W). Integration times were 6 500 s in each passband and at each position. 81 confirmed cluster members are located within the boundaries of the HST mosaic. Accurate magnitudes and colors were determined from the WFPC2 images. Morphological classifications were performed by PvD, MF, and DF, using the F814W images (restframe $\sim B$). The classification methods are described in detail in Fabricant et al. (in prep.) and van Dokkum et al. (in prep.).

6.3 Mergers at $z = 0.83$

The most surprising result of our survey of MS 1054–03 is the high fraction of galaxies classified as "merger/peculiar". We classified 17 % as mergers, compared to 22 % ellipticals, 22 % S0s, and 39 % spirals. Images of the mergers are displayed in Fig. 6.1(a) [Plate 5, page 60], which shows the sixteen most luminous galaxies in MS 1054–03 ordered by total I band luminosity, and Fig. 6.1(b), which shows all fainter mergers. The mergers display a variety of features: double nuclei (e.g., 997), tidal tails (e.g., 1760), and interacting doubles with distorted morphologies (e.g., 1340). The mergers are unresolved in our ground based images. We emphasize that all mergers are spectroscopically confirmed cluster members.

The merger fraction of 17 % is significantly higher than in clusters at lower redshift, as discussed in the Introduction. Furthermore, as demonstrated in Fig. 6.1 [Plate 5, page 60] the mergers in MS 1054–03 extend to high luminosities: five of the sixteen brightest galaxies were classified as mergers. Only seven out of sixteen were classified as ellipticals or S0s, two of which (1584 and 710) have a luminous companion within $20\,h_{50}^{-1}$ kpc. The median luminosity of the mergers is $M_B^T \approx -22$ ($\sim 2L_*$ at $z = 0.83$).

The majority of the mergers will probably evolve into elliptical galaxies (e.g., Toomre & Toomre 1972, Barnes 1998), thereby increasing the number fraction of massive ellipticals at later times. However, not all mergers form ellipticals. Simulations indicate that disks can survive mergers between galaxies of very different mass (Barnes 1998), and so some mergers may evolve into S0s (e.g., galaxy 1583). In most cases there is no evidence for the presence of gas to form a new disk: only 15 % of the mergers have EW [O II] 3727 Å > 5 Å.

Since the merger fraction is comparable to the elliptical fraction and merger timescales are short (< 1 Gyr; e.g., Rix & White 1989), the implication is that more than ~ 50 % of present-day cluster ellipticals (and probably a small fraction of S0s) were assembled in mergers at $z < 1$. A direct consequence is that samples of ellipticals at $z \geq 1$ are special subsets of samples of ellipticals at $z = 0$.

A possible concern is that some of the mergers are misclassified. Several show two galaxies separated by $\sim 1''$ ($10\,h_{50}^{-1}$ kpc) in a common envelope without obvious tidal features (e.g., galaxies 997 and 1163). One could argue that these objects are not bound, but chance projections along the line of sight. However, the probability of a chance projection within $1''$ is smaller than 10^{-3}. Furthermore, for the brightest mergers we can constrain the velocity differences between the galaxies from our spectroscopy. No double peaks were seen in the cross-correlation functions, implying $\Delta v < 500\,\mathrm{km\ s^{-1}}$. Both arguments are strong evidence that the galaxies are bound, and that we are witnessing mergers in progress.

6.4 Mechanism

The merger fraction in MS 1054–03 is surprisingly high, given the high velocity dispersion of the cluster ($\approx 1150\,\mathrm{km\ s^{-1}}$; Tran et al. 1999). Since the progenitors of the mergers must have had low relative velocities, the mergers are probably taking place in cold subclumps which are falling into the cluster. This is supported by the spatial distribution of the mergers, shown in Fig. 6.2. The mergers occur preferentially in the outskirts of the cluster, consistent with recent infall.

Furthermore, the cluster itself is irregular and elongated, as indicated by the iso-density contours in Fig. 6.2 and the x-ray distribution (Donahue et al. 1998). Our data suggest that the cluster consists of three clumps at the same radial velocity. We conclude that the mergers are possible because the cluster is viewed before final virialization, and hence before stripping of the halos of infalling subclumps.

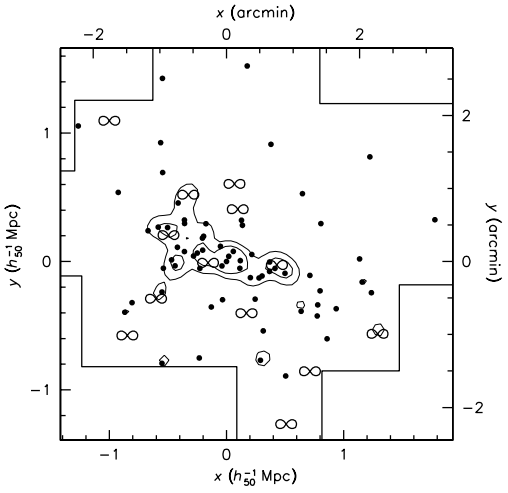

Figure 6.2: Spatial distribution of confirmed cluster members in MS 1054–03. Iso-density contours were derived from our photometric catalog. Note the filamentary galaxy distribution. Mergers are indicated by ∞ symbols. The mergers are preferentially found in the outskirts of the cluster, indicating they probably reside in cold infalling clumps.

6.5 Assembly Time versus Star Formation Epoch

In most cases the merging galaxies are bulge-dominated, red, and have no detected [O II] 3727 Å emission. Hence, they are mergers between ellipticals, S0s or Sas. The most striking examples of these (nearly) dissipationless mergers are galaxies 997 and 1163. In contrast to mergers in the nearby field (Liu & Kennicutt 1995), the star formation rate is very low, although several galaxies have enhanced Balmer lines indicating a modest star burst. A major puzzle is how and when the progenitors of the mergers lost their gas.

The ages of the mergers relative to the other cluster galaxies can be estimated from their location in the color-magnitude plane. Figure 6.3 shows the color-magnitude relation of confirmed members of MS 1054–03. Mergers are indicated with ∞ symbols. The median color of the mergers is modestly bluer (by ≈ 0.08 magnitudes in $U-B$) than the CM relation defined by the early-type galaxies, indicating that their luminosity weighted ages are $\approx 40\,\%$ lower (Worthey 1994). Assuming galaxies on the CM relation formed their stars at $z \geq 3$ (van Dokkum et al. 1998b), the stars in the mergers have a luminosity weighted mean formation redshift $z_* \gtrsim 1.7$. We conclude that the mean stellar ages of present-day cluster ellipticals are much larger than the ages of their last major mergers. We note in passing that only three of the mergers satisfy the Butcher & Oemler (1978) criteria for a blue galaxy. The blue fraction in MS 1054–03 is $\sim 20\,\%$; $\sim 75\,\%$ of the blue galaxies are spirals.

We test whether the colors of the mergers are consistent with measurements of the scatter in the CM relation at $z < 1$. The intrinsic scatter in the CM relation of the existing Es and E/S0s at $z = 0.83$ is low at 0.027 ± 0.013 in restframe $U-B$, consistent with the results of Stanford, Eisenhardt, & Dickinson (1998). The scatter in the combined sample of ellipticals and mergers (i.e., the sample of *future* ellipticals) is much higher, at 0.054 ± 0.011. This scatter will decrease at later times, because the fractional age differences between the galaxies will be smaller (e.g., van Dokkum et al. 1998a). We have evolved the CM relation forward in time using the simple models presented in van Dokkum et al. (1998a), and find that the $U-B$ scatter in the CM relation of ellipticals and mergers will be ≈ 0.035 at $z = 0.5$, and only ≈ 0.015 at $z = 0$. These numbers are consistent with the observed scatter in the CM relation at low and intermediate redshift (Bower, Lucey, & Ellis 1992; Ellis et al. 1997; Stanford et al. 1998; van Dokkum et al. 1998a).

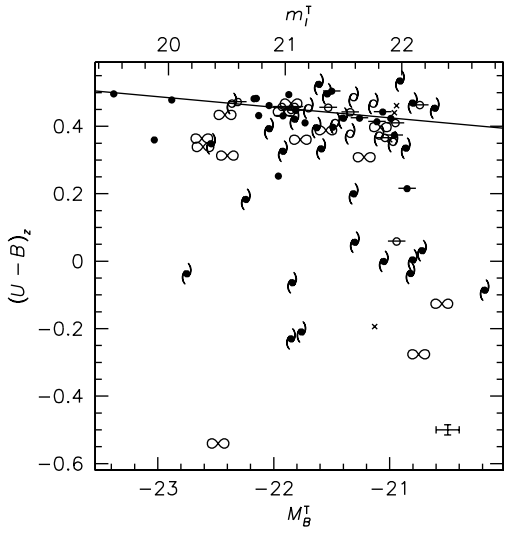

Figure 6.3: Color-magnitude relation of spectroscopically confirmed members of MS 1054–03. Mergers are indicated by ∞ symbols, ellipticals by solid circles. The mergers are only ≈ 0.08 magnitudes bluer than the CM relation defined by the early-type galaxies (solid line).

6.6 Discussion

The large number of mergers in MS 1054–03 implies strong evolution in the merger fraction from $z = 0$ to $z = 0.83$. This is illustrated in Fig. 6.4, which shows the evolution of the merger fraction in rich clusters with redshift. Solid symbols are CL 1358+62 at $z = 0.33$ and MS 1054–03 at $z = 0.83$. We determined the merger fraction in CL 1358+62 from a sample of 194 spectroscopically confirmed cluster members imaged with WFPC2 (van Dokkum et al. 1998a). The merger fraction in this cluster can be compared directly to that in MS 1054–03, since the sample selection, field size (in Mpc) and classification method are identical. Merger fractions for other rich clusters were estimated from the literature; in order of increasing redshift from Dressler (1980), LH88, C98, LPM92, and D94. These merger fractions are based on ground based imaging of blue galaxies (LH88, LPM92) or visual classifications of HST images (D94, C98). The evolution of the merger rate can be parameterized by $f \propto (1+z)^m$. We find $m = 6.0^{+0.5}_{-2.7}$. The best fit is indicated with the solid line.

It is interesting to compare the evolution of the merger fraction in clusters to that in the field. The broken line in Fig. 6.4 is a fit to the fraction of field galaxies in close pairs, from Patton et al. (1997). A direct comparison with the cluster data is difficult because the latter are based on visual classifications, which include both close pairs and merger remnants. We note, however, that these fractions are comparable in the outer parts of MS 1054–03. Although the normalization is uncertain, the *rate* of evolution can be compared directly. Both the cluster environment and the field show strong evolution. The evolution in clusters might even be stronger than in the field. This result is mainly driven by the very low merger fraction in low redshift clusters. The rapid evolution in the cluster environment could be due to an enhanced accretion rate onto clusters at high redshift, and/or enhanced merging during the collapse of massive clusters.

The increase with redshift of the merger rate of massive galaxies is in qualitative agreement with predictions from hierarchical galaxy formation models (e.g., Kauffmann 1996, Baugh et al. 1996), although it is a challenge to explain both the recent assembly of massive early-types and the early formation of their stars. The presence of the mergers in MS 1054–03 is direct evidence against formation of massive ellipticals in a "monolithic" collapse at very

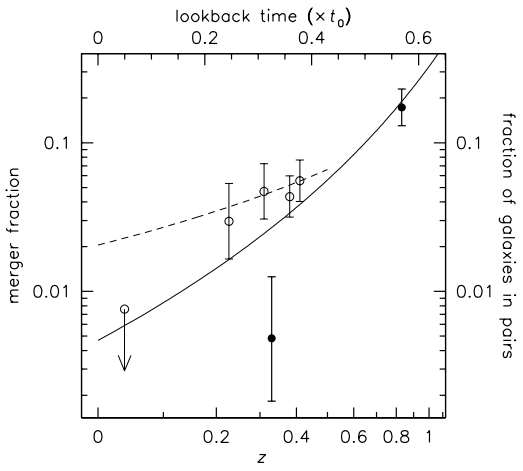

Figure 6.4: Evolution of the merger fraction in clusters. The solid symbols are the clusters CL1358+62 at $z = 0.33$ and MS 1054–03 at $z = 0.83$ from our study. Literature studies of rich clusters are indicated by open symbols. The solid line is a fit to the cluster data. The broken line is a fit to the fraction of field galaxies in close pairs from Patton et al. (1997). The merger fraction evolves rapidly in clusters and in the field, possibly even stronger in clusters.

high redshift.

Assuming merging does not alter the shape of the mass function, the mergers cause an increase in M_* of $\approx 15\,\%$. This can be contrasted to the strong evolution in the number density of massive field galaxies inferred by Kauffmann & Charlot (1998) from the lack of luminous K-band selected galaxies at $z > 1$. Although this result is still uncertain, the implication may be that massive galaxies in the field were assembled more recently than those in clusters.

This study demonstrates that large field studies with HST, in combination with deep spectroscopy from the ground, can show directly how galaxy formation proceeded. The large field was essential, since the mergers are preferentially located in the outskirts of the cluster. More wide field observations of high redshift clusters would be valuable to test whether MS 1054–03 is typical for its redshift. Studies of early-type galaxies in groups and the field at high redshift are necessary to establish whether their evolution has an environmental dependence.

Acknowledgements

Support from the University of Groningen, the Leids Kerkhoven-Bosscha Fonds, and STScI grants GO07372.01-96A and GO05991.01-94A is gratefully acknowledged.

References

Barnes, J. E. 1998, in After the Dark Ages: When Galaxies Were Young, 9th October Astrophysics Conference, University of Maryland, in press (astro-ph/9811242)
Baugh, C. M., Cole, S., & Frenk, C. S. 1996, MNRAS, 283, 1361
Bower, R. G., Lucey, J. R., & Ellis, R. S. 1992, MNRAS, 254, 601
Butcher, H., & Oemler, A. 1978, ApJ, 219, 18
Couch, W. J., Barger, A. J., Smail, I., Ellis, R. S., Sharples, R. M. 1998, ApJ, 497, 188 [C98]
Donahue, M., Voit, G. M., Gioia, I., Lupino, G., Hughes, J. P., Stocke, J. T. 1998, ApJ, 502, 550
Dressler, A. 1980, ApJ, 236, 351
Dressler, A., Oemler, A., Jr., Sparks, W. B., & Lucas, R. A. 1994, ApJ, 435, L23 [D94]
Dressler, A., Oemler, A., Jr., Couch, W. J., Smail, I., Ellis, R. S., Barger, A., Butcher, H., Poggianti, B. M., & Sharples, R. M. 1997, ApJ, 490, 577
Ellis, R. S., Smail, I., Dressler, A., Couch, W. J., Oemler, A., Jr., Butcher, H., & Sharples, R. M. 1997, ApJ, 483, 582
Kauffmann, G. 1996, MNRAS, 281, 487

Kauffmann, G., & Charlot, S. 1998, MNRAS, 297, L23
Lavery, R. J., & Henry, J. P. 1988, ApJ, 330, 596 [LH]
Lavery, R. J., Pierce, M. J., & McClure, R. D. [LPM] 1992, AJ, 104, 2067
Liu, C. T., & Kennicutt, R. C., Jr. 1995, ApJ, 450, 547
Lubin, L. M., Postman, M., Oke, J. B., Ratnatunga, K. U., Gunn, J. E., Hoessel, J. G., & Schneider, D. P. 1998, AJ, 116, 584
Merritt, D. 1984, ApJ, 276, 26
Oke, J. B., et al. 1995, PASP, 107, 375
Patton, D. R., Pritchet, C. J., Yee, H. K. C., Ellingson, E., & Carlberg, R. G. 1997, ApJ, 475, 29
Rix, H-W. R., White, S. D. M. 1989, MNRAS, 240, 941
Roos, N., & Aarseth, S. J. 1982, A&A, 114, 41
Searle, L., Sargent, W. L. W., & Bagnuolo W. G. 1973, ApJ, 179, 427
Stanford, S. A., Eisenhardt, P. R., & Dickinson, M. 1998, ApJ, 492, 461
Toomre, A., & Toomre, J. 1972, ApJ, 178, 623
Tran, K-V. H., Kelson, D. D., van Dokkum, P. G., Franx, M., Illingworth, G. D., & Magee, D. 1999, ApJ, in press
van Dokkum, P. G., Franx, M., Kelson, D. D., Illingworth, G. D. I., Fisher, D., & Fabricant, D. 1998a, ApJ, 500, 714 **[Chapter 5]**
van Dokkum, P. G., Franx, M., Kelson, D. D., & Illingworth, G. D. 1998b, ApJ, 504, L17 **[Chapter 4]**
Worthey, G. 1994, APJS, 95, 107

7 HST Photometry and Keck Spectroscopy of the Rich Cluster MS 1054–03 at $z = 0.83$

ABSTRACT

We present a photometric and spectroscopic study of the galaxy population of the rich X-ray cluster MS 1054–03 at $z = 0.83$. We obtained a large mosaic of HST WFPC2 images in two filters of this cluster. The Keck telescope was used to measure redshifts for 186 galaxies in the MS 1054–03 field. We present redshifts, morphologies, and accurate colors of 81 spectroscopically confirmed cluster members within the HST mosaic. We study the color-magnitude (CM) relation in MS 1054–03 as a function of morphology. The early-type galaxies in MS 1054–03 follow a remarkably tight and well defined relation, with observed scatter 0.032 ± 0.011 in restframe $U-B$. The slope and scatter of the relation are very similar to those of the nearby Coma cluster. There is no significant dependence of the CM relation on radius in the cluster, although the data are consistent with the trend observed in the colors of S0 galaxies in the cluster CL 1358+62 at $z = 0.33$. Early-type galaxies constitute only 44 % of the galaxy population. The remainder consists of spirals (39 %) and mergers (17 %). These last two classes have a larger scatter in their colors than the early-type galaxies, and are bluer on average. Using simple prescriptions for the star formation histories of the galaxies we evolve the CM relation at $z = 0.83$ forward in time. Assuming mergers evolve into early-types we find that the colors of local counterparts of the mergers are indistinguishable from other luminous cluster early-types. The evolution of the spirals is difficult to predict because they are still forming stars at $z = 0.83$. The low fraction of early-types in MS 1054–03 and the presence of mergers demonstrate that morphological evolution should be taken into account in models for the evolution of the scatter in the CM relation. A generic model with continuous formation of early-type galaxies between $0 < z < 2$ by truncation of star formation in their progenitors provides a good fit to the observed scatter at $0 < z < 1$, provided that galaxies are classified as early-types 1 Gyr after their star formation ceases.

7.1 Introduction

There is good observational evidence for evolution in the galaxy population of rich clusters. Examples are the Butcher-Oemler effect (Butcher & Oemler 1978, 1984), the large number of star forming and post starburst galaxies in intermediate redshift clusters (e.g., Dressler & Gunn 1983, Couch & Sharples 1987, Barger et al. 1996, Fisher et al. 1998, Poggianti et al. 1999), and the enhanced spiral fraction in clusters at $z \approx 0.5$ (Dressler et al. 1997).

Studies of the redshift evolution of the color-magnitude (CM) relation (Ellis et al. 1997; van Dokkum et al. 1998a; Stanford et al. 1998) and the Fundamental Plane (van Dokkum et al. 1998b) seem to be at odds with these results. The scatter and zeropoint of these relations provide constraints on the star formation epoch of galaxies (e.g., Bower, Lucey, & Ellis 1992 [hereafter BLE92], van Dokkum et al. 1998a). The scatter in the CM relation of early-type galaxies is very low, even in clusters at $z > 0.5$ (Ellis et al. 1997, Stanford et al. 1998). These results indicate an early and brief star formation epoch of early-type galaxies (e.g., Stanford et al. 1998). Similarly, the slow evolution of the zeropoint and slope of the CM relation (Stanford et al. 1995, 1998; Kodama et al. 1998) and the zeropoint of the Fundamental Plane (van Dokkum & Franx 1996, Kelson et al. 1997, Bender et al. 1998, van Dokkum et al. 1998b) suggest high formation redshifts of early-type galaxies. van Dokkum et al. (1998b) find that the luminosity weighted formation redshift of the stars in massive early-type galaxies $z_{\rm form} > 2.8$, for $q_0 = 0.15$ and a Salpeter IMF.

Because early-type galaxies dominate the galaxy population of local rich clusters (Dressler 1980) it seems hard to resolve this apparent conflict. However, as pointed out by, e.g., Franx & van Dokkum (1996) studies of early-type galaxies in high redshift clusters may suffer from selection effects. In particular, if early-type galaxies were formed in mergers or experienced star bursts samples of early-type galaxies at high redshift are special subsets of samples of low redshift early-types. In that case studies of the CM relation or the Fundamental Plane at high redshift are biased towards the progenitors of the oldest present-day early-types.

The importance of such biases can be quantified with large samples of spectroscopically confirmed galaxies in high redshift clusters. As an example, if mergers occur frequently at high redshift a fraction of the galaxy population is expected to be involved in these mergers. Mergers may take only a short time (e.g., Barnes 1998); therefore, large samples are required to determine the relevance of this process. Spectroscopic confirmation is crucial, because the field contamination among non-early-types is large and uncertain. In the absence of spectroscopy a field correction needs to be applied to determine the merger fraction in clusters. This field correction requires subtraction of a large uncertain number from another large number (see, e.g., Barger et al. 1996).

In van Dokkum et al. (1998a) we studied morphologies and the CM relation of a sample of 194 spectroscopically confirmed galaxies in the cluster CL 1358+62 at $z = 0.33$. A population of mildly blue S0s was found in the outskirts of the cluster. It was inferred that these galaxies had likely been accreted from the field and had thereafter stopped forming stars. The mildly blue S0s in CL 1358+62 are of low luminosity; massive cluster galaxies formed apparently formed at $z > 0.3$.

Recently it has become possible to study cluster galaxies out to $z \sim 1$ (e.g., Lubin et al. 1998, Postman et al. 1998). Here, we present a large area survey with the W. M. Keck Telescope and the Hubble Space Telescope (HST) of the cluster MS 1054–03 at $z = 0.83$. The most striking result of our survey is the discovery of a large number of luminous mergers. Properties of the mergers and implications of their existence are discussed in van Dokkum et al. (1999). In this paper, we present redshifts, morphologies, and accurate colors of all 81 spectroscopically confirmed cluster members within the $6' \times 4'$ HST field. The num-

ber of confirmed cluster galaxies observed with HST is second only to that of the cluster CL 1358+62 at $z = 0.33$ (van Dokkum et al. 1998a). Furthermore, we present the color-magnitude relation of this high redsfhift cluster and quantify the effects of morphological evolution on the observed scatter in the CM relation. We will assume $H_0 = 50\,\mathrm{km\ s^{-1}\ Mpc^{-1}}$ and $q_0 = 0.15$.

7.2 Data

7.2.1 Spectroscopy

We have conducted a spectroscopic survey of the MS 1054–03 field, using the LRIS spectrograph (Oke et al. 1995) on the 10 m W. M. Keck II Telescope. The main purpose of the survey was to measure redshifts for an I magnitude limited sample. In addition to the redshifts we have determined spectral types of the galaxies.

Sample Selection and Observations

Targets for the spectroscopy were selected from a photometric catalog of objects in the MS 1054–03 field. The catalog was created from a 900 s Keck I-band image of the cluster, centered on the Brightest Cluster Galaxy (BCG), and spanning $5' \times 7'$. The seeing in the image is $1\farcs0$. Objects were detected with FOCAS (Valdes et al. 1995). I band magnitudes were measured in a $3''$ diameter aperture. The resulting catalog contains 412 objects with $20.0 < I < 22.7$. These objects were selected as potential targets for the spectroscopy. The magnitude of the BCG is $I = 20.2$.

Six slitmasks were designed, with ~ 40 slitlets each. Objects with $20.0 < I < 22.2$ were given the highest priority. Objects located outside the boundaries of our HST mosaic (see Sect. 7.2.2) were given low priority irrespective of their magnitude. The positions and position angles of the masks were chosen to maximize the total number of slitlets within the HST mosaic.

The MS 1054–03 field was observed 1998 February 28 and March 1. All six slitmasks were exposed, using the 400 lines $\mathrm{mm^{-1}}$ grating blazed at 8500 Å, and $1\farcs2$ wide slits. Five masks were exposed for 2×20 minutes, and one mask for 20 minutes. The seeing was $\approx 0\farcs8$ during the observations, and conditions were photometric. The instrumental resolution, as measured from sky lines, is ≈ 7 Å FWHM at 7500 Å. The wavelength coverage depends on the position of the slitlet in the multislit mask, but is typically 5700 – 9500 Å. The [O II] 3727 Å doublet and the 4000 Å break redshifted to $z = 0.83$ are covered in all slitlets.

Reduction

The reduction involved bias subtraction, flatfielding, removal of cosmic rays, rectification, and sky subtraction. Critical steps in the reduction process were flatfielding and cosmic ray removal. Flatfielding is difficult because the Tektronix CCD has severe fringing at $\lambda \gtrsim 7500$ Å. The fringes have phases $\lambda \sim 20$ Å, and amplitudes to $\sim 8\,\%$. The signal-to-noise in the sky subtracted spectra critically depends on the ability to flatfield out the fringe pattern. For this reason we took flatfield exposures at a range of hour angles and grating angle settings, bracketing the hour angle and grating angle at the time of the observations. The flatfields that produced the lowest noise in the sky lines were used. This procedure reduced the amplitude of the fringes to $\approx 0.5\,\%$.

Cosmic rays were removed in a similar way as described by van Dokkum & Franx (1996). The galaxy spectra and sky lines were fitted with appropriate functions and subtracted. Pixels that deviated significantly from the expected noise in the subtracted functions were flagged as possible cosmic rays. Several slits in the masks were tilted in order to cover more than one object with the same slit. These tilted slits produced tilted sky lines in the 2D spectra, which were not completely removed by the fitting functions. Residuals from sky lines in these slits were removed interactively. After subtraction of the cosmic rays, the frames were carefully checked by eye to ensure that only cosmic rays were removed.

For each row in each slitlet a wavelength solution was obtained from the sky lines. Wavelengths of unblended sky lines (the [O I] 5577, 6300 Å lines and the OH P1 lines) were taken from the Osterbrock et al. (1996) catalog. The 2D galaxy spectra were corrected for the S-distortion and transformed to a common wavelength scale. The sky spectrum was determined from the edges of each slitlet, and subtracted. Finally, 1D spectra were extracted from the 2D spectra using APSUM in IRAF.

Redshifts and Completeness

A total of 256 spectra were extracted from the 2D data. This number includes objects that were unintentionally covered by slits pointed at other objects. Redshifts were measured from emission lines using SPLOT in IRAF, or determined from absorption lines using the cross-correlation routine XCSAO. For the cross-correlations two template spectra were used: the spectrum of the nearby early-type galaxy NGC 7331, and the spectrum of the E+A galaxy 209 in CL 1358+62 (Fisher et al. 1998). The galaxies and the templates were cross-correlated in the 3750 – 4500 Å restframe wavelength range. Redshifts could be determined from 200 spectra. Ten objects turned out to be stars, and four objects were observed twice. Therefore, the number of galaxies with redshifts is 186.

We investigate the completeness of the spectroscopic sample by comparing the number of galaxies with measured redshifts to the number of galaxies in the photometric catalog. Figure 7.1(a) shows the completeness as a function of I magnitude, calculated in ± 0.25 magnitude bins around each galaxy. The sample is 65 % complete for $20.0 < I < 22.2$, and 16 % complete for $22.2 \leq I < 22.7$. Within the boundaries of the HST mosaic the completeness is 73 % for $20.0 < I < 22.2$, and 17 % for $22.2 \leq I < 22.7$.

As is often the case in this type of survey (e.g., Lilly 1995, Fisher et al. 1998) the incompleteness at the faint end of the sample is primarily caused by sparse sampling, and not by the inability to measure redshifts of observed galaxies. The success rate of measuring the redshift of observed objects is plotted in Fig. 7.1(b). The success rate is still ≈ 80 % at $I = 22.7$. There are 34 galaxies with $20.0 < I < 22.7$ that were observed but do not have a redshift. It may be that a large fraction of these galaxies are red early-type galaxies in the cluster, since it is easier to determine the redshift of galaxies with emission lines. We test whether the ability to measure the redshift is a function of color in Fig. 7.2, which shows the distributions of confirmed cluster galaxies, confirmed field galaxies, and galaxies without redshift in the $R-I$ versus $B-R$ plane. The B and R magnitudes were determined from images kindly provided by G. Luppino (Luppino & Kaiser 1997); the $R-I$ and $B-R$ colors were normalized to the colors of the BCG. Only a small fraction of the galaxies without redshift have colors consistent with those of red early-types in the cluster. We conclude that the sample of spectroscopically confirmed cluster members is not significantly biased against red galaxies.

Figure 7.3 shows the redshift distribution. The peak at $z = 0.83$ is conspicuous, but we also find peaks at lower redshifts. In particular, there is a concentration of 14 galaxies at $z = 0.547$, with a dispersion of only ~ 200 km s^{-1}. MS 1054–03 is well separated from the field in redshift space. In the redshift range $0.78 < z < 0.87$ all galaxies have redshifts in the

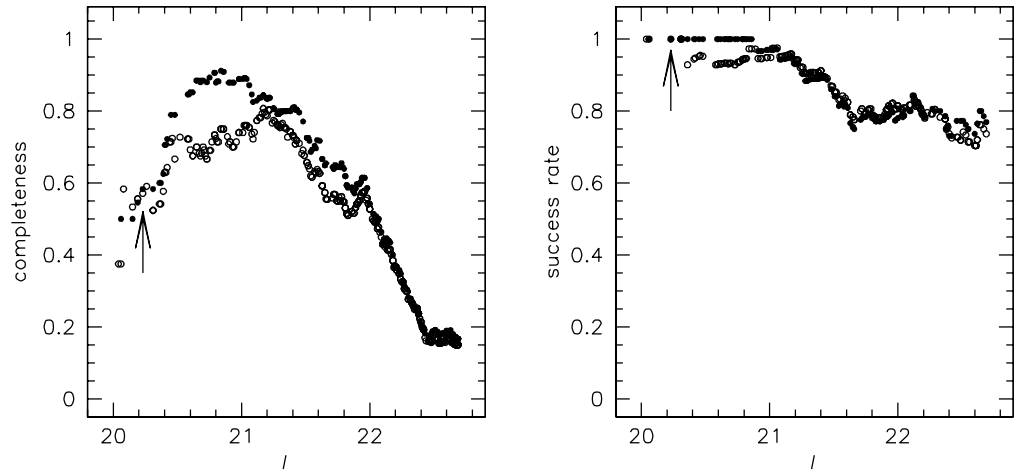

Figure 7.1: (a) The completeness as a function of magnitude, calculated by dividing the number of galaxies with measured redshift by the number of galaxies in the photometric catalog, in ± 0.25 mag bins centered on each galaxy. Open symbols are for the full sample, solid symbols for objects covered by our HST imaging. The arrow indicates the BCG. In (b), the success rate of measuring the redshift of observed objects is plotted.

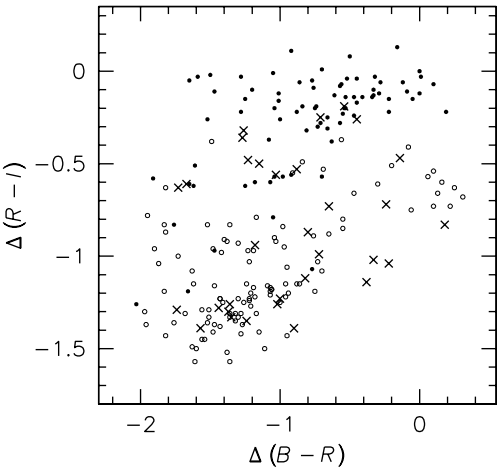

Figure 7.2: The distribution in the $R-I$ versus $B-R$ plane of spectroscopically confirmed cluster galaxies (filled circles), spectroscopically confirmed field galaxies (open circles), and observed galaxies for which no redshift could be obtained (crosses). The sample of spectroscopically confirmed cluster members is not biased against red galaxies.

interval $0.8132 < z < 0.847$, i.e., within $\pm 2.7\sigma_{\rm cl}$ (Tran et al. 1999). The distinction between cluster galaxies and field galaxies is therefore unambiguous.

The number of cluster members in our spectroscopic sample is 80. Their redshifts are listed in Table 1. Two of the cluster members were observed serendipitously, in slits pointed at other objects. These galaxies have $I \sim 24$, and will not be considered in our subsequent analysis. The total number of spectroscopically confirmed members of MS 1054–03 is now 89. This number includes 3 galaxies from Donahue et al. (1998), 3 galaxies from Tran et al. (1999), and 3 galaxies from van Dokkum et al. (in prep).

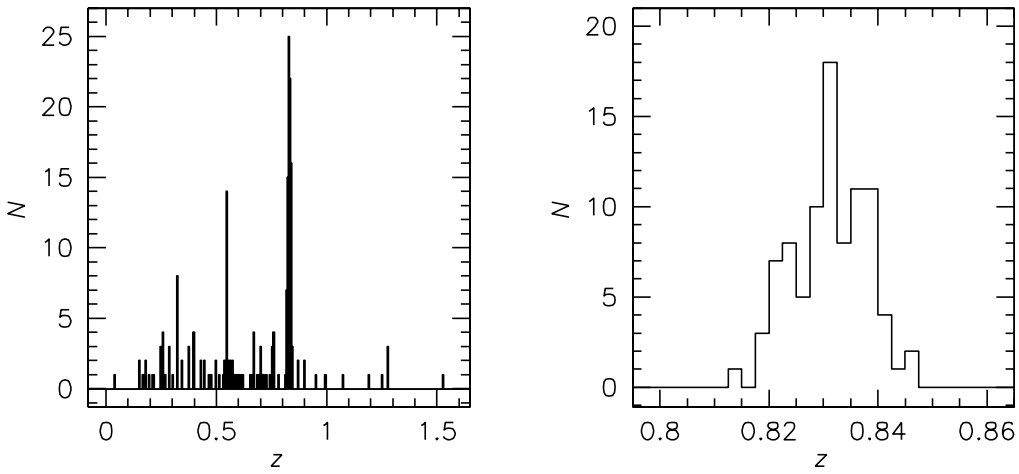

Figure 7.3: Redshift distribution of galaxies in our spectroscopic sample. The peak at $z = 0.83$ is conspicuous, and well separated from the field. We find at least two peaks at lower redshifts.

Spectral Types

We have measured equivalent widths of the [O II] 3727 Å emission line and the Hδ 4102 Å Balmer line. The strength of the [O II] line is a measure of ongoing star formation, and the strength of the Hδ line of recent star formation activity (e.g., Barbaro & Poggianti 1997). We used line strength index definitions of Fisher et al. (1998). EW Hδ is positive if in absorption, and EW [O II] 3727 Å is positive if in emission. The restframe equivalent widths and their associated errors are listed in Table 1. For most galaxies the errors are a few Å.

Based on the strengths of [O II] and Hδ spectral types were assigned to the galaxies. The definitions of the spectral types are analogous to those of Fisher et al. (1998). The spectral types are "absorption", "emission", and "E+A" (Dressler & Gunn 1983). Emission line galaxies have EW [O II] ≥ 5 Å. Galaxies with EW [O II] < 5 Å and EW H$\delta \geq 4$ Å are "E+A" galaxies. The spectral types are listed in Table 2. Spectral types which are 1σ removed from another spectral type (as determined from the errors in EW [O II] 3727 Å and EW Hδ) are labeled with a question mark.

In our restframe *B* selected sample of 78 cluster galaxies, there are 52 absorption line galaxies (67 %), 15 emission line galaxies (19 %), and 11 E+A galaxies (14 %). The number fractions of the various spectral types are not significantly different from those in intermediate redshift clusters (e.g., Couch & Sharples 1987, Balogh et al. 1998, Fisher et al. 1998, Poggianti et al. 1999). The fraction of emission line galaxies in MS 1054–03 is significantly lower than that of the optically selected massive cluster CL 1604+4304 at $z = 0.89$, as determined by Postman et al. (1998). These authors find that 11 out of 22 cluster galaxies have EW [O II] > 15 Å. In contrast, only 7 out of 78 galaxies in MS 1054–03 have EW [O II] > 15 Å. We note, however, that the Postman et al. (1998) sample extends to fainter magnitudes than our sample. Furthermore, our sample was selected in restframe *B* and the Postman et al. (1998) sample in restframe *U*. Finally, CL 1604+4304 is an optically selected cluster whereas MS 1054–03 was selected in X-rays.

As shown in Fig. 7.4 the emission line galaxies in MS 1054–03 are less concentrated toward the center of the cluster than the other galaxies. The fraction of emission line galaxies

TABLE 1
SPECTROSCOPIC DATA

Id	z	EW Hδ	error	EW O II	error	type
514	0.8398	–2.5	3.0	–4.4	3.2	abs
564	0.8322	3.2	4.0	39.0	6.8	emi
573	0.8362	3.7	2.8	1.0	3.1	abs?
661	0.8470	1.0	2.1	5.4	2.2	emi?
675	0.8417	3.2	2.3	1.9	3.1	abs?
696	0.8322	1.4	1.4	–0.2	1.5	abs
703	0.8323	–0.5	3.8	–1.1	3.7	abs
710	0.8344	0.4	1.2	1.2	1.5	abs
742	0.8307	0.3	2.7	2.7	3.0	abs?
777	0.8323	3.7	1.6	–2.9	1.9	abs?
793	0.8276	5.3	2.6	2.4	3.1	E+A?
796	0.8235	2.9	1.6	–0.8	1.8	abs?
997	0.8389	0.2	0.7	1.0	0.8	abs
1035	0.8307	8.1	2.4	4.3	2.9	E+A?
1088	0.8184	1.0	2.5	–3.1	2.1	abs
1091	0.8449	3.7	1.6	4.6	2.5	abs?
1103	0.8222	5.7	1.9	5.0	1.9	E+A?
1114	0.8317	0.5	2.2	–2.1	2.6	abs
1119	0.8225	–4.2	3.0	–4.1	2.3	abs
1163	0.8338	3.7	1.2	1.1	1.7	abs?
1198	0.8313	1.7	2.4	5.2	2.9	emi?
1209	0.8379	2.5	1.5	0.4	2.0	abs?
1215	0.8394	2.2	1.7	3.4	2.3	abs?
1280	0.8372	0.4	1.3	–0.3	1.7	abs
1294	0.8352	–2.5	1.0	–0.3	1.1	abs
1298	0.8363	1.5	2.7	5.9	4.3	emi?
1304	0.8335	2.6	1.3	–0.4	1.6	abs
1305	0.8209	0.5	3.0	–4.2	2.5	abs?
1325	0.8311	2.1	1.0	–0.8	1.2	abs
1329	0.8352	3.2	2.5	3.5	3.8	abs?
1340	0.8403	2.7	3.1	5.1	3.6	emi?
1355	0.8355	1.1	1.3	–2.5	1.7	abs
1359	0.8180	0.9	1.7	–1.7	1.6	abs
1396	0.8299	–2.6	2.1	–3.5	2.6	abs
1403	0.8132	2.8	1.9	14.7	2.2	emi
1405	0.8363	1.2	1.4	0.6	2.0	abs
1406	0.8206	–2.2	1.8	2.8	1.8	abs
1422	0.8330	–2.8	2.9	2.5	2.2	abs
1430	0.8240	5.4	1.2	–0.3	1.3	E+A
1434	0.8248	–1.8	2.3	–4.5	2.0	abs
1435	0.8197	0.9	2.6	–0.8	2.7	abs
1439	0.8213	4.2	2.8	–2.3	2.6	E+A?
1457	0.8420	2.7	1.2	–3.8	1.3	abs
1459	0.8461	5.6	0.9	5.9	1.2	emi?
1477	0.8274	1.2	2.6	4.5	3.0	abs?
1481	0.8258	–0.6	2.0	–4.4	2.0	abs
1484	0.8318	1.0	1.0	–0.1	1.2	abs

TABLE 1 (CONTINUED)

Id	z	EW Hδ	error	EW O II	error	type
1486	0.8332	0.1	3.4	−3.8	4.0	abs
1492	0.8280	1.1	2.4	−1.1	2.5	abs
1493	0.8334	2.9	2.9	0.6	3.6	abs?
1519	0.8301	1.4	2.1	−4.5	2.3	abs
1520	0.8310	0.1	2.7	1.5	2.8	abs
1567	0.8279	3.4	1.3	−2.3	1.4	abs?
1583	0.8261	6.9	0.6	0.4	0.7	E+A
1584	0.8313	−0.4	1.6	1.1	2.1	abs
1585	0.8369	4.4	3.1	3.8	3.3	E+A?
1635	0.8363	1.3	1.7	−1.7	2.7	abs
1639	0.8377	5.4	2.0	8.1	2.3	emi
1650	0.8294	7.1	2.8	3.9	3.1	E+A?
1651	0.8241	0.7	3.5	−3.4	3.6	abs?
1656	0.8223	2.0	1.3	0.2	1.5	abs
1692	0.8253	1.7	2.9	1.6	3.0	abs?
1701	0.8317	1.2	1.7	−3.7	2.0	abs
1733	0.8347	0.5	4.9	23.0	5.6	emi
1758	0.8374	5.1	2.4	−3.0	3.4	E+A?
1760	0.8246	5.6	1.2	1.3	1.4	E+A
1763	0.8390	3.9	4.1	20.8	4.7	emi
1801	0.8328	0.6	1.1	51.9	1.6	emi
1834	0.8394	7.6	1.3	3.1	1.8	E+A
1855	0.8210	2.7	2.4	17.8	3.8	emi
1896	0.8227	2.5	3.4	20.6	3.1	emi
1929	0.8400	2.8	1.5	−2.7	1.7	abs?
1942	0.8307	1.8	1.2	2.1	1.5	abs
1986	0.8253	0.4	1.5	0.1	1.7	abs
2011	0.8413	−4.2	3.2	32.5	3.4	emi
2130	0.8250	3.1	4.2	10.2	4.5	emi
2152	0.8319	−0.8	1.0	2.8	0.8	abs
2174	0.8382	−1.6	2.6	−2.4	3.3	abs
1888X	0.8286	−11.8	9.2	66.5	14.9	emi
2297X	0.8240	−1.4	5.8	64.0	11.9	emi

is 6 % within a radius of $0.5\,h_{50}^{-1}$ Mpc, and 31 % outside $R = 0.5\,h_{50}^{-1}$ Mpc. These numbers are similar to those found for low and intermediate redshift clusters (e.g., de Theije & Katgert 1999, Balogh et al. 1998). The E+A galaxies in MS 1054–03 seem to reside at intermediate radii, also similar to what is found at lower redshift (Fisher et al. 1998).

7.2.2 HST WFPC2 Imaging

We have obtained a large HST WFPC2 mosaic of MS 1054–03, consisting of six slightly overlapping pointings in two filters. The MS 1054–03 field was observed with the F606W and F814W filters on 1998 May 30. Six exposures were taken in each filter and at each position, giving a total of 72 exposures. In order to improve the sampling the six exposures at each position were split in two sets of three, with relative offsets between the sets of 5.5

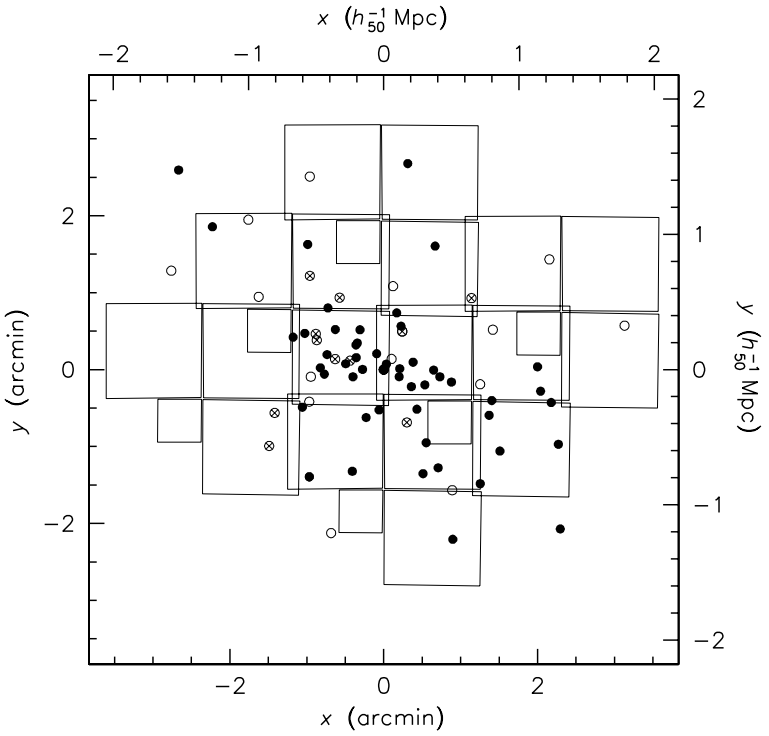

Figure 7.4: Spatial distributions of galaxies with different spectral types. Filled circles are absorption line galaxies, open circles are emission line galaxies, and open circles with crosses are E+A galaxies. The emission line galaxies have a less concentrated distribution than the other galaxies. The layout of the HST WFPC2 mosaic is overplotted.

pixels in x and y. Furthermore, the three exposures in each set were shifted relative to each other by ± 3.0 pixels, to facilitate the identification of hot pixels. Total exposure times were 6500 s in each filter for each pointing. The layout of the field is shown in Fig. 7.4, and Fig. 7.5 [Plate 6, page 61]. The area of the mosaic is 25 arcmin^2, or $8\,h_{50}^{-2}$ Mpc^2.

Reduction

The pipeline reduction was performed at the Space Telescope Science Institute (STScI). Further processing involved masking of bad pixels and bad columns, shifting the exposures to a common position on the sky, sky subtraction, identifying cosmic rays and hot pixels, and combining the images.

The most labour intensive step in this process is the cosmic ray removal. We experimented with the CRREJECT task in the STSDAS package, but found that the quality of the combined image is quite sensitive to the choice of input parameters. In particular, the noise in the final combined image can be higher than expected from the noise in the individual input images.

We followed therefore a different strategy. We compared the exposures with integer pixel shifts in each set of three, and removed cosmic rays in several steps. First, the expected noise $\sigma_{\rm exp}$ in each pixel was calculated from the minimum of the three exposures. Then, the task GCOMBINE was used to identify cosmic rays, with $\sigma_{\rm exp}$ as the input noise model. The output

of GCOMBINE is a cosmic ray cleaned average of the three exposures, an image containing the number of cosmic rays found, and an output noise map $\sigma_{\rm true}$ based on the actual variation in each pixel. Finally, the noise model and the measured noise were compared to identify pixels affected by cosmic rays in two of the three exposures. The method proved to work very well. In particular, in no cases were the central pixels of stars or galaxies mistaken for cosmic rays.

After identifying the cosmic rays each set of three exposures with integer pixel shifts was averaged, excluding the flagged pixels. As a result there are two images of each field and in each filter, shifted with respect to each other by 5.5 pixels. The images separated by 5.5 pixels were interlaced, producing one image of each field in each filter, with a resolution of $0\farcs071\,{\rm pixel}^{-1}$. Interlacing leaves the pixel values intact, and there is no loss of information. The interlacing procedure is explained in detail in the Appendix.

A color image of the full HST mosaic is shown in Fig. 7.5 [Plate 6, page 61]. The red cluster galaxies are conspicuous. The cluster is elongated, and has significant substructure.

Photometry

There are 81 spectroscopically confirmed cluster members in the HST WFPC2 mosaic. Figure 7.6 shows the F814W images of these galaxies, at $0\farcs1$ resolution. Total ("best") magnitudes of these galaxies were determined from the HST data using the SExtractor program (Bertin & Arnouts 1996). Colors were determined from the HST data using PHOT in IRAF. The colors were measured within the effective radii of the galaxies, which were derived from fits of the galaxy images to $r^{1/4}$ laws convolved with the PSF (see van Dokkum et al. 1998a). In order to limit the influence of the HST WFPC2 PSF, the images were CLEANed (Høgbom 1974; see Appendix) before these measurements.

The observed F606W and F814W bands roughly correspond to restframe U and B for objects redshifted to $z = 0.83$. Following the method outlined in van Dokkum & Franx (1996) transformations were computed from the observed bands to redshifted B (denoted B_z), and $(U-B)_z$ colors:

$$B_z = F814W - 0.03(F606W - F814W) + 1.23 \tag{7.1}$$

$$(U-B)_z = 0.76(F606W - F814W) - 1.14. \tag{7.2}$$

The zero points of the $F814W$ and $F606W$ filters are taken from the HST Data Handbook (STScI, Baltimore). Total B_z magnitudes were converted to total absolute $M_B^{\rm T}$ magnitudes using $H_0 = 50\,{\rm km\,s^{-1}\,Mpc^{-1}}$ and $q_0 = 0.15$.

The photometric accuracy can be assessed empirically, by comparing the two independent measurements of colors of objects in the overlapping regions between the six HST pointings. From this comparison we find that the average photometric uncertainty in the color is 0.016 for a single measurement. In our analysis of the scatter in the CM relation, this number is subtracted in quadrature from the measured scatter.

7.3 Morphologies

7.3.1 Visual Classifications

The $F814W$ HST WFPC2 images of spectroscopically confirmed members were visually classified by three of us (PGvD, MF, and DF). The images were compared to images of

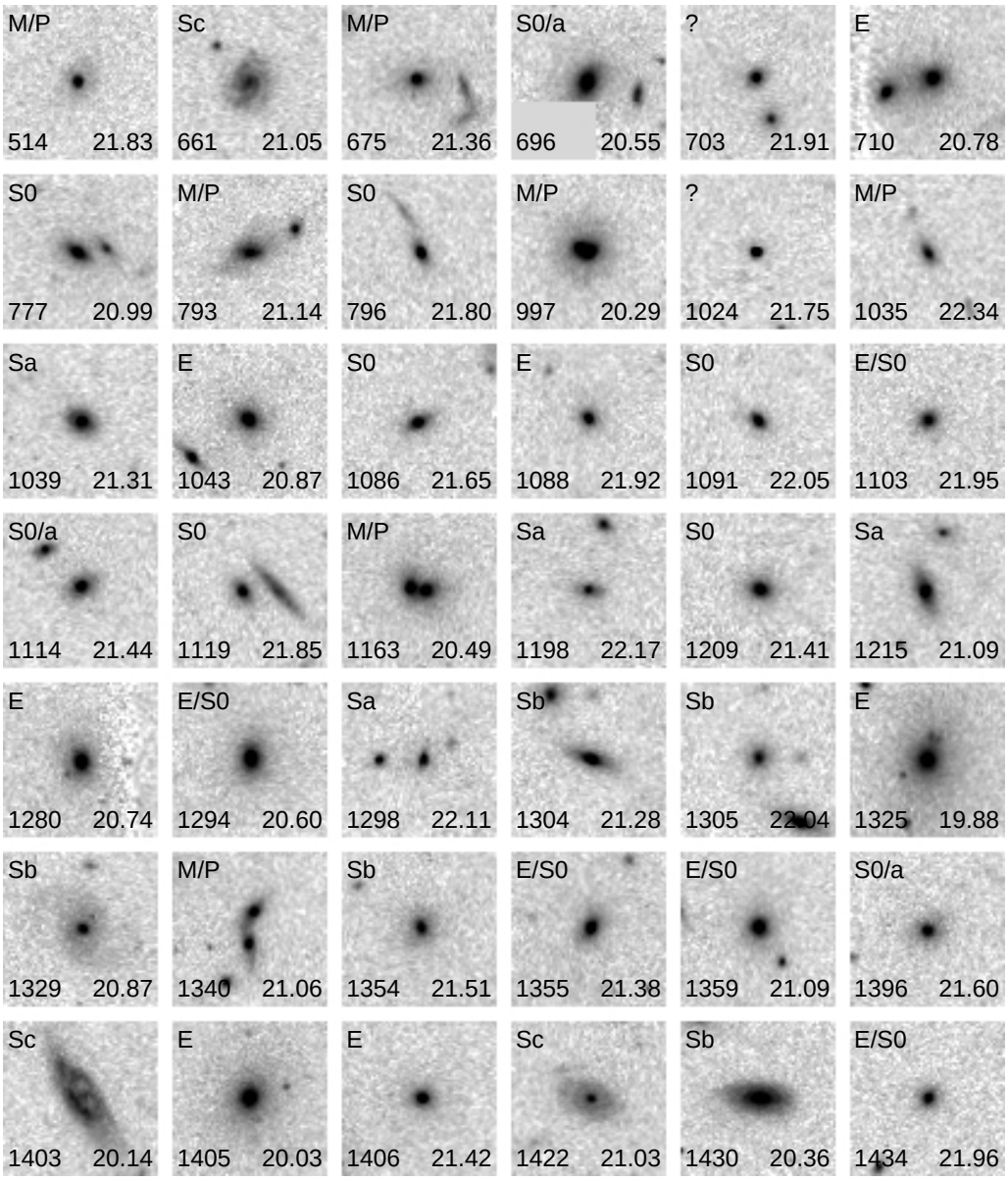

Figure 7.6: *Hubble Space Telescope* WFPC2 F814W images of spectroscopically confirmed cluster members in MS 1054–03. Each image is $6\farcs4 \times 6\farcs4$, with $0\farcs1$ pixels. At the distance of MS 1054–03, this corresponds to $61 \times 61\, h_{50}^{-1}$ kpc. The number in the lower right is total F814W magnitude. Morphological classifications are in the upper left.

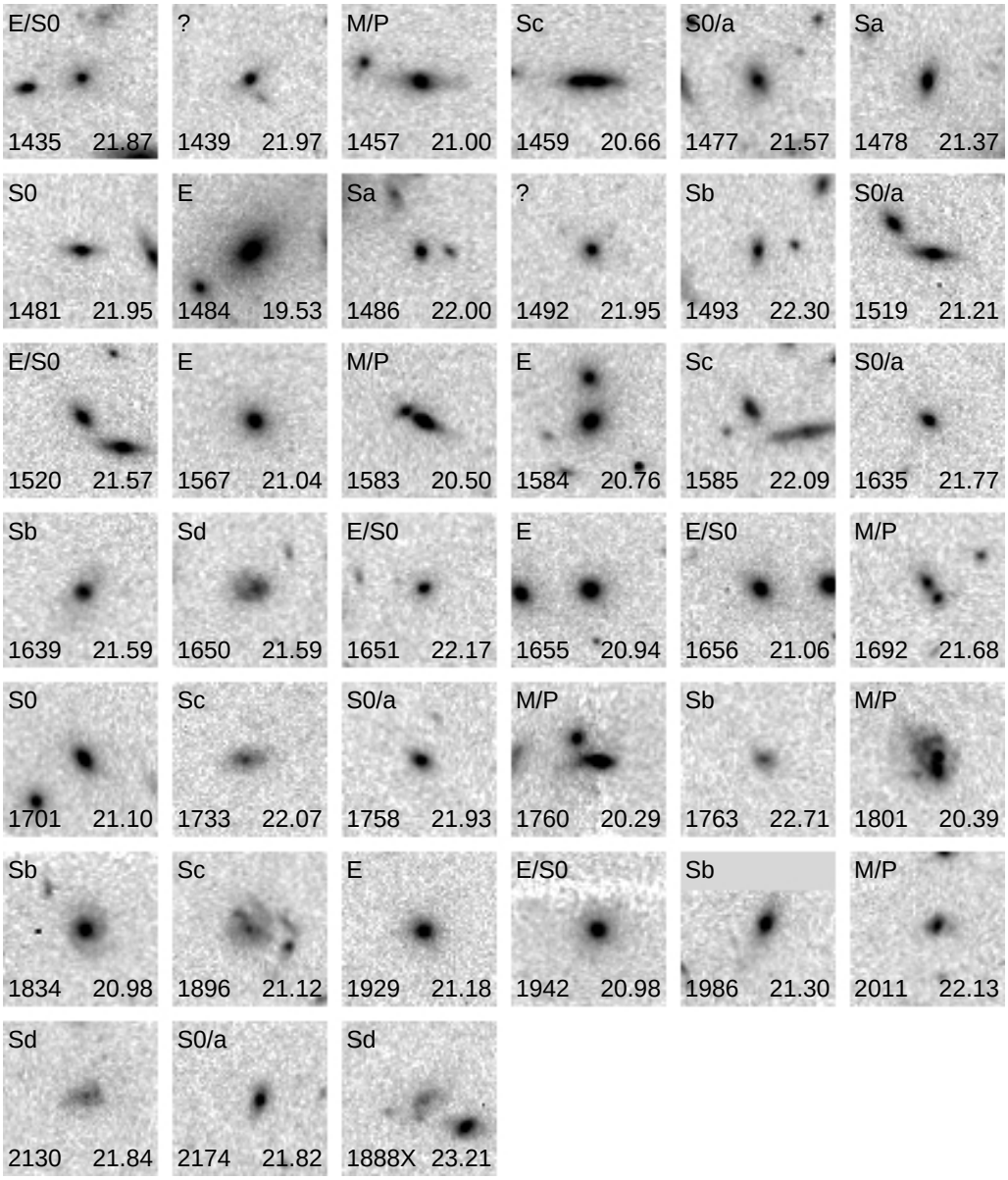

Figure 7.6: (Continued)

TABLE 2
MORPHOLOGIES AND PHOTOMETRY

Id	x ($''$)	y ($''$)	morph	F814W^T	B_z^T	$(U-B)_z$	$\Delta(U-B)_z$
514	53.8	–132.4	M/P	21.83	23.00	0.402	–0.034
661	53.4	–94.1	Sc	21.05	22.24	–0.064	–0.520
675	75.2	–89.0	M/P	21.36	22.53	0.393	–0.053
696	–58.1	–83.7	S0/a	20.55	21.72	0.467	–0.011
703	–24.5	–79.3	?	21.91	23.08	0.360	–0.073
710	30.6	–81.2	E	20.78	21.95	0.432	–0.035
777	90.6	–63.5	S0	20.99	22.16	0.431	–0.023
793	–89.3	–59.6	M/P	21.14	22.31	0.365	–0.087
796	33.1	–57.0	S0	21.80	22.97	0.413	–0.027
997	136.2	–58.3	M/P	20.29	21.47	0.343	–0.141
1024	81.7	–44.8	?	21.75	22.95	–0.194	–0.627
1035	18.0	–41.2	M/P	22.34	23.53	–0.122	–0.543
1039	67.3	–40.9	Sa	21.31	22.49	0.333	–0.124
1043	–91.6	–41.7	E	20.87	22.04	0.461	–0.004
1086	98.9	–38.8	S0	21.65	22.82	0.424	–0.022
1088	–13.7	–37.4	E	21.92	23.09	0.423	–0.011
1091	82.2	–35.7	S0	22.05	23.23	0.215	–0.217
1103	–85.1	–33.8	E/S0	21.95	23.14	0.059	–0.375
1114	–3.6	–31.4	S0/a	21.44	22.61	0.410	–0.040
1119	25.8	–30.9	S0	21.85	23.02	0.442	0.003
1163	–63.5	–29.4	M/P	20.49	21.66	0.438	–0.039
1198	–58.1	–25.1	Sa	22.17	23.36	0.031	–0.395
1209	84.3	–24.1	S0	21.41	22.58	0.504	0.050
1215	130.6	–25.7	Sa	21.09	22.26	0.421	–0.038
1280	122.3	–16.9	E	20.74	21.91	0.482	0.011
1294	21.5	–13.3	E/S0	20.60	21.77	0.472	–0.002
1298	75.2	–11.4	Sa	22.11	23.28	0.469	0.042
1304	32.0	–11.9	Sb	21.28	22.45	0.396	–0.060
1305	29.4	–13.6	Sb	22.04	23.22	0.335	–0.097
1325	52.8	–9.8	E	19.88	21.05	0.360	–0.120
1329	–24.0	–5.7	Sb	20.87	22.04	0.393	–0.058
1340	45.5	–1.6	M/P	21.06	22.23	0.472	0.030
1354	38.8	–8.2	Sb	21.51	22.68	0.424	–0.021
1355	43.7	–5.6	E/S0	21.38	22.55	0.455	0.002
1359	38.9	–0.4	E/S0	21.09	22.26	0.457	–0.005
1396	119.9	2.1	S0/a	21.60	22.77	0.486	0.042
1403	–56.9	–5.6	Sc	20.14	21.33	–0.037	–0.507
1405	–46.3	–3.6	E	20.03	21.20	0.478	0.000
1406	–49.4	1.4	E	21.42	22.59	0.398	–0.050
1422	22.9	5.8	Sc	21.03	22.23	–0.230	–0.681
1430	–26.3	6.9	Sb	20.36	21.54	0.348	–0.133
1434	–21.5	9.3	E/S0	21.96	23.13	0.410	–0.026
1435	–29.7	4.5	E/S0	21.87	23.04	0.366	–0.067
1439	–37.9	8.2	?	21.97	23.14	0.461	0.029
1457	–16.5	0.1	M/P	21.00	22.17	0.448	–0.013
1459	6.1	8.3	Sc	20.66	21.84	0.183	–0.288
1477	12.5	0.7	S0/a	21.57	22.74	0.378	–0.069
1478	–4.1	–3.7	Sa	21.37	22.54	0.496	0.041

TABLE 2 (CONTINUED)

Id	$x('')$	$y('')$	morph	F814W^1	B_z^1	$(U-B)_z$	$\Delta(U-B)_z$
1481	12.0	–5.6	S0	21.95	23.12	0.373	–0.065
1484	0.0	0.0	E	19.53	20.70	0.496	0.005
1486	2.0	4.3	Sa	22.00	23.17	0.534	0.097
1492	–5.5	12.4	?	21.95	23.12	0.440	0.005
1493	–44.2	11.7	Sb	22.30	23.47	0.454	0.030
1519	–20.6	20.7	S0/a	21.21	22.38	0.454	–0.002
1520	–21.7	19.2	E/S0	21.57	22.74	0.442	–0.004
1567	–70.7	25.2	E	21.04	22.21	0.494	0.033
1583	–52.2	22.9	M/P	20.50	21.68	0.318	–0.165
1584	–61.6	28.2	E	20.76	21.93	0.483	0.011
1585	–53.0	27.9	Sc	22.09	23.28	0.004	–0.426
1635	–18.5	31.1	S0/a	21.77	22.94	0.467	0.027
1639	85.1	31.1	Sb	21.59	22.77	0.200	–0.241
1650	14.4	29.7	Sd	21.59	22.78	0.056	–0.386
1651	13.5	33.9	E/S0	22.17	23.34	0.463	0.038
1655	–37.9	34.1	E	20.94	22.12	0.252	–0.214
1656	–37.8	31.2	E/S0	21.06	22.23	0.448	–0.011
1692	10.1	44.2	M/P	21.68	22.86	0.313	–0.127
1701	–43.5	48.1	S0	21.10	22.27	0.447	–0.013
1733	187.8	34.3	Sc	22.07	23.26	–0.036	–0.463
1758	68.4	55.7	S0/a	21.93	23.11	0.354	–0.082
1760	–34.4	56.1	M/P	20.29	21.46	0.369	–0.108
1763	–97.6	56.8	Sb	22.71	23.90	–0.086	–0.493
1801	7.2	65.1	M/P	20.39	21.60	–0.536	–1.007
1834	–57.6	73.1	Sb	20.98	22.16	0.326	–0.139
1896	129.2	86.0	Sc	21.12	22.32	–0.210	–0.654
1929	40.1	96.3	E	21.18	22.35	0.410	–0.050
1942	–59.3	97.6	E/S0	20.98	22.15	0.457	–0.005
1986	–133.6	111.4	Sb	21.30	22.47	0.524	0.070
2011	–105.6	116.9	M/P	22.13	23.33	–0.271	–0.698
2130	–57.7	150.5	Sd	21.84	23.03	–0.001	–0.424
2174	18.7	160.7	S0/a	21.82	22.99	0.372	–0.068
1888X	–90.2	101.4	Sd	23.21	24.23	–0.194	–0.752

nearby galaxies from the survey by Jansen et al. (1999). The classification system is identical to that of Fabricant et al. (1999), and similar to the system of Smail et al. (1997). In order to extract as much information as possible from our data the galaxies were displayed in several formats. Of each galaxy, we inspected the image at the original 0.″1 WFC resolution, the interlaced image at 0.″071 resolution, the CLEANed interlaced image, and the interlaced image convolved with a $\sigma = 0.''11$ Gaussian. The latter image brings out faint outer structure.

The classifications of the three classifiers were compared to assess their internal errors. In general, classifications agreed within the broad categories of early-type, spiral, or merger. If galaxy types are binned in the two categories early-types (E, E/S0, S0) and other types the three classifiers agreed exactly on 76 % of all galaxies. To combine the classifications we used the same combination rules as Fabricant et al. (1999). The classifications are listed in Table 2.

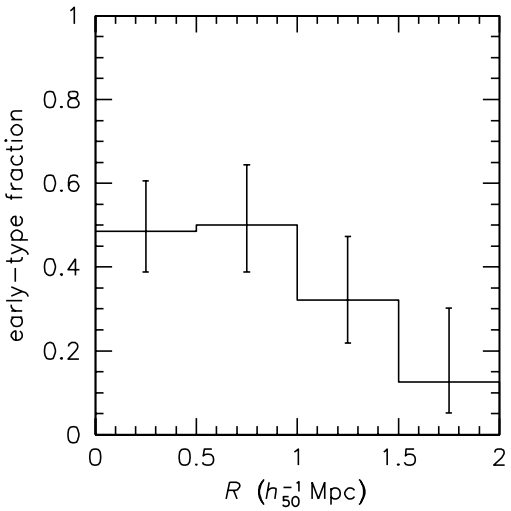

Figure 7.7: Early-type fraction plotted against R, the projected distance from the BCG. The histogram shows the average early-type fraction in $0.5\,h_{50}^{-1}$ Mpc wide bins. The early-type fraction is low, even in the central regions of the cluster.

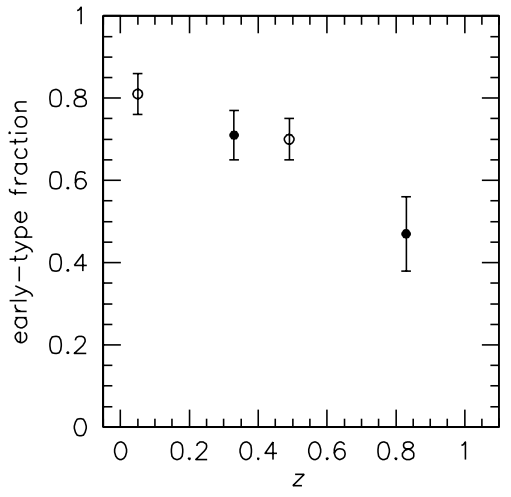

Figure 7.8: Evolution of the early-type fraction in rich clusters. The early-type fraction in MS 1054–03 is lower than the early-type fraction in clusters at lower redshift, indicating strong evolution in the nunber density of early-type galaxies.

7.3.2 Morphological Fractions

We find that the relative fractions of ellipticals, S0s, spirals, and mergers are 22 %, 22 %, 39 %, and 17 % respectively, where E/S0s and S0/as are evenly split between their neighboring types. One of the most striking results of our survey is the high fraction (17 %) of galaxies classified as mergers. Properties of the mergers and implications of their existence are discussed by van Dokkum et al. (1999). The ratio of ellipticals to S0 galaxies is ~ 1. This quantity is somewhat uncertain, because it is very difficult to distinguish ellipticals from S0s (see, e.g., Jørgensen & Franx 1994, Andreon 1998). The fraction of early-type galaxies (E+E/S0+S0) is better determined (see, e.g., Fabricant et al. 1999). We find that only 34 out of 77 classified galaxies (44 %) are early-types.

In Fig. 7.7 we test whether the early-type fraction is a function of R, the projected distance from the BCG. The histogram shows the average early-type fraction in $0.5\,h_{50}^{-1}$ Mpc wide bins.

We find that the radial dependence of the early-type fraction is weak for $R \lesssim 1\,h_{50}^{-1}$ Mpc. Even in the central regions of the cluster the early-type fraction is $< 50\,\%$. At $R > 1\,h_{50}^{-1}$ Mpc the early-type fraction is $\sim 20\,\%$.

MS 1054–03 has an irregular and elongated appearance (cf. Fig. 7.5 [Plate 6, page 61]). We test whether the low early-type fraction in the central regions of MS 1054–03 is related to substructure, by calculating the early-type fraction within apertures centered on the three most luminous galaxies in the cluster. Their positions coincide with those of the three strongest peaks in the luminosity density distribution. The early-type fractions in the immediate vicinity of these three galaxies are in fact somewhat lower than the average fraction in the central region of the cluster: they are 33 %, 38 % and 38 % within circles with radii $R = 0.25\,h_{50}^{-1}$ Mpc centered on galaxies 1484, 1325 and 1405 respectively. Within $R = 0.5\,h_{50}^{-1}$ Mpc these fractions are 47 %, 43 % and 50 %. We conclude there is no evidence for a strong dependence of the early-type fraction on luminosity density.

We can compare the early-type fraction in MS 1054–03 to the early-type fractions in rich clusters at lower redshift, using data from Fabricant et al. (1999) of CL 1358+62 at $z = 0.33$, and data from Dressler et al. (1997) of rich clusters at $z \approx 0.04$ and $z \approx 0.5$. The WFPC2 data of Dressler et al. (1997) only cover the central regions of the $z \approx 0.5$ clusters. For consistency with Dressler et al. (1997) we calculate the early-type fractions in all clusters within a projected radius $R = 635\,h_{50}^{-1}$ kpc. The evolution of the early-type fraction is shown in Fig. 7.8. The early-type fraction at $z = 0.83$ is significantly lower than in rich clusters at lower redshift, which may imply strong evolution in the number density of early-type galaxies. In the following Section we will study the color-magnitude relation in MS 1054–03, to constrain the star formation histories of the early-types, mergers, and spirals. In Sect. 7.7 we will discuss the connection between the evolution of the early-type fraction and the evolution of the CM relation.

7.4 The Color-Magnitude Relation

7.4.1 The CM Relation for Different Morphologies

The color-magnitude relation of spectroscopically confirmed cluster members is shown in Fig. 7.9. There is a strong trend with morphology. Most early-type galaxies follow a tight and well defined relation, but there are four early-types which are fairly blue. We stress that these blue early-types are spectroscopically confirmed cluster members. The most luminous blue elliptical (1325) has an overall red color and a small blue feature 0.5 arcsec from the center. This may be a lensed background galaxy, a star forming region, or a small cluster galaxy which may be merging with the luminous elliptical. The other blue elliptical is uniformly blue. Luminous blue early-types are very rare in clusters at lower redshift (e.g., van Dokkum et al. 1998a). The spirals are, on average, bluer than the early-types and have a large scatter. The mergers are also somewhat bluer than the early-type galaxies, but follow a much tighter CM relation than the spirals.

We determined the form of the CM relation from a fit to the early-type galaxies, and subtracted this fit from the observed relation. For each morphological subsample we then computed the offset and scatter in the CM relation from the distribution of residuals. Excluding the four bluest galaxies, the fit to the early-type galaxies (Es, E/S0s, and S0s) has the form

$$(U-B)_z = -0.031(M_B^T + 22) + 0.449. \qquad (7.3)$$

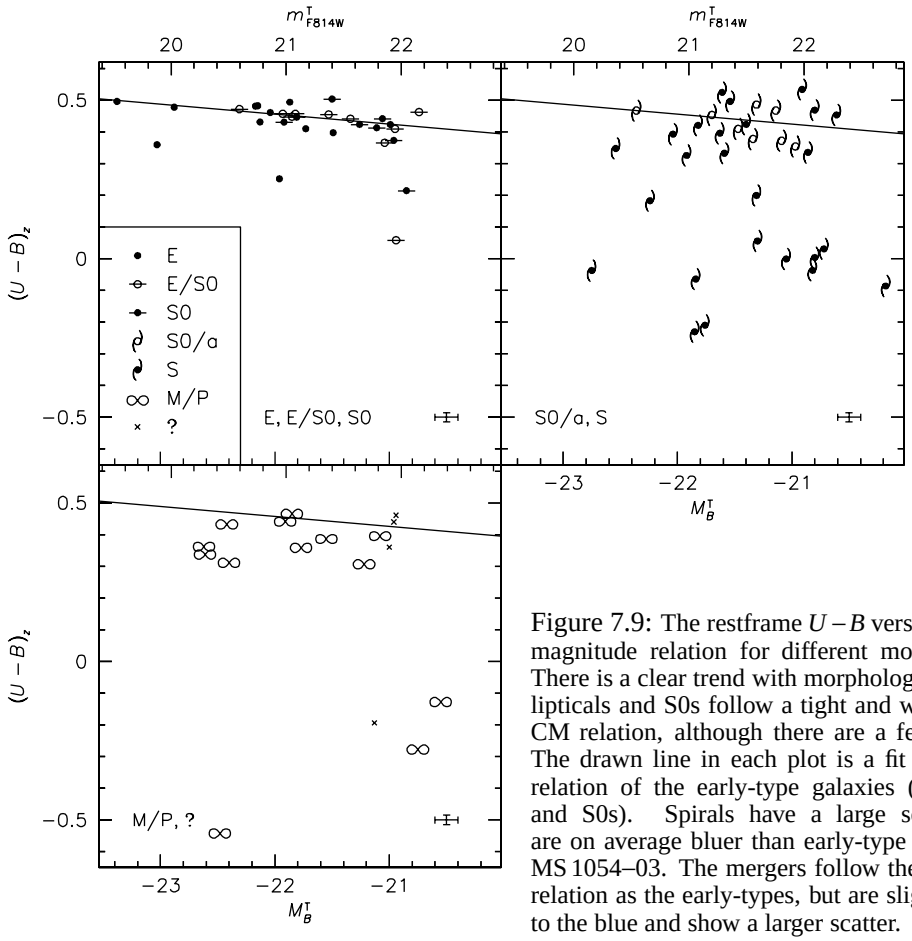

Figure 7.9: The restframe $U-B$ versus B color-magnitude relation for different morphologies. There is a clear trend with morphology. Most ellipticals and S0s follow a tight and well-defined CM relation, although there are a few outliers. The drawn line in each plot is a fit to the CM relation of the early-type galaxies (Es, E/S0s, and S0s). Spirals have a large scatter, and are on average bluer than early-type galaxies in MS 1054–03. The mergers follow the same CM relation as the early-types, but are slightly offset to the blue and show a larger scatter.

The predicted colors from the CM relation were subtracted from the observed colors. For each morphological subsample the mean and scatter in the distribution of residuals $\Delta(U-B)_z$ were computed using the biweight statistic (Beers, Flynn, & Gebhardt 1990). Uncertainties in the scatter were determined from bootstrap resampling. The results are listed in Table 3.

The observed scatter in the early-type galaxies is low at 0.032 ± 0.011. The intrinsic scatter is 0.028 ± 0.012. This scatter is much smaller than that of the full sample (0.097 ± 0.027). Because of the small number of early-type galaxies (30) the offsets and scatter in the subsamples of Es, E/S0s and S0s have large uncertainties, and the differences between these three subsamples are not significant. The scatter in the ellipticals is 0.045 ± 0.019.

From Table 3 we can see that the spirals and mergers are more heterogeneous in their colors than the early-type galaxies, but the spirals much more so than the mergers. The mergers follow the same CM relation as the early-types, but are slightly offset to the blue and show a larger scatter. The average offset between the CM relation of the early-types and the mergers is only -0.07 ± 0.02 magnitudes. The scatter in the CM relation of the mergers is comparable to their mean offset from the early-types, and roughly twice that of the ellipticals.

TABLE 3
OFFSET AND SCATTER OF THE CM RELATION

Sample	N	Offset	Error	Obs. Scatter	Error
E,E/S0,S0	30	0.000	0.006	0.032	0.011
S	26	–0.219	0.047	0.255	0.025
M/P	13	–0.066	0.019	0.073	0.029
E	12	–0.003	0.012	0.045	0.019
E,E/S0,M/P	35	–0.024	0.010	0.054	0.011
All	81	–0.023	0.010	0.097	0.027

7.4.2 Radial Dependence of the Color-Magnitude Relation

In the cluster CL 1358+62 at $z = 0.33$ the scatter and offset of the color-magnitude relation are dependent on R, the projected distance to the BCG: S0 galaxies in the outer parts of CL 1358+62 have a larger scatter in the CM relation and a bluer mean color than S0s in the inner parts (van Dokkum et al. 1998a). If this trend is caused by an age gradient in the cluster one might expect it is stronger at higher redshift. In Fig. 7.10 the residuals from the CM relation are plotted against R. There is no significant correlation between $\Delta(U-B)_z$ and R for the early-type galaxies. The trend observed in CL 1358+62 is indicated by the broken line in Fig. 7.10; our data are consistent with this trend.

We conclude that the scatter in the CM relation at $z = 0.83$ is mainly driven by spirals and (to a lesser extent) mergers. Although there are a few fairly blue early-types, most of the early-type galaxies follow a well-defined color-magnitude relation with small scatter. In our data there is no significant trend with distance from the BCG; we do not have sufficient data to confirm or rule out a similar trend as seen in the colors of S0s in the cluster CL 1358+62 at $z = 0.33$.

7.5 Evolution of the Color-Magnitude Relation of Early-Type Galaxies

The slope and scatter of the CM relation of early-type galaxies can be compared to data at lower redshift. Fig. 7.11(a) shows the evolution of the slope of the CM relation as a function of redshift. Data points are from BLE92 for the Coma cluster, van Dokkum et al. (1998a) for CL 1358+62 at $z = 0.33$, and Ellis et al. (1997) for three clusters at $z \approx 0.55$. We have used the Worthey (1994) models to transform $U-V$ (BLE92 and Ellis et al. 1997) and $B-V$ colors (van Dokkum et al. 1998a) to $U-B$ colors. For solar metallicity these models give $\Delta(U-B) = 1.4\Delta(B-V)$ and $\Delta(U-B) = 0.6\Delta(U-V)$. The samples of BLE92 and Ellis et al. (1997) only cover the inner parts of the clusters. For CL 1358+62 and MS 1054–03 we determined the slope for the inner parts of the cluster as well as for the whole sample.

A fit to the evolution of the slope in the inner parts of the clusters gives $\delta(U-B)_z/\delta B_z = (0.013 \pm 0.016)z - (0.041 \pm 0.008)$. We conclude that the data are consistent with a constant slope with redshift. If the slope in the relation at $z = 0$ is (partly) due to a systematic age gradient, such that high luminosity galaxies have higher luminosity weighted ages than low luminosity galaxies, one might expect the slope to become steeper at higher redshift (e.g., Kodama et al. 1998). There is no evidence for such an effect in the data presented here, confirming the results of Stanford et al. (1998) and Kodama et al. (1998), who used ground based photometry and HST morphologies to determine the slope and scatter of the CM relation of

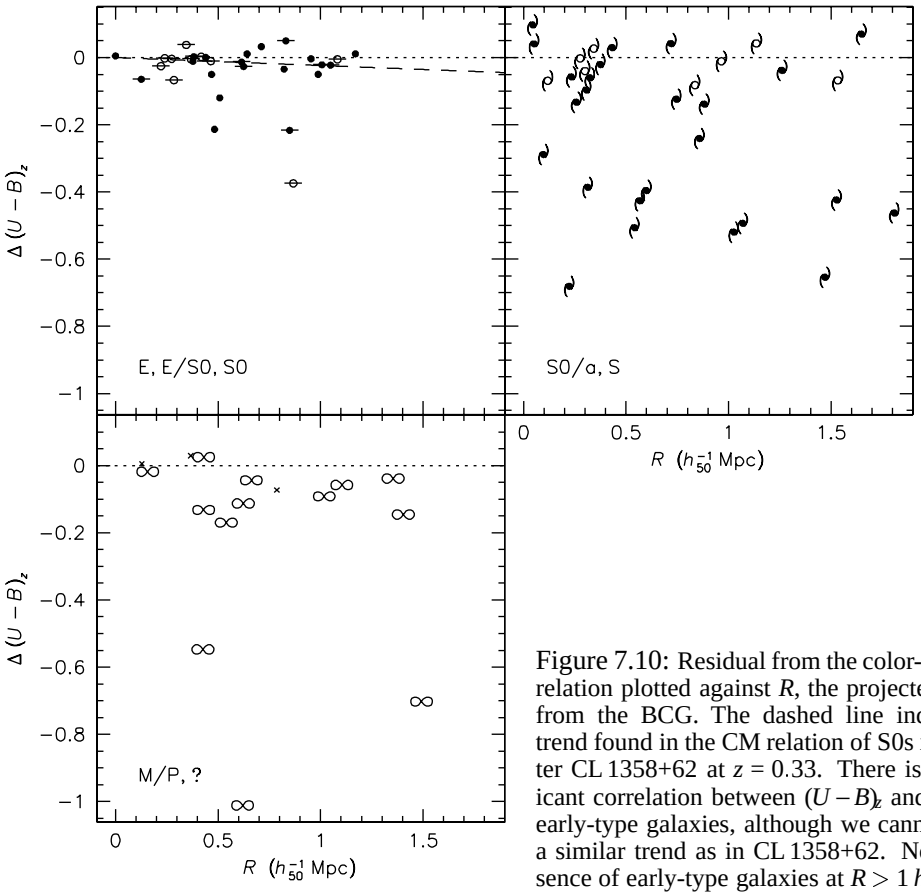

Figure 7.10: Residual from the color-magnitude relation plotted against R, the projected distance from the BCG. The dashed line indicates the trend found in the CM relation of S0s in the cluster CL 1358+62 at $z = 0.33$. There is no significant correlation between $(U-B)_z$ and R for the early-type galaxies, although we cannot exclude a similar trend as in CL 1358+62. Note the absence of early-type galaxies at $R > 1\,h_{50}^{-1}$ Mpc.

early-type galaxies in clusters at $0 < z < 1$.

The evolution of the scatter in the CM relation of early-type galaxies is shown in Fig. 7.11(b). The scatter is remarkably low at all redshifts. In particular, the scatter at $z = 0.83$ is very similar to the scatter at $z = 0$. This is remarkable, because the scatter in the CM relation might be expected to increase with redshift due to increasing fractional age differences between galaxies (see, e.g., BLE92, van Dokkum et al. 1998a). Our result is consistent with the results from Stanford et al. (1998).

We conclude that there is no strong redshift dependence of the slope and scatter of the CM relation of early-type galaxies. In particular, the scatter in the CM relation of MS 1054–03 at $z = 0.83$ is almost identical to the scatter in the CM relation of the nearby Coma cluster. In the following Sections, we will model the color and luminosity evolution of galaxies in an effort to reconcile this result with the strong evolution of the early-type fraction in clusters.

7.6 Predicted Color Evolution of Mergers and Ellipticals

An important question is how the colors and luminosities of the mergers will evolve with time. Here, we assume all mergers will evolve into ellipticals or E/S0s, and evolve the CM

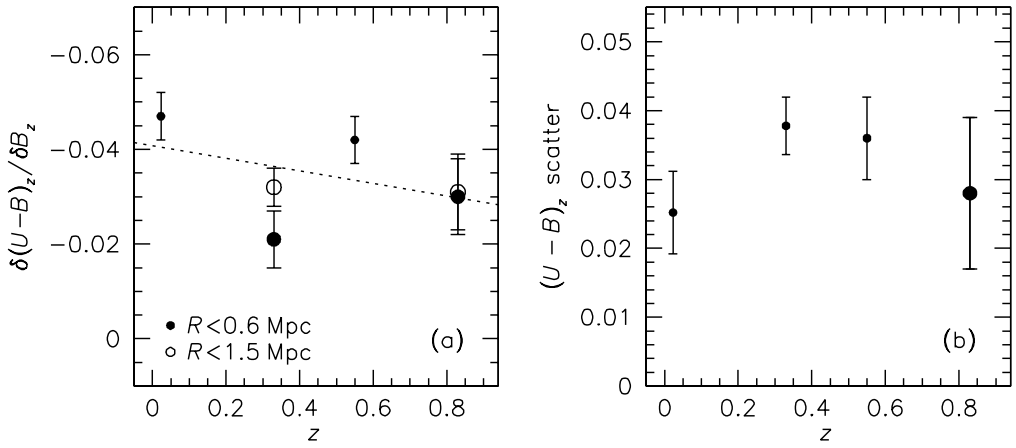

Figure 7.11: Evolution of the slope (a) and scatter (b) of the CM relation of early-type galaxies. In order of increasing redshift the data points in (a) and (b) are from BLE92 (z = 0.023), van Dokkum et al. (1998a) (z = 0.33), Ellis et al. (1997) (z = 0.55), and this study (z = 0.83). The data are consistent with a constant slope and scatter.

relation of the combined sample of mergers, ellipticals, and E/S0s forward in time. We note that the color evolution of the spirals is very difficult to predict, because they are still forming stars at z = 0.83.

7.6.1 Modeling Color Evolution

We assume that the star formation rate in all galaxies was constant from z = 10 to an abrupt truncation at $z = z_2$. Furthermore it is assumed that all galaxies on the CM relation have identical ages, and that the distance to the CM relation depends on the age only. For consistency with the luminosity evolution of early-type galaxies to z = 0.83 inferred from the Fundamental Plane (van Dokkum et al. 1998b) we take z_2 = 3 for galaxies on the CM relation. As shown in Appendix 7.B we can calculate the truncation redshift z_2 for each galaxy from its distance to the CM relation $\Delta(U-B)_z$ under these assumptions.

Fig. 7.12 shows the CM relation of ellipticals, E/S0s and mergers at z = 0.83, and the predicted CM relations at z = 0.5, z = 0.3, and at z = 0. In each panel, the line indicates the CM relation of early-type galaxies at z = 0.83. The scatter in the sample of Es and E/S0s and the scatter in the combined sample of Es, E/S0s, and mergers are indicated in the lower right corner of each panel. Observational errors were subtracted in quadrature from the scatter at z = 0.83; at lower redshifts the predicted scatter was corrected by the same fraction as the correction at z = 0.83.

Galaxies on the CM relation fade by $\Delta B \approx 0.9$ magnitudes and become redder by $\Delta(U-B) \approx 0.2$ magnitudes between z = 0.83 and z = 0. Blue galaxies evolve faster than red galaxies, because young stellar populations evolve faster than old stellar populations. The scatter in the CM relation of the combined sample of Es, E/S0s and mergers decreases with time, from 0.055 at z = 0.83 to 0.016 at z = 0. The implication is that the present-day counterparts of the z = 0.83 mergers have the same colors as luminous early-type galaxies. Note that the merger remnants are among the most luminous galaxies at z = 0; they will have absolute magnitudes in the range $-22 \lesssim M_B^{\rm T} \lesssim -20$.

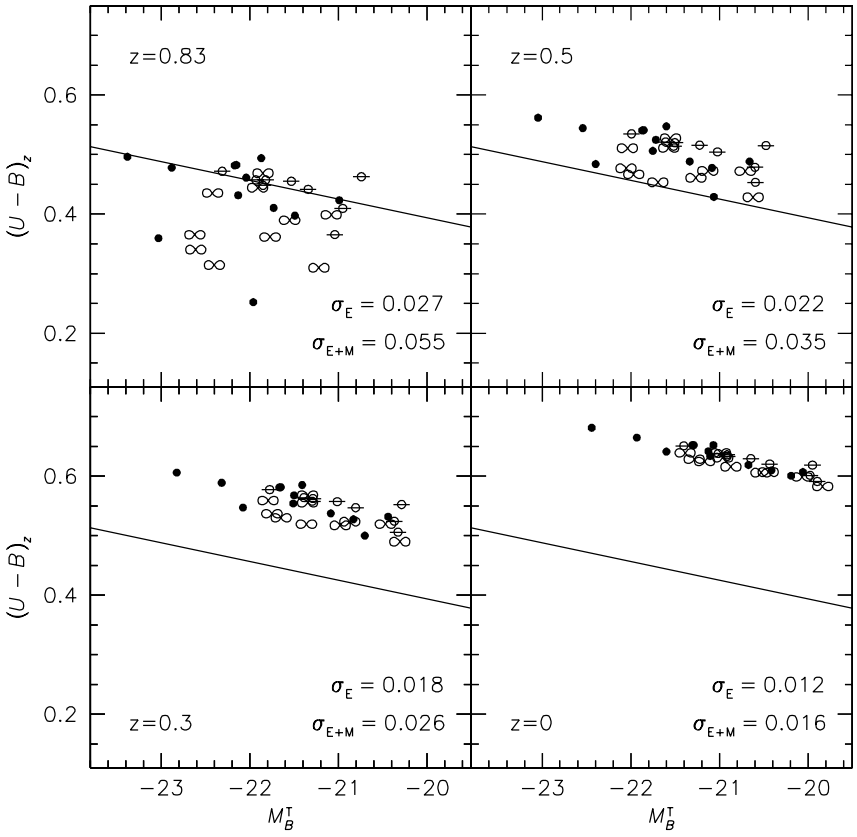

Figure 7.12: Color and luminosity evolution of ellipticals, E/S0s and mergers in MS 1054–03. The panels show the observed CM relation at $z = 0.83$, and predicted CM relations at $z = 0.5$, $z = 0.3$, and $z = 0$. The CM relation was evolved forward in time using models described in Sect. 7.B. Galaxies become progressively fainter and redder with time. The scatter in the CM relation decreases, because the fractional age differences between galaxies become smaller.

7.6.2 Evolution of the Scatter

The predicted redshift evolution of the scatter in the CM relation of the combined sample of ellipticals and mergers is shown in Fig. 7.13. At each redshift the predicted scatter was calculated from the predicted colors, using the same method as used for the observations. Assuming a merger timescale of 1 Gyr, the mergers seen at $z = 0.83$ will all be completed at $z \sim 0.65$. The data points at $z < 0.83$ show the scatter in the CM relation of ellipticals, from BLE92, van Dokkum et al. (1998a), and Ellis et al. (1997). The scatter in the CM relation of ellipticals at $z < 0.83$ is well fitted by the predictions.

Figure 7.13 demonstrates the effect of morphological evolution on the scatter in the CM relation. The scatter in the colors of all progenitors (i.e., the ellipticals and the mergers) of low redshift ellipticals is much higher at $z = 0.83$ than the scatter in the colors of the ellipticals alone.

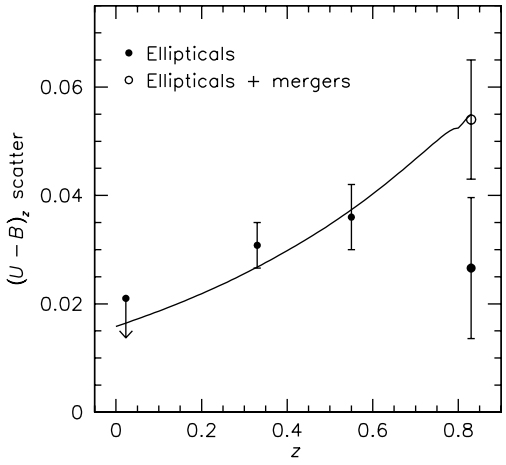

Figure 7.13: Predicted and observed evolution of the scatter in the CM relation of ellipticals and mergers. The solid line shows the predicted scatter at $z < 0.83$, assuming all mergers have evolved into ellipticals at $z \lesssim 0.65$. Data points are from BLE92 ($z = 0.023$), van Dokkum et al. (1998a) ($z = 0.33$), Ellis et al. (1997) ($z = 0.55$), and the present study ($z = 0.83$). The model predictions are consistent with the observed scatter at $z < 0.83$.

7.7 The Effect of Morphological Evolution on the Scatter in the Color-Magnitude Relation of Early-Type Galaxies

We have demonstrated that the formation of ellipticals by mergers has an effect on the measured evolution of the scatter in the CM relation of ellipticals at high redshift. Here, we take a broader view and examine the effects of the overall evolution of the early-type fraction in clusters. We do not want to resolve the issue to what extend this evolution is due to mergers forming ellipticals or spirals forming S0s, but treat these transformations as one process.

We take the observed evolution of the early-type galaxy fraction in clusters, and calculate the expected effect on the measured scatter in their CM relation. We assume the early-type fraction increases with time because star forming galaxies are transformed into early-type galaxies. We furthermore assume these systems are classified as early-types some time ($\sim$ 1 Gyr) after star formation ceased.

The observed evolution of the early-type fraction is repeated in Fig. 7.14*a*. The line is a linear least squares fit to the data, of the form $f_{\rm early} = 0.85 - 0.43z$. Extrapolating this fit to higher redshifts gives a formation epoch of $0 < z < 2$ for cluster early-type galaxies, with the formation rate linear in redshift.

We calculated the predicted evolution of the scatter in the CM relation and the evolution of the zeropoint of the Fundamental Plane using Monte Carlo simulations. The star formation history of each galaxy in the simulations is described by the continuous truncated star formation model described in van Dokkum et al. (1998a) and Sect. 7.8. In Fig. 7.14*b* and *c* the predictions of this model are shown for various values of Δt, the time interval between truncation of star formation and classification as early-type galaxy. Excellent fits to the observations are obtained for $\Delta t \sim 1$ Gyr.

The modeling demonstrates that morphological transformations of galaxies can "artificially" cause a roughly constant, low scatter in the CM relation. The low early-type fraction and the presence of the mergers in MS 1054–03 provide direct evidence for such morphological transformations. The main aspects of our model are formation of early-type galaxies by truncation of star formation, combined with the assumption that early-type galaxies are recognized as such $\sim$ 1 Gyr after star formation ceased. The formation rate of early-type galaxies is specified by the observed evolution of the early-type fraction.

We emphasize the approximate nature of our modeling. In particular, galaxy transforma-

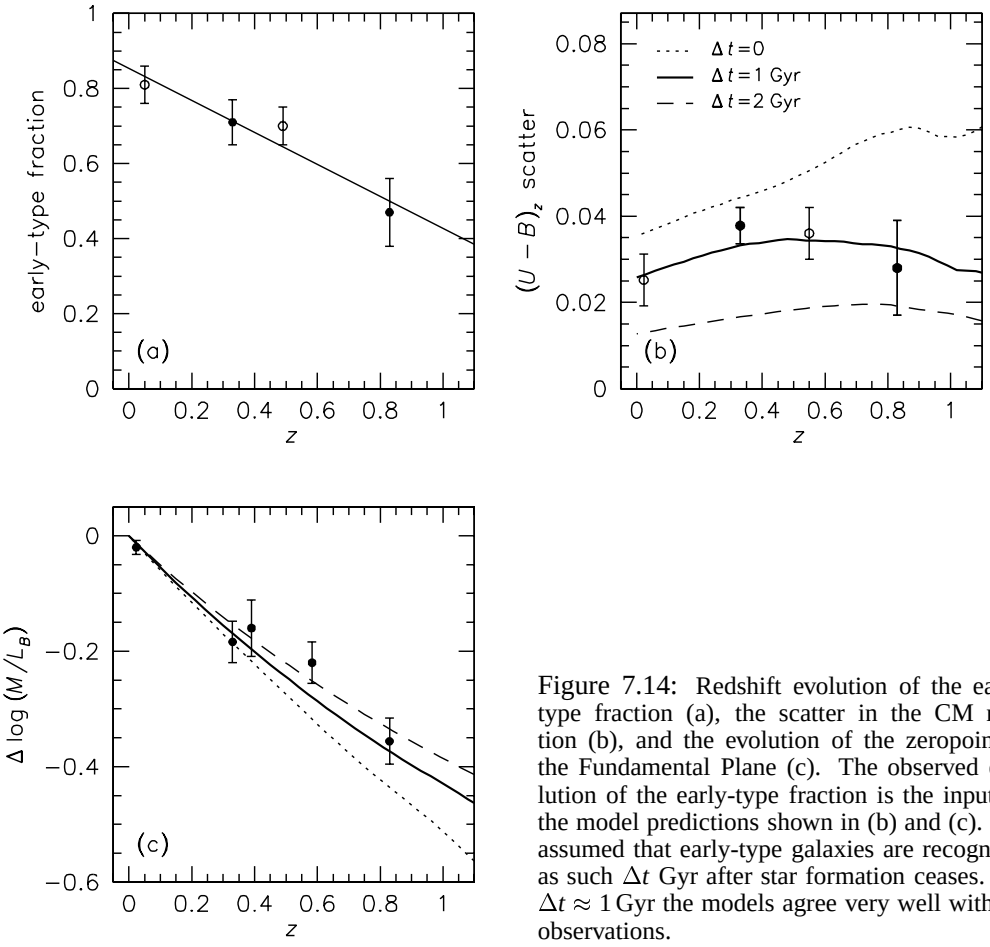

Figure 7.14: Redshift evolution of the early-type fraction (a), the scatter in the CM relation (b), and the evolution of the zeropoint of the Fundamental Plane (c). The observed evolution of the early-type fraction is the input for the model predictions shown in (b) and (c). It is assumed that early-type galaxies are recognized as such Δt Gyr after star formation ceases. For $\Delta t \approx 1$ Gyr the models agree very well with the observations.

tions may not occur continuously, but could be triggered by the infall of galaxies or groups from the field (e.g., Abraham et al. 1996, van Dokkum et al. 1998a, 1999). Also, the star formation histories of galaxies may be better described by other models, e.g., a combination of an exponentially decreasing star formation rate followed by a small star burst (see, e.g., Barger et al. 1996). Given the simplicity of our approach the excellent fits to the observations are encouraging.

7.8 Summary and Conclusions

We have presented a large format two color HST WFPC2 mosaic of the cluster MS 1054–03 at $z = 0.83$. Furthermore, we have presented a spectroscopic survey of this field with the 10 m W. M. Keck telescope. This combination has yielded a sample of 81 I selected spectroscopically confirmed cluster members imaged with WFPC2, currently the largest sample of confirmed cluster galaxies at $z > 0.5$ observed with HST.

We have studied the morphologies and colors of these galaxies. The most striking result of our survey of MS 1054–03 is the high fraction of mergers among the $L > L_*$ cluster population

(van Dokkum et al. 1999). In the present paper we have presented a quantitative study of the color-magnitude relation in MS 1054–03, and discussed the implications of morphological evolution of cluster galaxies.

The color-magnitude relation is a strong function of morphology. Most early-type galaxies follow a remarkably tight and well defined relation, consistent with results based on ground based color measurements in 17 clusters at $0.3 < z < 0.9$ by Stanford et al. (1998). The slope and scatter of the relation are very similar to those of the Coma cluster. There is no significant dependence of the CM relation on radius in the cluster. The data are insufficient to rule out or confirm the weak trend observed in the cluster CL 1358+62 at $z = 0.33$ (van Dokkum et al. 1998a).

Early-type galaxies constitute only 44 % of the galaxy population in MS 1054–03. Spirals and mergers, which make up the other 56 % of the galaxy population, have a larger spread in their colors than the early-type galaxies and are on average bluer, but the spirals more so than the mergers. The mergers follow a similar CM relation as the ellipticals, and are only modestly bluer. The scatter in the CM relation of the mergers is similar to the difference in mean color between the mergers and the ellipticals. Using a simple prescription for the star formation histories we have evolved the CM relation of ellipticals and mergers forward in time. The merger remnants have almost identical colors as other luminous early-type galaxies at $z = 0$.

Taking the observed increase in the early-type fraction with time as input for our modeling, we have calculated the effect of morphological transformations on the scatter in the CM relation of early-type galaxies. The roughly constant, low scatter in the CM relation at $0 < z < 1$ can be successfully reproduced, provided that the transforming systems are classified as early-types roughly 1 Gyr after star formation ceased. The success of this model demonstrates that the low scatter in the CM relation of early-type galaxies does not require that all early-types formed their stars in a short period at very high redshift (as suggested by, e.g., Ellis et al. 1997, Stanford et al. 1998, and Kodama et al. 1998). We note that all "standard" models predict a continuous increase of the scatter with redshift, because the fractional age differences between galaxies become larger at larger lookback times.

The most important assumption in our study is that MS 1054–03 is a typical cluster for its redshift. As discussed in vD99, the large fraction of mergers in this cluster may be related to its unvirialized state. More large field observations of distant clusters would be valuable. Furthermore, it will be interesting to extend this type of study to lower density regions.

References

Abraham, R. G., Smecker-Hane, T. A., Hutchings, J. B., Carlberg, R. G., Yee, H. K. C., Ellingson, E., Morris, S., Oke, J. B., & Rigler, M. 1996, ApJ, 471, 694
Andreon, S. 1998, ApJ, 501, 533
Balogh, M. L., Schade, D., Morris, S. L., Yee, H. K. C., Carlberg, R. G., & Ellingson, E. 1998, ApJ, 504, L75
Barbaro, G., & Poggianti, B. M. 1997, A&A, 324, 490
Barger, A. J., Aragon-Salamanca, A., Ellis, R. S., Couch, W. J., Smail, I., & Sharples, R. M. 1996, MNRAS, 279, 1
Barnes, J. E. 1998, in After the Dark Ages: When Galaxies Were Young, 9th October Astrophysics Conference, University of Maryland, in press (astro-ph/9811242)
Bender, R., Saglia, R. P., Ziegler, B., Belloni, P., Greggio, L., Hopp, U., & Bruzual, G. 1998, ApJ, 493, 529
Bertin, E., & Arnouts, S. 1996, A&AS, 117, 393
Bower, R. G., Lucey, J. R., & Ellis, R. S. 1992, MNRAS, 254, 601 [BLE92]
Bruzual, G., & Charlot, S. 1996, in preparation
Butcher, H., & Oemler, A. 1978, ApJ, 219, 18
Butcher, H., & Oemler, A. 1984, ApJ, 285, 426

Couch, W. J., & Sharples, R. M. 1987, MNRAS, 229, 423
de Theije, P. A. M., & Katgert, P. 1999, A&A, 341, 371
Donahue, M., Voit, G. M., Gioia, I., Lupino, G., Hughes, J. P., & Stocke, J. T. 1998, ApJ, 502, 550
Dressler, A. 1980, ApJ, 236, 351
Dressler, A., & Gunn, J. E. 1983, ApJ, 270, 7
Dressler, A., Oemler, A., Jr., Couch, W. J., Smail, I., Ellis, R. S., Barger, A., Butcher, H., Poggianti, B. M., & Sharples, R. M. 1997, ApJ, 490, 577
Ellis, R. S., Smail, I., Dressler, A., Couch, W. J., Oemler, A., Jr., Butcher, H., & Sharples, R. M. 1997, ApJ, 483, 582
Fabricant, D., et al. 1999, in preparation
Fisher, D., Fabricant, D., Franx, M., & van Dokkum, P. G. 1998, ApJ, 498, 195
Franx, M., & van Dokkum, P. G. 1996, in New Light on Galaxy Evolution (IAU 171), R. Bender & R. L. Davies, Eds., Kluwer, p. 233
Fruchter, A. S., Hook, R. N. 1999, preprint (astro-ph/9808087)
Høgbom, J. A. 1974, A&AS, 15, 417
Jansen, R. A., et al. 1999, in preparation
Jørgensen, I., & Franx, M. 1994, ApJ, 433, 553
Kelson, D. D., van Dokkum, P. G., Franx, M., Illingworth, G. D., & Fabricant, D. 1997, ApJ, 478, L13 **[Chapter 3]**
Kennicutt, R. C., Jr. 1992, ApJ, 388, 310
Kodama, T., Arimoto, N., Barger, A. J., & Aragon-Salamanca, A. 1998, A&A, 334, 99
Krist, J. 1995, in Astronomical Data Analysis Software and Systems IV, ASP Conference Series, 77, R. A. Shaw, H. E. Payne, and J. J. E. Hayes, eds., p. 349
Lilly, S. 1993, ApJ, 411, 501
Lubin, L. M., Postman, M., Oke, J. B., Ratnatunga, K. U., Gunn, J. E., Hoessel, J. G., & Schneider, D. P. 1998, AJ, 116, 584
Luppino, G. A., & Kaiser, N. 1997, ApJ, 475, 20
Oke, J. B., Cohen, J. G., Carr, M., Cromer, J., Dingizian, A., Harris, F. H., Labrecque, S., Lucinio, R., Schaal, W., Epps, H., & Miller, J. 1995, PASP, 107, 375
Osterbrock, D. E., Fulbright, J. P., Martel, A. R., Keane, M. J., Trager, S. C., & Basri, G. 1996, PASP, 108, 277
Poggianti, B., Smail, I., Dressler, A., Couch, W., Barger, A., Butcher, H., Ellis, R., & Oemler, A., Jr. 1999, ApJ, in press (astro-ph/9901264)
Postman, M., Lubin, L. M., & Oke, J. B. 1998, AJ, 116, 560
Smail, I., Dressler, A., Couch, W. J., Ellis, R. S., Oemler, A., Jr., Butcher, H., & Sharples, R. M. 1997, APJS, 110, 213
Stanford, S. A., Eisenhardt, P. R. M., & Dickinson, M. 1995, ApJ, 450, 512
Stanford, S. A., Eisenhardt, P. R., & Dickinson, M. 1998, ApJ, 492, 461
Tran, K-V. H., Kelson, D. D., van Dokkum, P. G., Franx, M., Illingworth, G. D., & Magee, D. 1999, ApJ, in press (astro-ph/9902349)
Valdes, F. G., Campusano, L. E., Velasquez, J. D., & Stetson, P. B. 1995, PASP, 107, 1119
van Dokkum, P. G., & Franx, M. 1996, MNRAS, 281, 985 **[Chapter 2]**
van Dokkum, P. G., Franx, M., Kelson, D. D., Illingworth, G. D., Fisher, D., & Fabricant, D. 1998a, ApJ, 500, 714 **[Chapter 5]**
van Dokkum, P. G., Franx, M., Kelson, D. D., Illingworth, G. D. 1998b, ApJ, 504, L17 **[Chapter 4]**
van Dokkum, P. G., Franx, M., Fabricant, D., Kelson, D. D., Illingworth, G. D. 1999, ApJ Letters, submitted **[Chapter 6]**
Vazdekis, A., Casuso, E., Peletier, R. F., & Beckman, J. E., 1996, APJS, 106, 307
Worthey, G. 1994, APJS, 95, 107

7.A Resolution Enhancement

7.A.1 Combination of Interlaced Images

As is well known, the $0\farcs1 \times 0\farcs1$ WFC pixels undersample the HST WFPC2 PSF. The sampling can be improved by obtaining multiple exposures of the same field, offset by subpixel shifts. The shifted exposures can be "drizzled" on a finer grid (see Fruchter & Hook 1999 and

references therein). If the offsets between the exposures are precisely 0.5 pixels, the images are interlaced. In this special case there is a one-to-one correspondence between pixels in the original image and in the higher resolution output image. The improvement in the sampling is a factor $\sqrt{N}$, with $N = 2$ or $N = 4$ the number of independent positions.

The present observations are taken at two independent positions, offset by ± 5.5 pixels. In the $N = 2$ case, the two exposures sample an (x, y) grid which is rotated by 45° with respect to the original grid. This is illustrated in Fig. 7.15. The sampling distance in the combined image is $0\farcs1/\sqrt{2} = 0\farcs071$.

We combined the two offset exposures of each field by copying the pixels on a finer grid. The transformations from the offset input images I^A and I^B to the interlaced output image I^{AB} are

$$I^{AB}_{n+i-j,i+j-1} = I^A_{i,j} \quad (7.4)$$

$$I^{AB}_{n+i-j,i+j} = I^B_{i,j}, \quad (7.5)$$

with $n \times n$ the size of the input images, and $i, j = 1, 2, ..., n$. The output image has a size $2n \times 2n$. The area of the output image containing data is $\sqrt{2}n \times \sqrt{2}n = 2n^2$ pixels.

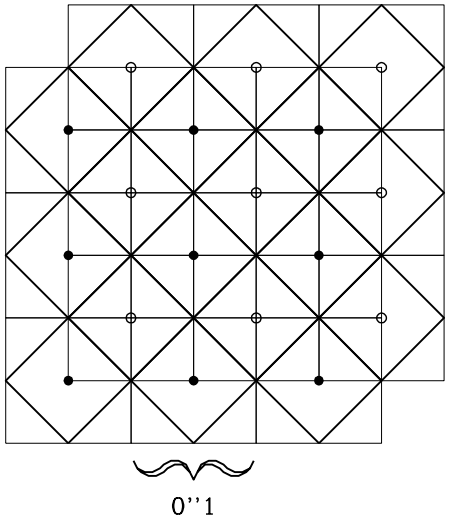

Figure 7.15: Illustration of interlacing using two independent positions. Solid circles are the centers of pixels in the first exposure, open circles are the centers of pixels in the second, offset, exposure. The solid circles and open circles sample a grid that is rotated by 45° with respect to the original grid. The output pixels are indicated by heavy lines. The output pixel size is $0\farcs1/\sqrt{2}$.

7.A.2 Image Restoration

Although the interlacing improved the sampling by a factor $\sqrt{2}$, the improvement in resolution is much smaller. This is caused by the wings of the PSF, and the subpixel response function (e.g., Krist 1995). In order to obtain high resolution images of the cluster galaxies, and to correct the photometry for the effects of the PSF (see van Dokkum et al. 1998a), the interlaced images were restored using CLEAN (Høgbom 1974).

The CLEAN algorithm requires a model for the PSF. For all cluster galaxies subsampled PSFs appropriate for the positions of the galaxies on the WFC chips were created using Tiny Tim (Krist 1995), version 4b. The exposures were mimiced by creating a copy of each subsampled PSF and shifting it by $0\farcs05$ in x and y. The PSFs were then rebinned to the WFC

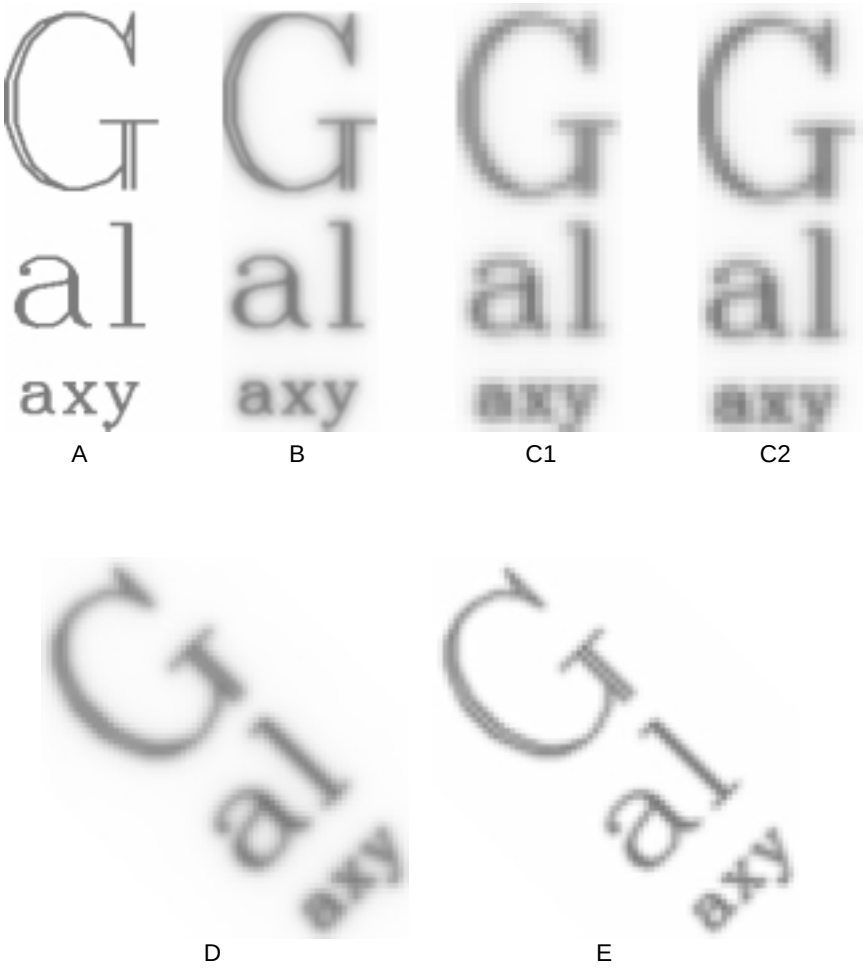

Figure 7.16: Effect of resolution enhancement as a result of interlacing and subsequent CLEANing. **A**: Original ("true") image of dimensions $2\farcs1 \times 5\farcs5$; **B**: image A convolved with HST WFPC2 PSF; **C1**, **C2**: image B sampled at WFPC2 $0\farcs1$ resolution and convolved with the subpixel response function, at two positions with relative offsets of $0\farcs05$ in x and y; **D**: interlaced combination of images C1 and C2, at $0\farcs071$ resolution; **E**: CLEAN restoration of image D.

resolution, and convolved with the subpixel response function using the kernel given in Krist (1995). Finally, each PSF was combined with its $0\farcs05$ shifted copy in the same way as the actual exposures. The effect of interlacing and subsequent CLEANing on noiseless data is demonstrated in Fig. 7.16. Note that most of the degradation of image **A** is caused by the coarse sampling of the PSF by the $0\farcs1$ pixels.

7.B Modeling Color and Luminosity Evolution

It is assumed age differences are the only contributor to the scatter in the color-magnitude relation. The color and luminosity evolution of a galaxy depend on the passband, the IMF, the metallicity, and the star formation history. For simplicity, we assume a Salpeter IMF and solar metallicity. We furthermore assume that the star formation rate in the galaxies was constant from $z = z_1$ to $z = z_2$, with an abrupt truncation at $z = z_2$. As shown by van Dokkum et al. (1998a) the luminosity evolution in the truncated star formation model is given by

$$L_B \propto \left[\sqrt{(t-t_1)(t-t_2)}\right]^{\kappa_B}, \tag{7.6}$$

and the color evolution by

$$\frac{L_B}{L_U} \propto \left[\sqrt{(t-t_1)(t-t_2)}\right]^{\kappa_U-\kappa_B}, \tag{7.7}$$

with t_1 the time of onset of star formation, t_2 the time of truncation, and t the age of the Universe at the epoch of observation. The coefficients κ_B and κ_U describe the luminosity evolution of a single age stellar population: $L \propto (t-t_0)^{-\kappa}$, with t_0 the time of formation of the population. These coefficients can be calculated from stellar population synthesis models. As shown in Fig. 7.17 the rate of evolution is similar in the Worthey (1994), Bruzual & Charlot (1996) and Vazdekis et al. (1996) models. Figure 7.17 also demonstrates that our powerlaw approximation for the color evolution is reasonable, even for fairly young stellar populations. Using Worthey (1994) we find $\kappa_B = 0.93$ and $\kappa_U = 1.08$ for solar metallicity and a Salpeter IMF.

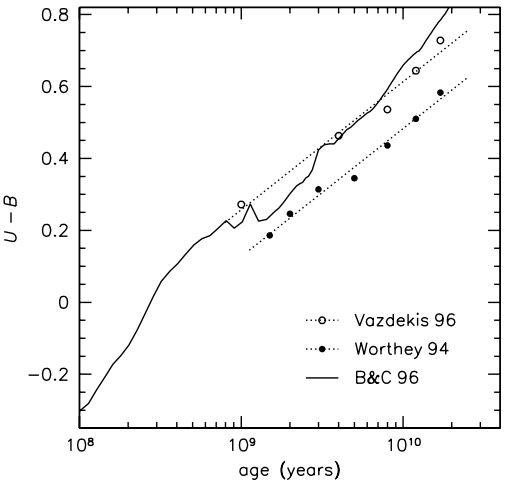

Figure 7.17: Predicted color evolution of single age stellar populations from various stellar population synthesis codes (Worthey 1994, Bruzual & Charlot 1996, and Vazdekis et al. 1996). The color evolution can be approximated by a power law. The coefficient of the powerlaw is similar in the three population synthesis codes.

For consistency with the luminosity evolution derived from the Fundamental Plane (van Dokkum et al. 1998b) we take $z_1 = 10$ and $z_2 = 3$ for galaxies on the CM relation. Assuming $z_1 = 10$ for all galaxies in MS 1054–03, the value of z_2 can be calculated from the observed $\Delta(U-B)_z$, for each galaxy. Since

$$(U-B)_{\rm evo} = 0.543(\kappa_U-\kappa_B)[\ln(t-t_1)+\ln(t-t_2)]+C \tag{7.8}$$

the color difference between two galaxies with the same t_1 and truncation times t_2^A and t_2^B is

$$\Delta(U-B)_{\rm evo} = 0.543(\kappa_U - \kappa_B)\left[\ln(t-t_2^A) - \ln(t-t_2^B)\right]. \quad (7.9)$$

Note that the expression for the color difference only depends on the time of truncation t_2, and is independent of t_1, the time of the onset of star formation.

The observed residual from the CM relation $\Delta(U-B)_{\rm obs}$ is inflated due to the increased luminosity of young galaxies. The relation between $\Delta(U-B)_{\rm evo}$ and the observed color residual is given by

$$\Delta(U-B)_{\rm obs} = \left(1 + \frac{\alpha}{1.086}\frac{\kappa_B}{\kappa_B - \kappa_U}\right)\Delta(U-B)_{\rm evo} = 1.22\Delta(U-B)_{\rm evo}, \quad (7.10)$$

where α is the slope of the CM relation (see van Dokkum et al. 1998a) Combining Eq. 7.9 and Eq. 7.10 yields

$$\ln(t-t_2^B) = \ln(t-t_2^A) - \frac{0.82\Delta(U-B)_{\rm obs}}{0.543(\kappa_U - \kappa_B)} \quad (7.11)$$

Taking $z_2 = 3$ for galaxies having $\Delta(U-B)_{\rm obs} = 0$ (i.e., galaxies on the CM relation) we find

$$\ln(t_{0.83} - t_2) = -1.198 + 10.07\Delta(U-B)_z \quad (7.12)$$

with $t_{0.83}$ the age of the Universe at the epoch of observation (note that $t_{0.00} \equiv 1$).

A consequence of Eq. 7.12 is that galaxies with $\Delta(U-B)_z < -0.2$ have $z_2 \approx 0.83$, i.e., they are still forming stars at $z \approx 0.83$. The fact that 15 out of 20 galaxies with $\Delta(U-B)_z < -0.2$ have EW [O II] 3727 Å > 5 Å lends some support to our modeling. Galaxies with $\Delta(U-B)_z > 0.064$ have $z_2 > 10$, which is not allowed in the present model. There are only two galaxies in our sample which have $\Delta(U-B)_z > 0.064$: 1486 and 1986. They are both spirals, and their colors are probably affected by dust. For these galaxies we have set $z_2 = z_1 = 10$.

Given the values of t_1 and t_2 we can calculate the color and luminosity of each galaxy at time t using Eq. 7.6 and Eq. 7.7. We note that our results are not very dependent on the assumed star formation history. As shown by van Dokkum et al. (1998a), the evolution of the scatter in the CM relation is mainly driven by the mean luminosity weighted ages of the galaxies, and this parameter is well constrained by the luminosity evolution derived from the Fundamental Plane.

Nederlandse samenvatting

Sterrenstelsels

Sterren zijn niet zomaar willekeurig in het Heelal verspreid maar zijn gegroepeerd in sterrenstelsels. Dit proefschrift gaat over de manier waarop sterrenstelsels zijn ontstaan, en hoe hun eigenschappen zijn veranderd in de loop van de tijd. De zon is een onbeduidend sterretje in een spiraalarm van het spiraalstelsel "De Melkweg". Alle sterren die 's nachts met het blote oog te zien zijn behoren tot de Melkweg. Zoals veel andere sterrenstelsels is de Melkweg plat: het is een roterende schijf, met in het midden een verdikking. Ware het geen heiligschennis dan zou men dit prachtige dynamische systeem met een spiegelei vergelijken. De zon bevindt zich in deze schijf. Je ziet meer sterren in het vlak van de schijf dan loodrecht daarop; de Melkweg vormt daarom een wazige band aan de hemel. Het aantal sterren in de Melkweg bedraagt ongeveer 100 miljard.

Op enkele uitzonderingen na zijn sterrenstelsels buiten onze eigen Melkweg alleen te zien met telescopen; doordat de sterrenstelsels erg ver van ons vandaan staan zijn zij niet zichtbaar met het blote oog. Het is vergeven van de sterrenstelsels in het Heelal. Op een opname van een klein stukje van de hemel met een gevoelige telescoop zijn er duizenden te zien. Elk sterrenstelsel herbergt miljarden sterren. Het licht van deze sterren vloeit samen tot een wazig vlekje, een klein spiegeleitje temidden van duizenden andere.

Niet alle sterrenstelsels zien er uit als onze eigen Melkweg. Sommige zijn niet plat maar rond, of gevormd als een rugby-bal (de "elliptische stelsels"). Kleine sterrenstelsels zijn vaak onregelmatig van vorm. Verder zijn er grote en kleine sterrenstelsels, heldere en zwakke, rode en blauwe. Ze komen veel voor in kleine groepjes, bestaande uit een paar grote en een handvol kleintjes, maar ook in concentraties van duizenden stelsels die samen gigantische dynamische systemen vormen ("clusters"). De eigenschappen van sterrenstelsels blijken samen te hangen met hun omgeving: sterrenstelsels in groepjes zijn bijvoorbeeld blauwer dan sterrenstelsels in clusters. In dit proefschrift gaat het over zogenaamde "vroeg-type" stelsels; de verzamelnaam voor elliptische stelsels en S0 stelsels. S0s (uitgesproken als "Es-nul") zijn eigenlijk elliptische stelsels met een platte schijf, een tussenvorm tussen spiraalstelsels en elliptische stelsels. Deze vroeg-type stelsels komen vooral voor in clusters; spiraalstelsels zoals de Melkweg vind je daarentegen vooral in kleine groepjes. Op de voorkant van dit proefschrift staat een opname door de Hubble Space Telescope van een zeer ver weg staande cluster. Veel van de rode objecten zijn vroeg-type stelsels.

Evolutie

Het Heelal is ongeveer 14 miljard jaar oud. In het begin was het Heelal woest en vol met elementaire deeltjes; van sterren of sterrenstelsels was nog geen sprake. Een belangrijke vraag in de astronomie is hoe en wanneer sterrenstelsels zijn ontstaan, en wat de verklaring is voor de grote verscheidenheid aan eigenschappen.

Er zijn verschillende manieren om tot een antwoord op deze vraag te komen. Tot voor kort was de belangrijkste methode het toetsen van modelvoorspellingen aan de waargenomen eigenschappen van stelsels. Een populair model voor de vorming van elliptische stelsels is bijvoorbeeld dat zij 10 tot 13 miljard jaar geleden zijn ontstaan, en dat er sindsdien geen nieuwe sterren meer gevormd zijn. Dit model voorspelt dat er geen jonge sterren in deze

elliptische stelsels voorkomen; dit zou namelijk betekenen dat er recent nog sterren werden gevormd. Door het vergelijken van het licht van elliptische stelsels met dat van sterren van diverse leeftijden in onze Melkweg kan een dergelijk model getoetst worden aan de werkelijkheid.

In dit proefschrift wordt gebruik gemaakt van een meer directe methode. Met grote telescopen is het tegenwoordig mogelijk sterrenstelsels tot op extreem grote afstanden waar te nemen. De vage vlekjes die met grote telescopen te zien zijn staan zo verschrikkelijk ver weg dat het licht van deze objecten miljarden jaren nodig heeft om ons te bereiken. Ter vergelijking, en om enig idee te geven van de afstanden waar het hier om gaat, het licht doet er 1 seconde over om vanaf de maan de aarde te bereiken; de afstand tot de Zon is acht lichtminuten, en de afstand tot de dichtst bijzijnde sterren bedraagt enkele lichtjaren.

Sterrenkundigen kijken dus terug in de tijd; een telescoop is niets minder dan een tijdmachine. Hoe groter de afstand tot het object, hoe meer tijd er verstreken is sinds de straling door het object werd uitgezonden, en hoe verder we in het verleden kijken. Door het vergelijken van de eigenschappen van sterrenstelsels op verschillende afstanden kan de ontstaansgeschiedenis van deze sterrenstelsels worden achterhaald. Het werk is vergelijkbaar met dat van paleontologen: zoals de paleontoloog restjes blad, bot en tanden met veel toewijding uit weerbarstige rotsen beitelt om de evolutie van planten en dieren te achterhalen, zo construeert de astro-paleontoloog de geschiedenis van het Heelal.

Het onderzoek

In dit proefschrift worden sterrenstelsels in clusters op verschillende afstanden met elkaar vergeleken. Uit de verschillen tussen de sterrenstelsels wordt afgeleid hoe zij evolueren. De reden waarom nu juist sterrenstelsels in clusters worden onderzocht is dat je op die manier eenvoudig een grote groep sterrenstelsels die allemaal op dezelfde afstand staan kunt bestuderen. Figuur 1 laat zien hoe oud het Heelal was toen het licht werd uitgezonden van sterrenstelsels in de vier verre clusters die in dit proefschrift beschreven worden. De Coma cluster is in de meeste hoofdstukken het nabije referentiepunt waarmee de verre clusters worden vergeleken; deze cluster staat “slechts” op zo’n 400 miljoen lichtjaar afstand. Het licht van sterrenstelsels in de verste cluster (MS 1054–03) werd uitgezonden toen het Heelal minder dan de helft van haar huidige leeftijd had. Op de voorkant van dit proefschrift staat een opname die wij met de Hubble Space Telescope van deze cluster gemaakt hebben. De Hubble Space Telescope maakt heel gedetailleerde opnamen van kleine stukjes van de hemel. De afbeelding op de voorkant van dit proefschrift (waarop enkele duizenden sterrenstelsels te zien zijn) beslaat een even groot deel van de hemel als een straaljager op tien kilometer hoogte, en is zo gedetailleerd dat je op het horloge van de piloot zou kunnen zien hoe laat het is.

Evolutie van de lichtkracht van sterrenstelsels

Er zijn diverse eigenschappen die je kunt meten; bijvoorbeeld de kleur of de grootte van de sterrenstelsels. Het bijzondere van het onderzoek in dit proefschrift is dat ook de massa (onnauwkeurig gezegd, het gewicht) van de centrale delen van sterrenstelsels wordt gemeten. Het is belangrijk om deze massa’s te kennen; eigenschappen zoals kleur en helderheid van sterrenstelsels zijn weliswaar veel eenvoudiger te bepalen, maar het is erg moeilijk sterrenstelsels op verschillende afstanden te vergelijken wanneer de massa niet bekend is. Je weet namelijk niet of een bepaald stelsel helder is omdat de sterren die het bevat erg helder zijn, of omdat het gewoon heel veel sterren bevat (en dus heel zwaar is). Wat je eigenlijk wilt weten is

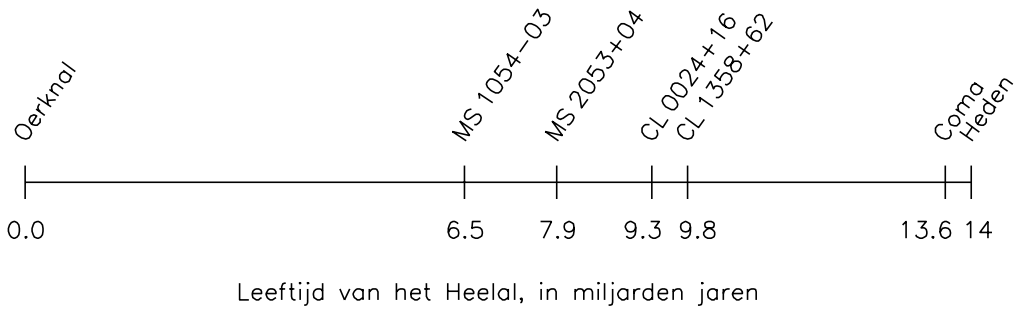

Figuur 1: Schematische weergave van de afstanden tot de clusters die in dit proefschrift beschreven worden. De figuur geeft aan hoe oud het Heelal was toen sterrenstelsels in de clusters het licht uitzonden dat wij nu opvangen.

de verandering in de verhouding tussen massa en lichtkracht van sterrenstelsels, toepasselijk de "massa-lichtkracht" verhouding genoemd.

De lichtkracht verandert omdat sterren in de sterrenstelsels sterven. Naarmate er meer sterren uitdoven wordt de lichtkracht van het sterrenstelsel kleiner. De massa van het sterrenstelsel blijft ongeveer constant: de resten van de uitgedoofde sterren (gas, witte dwergen, zwarte gaten) zijn weliswaar niet meer zichtbaar, maar dragen nog wel bij aan de massa. In mijn onderzoek vergelijk ik de massa-lichtkracht verhouding van sterrenstelsels op verschillende afstanden (en dus tijdstippen). Op deze manier kan de snelheid waarmee de helderheid van een sterrenstelsel verandert heel nauwkeurig bepaald worden. De bepaling van de evolutie van de massa-lichtkracht verhouding wordt beschreven in de Hoofdstukken 2, 3, en 4.

Uit de waargenomen evolutie van de lichtkracht kan worden afgeleid hoe oud de sterren in de sterrenstelsels zijn. Wanneer een generatie van sterren net gevormd is bestaat zij uit zeer veel lichte sterretjes en een handvol zware sterren. Zware sterren leven kort, maar spectaculair. Zij jagen in een paar miljoen jaar hun hele voorraad brandstof (waterstof en helium) erdoor, iets waar lichtere sterren (zoals de Zon) miljarden jaren over doen. Zware sterren zijn dan ook extreem helder; hoewel ze in de meerderheid zijn, stralen lichte sterren samen toch veel minder licht uit. Na korte tijd sterven de zware sterren echter uit en zien we alleen nog het licht van lichte en middelzware sterren. Aangezien deze sterren een veel langere levensduur hebben dan de zware sterren verandert de lichtkracht van de populatie nu veel langzamer dan eerst. Naarmate de sterpopulatie ouder is zal de lichtkracht dus langzamer afnemen. Uit de waargenomen verandering van de lichtkracht over een tijdsspanne van miljarden jaren is dan ook de leeftijd van de sterpopulatie af te leiden: zien we een snelle verandering dan is de populatie jong, is de verandering maar klein dan is de populatie oud.

In de praktijk blijkt de lichtkracht langzaam af te nemen in de loop van de tijd: in de afgelopen acht miljard jaar tijd is de lichtkracht ongeveer gehalveerd. Deze langzame verandering duidt erop dat de sterren in vroeg-type stelsels zeer oud zijn, minstens twaalf miljard jaar (er van uitgaande dat het Heelal veertien miljard jaar oud is).

Morfologische evolutie

De weeg-en-dateer methode kan goed gebruikt worden voor vroeg-type stelsels. Van deze stelsels zijn de massa en de lichtkracht tamelijk eenvoudig te bepalen met grote aardse telescopen (zoals de Keck telescoop op Hawaii, met een spiegeldiameter van tien meter de grootste op aarde) en de Hubble Space Telescope. Hoewel de evolutie van de lichtkracht van deze stelsels zeer nauwkeurig bepaald kan worden is er toch een probleem. De achterliggende

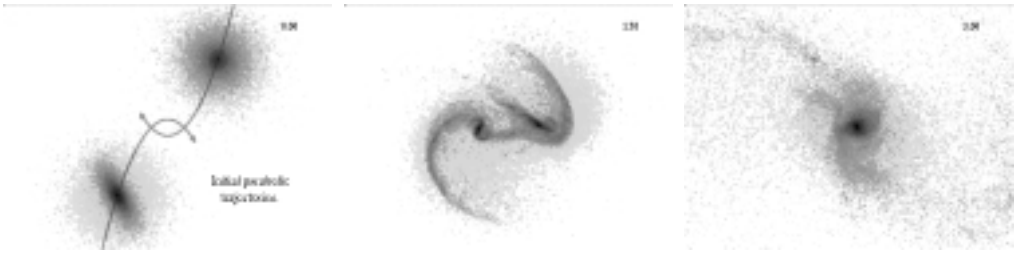

Figuur 2: Simulatie van de botsing van twee sterrenstelsels (met dank aan Dr. J. Barnes). Na drie miljard jaar zijn de stelsels samengesmolten tot een nieuw, groter en zwaarder stelsel. Eén van de resultaten van dit proefschrift is dat dergelijke botsingen veel voorkwamen acht miljard jaar geleden. Afbeeldingen van deze waargenomen botsingen staan op de achterkant van het proefschrift.

aanname van dit soort onderzoek is namelijk dat de vroeg-type sterrenstelsels die je op zeer grote afstanden ziet vergelijkbaar zijn met de voorouders van vroeg-type sterrenstelsels die je in de nabije omgeving ziet. Het is echter maar de vraag of dat echt zo is, en of je geen appels met peren aan het vergelijken bent.

De morfologieën van sterrenstelsels kunnen namelijk veranderen. Het kan zijn dat een deel van de vroeg-type sterrenstelsels in nabije clusters er heel anders uitzag in het verleden, bijvoorbeeld als spiraalstelsels. Als dat zo is dan vertegenwoordigen de vroeg-type stelsels in de verre clusters maar een deel van de voorouders van vroeg-type stelsels in nabije clusters. Om een voorbeeld te geven: in het paleontologisch onderzoek naar de voorouders van de mens heeft men zich tot nu toe geconcentreerd op primaten. Stel je eens voor dat mensachtigen zijn voortgekomen uit ezels. In dat geval zal men minder en minder primaten vinden naarmate men oudere steenlagen onderzoekt, en meer en meer ezels. Wil men een volledig beeld krijgen van de evolutie van de mens, dan zou men eigenlijk zowel fossiele ezels als primaten moeten onderzoeken.

Hoewel de evolutie van ezel tot mens voor sommigen misschien moeilijk voor te stellen is ligt de situatie bij sterrenstelsels enigszins anders. Zolang de verschillende verschijningsvormen van sterrenstelsels bekend zijn is al gespeculeerd over overgangen tussen de vormen. Veel van de morfologische kenmerken hangen bijvoorbeeld samen met stervorming: de vorming van sterren vindt plaats in kleine klontjes temidden van stof en gruis en dit geeft een sterrenstelsel als geheel een brokkelig aanzien. In de Melkweg vindt veel stervorming plaats; je kunt zelf vaststellen dat de Melkwegband aan de hemel dan ook niet egaal is, maar nogal rafelig. Vroeg-type stelsels zijn egaal en gelijkmatig van vorm en kleur, en hebben nauwelijks of geen stervorming. Het is niet zo moeilijk voor te stellen dat wanneer stervorming in een spiraalstelsel stopt (bijvoorbeeld omdat al het gas waaruit sterren gevormd werden op is) het stelsel meer en meer op een vroeg-type stelsel zal gaan lijken.

Verder kunnen sterrenstelsels op elkaar botsen. Door zulke botsingen worden alle structuren (zoals een schijf) vernietigd en ontstaat een grote bal sterren. Zo hebben simulaties laten zien dat de botsing van twee spiraalstelsels kan leiden tot de vorming van een elliptisch stelsel. Een voorbeeld van een dergelijke simulatie is te zien in Figuur 2. Wijzelf vliegen trouwens met een vaartje van 400.000 km per uur op het Andromeda sterrenstelsel af (dat nu al op een heldere herfstnacht met het blote oog te zien is!). Grote zorgen hoeven we ons gelukkig niet te maken: de afstanden tussen sterren zijn zo groot dat de botsing van de stelsels geen botsingen van individuele sterren of planeten tot gevolg zal hebben (de stelsels “schuiven in elkaar”), en verder duurt het nog ruim vier miljard jaar voordat het zover is.

De vorming van vroeg-type stelsels

Het belang van morfologische evolutie van sterrenstelsels kan bepaald worden door niet alleen naar een bepaalde soort stelsels te kijken, maar naar alle sterrenstelsels op een zekere afstand. Als een paleontoloog alle 100.000 jaar oude fossielen bestudeert kan hij er zeker van zijn dat er voorouders van de mens tussen zitten. Deze aanpak wordt gevolgd in de Hoofdstukken 5, 6 en 7. In deze hoofdstukken worden niet alleen de vroeg-type stelsels in verre clusters onderzocht maar er wordt ook gekeken naar alle andere stelsels die deel uitmaken van de clusters.

Er worden twee manieren gebruikt om er achter te komen of morfologische evolutie veel voorkomt. De eerste manier is het bepalen van de fractie van vroeg-type stelsels: als vroeg-type stelsels gevormd worden uit andere typen sterrenstelsels is de verwachting dat er minder vroeg-type stelsels en meer andere types waren in het verleden. De andere manier is het zoeken naar overgangsvormen. Net als bij de reconstructie van de evolutie van de mens is het vinden van overgangsvormen een cruciaal aspect van het bewijzen van morfologische evolutie. Aangezien simulaties aangeven dat deze overgangen tamelijk vlug verlopen (in minder dan een miljard jaar) moeten veel sterrenstelsels onderzocht worden om deze overgangen op heterdaad te betrappen.

In de Hoofdstukken 5, 6 en 7 worden twee morfologische overgangen besproken: de overgang van spiraalstelsels (zoals de Melkweg) naar S0 stelsels (bollen met structuurloze schijven), en de overgang naar grote elliptische stelsels door botsingen van kleinere stelsels. In Hoofdstuk 5 wordt aannemelijk gemaakt dat de overgang van spiraalstelsel naar S0 op grote schaal optreedt in clusters. Er wordt voor het eerst een populatie gevonden van jonge S0 stelsels, dat wil zeggen stelsels die tot voor kort nog sterren vormden maar zojuist zijn “uitgedoofd”. Deze pas gevormde vroeg-type stelsels bevinden zich in de buitengebieden van de cluster. Zij houden zich daar waarschijnlijk op omdat zij recentelijk de cluster zijn binnengevallen vanuit het omringende gebied. Het binnendringen van clusters kan alleen tegen een prijs: de clusters zitten boordevol heet gas dat Röntgen-straling uitzendt, en het is waarschijnlijk dat sterrenstelsels door de botsing met dit hete gas een groot deel van hun koude gas (waaruit sterren kunnen worden gevormd) kwijtraken. Het lijkt er dan ook op dat de binnendringende stelsels spiraalstelsels waren, die hun gas kwijt zijn geraakt bij het binnendringen van de cluster en vervolgens in S0 stelsels zijn veranderd. Dit scenario is ook al bedacht door andere astronomen, onder meer op grond van het kleine aantal S0 stelsels in verhouding tot het aantal spiraalstelsels in andere verre clusters.

In Hoofdstuk 6 wordt voor het eerst bewezen dat botsingen tussen sterrenstelsels in clusters acht miljard jaar geleden veelvuldig voorkwamen. In de meest verafgelegen (en dus jongste) cluster die in dit proefschrift wordt beschreven bestaat maar liefst 17 % van de sterrenstelsels uit “wrakken” van zojuist gebotste stelsels of uit paren van botsende stelsels. De opnamen die de Hubble Space Telescope van deze objecten maakte staan op de achterkant van het proefschrift. Simulaties laten zien dat dergelijke botsingen leiden tot de samensmelting van de stelsels tot elliptische stelsels. Uit het grote aantal botsingen wordt afgeleid dat minstens de helft van de elliptische stelsels in clusters is ontstaan door samensmelting van kleinere stelsels in de afgelopen acht miljard jaar. Een gedetailleerde bestudering van de stelsels toont aan dat de sterren in de samensmeltende stelsels al behoorlijk oud zijn, en dat er maar heel weinig nieuwe sterren worden gevormd tijdens de botsingen.

Het komt er dus op neer dat de *sterren* in vroeg-type stelsels erg oud zijn, maar dat de sterren*stelsels* relatief kort geleden gevormd zijn. In Hoofdstuk 7 wordt een model beschreven dat zowel de morfologische evolutie van sterrenstelsels in clusters als de evolutie van hun sterpopulaties goed weet te beschrijven.

Implicaties

De ontdekking van het grote aantal botsende stelsels in het verleden heeft verstrekkende implicaties. Het bestaan van deze objecten is een overtuigend bewijs tegen vorming van sterrenstelsels in een zogenaamde "monolitische ineenstorting" in het vroege Heelal. In deze theorie zijn sterrenstelsels al snel na de oerknal gevormd, uit enorme samentrekkende gaswolken. Dit was lange tijd het meest populaire model voor de vorming van sterrenstelsels; je kunt met een gerust hart aannemen dat er astronomen waren die eerder zouden geloven dat mensen uit ezels zijn voortgekomen dan dat grote sterrenstelsels door botsingen van kleintjes zijn gevormd.

De belangrijkste alternatieve theoriën proberen de vorming van sterrenstelsels te verklaren uit kleine verstoringen in de kosmische achtergrondstraling. In deze "hiërarchische" theoriën worden grote structuren onder invloed van de zwaartekracht gevormd door samensmeltingen van kleinere structuren. Dergelijke theoriën doen tamelijk specifieke voorspellingen voor de evolutie van donkere materie, maar de voorspellingen voor de vorming en eigenschappen van sterren en sterrenstelsels zijn nog vrij onzeker. In grote lijn kunnen in het vroege Heelal alleen kleine sterrenstelseltjes vormen, die vervolgens botsen met andere kleine sterrenstelsels en samensmelten tot grotere stelsels. Het duurt op deze manier lang voordat zware sterrenstelsels zijn gevormd; je hebt daar immers behoorlijk wat generaties van botsingen voor nodig. De ontdekking van de botsende stelsels is in overeenstemming met het principe van hiërarchische vorming. De meest specifieke modellen namen aan dat bij dergelijke botsingen veel nieuwe sterren worden gevormd, en uit het feit dat de meeste sterren in de botsende stelsels al lang voor de botsingen gevormd waren valt af te leiden dat deze modellen nog incompleet zijn.

Curriculum Vitae

Op 29 juni 1972 werd ik geboren te Zwolle. In juni 1990 behaalde ik aan het Lambert Franckens College te Elburg het VWO diploma Athenaeum.

In september 1990 begon ik aan de studie sterrenkunde aan de Rijksuniversiteit Groningen. Een jaar later behaalde ik het propaedeutisch examen. Tijdens mijn doctoraalfase werkte ik met dr. R. Peletier aan de lichtverdeling in spiraalstelsels, en met prof. dr. M. Franx aan de kernen van elliptische stelsels. In 1994 ondernam ik een reis naar La Silla (Chili) om waarnemingen te doen met de 0,9 m Nederlandse Telescoop. Ook was ik dat jaar lid van het afdelingsbestuur Sterrenkunde, en van de studentenorganisatie β-stuff. Daarnaast richtte ik samen met drs. M. Zwaan een bedrijf op dat bemiddelde op het gebied van studiebegeleiding. In december 1994 legde ik het doctoraalexamen sterrenkunde af.

Op 1 januari 1995 trad ik in dienst als assistent in opleiding bij de Rijksuniversiteit Groningen. Onder leiding van prof. dr. M. Franx en prof. dr. G. D. Illingworth (Lick Observatory, Santa Cruz, California) deed ik onderzoek aan de evolutie van sterrenstelsels. Behalve met mijn promotores werkte ik in de periode 1995 – 1999 samen met dr. D. Fabricant, dr. D. Fisher en dr. D. Kelson.

Ik bracht vijf werkbezoeken aan het Lick Observatory te Santa Cruz, twee aan het Harvard-Smithsonian Center for Astrophysics te Cambridge (Massachusetts), en verscheidene korte bezoeken aan andere instituten. In 1996 nam ik deel aan een winterschool in Jeruzalem. Ik bezocht conferenties in Heidelberg, München ($2\times$), Canberra, Rome en New Brunswick, en gaf colloquia in Cambridge (Engeland), München en Utrecht. Gedurende mijn onderzoek heb ik waarnemingen verricht met de 3,6 m New Technology Telescope op La Silla (Chili), tweemaal met de 4,2 m William Herschel Telescope op La Palma, en zeven keer met de 10 m W. M. Keck Telescope op Hawaii.

Naast mijn onderzoek verzorgde ik in 1996 en 1997 een deel van het college Sterrenkunde 2 en was ik voorzitter van schaakvereniging De Spassky's. Vanaf april 1998 werkte ik als gastonderzoeker bij de Leidse Sterrewacht. Na mijn promotie zal ik als Hubble Fellow verbonden zijn aan het California Institute of Technology in Pasadena.

Acknowledgements

No thesis is solely the work of the author. Assistance comes from a variety of sources in as many different ways. I am grateful to the following people and institutions for their support.

First of all my advisors Marijn Franx and Garth Illingworth, for their unending enthusiasm and involvement. They have always given me the freedom to pursue my own interests.

Having had Marijn as my advisor for five years deserves a special thanks. It has been both hard labour and fun to work with Marijn, whose personality and intelligence have – during all these years – never failed to impress and amuse me. The trust he has always placed in me is inspiring and I will never forget the moment when I was first allowed – after two years of working under his guidance – to mow his lawn on my own.

During several visits I enjoyed the hospitality of the Harvard-Smithsonian Center for Astrophysics and the University of California, Santa Cruz. I gratefully acknowledge the Leids Kerkhoven-Bosscha Fonds and the University of Groningen for their generous financial support of my outward bound journeys. As a Dutch graduate student I have profited tremendously from the excellent opportunities to visit conferences and Universities abroad.

For their advice, friendship and hospitality I thank Dan Kelson and Dan Fabricant.

In Groningen dank ik Tjeerd van Albada en Donald Staal voor het inzetten van hun organisatietalent bij mijn verhuizing naar Leiden. Tevens dank ik de leden van de beoordelingscommissie, Tjeerd, Renzo en Frank, voor hun interesse en commentaar. Ik dank het Kapteyn Instituut en haar bewoners voor acht goede jaren, en de Leidse Sterrewacht voor haar gastvrijheid gedurende het laatste jaar van mijn onderzoek. In het bijzonder dank ik Tim de Zeeuw voor zijn wijze raad op alle terreinen des levens.

Ik dank Martin, Ilse, Pim, Paul, Henk, Jolanda en Mangala voor hun vriendschap, en JM voor alle goede en slechte films en maaltijden tot nu toe samen genuttigd, en de toekomstige. De afstand tussen Las Vegas en Pasadena is maar klein; moge mijn huis een welkome afwisseling zijn van de Strip.

Mijn ouders dank ik voor hun niet aflatende vertrouwen. Zij hebben mij altijd de ruimte gegeven om te doen wat mij goeddunkte. Ik dank Henno voor zijn stimulerende aanwezigheid het afgelopen jaar. Zijn kritische houding ten opzichte van wetenschappers was amusant.

Op deze plaats roep ik mijn paranimfen op zich met elkaar te verzoenen.

Tenslotte dank ik Hester voor het doorbladeren van de Nederlandse samenvatting, voor haar consequente desinteresse in sterrenkunde, en voor drie onvergetelijke jaren. Je scherpe geest doet me telkens weer versteld staan.